Nutritional Regulation of Neural Stem Cell Reactivation in *Drosophila Melanogaster*

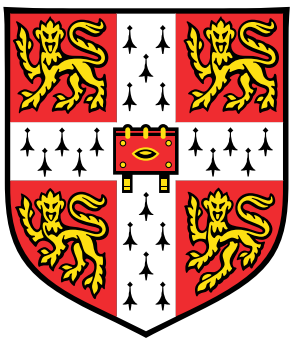

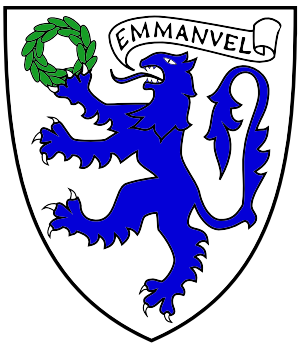

Jun Liu

Department of Physiology, Development and Neuroscience

University of Cambridge

This dissertation is submitted for the degree of

Doctor of Philosophy

Emmanuel College

2014

I would like to dedicate this thesis to my mother and grandmother. I hope that this achievement will make you proud.

Declaration

The work described in this thesis was performed in Professor Andrea Brand's laboratory at the Gurdon Institute, University of Cambridge. I hereby declare that except where specific reference is made to the work of others, the contents of this dissertation are original and have not been submitted in whole or in part for consideration for any other degree or qualification in this, or any other University. This dissertation is the result of my own work and includes nothing which is the outcome of work done in collaboration, except where specifically indicated in the text. This dissertation contains less than 60,000 words excluding appendices, bibliography and tables and has less than 150 figures.

Jun Liu
2014

Acknowledgements

First of all, I would like to thank my supervisor, Andrea Brand, for giving me the wonderful opportunity to work in her laboratory, and her guidance during the past four years. I am extremely grateful for the the present and past members of the Brand lab, who provided me with constant technical and emotional support, and made my time in the lab intellectually stimulating and enjoyable. In particular, I would like to thank Pauline Speder, for teaching me a variety of techniques, giving me practical guidance in my project, and being a fantastic friend. I also thank Paul Wu, who gave me plenty of encouragement and PhD survival tips during my troubled first year. I would like to thank Esteban Contreras for valuable scientific insights, life advice, and friendship. Many thanks to Jorge Buendia-Buendia, who continued to help me with bioinformatics analysis even after he officially completed his Master's degree. In addition, I am grateful to Tony Southall, for help with all aspects of the Targeted DamID experiments and beyond.

I would like to thank my supervisor, the Cambridge University Philosophical Society, and the fellowship office of Williams College, MA, USA, for providing generous financial support during the past four years.

Finally, I would like to express my deepest gratitude to friends and family members who trusted in me and supported me during difficult times. Thank you Christoph for being a patient and encouraging partner throughout my PhD. Thank you Diane for being the best friend and study-buddy one can hope for. Many thanks to my supportive parents, grandmother, cousins and the rest of my extended family for their love on the other side of the globe. Finally, I would like to thank Daniel, without whose support I would not have dreamt of winning the Herschel Smith Fellowship in the first place.

Abstract

In order to coordinate brain development with the growth of the organism, neurogenesis is highly dependent on the organism's nutritional intake. The transition between neural stem cell (NSC) quiescence and reactivation is a key point of regulation during neurogenesis, and in *Drosophila*, this process is tightly coupled to nutrient availability. Post-embryonic NSCs in *Drosophila* only exit quiescence when larvae are fed a diet containing essential amino acids. The fat body, a functional homologue of the liver and adipose tissue, acts as a systemic nutrient sensor. Existing evidence from both *in vivo* and *in vitro* studies suggest that upon sensing dietary amino acids, the fat body secretes unknown factor(s) that induce glial secretion of insulin/IGF-peptides, which are sensed by underlying NSCs to trigger their reactivation.

Despite recent work on nutritional regulation of NSC reactivation, key questions still remain: what are the signal(s) from the fat body, and how do they interact with the glial cells to induce glial production of DIlps? In addition, a number of glial subtypes are closely associated with the NSCs, but each subtype's individual contribution to NSC reactivation remains elusive. In order to search for the unknown fat body factor(s) and investigate how they interact with the glial cells, I compared the transcriptome of the fat body under fed and starvation conditions during the time window of NSC reactivation. I identified an extracellular matrix protein (ECM), Collagen IV, as a secreted fat body signal whose deposition on the CNS is required for NSC reactivation. Collagen IV recruits glial-derived Perlecan^{Trol}, another ECM protein and a known requirement for NSC reactivation, to the vicinity of NSCs. Both ECM proteins are indispensable for the induction of glial insulin/IGF signalling.

NSCs are separated from the hemolymph by a blood brain barrier (BBB). In collaboration with Pauline Speder and Jessie Van Buggenum (Andrea Brand lab), we confirmed crucial roles of the two BBB glial populations as a nutrient-sensitive NSC niche and identified each subpopulation's contribution to NSC reactivation. Transcriptional profiling revealed that both BBB glial populations transcribe Dilp6 and perineurial glia is the source of Perlecan^{Trol}. Together, Collagen IV and Perlecan^{Trol} trigger NSC reaction via binding to their integrin receptors and subsequent induction of insulin signalling from the BBB glia.

Glossary

Abbreviation	Full name
BBB	Blood brain barrier
CG	Cortex glia
CNS	Central nervous system
CSF	Cerebral spinal fluid
Dam	DNA adenine methyltransferase
DamID	DNA adenine methyltransferase identification
DAPI	4',6-diamidino-2-phenylindole
DAVID	Database for Annota- tion, Visualisation and Integrated Discovery
dH2O	deonised H2O
DIlp	Drosophila insulin-like peptide
Dlg	Discs large
DNA	Deoxyribonucleic acid
Dpn	Deadpan
ECM	Extracellular matrix
FDR	False discovery rate
FGF	Fibroblast growth factor
FISH	Fluorescence in situ hybridisation
GAL4	GAL4 activation domain
GFP	Green fluorescent protein
GO	Gene ontology
GO	Gene ontology
Hh	Hedgehog
hph	hours post hatching
IGF	Insulin-like growth factor
IGF1R	Insulin-like growth factor 1 receptor

IPC	Insulin producing cell
JAK/STAT	Janus kinase/Signal transducer and activator of transcription
KEGG	Kyoto Encyclopedia of Genes and Genomes
LPC	Lamina precursor cell
NSC	Neural stem cell
PBS	Phosphate-buffered saline
PCR	Polymerase chain reaction
PG	Perineurial glia
PH3	Phospho-Histone 3
Pha	Phalloidin
Pol II	RNA Polymerase II
RFP	Red fluorescent protein
RNA	Ribonucleic acid
RNAi	RNA interference
SGZ	Subgranular zone
ShiDN	Dominant negative Shibire
ShmiR	Small hairpin-based mi- croRNA
Slif	Slimfast
SPG	Subperineurial glia
STRING	Search Tool for the Retrieval of Interacting Genes/Proteins
SVZ	Subventricular zone
Syx5	Syntaxin5
TaDa	Targeted DamID
TOR	Target of Rapamycin
UAS	Upstream activating sequence
VEGF	Vascular endothelial growth factor
VNC	Ventral nerve cord
VNC	Ventral nerve cord
VZ	Ventricular zone
WT	Wild type

Contents

Chapter 1

Introduction

1.1 An Overview of Mammalian Neural Development

1.1.1 Prenatal Neurogenesis and the Emergence of NSCs

The central nervous system (CNS) is the part of the nervous system consisting of the brain and the spinal cord. It exists in all bilaterally symmetric multicellular animals, such as insects and mammals, and it is considered the commanding centre of the organism. The CNS integrates information that it receives from the rest of the body, while exerting influences on its activities in response to the organism's internal needs and stimuli from the environment. The brain, in particular, exerts many higher cognitive functions such as thinking, learning, and decision making, which are hallmarks for higher organisms such as mammals. Therefore, the normal functions and well-being of an animal are highly dependent on a well-formed CNS and the maintenance of its health throughout life. The formation of the mammalian CNS is a complex process. The emergence of the neuronal tissues, or neural differentiation, occurs during early stages of embryogenesis, soon after germ layer differentiation. The tissues of the CNS are derived from a clearly defined neuroectoderm, called the neural plate, which lies along the dorsal midline of the embryo. For a review, see (Kennea & Mehmet, 2002). The neural plate is formed by the local suppression of signalling molecules that induce non-neural differentiation. Such molecules include the bone morphogenetic proteins (BMPs), which instruct epidermal differentiation and other transforming growth factor-beta (TGF-beta) superfamily molecules (Kintner, 2002; Wilson & Edlund, 2001).

The neural plate then gives rise to all cell types of the mature CNS. This process is precisely regulated, both spatially and temporally, by a variety of intrinsic factors and external

signalling molecules such as BMP signalling and sonic hedgehog signalling (Briscoe & Ericson, 2001; Lee & Pfaff, 2001). Cellular growth and proliferation of the neural plate gradually lead to the closure of the neural groove, which then forms the neural tube. The cavity of the neural tube later gives rise to the ventricular system, while the epithelial layer of the neural tube give rise to stem cells that will then produce the neuronal and glial cells of the developing CNS (Kennea & Mehmet, 2002).

Initially, the single layer of neuroepithelial lining consists of morphologically similar stem cells. These cells are defined as neural stem cells (NSCs) due to their ability to self-renew and their potential to generate all CNS cell types of the mature brain. They can divide asymmetrically, in which one daughter cell retains self-renewing capacity, while the other differentiates into specific cell types (Götz & Huttner, 2005). In addition, NSCs often produce intermediate progenitors that exist transiently and amplify the number of daughter cells through symmetric division, as reviewed in (Götz & Huttner, 2005). The NSCs and NSCs-derived progenitor cells eventually produce all three major cell types of the CNS: neurons, astrocytes and oligodendrocytes (Jan & Jan, 1998).

Because NSCs exhibit branched, astrocytes-like morphology, and express certain glial markers such as glycogen granules, astrocyte glutamate transporter (GLAST), glial fibrillary acidic protein (GFAP), they have been widely referred to as radial glia (Alvarez-Buylla & Garcia-Verdugo, 2002).

1.1.2 Mammalian Neurogenesis Continues Into Postnatal Life

In mammals, neurogenesis occurs mostly prenatally. But in addition to embryonic NSCs, multipotent and self-renewing NSCs also exist in the adult cerebral cortex. The cerebral cortex is arguably one of the most important areas of the mammalian CNS, which is the outermost layered structure. It contains approximately half of all neurons in the human brain and executes higher brain functions such as memory, attention, perceptual awareness, thought, language, and consciousness. For a review, see (Bystron *et al.* , 2008).

Neurons necessary for postnatal cortical functions are generated prior to birth. After the completion of prenatal cortical neurogensis program, most NSCs migrate to the cortex surface where they differentiate into astrocytes and lose their neurogenic potential. However, some NSCs remain in the postnatal/adult cerebral cortex in two specific regions: the subventricular zone (SVZ) and hippocampal subgranular zone (SGZ). These NSCs have been found to retain their neurogenic properties in the postnatal life (Götz & Huttner, 2005; Song *et al.* , 2002). Therefore, the existence of adult NSCs has important implications for

the maintenance, plasticity, and pathogenesis of the adult mammalian brain.

1.1.3 Quiescence Is a Physiologically Important State for the Adult NSCs

Adult NSCs can transit between states of quiescence and proliferation. The SVZ is a paired brain structure situated throughout the lateral walls of the lateral ventricles, whereas the SGZ is a narrow layer of cells situated between the granule cell layer and hilus of the dentate gyrus (Figure 1.1.1). NSCs of the SVZ and SGZ become quiescent (mitotically inactive) for most of adult life. However, in response to intrinsic and extrinsic stimuli, such as injury and exercise, they are able to exit quiescence to re-enter the cell cycle in postnatal animals (Ahn et al, 2005; Doetsch et al 1999, 2009; Morshead et al, 1994). Whereas quiescent NSCs exhibit radial-glia like morphology, activated NSCs retract their processes prior to re-entry into the cell cycle (Song et al, 2002) (Figure 1.1.1).

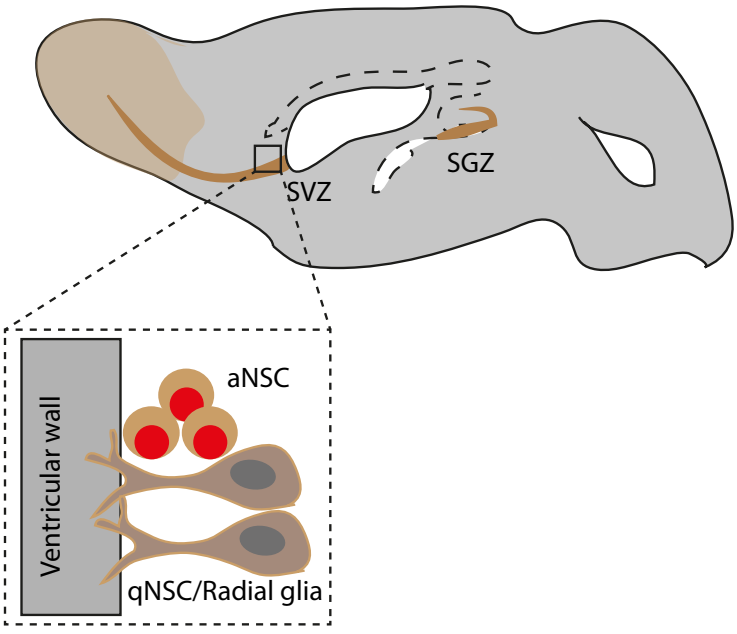

Fig. 1.1.1 Schematic of adult mammalian neurogenic zones. Schematic of mouse brain (sagittal view) shows the positions of two neurogenic zones, the subventricular zone (SVZ) of the lateral ventricle wall and subgranular zone (SGZ) of the hippocampal dentate gyrus. Modified from Ma et al, 2009

Quiescence is a physiologically important state for the NSCs as it helps to promote long-term maintenance and prevent stem cell exhaustion. Quiescence is a hallmark of adult stem

cells across diverse tissues, such as the brain, blood, muscles and the gut (as reviewed in (Orford & Scadden, 2008)). The view that quiescence state is a functionally important characteristic for adult stem cells was largely developed from experiments in the haematopoietic system, which is the most extensively studied adult stem cell system in mice and human (as reviewed in (Orford & Scadden, 2008)). Compelling evidence suggests that quiescence is essential for preventing the premature exhaustion of self-renewing haematopoietic stem cell (HSC) populations. Although adult stem cells are often considered immortal, they have clear limitations in their functions, and these limitations appear to be worsened by proliferative stress. For example, HSCs can give rise to the entire haematopoietic system upon transplantation, but after serial transplantation, HSCs gradually decline. Studies using genetic models that disrupt stem cell quiescence showed that proliferation results in stem cell exhaustion (Harrison *et al.* , 1978; Kamminga *et al.* , 2006). Cyclins and CDKs are important positive regulators of cell cycle progression, whereas cyclin-dependent kinase inhibitors (CDKI), such as P21, inhibit cell cycle progression and promote quiescence (Kippin *et al.* , 2005). Forced exit from quiescence and increased proliferation, such as in the case of a P21 knockout mouse, led to long-term loss of HSCs and increased susceptibility to stress-induced exhaustion (Cheng *et al.* , 2000; Yu *et al.* , 2006). Later studies revealed that the positive role of P21 on stem cell quiescence and long-term maintenance is also conserved in NSCs of the adult mammalian CNS (Kippin *et al.* , 2005; Porlan *et al.* , 2013). However, despite mounting evidence that support the idea of ectopic activation/proliferation being detrimental to adult stem cells maintenance, two HSC genetic models emerged in which shortened cell cycle/increased proliferation did not lead to stem cell exhaustion. This includes knockout of p18INK4c (Yu *et al.* , 2006; Yuan *et al.* , 2004), a CDKI, as well as over-expression of HOXB4, a hox transcription factor whose targets involve cell-cycle regulatory genes (Bowles *et al.* , 2006; Helgason *et al.* , 1996).

The mechanisms responsible for the effect of p18INK4c and HOXB4 are unknown, and moreover, it is unclear whether the mis-regulation of these genes can lead to similar degree of NSC expansion without compromising their long-term maintenance, as seen in the HSC system. The majority of studies in mammalian NSCs suggest that exogenously activating adult NSCs exhausts and diminishes this population long-term, such as via the activation of BMP signalling (Bonaguidi *et al.* , 2011; Mira *et al.* , 2010) or mutation in FoxO transcription factors (Paik *et al.* , 2009; Renault *et al.* , 2009). However, a recent report with an alternative BMP inactivation regime provided evidence that NSC pool is not only maintained but can be even increased in response to long-term inhibition of BMP signalling (Bond *et al.* , 2014). Although these results await further confirmation, they raise

the intriguing possibility that different modes of NSC activation, even via the same pathway (i.e. BMP signalling), can have opposite effects on the long term maintenance of the NSC pool.

1.2 Changes in Energy Metabolism Have Profound Impact on the Decision Between NSC Quiescence and Proliferation in Both Mammals and *Drosophila*

A dynamic balance must be achieved between states of quiescence and proliferation of the postnatal NSCs: uncontrolled proliferation can lead to the formation of tumours, whereas inability to exit quiescence may jeopardise NSCs' ability to promote regeneration after injury. Recently, a flurry of studies revealed that metabolic alterations due to diverse range of factors including nutrition, exercise, and diseases such as diabetes, not only affect brain structure but also cognitive functions in mammals (Lee *et al.* , 2002; Mehrabian *et al.* , 2012; Park *et al.* , 2010; Stranahan *et al.* , 2008b; van Praag *et al.* , 1999) (Figure 1.2.1). In many instances, such structural and cognitive changes of the brain can be associated with altered modes of neurogenesis (Lee *et al.* , 2000, 2002; van Praag *et al.* , 1999), although causative relationship between the two remains unproven.

Whereas dietary restriction promotes NSC maintenance (Lee *et al.* , 2000), excessive energy intake impairs neurogenesis. For example, a high fat diet impaired hippocampal neurogenesis in rats (Park *et al.* , 2010). Overeating as a result of impaired leptin signalling hampered hippocampal neurogenesis in mice (Stranahan *et al.* , 2008b). In addition, exercise enhanced postnatal neurogenesis in the brains of rodents (van Praag *et al.* , 1999). Furthermore, mutations in the chromatin remodelling protein, *CHD7*, which led to impaired neurogenesis in mice, can be rescued by voluntary exercise (Kim & Roberts, 2013). Importantly, imbalanced energy metabolism can also result from metabolic diseases. Diabetes, which leads to an imbalance in sugar levels, has been related to compromised memory and learning ability in rodents. The underlying cause of these cognitive impairments can be at least in part associated with reduced neurogenesis (Stranahan *et al.* , 2008a).

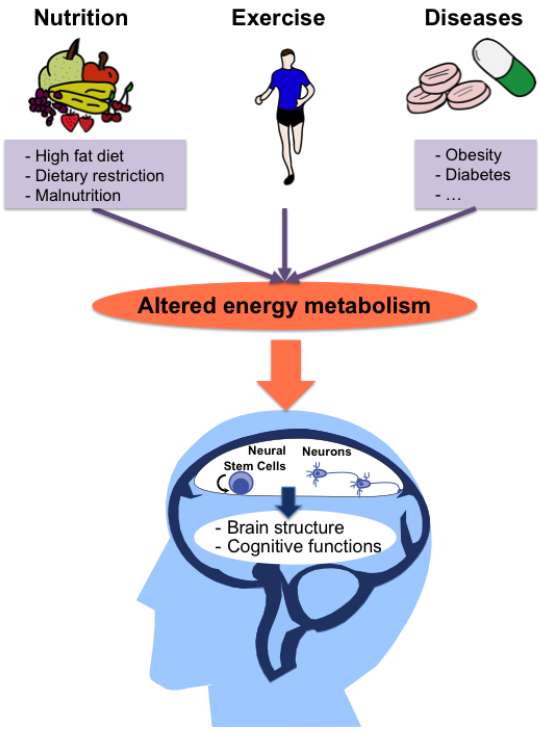

Fig. 1.2.1 Systemic metabolic states affect neurogenesis and neuronal functions. Altered systemic energy metabolism, as a result of diet, exercise or diseases, can have profound influence on the CNS, including proliferation and homeostasis of the NSCs.

1.3 *Drosophila* Larval CNS as a Model System for Investigating systemic regulation of NSC Quiescence/Reactivation

Studies in the past decade revealed remarkable similarities between the mammalian and *Drosophila* NSCs (also called neuroblasts). They can divide asymmetrically and self-renew. IN addition, like their mammalian counterparts, *Drosophila* NSCs extend characteristic projections during quiescence which are then retracted upon activation (Chell & Brand, 2010). Furthermore, the switch between quiescence and proliferation is not unique to mammalian NSCs. *Drosophila* NSCs transit through a developmentally regulated, stereotypical period of quiescence after the completion of embryonic neurogenesis program that gives rise to neurons and glia of the larval CNS. After larval hatching, quiescent NSCs will re-enter the cell cycle, or "reactivate", to initiate the onset of larval neurogenesis that produces neurons and glia of the adult CNS (Ito & Hotta, 1992; Truman & Bate, 1988). Importantly, their decision to exit quiescence and re-enter the cell cycle is critically dependent on the availability of dietary amino acids (Figure 1.2.2) (Britton & Edgar, 1998). Whereas newly-hatched larvae cultured on media lacking either nucleotide precursors, lipids, or vitamins were able to exit NSC quiescence and resume neurogenesis till the late second or early third instar stage, larvae cultured on medium lacking amino acids did not grow and their NSCs remained quiescent (Britton & Edgar, 1998). No single amino acid could rescue NSC cell cycle reactivation, suggesting that protein synthesis is required for this process. Therefore, like their vertebrate counterparts, *Drosophila* NSCs's decision to remain quiescent or reactivate is also heavily influenced by the metabolic state of the organism. This similarity makes *Drosophila* an attractive model organism to investigate mechanisms underlying regulation of NSC quiescence/reactivation, especially in response to changes in diet-induced systemic metabolic state.

Understanding the changes occurring in NSCs in response to altered global nutritional and metabolic states as well as the molecular basis of these changes will not only yield important insights into the maintenance of brain function during development and ageing. More importantly, it may help to pave the way towards battling the detrimental effects of metabolic pathologies on NSC homeostasis including diabetes, obesity, and neurodegenerative diseases.

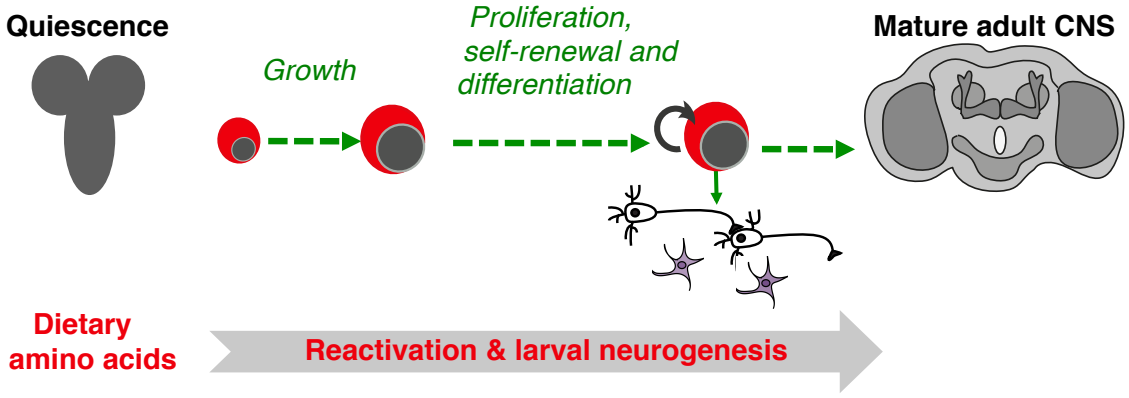

Fig. 1.3.1 Processes of *Drosophila* NSC reactivation. The *Drosophila* NSCs transit through a period of quiescence before the onset of a post-embryonic wave of neurogenesis. If larvae are fed dietary amino acid, NSCs will first start to enlarge and once they reach a certain size, will proliferate to self-renew and generate progenies which populate the adult CNS. Reactivation is defined as the sequential combination of enlargement and proliferation.

1.4 Systemic Energy Sensing in Mammals Involves Insulin/IGF Signalling

How do proliferating or quiescent NSCs respond to systemic energy state? Recent work have started to illuminate how signalling from distant organs that sense changes in systemic metabolic state can communicate such alterations to NSCs in the brain (Rafalski & Brunet, 2011; Spéder *et al.* , 2011). In mammals, the liver, pancreas and adipose tissue act as major energy sensing organs. In particular, the liver and pancreas couple the growth of distant organs with nutrient availability via IGFs (Insulin-like growth factors) and Insulin, respectively. In vertebrates, the pancreas secretes Insulin in response to glucose intake, whereas IGFs are secreted by the liver (Iresjö *et al.* , 2013; Livingstone & Borai, 2014) in response to dietary protein intake (Miura *et al.* , 2007). NSCs' response to dietary restriction is a good example of how systemic IGF/Insulin signalling can alter NSC behaviour in the brain. Systemic IGF–1 level decreases significantly in response to dietary restriction (Cohen *et al.* , 2009). Since IGF–1 is capable of crossing the mammalian blood-brain barrier (BBB) (Reinhardt & Bondy, 1994), it is possible that by reducing IGF–1 levels, dietary restriction may promote the maintenance of the NSC pool by preventing excessive proliferation and premature differentiation.

Recent studies showed that Insulin/IGF signalling pathway plays diverse and critical

roles during mammalian neurogenesis. IGFs are capable of promoting mammalian neurogenesis, including the production of neurons, astrocytes and oligodendrocytes, both *in vivo* and *in vitro* (Aberg *et al.* , 2003a,b; Arsenijevic *et al.* , 2001; Mason *et al.* , 2003). Further analysis shows that IGF–1 can shorten the duration of the cell cycle and increase the number of cells that re-enter the cell cycle (Hodge, 2004). Apart from its mitogenic effect on NSCs, IGF–1 can also direct differentiation towards specific lineages (Popken *et al.* , 2004). In response to exogenous IGF–1 stimuli, cultured NSCs proliferate or differentiate into mainly neuronal or oligodendrocyte cell types (Arsenijevic *et al.* , 2001; Brooker *et al.* , 2000; Drago *et al.* , 1991).

1.5 Fat Body-Derived Signals and Glial Insulin Signalling Control *Drosophila* NSC Reactivation in Response to Dietary Amino Acid Intake

Drosophila has recently emerged as a powerful model organism for studying inter-organ communication and systemic regulation of NSCs reactivation. Previous studies have revealed remarkable similarities between the mammalian and *Drosophila* NSCs, including similar division patterns and lineage outputs, as well as characteristic morphologies during NSC quiescence/reactivation. For a review, see (Brand & Livesey, 2011). Several signalling pathways govern the proliferation, self-renewal and differentiation of NSCs during development. For example, Notch signalling has been found to promote self-renewal and repress differentiation in *Drosophila* NSCs (Alexson *et al.* , 2006). In mammalian brains, activation of Notch signalling induces the expression of transcriptional repressor genes such as Hes1, leading to repression of proneural gene expression and maintenance of NSC/progenitor cells (Imayoshi *et al.* , 2010). In addition, Insulin/IGF signalling has recently been shown to act as a potent regulator of NSC proliferation *in vivo* in both flies and mammals (Chell & Brand, 2010; Lehtinen *et al.* , 2011; Sousa-Nunes *et al.* , 2011; Ziegler *et al.* , 2014, 2012). Furthermore, PTEN and PI3K, the downstream effectors of Insulin/IGF signalling, have been found to govern the transition from quiescence to proliferation in both systems (Groszer *et al.* , 2001, 2006; Peltier *et al.* , 2007).

Exploiting powerful genetic tools that are available in *Drosophila* led to the recent discovery that NSCs reactivate via a fat body and glial cell relay (Figure 1.4.1). Functionally homologous to vertebrate liver and adipose tissue, the *Drosophila* fat body functions as a systemic nutrient sensor and it coordinates organismal growth with nutrient availability. It

stores sugar in the form of glycogen and fat in the form of triacylglycerol. In addition, it is known to produce a large amount of secreted molecules circulating in the hemolymph, such as larval serum proteins, adipokines and enzymes. For a review, see (Andersen *et al.* , 2013). The fat body coordinates organismal growth with dietary amino acid availability partly through Slimfast (Slif), an essential amino acid transporter (Colombani *et al.* , 2003; Géminard *et al.* , 2009). In addition to serving as an amino acid passageway, Slif regulates fat body TOR (Target of Rapamycin) signalling. In both invertebrates and vertebrates (Colombani *et al.* , 2003), TOR signalling is a conserved strategy by which organisms coordinate nutrient availability with cellular growth and proliferation. Upon sensing dietary amino acids, TOR phosphorylates S6K (S6 kinase, a ribosome protein) and 4E-BP (Eukaryotic translation initiation factor 4E-binding protein), thereby activating protein translation (Abraham, 2002). This ultimately lead to the production and secretion of growth-promoting factors, known for a long time as "fat body derived mitogens (FBDMs)", and more recently as "fat body signals". Fat body-directed knockdown of Slif leads to fat body-specific TORC (TOR complexes) inhibition and systemic growth defects (Colombani *et al.* , 2003).

Compelling evidence suggests that NSCs' reactivation from quiescence is coupled to dietary amino acids and larval growth through signals transmitted from the fat body, both in tissue culture (Britton & Edgar, 1998) and *in vivo* (Sousa-Nunes *et al.* , 2011). NSCs in brains isolated from starved animals remain quiescent in culture even if amino acids or fat body alone were supplied to the media. NSCs were only able to reactivate when both factors are present (Britton & Edgar, 1998). This implies that amino acid-induced fat body factor(s), and not the amino acids themselves, are responsible for triggering NSC reactivation (Britton & Edgar, 1998). Except for the mushroom body NSCs and one ventral lateral NSC, the initiation of reactivation for all other NSCs in the brain and ventral nerve cord (VNC) are dependent on the availability of dietary amino acids and fat body signals (Britton & Edgar, 1998). A complementary *in vivo* experiment was carried out by disrupting fat body vesicle trafficking using a dominant negative dynamin ($Shibire^{DN}$), which resulted in reduced EdU labelling (a thymidine analog labelling S phase of cell cycle) in the CNS in early second instar larvae, indicating impaired NSC reactivation/proliferation (Sousa-Nunes *et al.* , 2011). However, even though convincing evidence suggests that the fat body signals are important for NSC reactivation, their identities remain unknown.

How are fat body signals sensed by NSCs in the brain? Glial cells in the CNS surround NSCs and insulate them from the systemic environment. In particular, two populations of glial cells, the perineurial glia and subperineurial glia, make up the *Drosophila* BBB. Recent work revealed that glial cells serve as a key relay to regulate NSC reactivation downstream

of nutrient sensitive fat body signals via the transcription and secretion of local insulin-like peptides (DIlps) (Chell & Brand, 2010; Sousa-Nunes *et al.* , 2011). In addition, gap junction-mediated coordination of DIlps release is essential for efficient NSC reactivation (Speder and Brand, 2014, accepted).

The insulin/IGF signalling pathway is highly conserved in mammals and flies (Goberdhan & Wilson, 2003). No homologue of IGF–1 has been identified in *Drosophila*, but there are 8 insulin-like peptides (DIlps) (Andersen *et al.* , 2013). They consist of two major pools: systemically circulating DIlps in hemolymph (blood equivalent) are secreted by insulin producing cells (IPCs, pancreas equivalent), fat body and imaginal discs (Colombani *et al.* , 2012; Okamoto *et al.* , 2009; Wang *et al.* , 2007). DIlps can also be produced locally and retained in peripheral tissues such as renal tubules, gut, and the brain (Chell & Brand, 2010; Garelli *et al.* , 2012; O'Brien *et al.* , 2011; Söderberg *et al.* , 2011). The 8 different DIlps have diverse spatial temporal expression patterns and serve different functions in the organism. Four of the DIlps (DIlp1, DIlp2, DIlp3, DIlp5) are expressed in the IPCs that share a common progenitor lineage (Wang *et al.* , 2007). They can be secreted into the circulating hemolymph to promote insulin signalling and tissue growth in many different target organs during larval stages. During the actively feeding larval stages, impaired growth of imaginal tissues delays the onset metamorphosis. DIlp8 is a secreted factor from the imaginal discs which is sufficient to delay metamorphosis without affecting tissue integrity. Therefore, it was proposed that DIlp8 coordinates the growth status of organs with developmental timing (Colombani *et al.* , 2012). DIlp6 is predominantly expressed in the fat body during the post-feeding pupal stage, and secreted into the hemolymph to instruct appropriate cellular division in distant organs. DIlp6 mutant shows reduced adult body size as a result of decreased cell number, and the phenotype can be rescued by fat body expression of DIlp6 alone (Okamoto *et al.* , 2009).

What are the sources and functions of locally-derived DIlps? Recent studies suggest that DIlp5 is expressed in principal cells of the renal tubule to regulate stress response locally (Nässel *et al.* , 2013). DIlp3 expression was detected in the midgut viseral muscle, and it regulates food-dependent proliferation of midgut stem cells (O'Brien *et al.* , 2011; Veenstra *et al.* , 2008). Although the precise identity of glial-derived DIlp(s) are unclear, evidence suggests that DIlp2 and DIlp6 are produced locally in the CNS and play a prominent role in NSC reactivation. This is because these are the only two *dIlps* whose transcripts are upregulated in the VNC during the time window of NSC reactivation (Chell & Brand, 2010). The *dIlp6* promoter was found to drive expression in glial cells of the CNS surface overlying the NSCs, suggesting that these glial cells might be the source of the signal that

reactivates NSCs (Chell & Brand, 2010). Interestingly, NSCs do not respond to systemic DIlps fluctuation: over-expression of DIlps in the fat body or in the IPCs, which elevate the level of circulating DIlps, were not able to ectopically reactivate NSCs from quiescent state (Sousa-Nunes *et al.* , 2011). Instead, the NSCs are controlled by local DIlps from the surrounding glial cells (Figure 1.4.1) (Chell & Brand, 2010; Sousa-Nunes *et al.* , 2011). Disruption of vesicle trafficking in glia impairs NSC reactivation when larvae are fed an amino acid rich diet, and forced expression of DIlps in CNS glial cells drive the reactivation of NSCs in the absence of dietary amino acids intake.

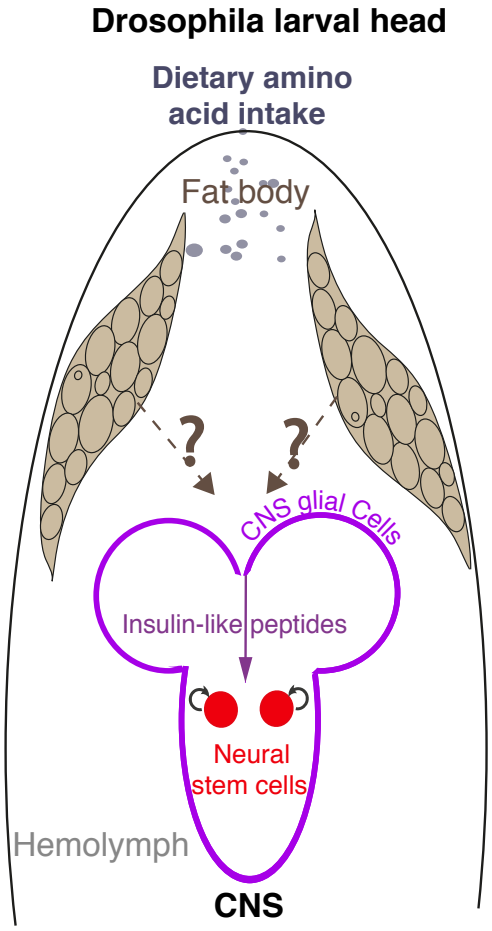

Fig. 1.5.1 NSC reactivation involves the fat body and a glial relay. Upon sensing dietary amino acids, the *Drosophila* fat body is known to secrete unidentified signal(s) into the hemolymph, which travel to the brain and induce the CNS glial cells to release *Drosophila* insulin-like peptides (DIlps). DIlps bind to insulin receptors on the NSC surface, leading to their reactivation

1.6 Local Insulin/IGF Signalling Also Plays an Important Role in Mammalian Neurogenesis

Local IGF expression has also been detected in the mammalian brain. As in the case of *Drosophila* NSC reactivation, the mammalian IGF-I exhibits peak expression which is temporally and spatially correlated with brain development (Popken *et al.* , 2004). In rodent brains, IGF–1 expression increases rapidly during late prenatal and early postnatal development and peaks in the first week of postnatal life, as seen with Northern blot analysis of rodent whole brain. This is a time window before and during rapid proliferation, differentiation and maturation of NSCs (Popken *et al.* , 2004). Expression of IGF–1 and IGF1R (IGF1 receptor) were also observed in cultured NSCs derived from both embryos and adults (Drago *et al.* , 1991).

The observation that local IGF-I overexpression without elevations in circulating IGF-I led to brain overgrowth further supports the idea that paracrine/autocrine IGF-I signalling has a more prominent impact on NSC proliferation than circulating IGF-I, at least during early phases of neurogenesis when IGF-I level is significantly higher in the brain than in the circulation (Joseph D'Ercole & Ye, 2008). What cell type(s) in the mammalian brain secrete IGF-I ligand, and is there an equivalent of insulin/IGF secreting glial niche as in *Drosophila*? IGF-I ligand expression has been reported in neurons (Bondy, 1991), astrocytes (Shetty *et al.* , 2005), and NSCs (Drago *et al.* , 1991). Whereas autocrine signalling and neuronal IGF-I may have an impact on NSCs, recent studies suggest a prominent role of astrocytic glia as the IGF-secreting NSC niche. Astrocyte-specific overexpression of IGF–1 in the mouse brain is capable of promoting brain overgrowth *in vivo* (Yan *et al.* , 2006; Ye *et al.* , 2004). In addition, IGF–1 expression is induced in stellate astrocytes in response to CNS injuries, and is believed to account for increased rate of NSC division following cortical ischemia (Yan *et al.* , 2006).

Until recently, studies of Insulin/IGF signalling and neurogenesis have almost entirely focused on IGF-I to the exclusion of IGF-II. Whereas fetal IGF-I showed clear expression in the neurogenic zones of VZ and SVZ, IGF-II expression has been detected predominantly in the neuroectoderm and was therefore deemed to be less relevant for neurogenesis (McDonald *et al.* , 2007). Studies in recent years uncovered a long-neglected neurogenic niche parallel to the *Drosophila* NSC niche at the brain-cerebral spinal fluid (CSF) interphase (Lehtinen *et al.* , 2011; Ziegler *et al.* , 2014, 2012). A novel role of local niche-derived IGF-II signalling in regulating NSC proliferation was uncovered (Figure 1.5.1). The ventricular system of mammalian CNS contains CSF and is continuous with the central canal of the

spinal cord. A network of capillaries enveloped by ependymal epithelium, called choroid plexus, line each of the ventricles. In addition to acting as a barrier to allow selective passage of particles from the blood to CSF, the choroid plexus ependymal epithelium also secretes growth factors such as FGF (Fibroblast growth factor), VEGF (Vascular endothelial growth factor), and IGF-II (Lehtinen *et al.* , 2011; Stopa *et al.* , 2001). CSF IGF-II signals to primary cilia of NSCs/neural progenitors of the surrounding SVZ and instructs cortical neurogenesis during development (Lehtinen *et al.* , 2011). The NSCs/neural progenitors express IGF receptors on their apical surface facing the CSF, which provides optimal spatial orientation to sample the CSF IGF-II ligands. Choroid plexus IGF-II expression is also developmentally regulated: a transient peak of CSF IGF-II occurs at mid to late embryonic neurogenesis in rodents (Lehtinen *et al.* , 2011) (Figure 1.5.1). Therefore, the regulation of NSCs by local Insulin/IGF signalling appears to be a conserved strategy evolved in both invertebrates and vertebrates.

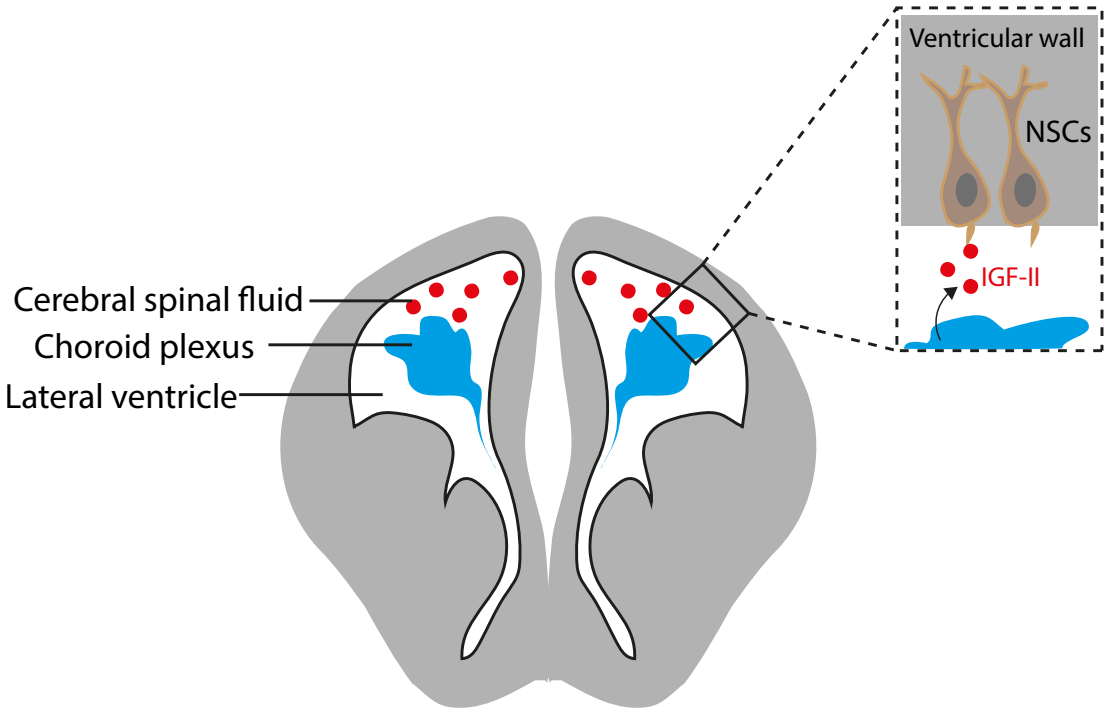

Fig. 1.6.1 Schematic of a IGF-II-dependent neurogenic niche at the Brain-CSF-Barrier. The choroid plexus secretes IGF-II into the CSF, which are sensed by receptors on the primary cilia of NSCs lining the ventricular wall. IGF-II binding to its receptor induces NSC proliferation.

1.7 An Emerging Role of CNS Glial Cells as a NSC Niche

Increasing evidence points to the critical role of glial cells as a NSC niche in both mammals and flies. In mammals, astrocytes have been shown to form a NSC niche and promote NSC proliferation *in vitro* (Song *et al.* , 2002), and *in vivo* by secreting neurotrophic factors including IGF–1 and FGF (Shetty *et al.* , 2005). Recently, it has been shown that Clusterin, a highly glycosylated protein secreted by astrocytes, is able to promote human neural precursor cell survival and differentiation *in vitro* (Cordero-Llana *et al.* , 2011).

In *Drosophila*, three types of glial cells are closely associated with NSCs (Figure 1.6.1). The *Drosophila* NSCs are isolated from the hemolymph (the equivalent of blood) by two populations of glial cells that comprise the *Drosophila* BBB—the subperineurial glia (SPG) and perineurial glia (PG) (Stork *et al.* , 2012). The third population, cortex glia (CG), are located between NSCs beneath the BBB. Subperineurial glial cells form septate junctions (equivalent of tight junctions) and create a physical barrier. The outermost perineurial glia are less well characterised, but they have been hypothesised to mediate signalling from the hemolymph to the CNS due to their localisation at the interface between the two (Stork *et al.* , 2008). Cortex glia have similar structures to mammalian astrocytes and may provide trophic support for the surrounding NSCs (Freeman & Doherty, 2006a).

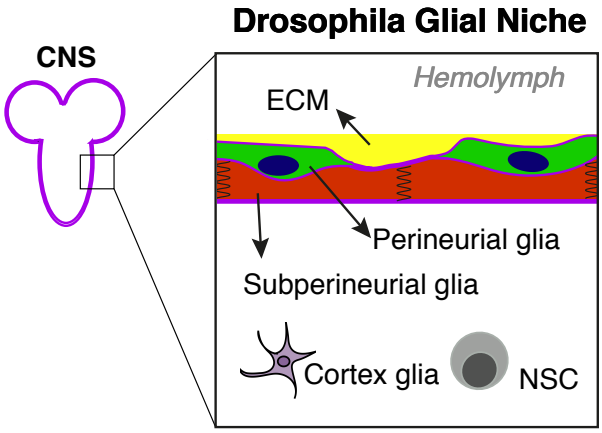

Fig. 1.7.1 Three major types of CNS glial cells are associated with reactivating NSCs. A closer look at the NSC niche reveals that NSCs are surrounded by three glial subtypes: the perineurial glia and subperineurial glia which together make up the blood brain barrier, and cortex glia.

Apart from DIlps, glial cells in *Drosophila* are known to secrete other factors that regulate NSC reactivation. The *anachronism* (*ana*) gene is expressed in a subset of glial cells and encodes a secreted glycoprotein whose mechanism of action is unknown (Ebens *et al.* , 1993). Loss of Ana function results in precocious NSC reactivation, with NSCs entering

their first S phase around eight hours early. However, a recent study provided evidence that Ana is also expressed in miR–124-expressing neurons/NSCs and that *ana* transcripts must be downregulated by the action of miR–124 during neuronal progenitor proliferation to ensure proper larval neurogenesis (Weng & Cohen, 2012).

1.8 Other Factors Known to Regulate NSC Reactivation in *Drosophila*

Apart from the unknown fat body signals, glial derived DIlps and Anachronism, another factor known to regulate NSC reactivation is Perlecan (called Trol in *Drosophila*, which stands for "Terribly reduced optic lobes", hereafter referred to as Perlecan$^{\text{Trol}}$). In *perlecan^{trol}* null mutants, NSC reactivation is severely impaired: NSCs enlarge, but never enter their first S phase (Datta, 1995). NSC proliferation defect in *perlecan^{trol}* mutants can be rescued by overexpression of the positive G1/S regulator cyclin E (Caldwell & Datta, 1998). These results indicate that growth and proliferation are at least partly uncoupled in larval NSCs. The *ana/perlecan^{trol}* double mutant displays the *ana* mutant phenotype of precocious NSC reactivation (Datta, 1995). This suggests that Perlecan$^{\text{Trol}}$ acts downstream of Ana to bypass or inactivate Ana's repressive effect on the cell cycle.

Perlecan^{trol} encodes a heparan sulfate proteoglycan (HSPG) (Park *et al.* , 2003; Voigt *et al.* , 2002). It is an important component of the extracellular matrix (ECM) that interacts with other ECM proteins, growth factors and receptors, to regulate cellular signalling (Lin, 2004a). Null mutations in *hedgehog* (*hh*) and *branchless* (*bnl*, an FGF homologue) dominantly enhance the impairment in NSC proliferation in a sensitised *perlecan^{trol}* mutant background (Park *et al.* , 2003). Although the origin of CNS Perlecan$^{\text{Trol}}$ protein is unclear, it is deposited on the brain surface throughout larval life (Park *et al.* , 2003), close to the reactivating NSCs. Thus Perlecan$^{\text{Trol}}$ may function to locally modulate Hh and FGF signalling in a manner important for NSC reactivation.

1.9 Regulators of NSC Quiescence/Reactivation in Mammalian Systems

1.9.1 Regulators of NSC Quiescence in Adult Mammalian Brain: an Overview

Work in the past decade started to identify the multitude of niche-dependent and intrinsic effectors of NSC quiescence/reactivation. NSC quiescence and reactivation are controlled by signalling pathways, niche adhesion, transcriptional factors, epigenetic programs, as well as neuronal activities. Several morphogens/signalling molecules have been shown to control the proliferation and NSCs in the SVZ, including Notch, Wnt, FGF–2, IGF-I, VEGF, BDNF, and BMPs, among others. Wnt (Lie *et al.* , 2005; Qu *et al.* , 2010), IGF-I (Aberg *et al.* , 2003a; Lichtenwalner *et al.* , 2001), BDNF (Scharfman *et al.* , 2005; Zigova *et al.* , 1998) and VEGF (Jin *et al.* , 2002) signalling promote NSC activation/proliferation and stimulate neurogenesis. In contrast, BMP (Mira *et al.* , 2010) and Notch (Imayoshi *et al.* , 2010) signalling maintains NSCs and/or promote quiescence. Activated by ligands produced by differentiating neural precursors in the neurogenic niches, BMP and Notch signalling provide negative feedback signals that maintain the quiescent state of SEZ and hippocampal NSCs (Ables & Drummond-Barbosa, 2010; Bonaguidi *et al.* , 2008; Ehm *et al.* , 2010; Imayoshi *et al.* , 2010; Mira *et al.* , 2010). The mechanisms of BMP signalling in regulating NSC quiescence will be discussed in further detail. More recently, neuronal activities via synaptic transmission to NSCs has been shown to regulate the decision between quiescence and reactivation (Song *et al.* , 2012). Optogenetical control of GABA release by interneurons in the DG has allowed for the observation that NSCs can respond to the level of GABA, switching from a quiescence to an activated one (Song *et al.* , 2012).

1.9.2 Transcription Factors

Among intrinsic factors, a number of transcription factors have been identified to promote activation of quiescent NSCs. Sox and bHLH factors are among the most extensively studied transcription factors in mammalian embryonic neurogenesis (Bylund *et al.* , 2003; Scott *et al.* , 2010). Interestingly, recent study by Venere et al demonstrated that Sox1 also regulates in NSC activation/proliferation in adult neurogenic niche. Although the exact mechanism is unknown, Sox1 expression is absent in quiescent NSCs but it marks activated NSCs in the post-natal DG that are able to produce neuronal precursors and generate astrocytes, as

shown by lineage tracing (Venere *et al.* , 2012). Interestingly, the fraction of Sox1-positive cells within the NSC population decreases with age, correlating with a decrease in neurogenesis. The orphan nuclear receptor Tlx is another transcription factor known to promote the switch from adult NSCs' switch from quiescence to proliferation. It acts to ensure the proliferative ability of postnatal NSCs by controlling their activation through genetic interaction with p53 and p21 (Niu *et al.* , 2011) as well as signalling pathways such as Wnt and BMP signalling (Qin *et al.* , 2014; Qu *et al.* , 2010). Ascl1 is a third transcription factor which has established roles in NSC activation. A recent study showed that when NSCs of the adult hippocampus receive activating signals, such as upon depletion of Notch signalling, they first induce the expression of the transcription factor Ascl1 before exiting quiescence (Andersen *et al.* , 2014). Moreover, inactivating Ascl1 blocks quiescence exit completely, rendering them unresponsive to activating stimuli. NSCs in both hippocampus and SVZ require Ascl1 to exit quiescence, and this is most likely due to the regulatory roles of Ascl1 on cell cycle genes (Andersen *et al.* , 2014).

On the other hand, a number of transcription factors promote NSC quiescence, including FoxO, Tis21, REST/NRSF and NFIX. The FoxO proteins are the most extensively-studied transcription factors promoting NSC quiescence and maintenance. In mice mutant for FoxO1, FoxO3, and FoxO4 or for FoxO3 alone, an initial increase of NSC proliferation is followed by a depletion of the NSC pool and a decline in long term neurogenesis (Paik *et al.* , 2009; Renault *et al.* , 2009). Recently, another transcription factor, Tis21 (Btg2/PC3), has been identified as a positive regulator of NSC quiescence both *in vitro* and *in vivo* (Farioli-Vecchioli *et al.* , 2009, 2014). Ablation of Tis21 in the SVZ causes an increase of proliferation of NSCs/progenitor cells, consistently with its anti-proliferative activity (Farioli-Vecchioli *et al.* , 2009). In Tis21 null SVZ and cultured neurospheres, the expression of BMP4 and its effectors Smad1/8, which are known to promote quiescence, are strongly reduced (Farioli-Vecchioli *et al.* , 2014). On the other hand, positive regulators of proliferation such as cyclins D1/2, A2, and E were strongly up-regulated (Farioli-Vecchioli *et al.* , 2014). A third quiescence-promoting transcription factor is the GLI–Kruppel class C2H2 zinc finger protein repressor element 1 (RE1)-silencing transcription factor (REST), also known as neuron-restrictive silencer factor (NRSF) (Schoenherr & Anderson, 1995). A recent study revealed a fundamental role for REST/NRSF in maintaining adult NSCs in a quiescent state by restraining the neurogenic program (Gao *et al.* , 2011). In REST/NRSF conditional knockout mice, hippocampal NSCs exit quiescence and enter neurogenic program to produce granule neurons. However, loss of REST/NRSF leads to a functional depletion of the adult hippocampal NSC pool and decreased granule neurons ultimately.

Mechanistically, REST/NRSF recruits its co-repressor complex to NSC chromatin to control neuronal target genes and maintain the undifferentiated state (Gao *et al.* , 2011).

Although a number of quiescence-inducing/maintaining transcription factors have been identified, no systematic approaches have been undertaken to investigate the transcriptional mechanisms involved in NSC quiescence/activation until the development of a cell culture-based NSC quiescence model (**?**). Martynoga et al first demonstrated that NSC cultures treated with pro-quiescence BMP signals acquire cellular and transcriptional characteristics of quiescent NSCs, and in a reversible manner (Martynoga *et al.* , 2013). Epigenomic profiling was performed on these cells to identify enhancers associated with quiescent state, and motif-enrichment analysis of these enhancers led to the discovery of NFIX as a key transcription factor promoting NSC quiescence. NFIX is required to induce the expression of a large portion of quiescence-specific genes. NFIX simultaneously suppresses a significant part of the gene expression program of proliferating NSCs. Furthermore, mutation of the NFIX gene *in vivo* results in a loss of quiescence for large proportion of hippocampal NSCs (Martynoga *et al.* , 2013).

1.9.3 Adhesion Molecules and ECM Proteins

A flurry of recent mammalian studies started to uncover the crucial functions of adhesion molecules and ECM proteins in regulating NSC quiescence/activation. Notably, the NSC microenvironment in the neurogenic subependymal zone of adult mammalian brain is associated with distinct ECM signatures in its quiescent and reactivated state, respectively (Kazanis *et al.* , 2010). ECM proteins including laminins and their integrin receptors are implicated in regulating NSCs' transition from quiescence to reactivation (Kazanis *et al.* , 2010). Furthermore, a transcriptome analysis of neurogenic regions of human and mouse fetal neocortex suggests that ECM proteins may be involved in neuronal progenitor self-renewal (Simone A Fietz, 2012). In this study, transcripts of perlecan, among many other ECM ligands, were highly enriched in the germinal zones consisting of neuronal progenitors compared to the cortical plates consisting of mature neurons. Other ECM transcripts, such as collagen IV, were present in the germinal zone and absent from the cortical plate.

Using an unbiased approach in a NSC cell-type specific manner, Martynoga et al performed epigenomic profiling in quiescent NSCs in culture to identify enhancers associated with quiescent state (Martynoga *et al.* , 2013). They showed that entry into quiescence involves major changes in the transcriptional profile of these cells and in particular, in their expression of cell adhesion and extracellular matrix (ECM) molecules (Martynoga

et al. , 2013), consistent with previous *in vivo* studies (Fietz *et al.* , 2010; Kazanis *et al.* , 2010). Another recent study provided convincing confirmation for the importance of adhesion molecules in regulating NSC quiescence/reactivation. Porlan et al showed that N-cadherin-mediated anchorage of NSCs to their niche in the adult murine subependymal zone modulates their quiescence *in vivo* (Porlan *et al.* , 2014). In addition, they identified MT5-MMP as a membrane-type metalloproteinase responsible for the shedding of the N-cadherin ectodomain in this niche. MT5-MMP-mediated cleavage of N-cadherin is required for proper activation of quiescent NSCs under physiological and regenerative conditions (Porlan *et al.* , 2014). The mechanisms of N-cadherin's action are unclear, but it was postulated that N-cadherin may mediate NSC reactivation via Wnt signalling (Porlan *et al.* , 2014).

1.9.4 BMP Signalling

In the past few years, BMP signalling emerged as a major mechanism governing the equilibrium between NSC quiescence and the cell cycle re-entry. The NSCs in the DG express BMP-receptor 1A (BMPR–1A) which binds to BMP–2 and BMP–4. This keeps NSCs in a quiescent state (Mira *et al.* , 2010). When noggin (a BMP antagonist) is present, it binds to the BMPs and prevent their binding to BMPR–1A. This in turn causes the NSCs to activate and enter cell cycle. Blockade of BMPs action with noggin or tissue-specific inactivation of BMPR-IA led to temporary increased NSC proliferation, but the eventual decline of the NSCs in hippocampus (Mira *et al.* , 2010). This suggests that BMP-dependent NSC quiescence is essential for NSC maintenance and long term neurogenic potential.

BMP signalling appears to be a key point of regulation in NSC quiescence/activation upon which many other regulatory factors and pathways converge. Exposure to exercise and learning promote neurogenesis, and BMP signalling is at least in part responsible for these effects (Gobeske *et al.* , 2009). Voluntary exercise reduces levels of hippocampal BMPs prior to and during NSC activation. Transgenic mice with decreased BMP signalling showed improved hippocampal cognitive performance and neurogenesis, mirroring the effects of exercise. In contrast, transgenic mice with increased BMP signalling showed reduced hippocampal neurogenesis and impaired cognition, which cannot be rescued by exercise, suggesting that reduced BMP signalling is required for environmental effects on neurogenesis (Gobeske *et al.* , 2009). Exercise and learning can cause a rapid increase in neurogenesis after as few as 7 days post-stimulation (Dalla *et al.* , 2007; Vaynman *et al.* , 2004). This suggests that mechanisms other than increased activation of quiescent NSCs

are necessary to generate such a rapid expansion of the new neuronal pool. A recent study showed that BMP signalling is not only important for the switch between NSC quiescence and proliferation; it is also involved in fine-tuning neurogenic efficiency at later stages of the NSC lineages after NSC activation (Bond *et al.* , 2014). Bond et al attempted to manipulate BMP signalling *in vivo* using virally mediated misexpression of BMP4 and noggin, or conditional ablation of BMP receptor type 2 (BMPRII) in different NSC/neural progenitor cell (NPC) subtypes. BMP signalling inhibition enhances neurogenesis by activating NPCs at multiple stages of the lineage and by accelerating their maturation (Bond *et al.* , 2014). Thus, BMP signalling represents a potential mechanism for rapidly expanding neuronal pools in response to environmental stimuli.

Intriguingly, altered BMP signalling also acts downstream of several transcription factors discussed earlier, including Tis21 and Tlx, as well as downstream of a key cyclin-dependent kinase inhibitor (CDKI), P21. Ablation of Tis21 impairs the expression of BMP4 and of its effectors Smad1/8, which is in part responsible for ectopic NSC activation in SVZ as well as in neurospheres (Farioli-Vecchioli *et al.* , 2014). Orphan nuclear receptor Tlx also regulates NSC activation and astrogenesis by modulating BMP signalling (Qin *et al.* , 2014). BMP pathway components such as BMP4, Hes1, and ID3, are transcriptionally upregulated in postnatal brains lacking Tlx. Furthermore, Tlx can directly bind the enhancer region of BMP4, and the downstream effectors Smad1/5/8 are activated in Tlx mutants. P21 is a CDKI and promotes NSC quiescence (Kippin *et al.* , 2005). Subependymal NSCs lacking P21 exhibit rapid expansion followed by depletion later in life (Kippin *et al.* , 2005). A recent study found that BMP2 is under direct transcriptional control by P21 and loss of P21 in NSCs resulted in increased level of secreted BMP2, leading to precocious NSC activation and proliferation (Porlan *et al.* , 2013).

1.10 An Overview of ECM Proteins at the Basement Membrane and Their Receptors Regulating CNS Functions

Extracellular matrix (ECM) and their receptors participate in most biological processes, and they play important roles during development, homeostasis and pathogenesis of the CNS. The *Drosophila* ECM are composed of many families of conserved molecules including collagens, proteoglycans, glycosaminoglycans and other non-collagenous glycoproteins (as reviewed in (Broadie *et al.* , 2011)). *Drosophila*, with its powerful and malleable genetics,

can serve as an important model system in understanding the principles of ECM-mediated functions in the CNS.

The basement membrane (BM) is a layer of non-cellular tissue that separates the epithelium, mesothelium and endothelium from underlying connective tissue. ECM proteins, in particular Collagen IV, Laminin, Nidogen, and Perlecan, as well as their receptors, are the key components of the BM. In addition to providing structural integrity of the BM and the underlying organs, ECM proteins and receptors also participate in cellular signalling. In the scope of this introduction, I will primarily focus on Collagen IV, Perlecan and the Integrin receptors.

1.10.1 Collagen IV

Type IV Collagen, or Collagen IV, is a unique member of the Collagen superfamily. In vertebrates the Collagen IV family contains 28 members (as reviewed in (Khoshnoodi *et al.* , 2008)). Unlike other collagens, Collagen IV only exists in the BM. In fact, it is the most abundant component of the BM, comprising 50% of its total protein contents (Kalluri, 2003). Collagen IV molecules consist of α chains bound in long helical trimers that assemble into a network through lateral and end-domain interactions (Yurchenco & Ruben, 1987). 6 genetically distinct α chains have been identified, which are designated $\alpha 1$ to $\alpha 6$ (Aouacheria *et al.* , 2006). In particular, the $\alpha 1$ like subunits and $\alpha 2$ like subunits are present in BM of all tissues in vertebrates, whereas the other 4 subunits have tissue-specific distributions, and their expressions are developmentally regulated (Pöschl *et al.* , 2004). Collagen IV is a non-fibrillar collagen, which differs from connective tissues' fibrillar collagens by the presence of globular NC (non-collagenous) domains at their C terminals (as reviewed in (Ortega & Werb, 2002)). The NC domains are critical because they seem to be responsible for ensuring that the α chains associate only with their appropriate binding partners, which give rise to only a limited number of heterotrimer combinations (as reviewed in (Ortega & Werb, 2002)).

In addition to providing a scaffold for assembly of other ECM proteins and mechanical stability of the BM, collagen IV is important for cellular interaction with the underlying BM. In vertebrates, this interaction is critical for a variety of processes, such as cell adhesion, migration, survival, proliferation, and differentiation for a large number of cell types [][Rubin:1981ii,Murray:1979vd,Setty:1998cj]. Collagen IV deficiency was shown to be involved in the pathogenesis of a variety of disorders, and kidney can be particularly affected by Collagen IV abnormalities. Alport's and Goodpasture's syndromes are the two

major kidney diseases in which Collagen IV deficiency is the main culprit (Borza, 2000; Mochizuki *et al.* , 1994). Recently, Collagen IV abnormality has been shown to be involved in pathogenesis of the CNS in mammals. Mutation in Collagen IV α1 subunit was shown to cause encephaloclastic porencephaly, which is characterized by structural defects in the cerebral vasculature and BM, leading to degenerative cavities and cerebral lesions (Gould *et al.* , 2005). Milder forms of the disease can cause patients to suffer from recurrent hemorrhagic strokes caused by weakened BM of the CNS vasculature (van der Knaap *et al.* , 2006).

Collagen IV is highly conserved from humans to *Drosophila*. In the *Drosophila* genome, two genes encode α-like subunits, named *viking* (*vkg*) and *collagen-at–25C* (*Cg25C*), hereby referred to as *collagen IV*^{vkg} and *collagen IV*^{cg25C}, respectively (Rodriguez *et al.* , 1996; Yasothornsrikul *et al.* , 1997). *collagen IV*^{vkg} encodes the alpha2 subunit and *collagen IV*^{cg25C} encodes the alpha1 subunit. A trimer of 2 alpha1 subunits and 1 alpha2 subunit form the Collagen IV molecule. *collagen IV*^{vkg} and *collagen IV*^{cg25C} are located head-to-head adjacent to each other in the genome, an arrangement that is conserved in the α1/2-like pair of Collagen IV genes in mammals (Rodriguez *et al.* , 1996). Whereas signalling events regulated by Collagen IV remains largely unexplored in vertebrates, recent work in *Drosophila* pioneered the investigation of a direct involvement of Collagen IV in growth factor signalling (Bunt *et al.* , 2010; Sawala *et al.* , 2012; Wang *et al.* , 2008). The most well-characterised signalling pathway mediated by Collagen IV is BMP signalling. Wang et al first demonstrated that interaction between Dpp (Decapentaplegic, a *Drosophila* BMP ligand) and Collagen IV is essential for the development of the *Drosophila* germarium and in early embryos (Wang *et al.* , 2008). In addition, Collagen IV-dependent BMP signalling has been shown to regulate renal tubule morphogenesis (Bunt *et al.* , 2010) and midgut stem cell proliferation (Tian & Jiang, 2014). Recently, Sawala et al showed that Collagen IV$^{\mathrm{Vkg}}$ facilitates Dpp gradient formation by physically binding to Dpp (Sawala *et al.* , 2012). In vertebrates, Collagen IV binds BMP4 and has been suggested to potentiate signalling in cultured cells (Wang *et al.* , 2008). These results suggest that Collagen IV can affect BMP signalling in both invertebrate and vertebrate development. Whether Collagen IV facilitate BMP signalling in the context of CNS development and homeostasis has not been explored in either vertebrate systems and *Drosophila* to date.

1.10.2 Perlecan

Perlecan is a heparan sulfate proteoglycan (HSPG) which consists of a 480-kDa protein core and three to four heparan sulfate chains (Iozzo *et al.* , 1994). A key feature of Perlecan are that it is secreted and a component of the BM, in contrast to other GPI linked or transmembrane proteoglycans like Dally and Syndecan. In vertebrates, it is produced during embryonic stage of development in many organs and is localized in BM, vessel walls, cartilage matrix and some other extracellular spaces (French *et al.* , 1999). In mice, deficiency of Perlecan lead to multiple defects and early lethality (Arikawa-Hirasawa *et al.* , 1999; Costell *et al.* , 1999). Major phenotypes include defective BM in the heart muscle and brain: exencephaly, an impaired endochondral ossification and an unstable cartilage matrix (Arikawa-Hirasawa *et al.* , 1999; Costell *et al.* , 1999). The complex phenotypes may be due to the fact that Perlecan binds to a diverse array of signalling molecules, as well as other ECM proteins such as laminins, nidogens and fibulins. Bindings sites with which Perlecan interacts with other molecules are present in different domains of the protein core as well as on the heparan sulfate side chains (Hopf *et al.* , 1999). These binding sites are particularly abundant in domains IV and V of Perlecan. Perlecan has been well characterised in the growth and morphogenesis of the skeleton and vascular system, and it is involved in FGF, PDGF, and VEGF signalling (Melrose *et al.* , 2008; Segev *et al.* , 2004; Whitelock *et al.* , 2008). Recent studies also revealed its potential role in BMP signalling (DeCarlo *et al.* , 2012), and TGF-beta signalling by interacting with the pro-domains of TGF-beta ligands (Sengle *et al.* , 2011). Its involvement in a diverse array of signalling pathways could be at least partly responsible for its essential roles in many aspects of brain functions. For example, Perlecan is required for mammalian neurogenesis (Girós *et al.* , 2007), promotes regeneration from ischemic stroke (Roberts *et al.* , 2012), and protects the brain from βamyloid fibre-induced neurotoxicity (Parham *et al.* , 2013).

Perlecan is well conserved in *Drosophila* and it shares nearly all the main domain structures of mammalian Perlecan except for domain I (Friedrich *et al.* , 2000; Voigt *et al.* , 2002). The *Drosophila* Perlecan is encoded by the gene *terribly reduced optical lobes (trol)*, and I hereby refer to it as *perlecan^{trol}*. As in mammals, the *Drosophila* Perlecan$^{\mathrm{Trol}}$ also interacts with other ECM proteins, growth factors and receptors, to regulate cellular signalling (Lin, 2004a). Early studies on Perlecan$^{\mathrm{Trol}}$ focused on its role on NSC reactivation. In *perlecan^{trol}* null mutants, NSC reactivation is severely impaired: NSCs enlarge, but never enter their first S phase (Datta, 1995). Null mutations in *hedgehog* (*hh*) and *branchless* (*bnl*, an FGF homologue) dominantly enhance the impairment in NSC proliferation in a sensitised *perlecan^{trol}* mutant background, suggesting that Perlecan$^{\mathrm{Trol}}$ may regulate NSC

reactivation by modulating Hh and FGF signalling pathways (Park *et al.* , 2003). A recent study supported Perlecan^{Trol}'s role in Hh signalling in a different context. *perlecan^{trol}* mutant lymph glands showed disrupted architecture and premature stem cell differentiation, and overexpression of hh in Perlecan^{Trol} mutants was able to rescue the premature differentiation phenotype (Grigorian *et al.* , 2013). Another study revealed a novel role of Perlecan^{Trol} in Wnt signalling. At the *Drosophila* neuromuscular junction (NMJ), Wnt/ Wingless (Wg) regulates the formation of both pre- and postsynaptic structures. Mutation in *perlecan^{trol}* resulted in diverse postsynaptic defects and overproduction of synaptic boutons at the NMJ. The postsynaptic defects of *perlecan^{trol}* mutants could be rescued by the postsynaptic activation of the Wnt pathway (Kamimura *et al.* , 2013). Whether Perlecan^{Trol} is also involved in BMP/TGF-beta signalling in *Drosophila*, and especially in the context of NSC reactivation, awaits further investigation.

1.10.3 Laminin and Nidogen

Laminins consist of the most abundant non-collagenous protein component in the BM. Laminin isoforms are heterotrimeric glycoprotein chains that are shaped like a three-pronged fork (reviewed in (Durbeej, 2010)). The heterotrimer consisting of one α, one β, and one γ chain. In vertebrates, five α, three β, and three γ chains have been identified that represent distinct gene products (reviewed in (Durbeej, 2010)). Laminins are essential for embryonic development, and have indispensable functions in major organs including muscle, nerve, skin, kidney, lung and the vasculature (reviewed in (Durbeej, 2010)).

The two *Drosophila* Laminins both share common β and γ chains (called LanB1 and LanB2, respectively), whereas there are two different α chains (LanA, or Laminin A and Wing blister, or Laminin W). The two α chains have distinct tissue-specific expression and distribution patterns (Kusche-Gullberg *et al.* , 1992; Martin, 1999). In *Drosophila*, deficiency in laminin leads to developmental morphogenesis defects in many organs including the heart, gut, CNS, and muscles (as reviewed in (Broadie *et al.* , 2011)). Laminin's role in CNS development includes promoting axon outgrowth and guidance both in culture (Takagi *et al.* , 1996) and *in vivo* (Garcia-Alonso *et al.* , 1996).

Nidogen, also known as entactin, accounts for 2–3% of all BM proteins. It is a glycoprotein which contains 10% carbohydrates in its composition (Timpl *et al.* , 1983). Nidogen can interact with several other BM components, including Collagen IV, Perlecan, Laminin, Fibrinogen and Fibronectin (as reviewed in (LeBleu *et al.* , 2007)). Together with Perlecan, it helps to structurally connect the BM network by linking Collagens and Laminins to each

other (as reviewed in (Yurchenco & Patton, 2009)). Despite being an ubiquitous component of the BM and having many binding partners, genetic analyses in mammals have shown that they are dispensable for the overall architecture of the BM (as reviewed in (Ho *et al.* , 2008)). Whereas the vertebrates have two Nidogen protein isoforms, only one exists in *Drosophila*. *Drosophila* Nidogen is a prominent component of BM (Wolfstetter & Holz, 2012), but there are few studies that investigated it at the functional level so far.

1.10.4 ECM Receptors

In *Drosophila*, ECM proteins bind a number of highly conserved ECM-receptors, including Integrins, Dystroglycan (Dg), Syndecan, and Glypicans (as reviewed in (Broadie *et al.* , 2011)). Dystroglycans are the transmembrane matrix receptor of the dystrophin-glycoprotein complex (DGC) and they are closely associated with muscular dystrophies (Cohn, 2005; Michele & Campbell, 2003). The sugar side chains of dystroglycan can mediate binding to many Laminin G-domain-containing ECM proteins, such as Laminins and Perlecan. The *Drosophila dystroglycan* has been shown to genetically interact with a diverse array of signalling pathways involved in the development and function of the CNS (Kucherenko *et al.* , 2008). Another class of ECM receptors belong to the HSPG family of proteins, including the glycosulphosphatidylinositol (GPI)-anchored glypicans Dally and Dlp (Van Vactor *et al.* , 2006), as well as the transmembrane protein Syndecan (Lin, 2004b). Like Dystroglycans, the HSPG receptors have also been shown to be involved in a number of signalling pathways (Alexopoulou *et al.* , 2007; Häcker *et al.* , 2005; Lin, 2004b; Morgan *et al.* , 2007).

Among all ECM receptors in *Drosophila*, most attention has been paid to the heterodimeric transmembrane Integrin receptors. Integrins are heterodimers of two single-pass type I transmembrane proteins, including an α and a β subunit. Integrin heterodimers are formed in the endoplasmic reticulum, where these two subunits are synthesised (Hynes, 1992). Mammalian genomes contain 18 α subunit and eight β subunit genes, which form a total of 24 α/β heterodimers that interact with a wide range of ECM proteins (Barczyk *et al.* , 2009; Bökel & Brown, 2002; Humphries *et al.* , 2006a). In comparison to the complexity of mammalian integrins, the *Drosophila* genome encodes only five α subunits and two β subunits. In particular, the position specific (PS) integrins βPS (*myospheroid, mys*), αPS1 (*inflated, if*) and αPS2 (*multiple edematous wings, mew*) are the most evolutionary conserved integrin subunits, whereas $\beta\nu$ (β*Int-*ν), αPS3 (*scab, volado*), αPS4 and αPS5 are less conserved (as reviewed in (Brown *et al.* , 2000)). Work in *Drosophila* has mostly

focused on the PS integrins (Brabant *et al.* , 1996; Brown, 1993; Gotwals *et al.* , 1994). The only βPS subunit, encoded by the *mys* locus, is likely to form heterodimers with all five known α subunits (as reviewed in (Brown *et al.* , 2000)).

In vertebrates, integrins can bind to many ECM ligands. Despite their wide variety, it is possible to cluster integrin-ligand combinations into four main classes, according to the structural basis of the molecular interaction (as reviewed in (Humphries *et al.* , 2006b)). The first class consists of RGD-binding integrins which have the ability to recognise ligands containing an RGD tripeptide active site, such as in Fibronectin and Vitronectin. The LDV-binding integrins recognise an acidic motif in their ligands, such as VCAM–1 and Fibronectin. For the third class, 4 α subunits containing an αA-domain combine with β1 integrin form a distinct Laminin/Collagen binding integrin subfamily. The structural basis for this interaction lies in a critical glutamate within a collagenous GFOGER motif. Finally, the fourth class consists of non-αA-domain-containing Lamimin binding integrins. Direct binding of Collagen IV to integrins has been biochemically confirmed in vertebrates: Purified $\alpha1\beta1$ and $\alpha2\beta1$ integrin complexes can directly bind Collagen IV, with $\alpha1\beta1$ showing higher binding affinity (Tuckwell & Humphries, 1996).

In *Drosophila*, only a small number of ECM proteins have been confirmed as integrin ligands, which includes two laminins (Henchcliffe *et al.* , 1993; Martin, 1999), tiggrin (Fogerty *et al.* , 1994), thrombospondin (Subramanian *et al.* , 2007) and tenectin (Fraichard *et al.* , 2010). Other ECM proteins, such as Collagen IV (Le Parco *et al.* , 1986) and tenasin (Graner *et al.* , 1998) are important in *Drosophila* but they have not been confirmed to be integrin ligands with biochemical assays. Nonetheless, a number of recent *in vivo* studies within different developmental contexts support the idea that Collagen IV exert its functions via its association with integrin receptors (Haigo & Bilder, 2011; Pastor-Pareja & Xu, 2011; Vanderploeg *et al.* , 2012).

What functions do integrins play during development? In *Drosophila*, most attention has been given to their adhesive and signalling roles in muscle attachment (Brown, 1993; Bunch *et al.* , 1998; Nievers *et al.* , 1999; Prokop *et al.* , 1998; Volk, 1999), morphogenesis of the gut (Borkowski *et al.* , 1995; Martin-Bermudo & Brown, 1999; Reuter *et al.* , 1993; Roote & Zusman, 1996), embryonic dorsal closure (Brabant & Brower, 1993; Brower *et al.* , 1995; Brown, 1994; Leptin *et al.* , 1989; Roote & Zusman, 1996) as well as adhesion of the wing blade (Brabant & Brower, 1993; Brabant *et al.* , 1996; Brower *et al.* , 1995; Ramírez-Weber & Kornberg, 1999). Furthermore, integrins play crucial roles during *Drosophila* neural development. *Drosophila* integrins were first implicated in regulating axon growth (Donady, 1972). Later, *Drosophila* laminins were found to act as Integrin ligands. They

promote axon outgrowth of cultured primary neurons and trigger cell spreading of neuronal BG2 cell lines and recruitment of βPS integrin into focal adhesion (Takagi *et al.* , 1996, 1998). These findings were partially confirmed by further *in vivo* analyses: Motor nerve patterns in mutant embryos lacking βPS integrin resulted in axonal navigational errors, although the outgrowth capacity of motor neurons were unchanged (Hoang & Chiba, 1998). A better defined axon-guidance role for integrins was explored in the context of CNS midline axon crossing mediated by the secreted ligand Slit and its receptor Roundabout (Robo). Loss of function mutation of integrin subunit genes led to phenotypes similar to slit/robo axon pathfinding defects (Stevens & Jacobs, 2002). Further studies found that Laminin A and Tiggrin are present in the CNS and may mediate integrin-dependent midline axon guidance: both *lanA* and *tig* genetically interact with *slit* mutations (Garcia-Alonso *et al.* , 1996). In addition to regulating axon guidance, integrins are also known to play a role in the formation of neural-muscular junctions (NMJ). βPS, $\beta\mu$, and αPS1–3 subunits are all present at *Drosophila* NMJs (Beumer *et al.* , 1999; Rohrbough *et al.* , 2000; Tsai *et al.* , 2008). Mutation in PS integrin subunits caused strong defects in the morphological differentiation and functional maturation of NMJ during CNS development (Beumer *et al.* , 1999; Rohrbough *et al.* , 2000). Although the exact mechanisms are unclear, it is hypothesised that integrins at the NMJ are important for interaction with other transmembrane partners and secreted signals. For example, the immunoglobulin family adhesion molecule Basigin (Bsg) is expression at the *Drosophila* NMJ (Besse *et al.* , 2007) and βPS and bsg mutant alleles show genetic interaction (Curtin *et al.* , 2007).

In addition, integrins are known to play major roles in the regulation of mammalian NSCs during development and homeostasis. Integrin receptors are widely expressed in both embryonic and adult NSCs. For example, the Laminin receptor $\alpha 6\beta 1$ integrin is present at high levels on both embryonic NSCs and on proliferating adult NSCs (Kazanis *et al.* , 2010; Shen *et al.* , 2008; Staquicini *et al.* , 2009). In the embryonic CNS, integrins anchor NSCs to their niche and maintain NSC polarity, which are important for NSC survival and proliferation, respectively (Radakovits *et al.* , 2009). Experiments that removed integrins in the developing CNS disrupted NSCs' basal processes' attachment to the basal lamina. This disruption in NSC niche architectural ultimately lead to the apoptosis of NSCs, suggesting that integrins are essential for NSC survival (Radakovits *et al.* , 2009). In addition, intraventricular injection of $\beta 1$ blocking antibodies in embryonic CNS caused reduction in NSC division, as a result of altered division cleavage plane (Loulier *et al.* , 2009). In adult neurogenic niche, integrins promote NSC activation and proliferation. For example, loss of αV$\beta 8$ integrin reduced NSC/or precursor cell proliferation in the SEZ (Mobley *et al.* ,

2009). Interestingly, another integrin receptor, $\beta 1$ integrin, is not present on quiescent adult NSC but upregulated when these cells activate to enter mitotic cell cycle (Kazanis *et al.* , 2010; Kokovay *et al.* , 2010). This suggests that changes in integrin receptor expression may mediate changes in ECM signalling that contributes to the activation of quiescent. Despite overwhelming evidence of integrins' role in mammalian NSC behaviour, whether integrin receptors play similar roles in *Drosophila* NSC survival, proliferation and activation remain undefined.

1.11 Advantage of Using *Drosophila* as a Model System to Investigate the Mechanisms of NSC Reactivation *in Vivo*

Studies using mammalian models to investigate mechanisms underlying NSC proliferation *in vivo* face a number of challenges. First of all, genetic manipulation in a NSC-specific manner is difficult. For example, the most widely used Nestin-cre mouse lines is not sufficiently specific, as it is expressed in radial glia/NSCs and intermediate intermediate progenitor cells (Gavériaux-Ruff & Kieffer, 2007). An even more problematic aspect of Nestin-cre has just emerged recently: a report showed that the only commercially available Nestin-cre line is insufficient for directing recombination in early embryonic NSCs (Liang *et al.* , 2012). These challenges can be largely resolved in *Drosophila*. The availability of multiple NSC specific GAL4 drivers in *Drosophila* enables misexpression and knockdown of candidate effectors in a cell type specific manner, and during any stage of development when GAL4 is used in combination with $GAL80^{ts}$ (Matsumoto *et al.* , 1978), a temperature sensitive inhibitor of GAL4.

The *Drosophila* model system offers a few other advantages for the study of systemic regulation of NSC reactivation. A large proportion of NSCs are conveniently localised on the surface of the VNC and they reactivate within a short time window, which makes observation and quantification more straightforward than in the rodent models. Due to short generation time of the organism, experiments that perturb cellular signalling components related to NSC reactivation can be performed with a speed unmatched by other model systems.

1.12 Summary of PhD findings

Despite recent exciting work on nutritional regulation of NSC reactivation, key questions still remain: what are the signal(s) from the fat body, and how do they interact with glial cells to induce glial secretion of DIlps? In addition, three glial subtypes are physically associated with the NSCs, including the perineurial glia, subperineurial glia, and cortex glia, but each subtype's individual contribution to NSC reactivation remains elusive.

To search for nutrient-responsive fat body factors and investigate the mechanisms by which they interact with the glial niche, I used the novel TaDa (Targeted DamID) Pol II transcriptional profiling technique (Southall *et al.* , 2013) to map fat body transcriptomes under fed and starved conditions. I identified Collagen IV as a key fat body factor crucial for coupling brain growth to the nutrient states of the organism. Secreted from the fat body in response to dietary amino acid availability, Collagen IV deposits on the CNS surface and controls NSC reactivation. NSCs are separated from the hemolymph by a BBB. In collaboration with Pauline Speder and Jessie Van Buggenum (Andrea Brand lab), we confirmed crucial roles of the two BBB glial populations as a NSC niche and identified each subpopulation's contribution to NSC reactivation: DamID glial transcriptional profiling identified subperineurial and perineurial glia as the source of CNS DIlps and perineurial glia as the source of Perlecan^{Trol}, an which is recruited to the CNS surface by fat body derived Collagen IV. Together, Collagen IV and Perlecan^{Trol} trigger NSC reaction and subsequent induction of insulin signalling from the BBB glia.

Chapter 2

Fat Body Targeted Dam ID (TaDa) Transcriptional Profiling Identified Regulators of CNS Development in Response to Nutrient Availability

2.1 Identification of Fat Body Derived Signals *in Vivo* Using TaDa Transcriptional Profiling

To confirm that the fat body secretes signals regulating CNS growth, I first assessed larval development when fat body secretion was impaired. A previous study showed the *in vivo* evidence for the requirement of putative fat body derived growth signals: disruption of vesicle trafficking in the fat body by expressing a dominant negative mutant of *shibire* (shi^{DN}), which encodes *Drosophila* Dynamin (Moline *et al.* , 1999), led to impaired NSC reactivation (fewer EdU positive cells) (Sousa-Nunes *et al.* , 2011). Shi^{DN} impaired endocytosis. Therefore, I used an approach to knock down secretion more specifically. Syntaxin 5 (Syx5) is a member of the SNARE complex and it is involved in ER-Golgi transport (Dascher *et al.* , 1994). Knockdown of *syx5* in *Drosophila* S2 cells specifically disrupted constitutive secretion while having little effect on other aspects of S2 cells' homeostasis (personal communication, Andrew Peden, University of Sheffield). Indeed, *in vivo* fat body knockdown (Lpp-GAL4) of *syx5* using RNAi resulted in arrested larval growth and reduced size of the CNS, confirming that fat body secreted signal(s) are required for CNS development (Figure 2.1.1). A second RNAi line against *syx5* showed the same phenotype, suggesting that the

growth phenotypes observed in *syx5* knockdown were likely not due to off-target effects of the RNAi constructs. The RNAi lines used in this experiment are listed in Appendix.

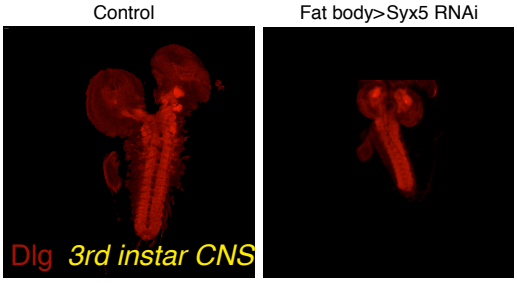

Fig. 2.1.1 Impairment of fat body secretion led to CNS underdevelopment. Disruption of fat body exocytosis by knocking down *Syntaxin 5* in the fat body (Lpp-GAL4) resulted in CNS underdevelopment (third instar larval CNS, 72 hph. Dlg: membrane marker).

Fat body derived growth signals may be transcriptionally regulated in response to feeding. Therefore, I assayed fat body transcriptomes in the first instar larvae under fed and starved conditions. Since dissection of fat body in a consistent manner is technically challenging from starved first instar larvae, I took advantage of the Targeted DamID (DNA adenine methyltransferase identification) technique, hereby referred to as "TaDa", to overcome this challenge (Southall *et al.* , 2013). This technique allowed me to obtain RNA Polymerase II (Pol II) binding profiles in the fat body cells *in vivo* without the need for dissection. Three fat body GAL4 drivers were tested, including Cg-GAL4, Lpp-GAL4, and Fb-GAL4. I expressed UAS-mCD8GFP under these fat body drivers and examined the expression patterns of GFP in embryonic and larval tissues. Lpp-GAL4 (Brankatschk & Eaton, 2010) was selected because of its tissue specificity (Figure 2.1.2). Driver specificity and onset of driver expression for all fat body drivers tested is summarised in Table 2.1.1. Workflow of the identification of fat body derived growth signals using TaDa is summarised in Figure 2.1.3.

A stringent fat body GAL4 driver (Brand & Perrimon, 1993) allowed me to obtain fat body Pol II binding profiles using a whole larval preparation. In addition, temporal control was achieved by combining the GAL4 system with a temperature sensitive repressor of GAL4, $GAL80^{ts}$ (Matsumoto *et al.* , 1978). I expressed the RNA Pol II-Dam fusion proteins in the fat body 0–24 hours post hatching (hph), which coincides with the reactivation time window of the majority of NSCs. Raw data from the TaDa transcriptional profiling experiments containing genes upregulated under fed or starved conditions, fold changes between the two conditions (on Log2 scale), and their corresponding false discovery rates (FDRs), can be found in my data deposition folder (see Chapter 8).

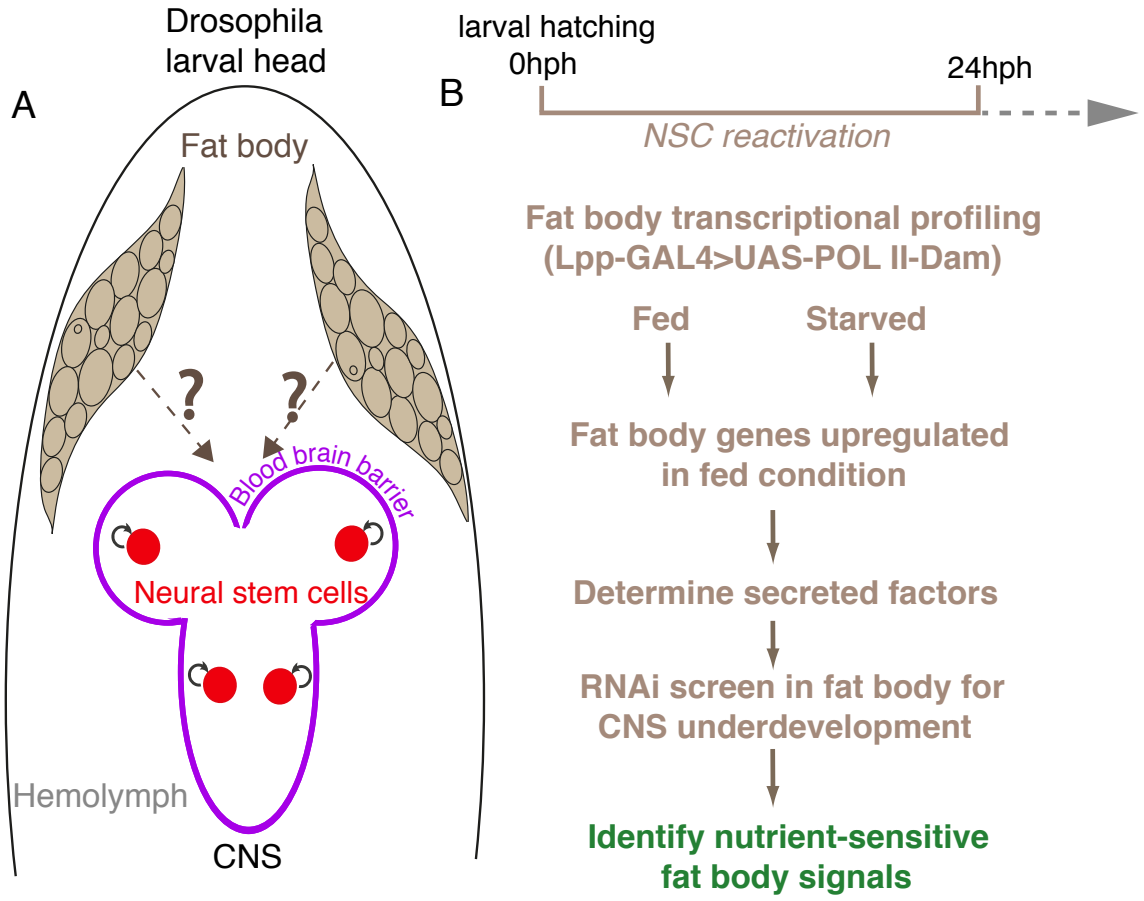

Fig. 2.1.2 Fat body transcriptional profiling identified factors that regulate CNS development in response to dietary amino acids. (A) Previous studies have shown that *Drosophila* fat body, the liver and adipose tissue equivalent, acts as a nutrient sensor in response to food in-take. It sends out unknown fat body signal(s), which induces CNS glial cells to secrete *Drosophila* insulin-like peptides (DIlps). The local DIlps in turn trigger NSC reactivation from quiescence. (B) A schematic workflow of the identification of nutrient-sensitive fat body signals following TaDa fat body transcriptional profiling.

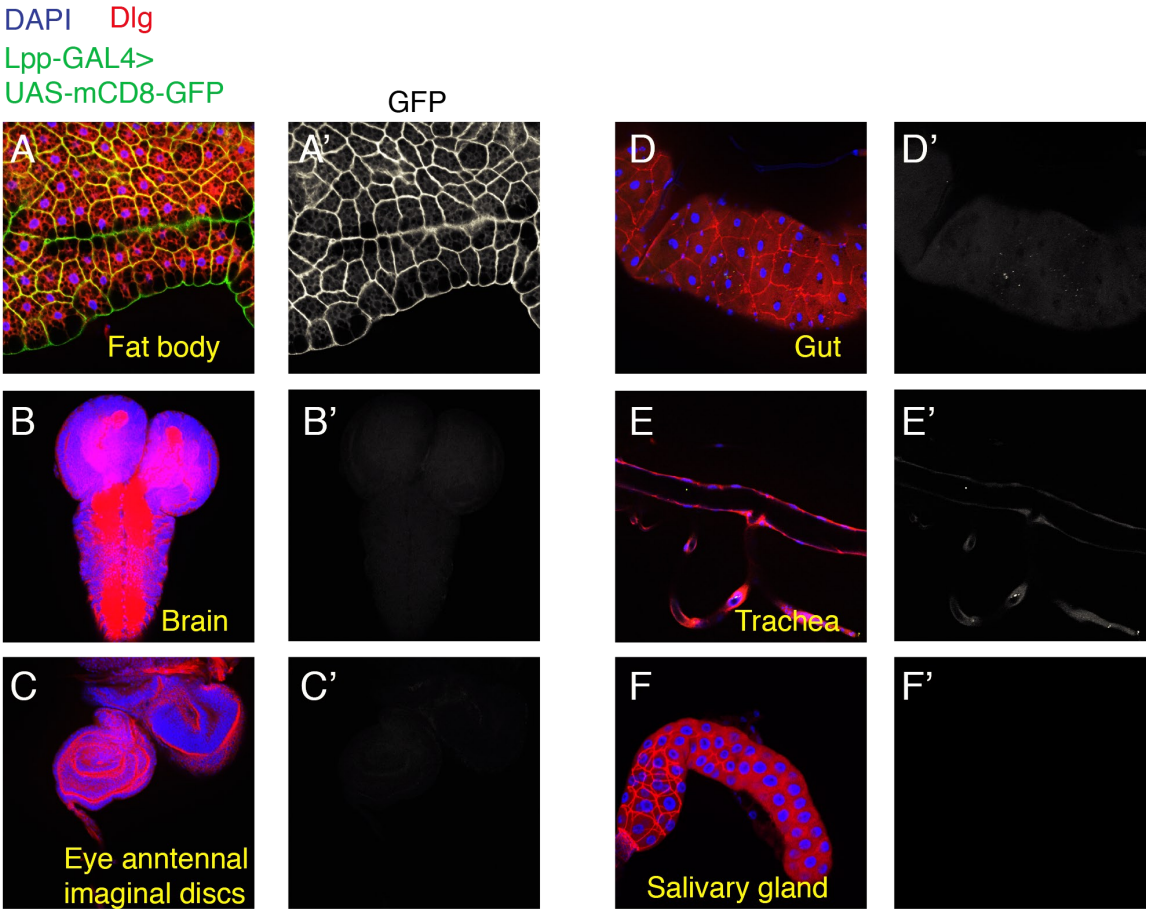

Fig. 2.1.3 Tissue specificity of Lpp-GAL4 driver (A-F) UAS-mCD8GFP was expressed under Lpp-GAL4 driver. GFP expression was assayed in fat body, gut, CNS, muscles, imaginal discs and salivary gland (A'-F'), and GFP signal was only detected in the fat body (A'). Larvae were reared at 25 ºC and dissected 72 hph. DAPI, DNA dye, blue; Lpp-GAL4>UAS-mCD8-GFP, green; Dlg, membrane marker, red.

Table 2.1.1 Driver specificity and onset of driver expression of all fat body drivers tested for fat body TaDa transcriptional profiling experiment

	CG-GAL4	**FB-GAL4**	**Lpp-GAL4**
Onset of GAL4 activity	Embryo	Embryo	Embryo
Expression pattern in fed larvae	Fat body, Hemocytes, Lymph gland	Fat body, Wing disc, CNS	Fat body
Expressed in starved larvae?	Yes	Yes	Yes
Driver strength	Strong	Very strong	Strong

2.2 Fat Body Transcriptional Profiling Identified Nutrient Sensitive Fat Body Signals and Signalling Pathways

Using a medium stringency threshold, 150 genes were significantly upregulated in the fat body under fed as compared to starved conditions, whereas 1370 genes were upregulated under starved conditions (>=1.5 fold change with FDR<=0.01). I found that fat body genes known to be upregulated under fed condition, such as *lsp–1* and *sug* (Farhadian *et al.* , 2012; Higami *et al.* , 2006), and fat body genes known to be upregulated under starved conditions such as *dIlp6* (Slaidina *et al.* , 2009) and autophagy genes (Scott *et al.* , 2004), were regulated as expected. I used two web based functional annotation tools, Gene Ontology (GO) and Database for Annotation, Visualisation and Integrated Discovery (DAVID) to investigate enriched processes and pathways among the differentially transcribed genes.

I first investigated genes upregulated under fed conditions. Many of the top GO terms correspond to processes related to the cell cycle, transcription, and translation. In addition, proteins encoded by genes upregulated under fed conditions form a dense interaction network according to known and predicted interactions, based on STRING (Search Tool for the Retrieval of Interacting Genes/Proteins) functional protein association network analysis (Franceschini *et al.* , 2013; von Mering *et al.* , 2005) (Figure 2.2.1)(http://string-db.org/). Recognisable clusters within the protein association network include “regulation of protein translation”, “protein folding”, “mRNA alternative splicing” and “extracellular matrix proteins” (Figure 2.2.1).

It is intriguing that significantly higher number of genes were upregulated under starved conditions compared to the number of genes upregulated under fed conditions in the fat body. Many of the top GO terms correspond to processes related to metabolism, consistent with the known role of fat body as a global metabolic sensor and coordinator (Colombani *et al.* , 2003). In particular, genes regulating sucrose and starvation metabolism are enriched in this gene set. This is consistent given the switch from a standard laboratory food to pure sucrose diet (Table 2.2.1). Starvation imposes tremendous stress on the organism. Transcriptome analysis revealed that many genes involved in stress response were upregulated under starved conditions, consistent with previous work describing an essential role of the fat body in coordinating stress response and the fact that starvation is stress-inducing (Karpac *et al.* , 2011) (Table 2.2.2).

In addition, many signalling pathways are enriched in the fat body under starved conditions. This includes the JAK/STAT (Janus kinase/Signal Transducer and Activator of Transcription) pathway, which is also known to be upregulated in response to stress (Dudley

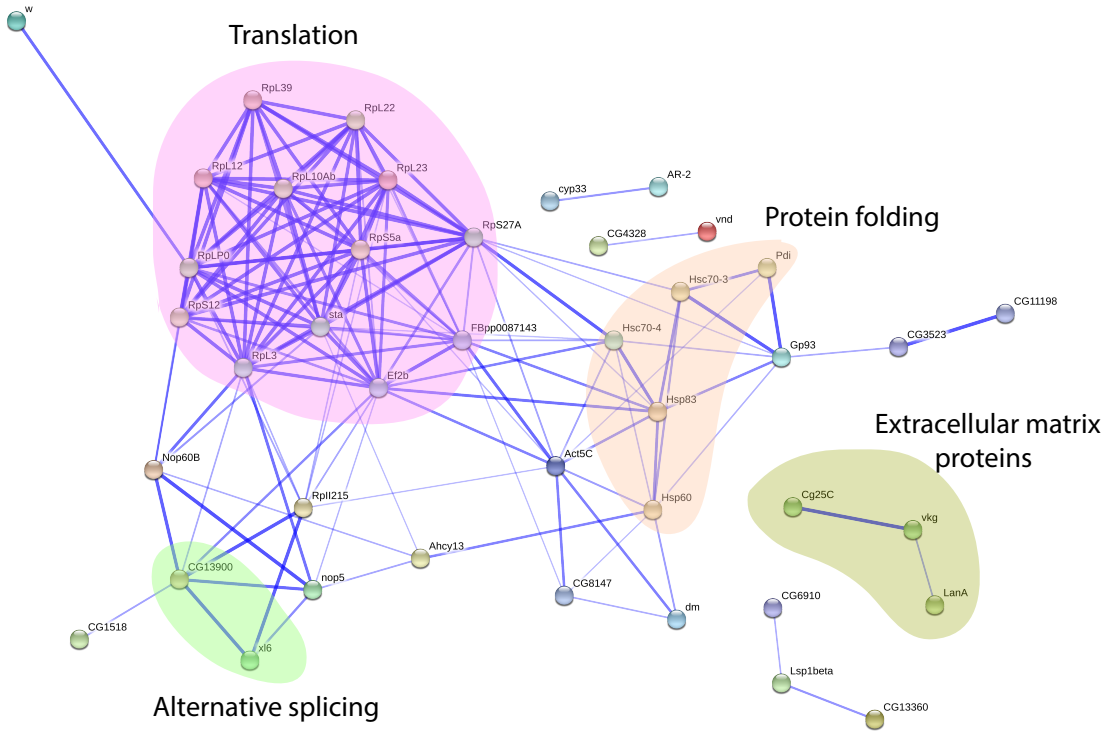

Fig. 2.2.1 Known and predicted interactions between the products of 150 genes differentially transcribed in the fat body under fed conditions. Analysis was performed using STRING with a medium confidence score of 0.4 and all interaction methods available. Clusters representing selected pathways and processes are highlighted. Single nodes are not displayed

Table 2.2.1 Genes involved in sugar and starch metabolism upregulated under starved conditions in the fat body.

Flybase ID	Gene Symbol
FBgn0034605	CG15661
FBgn0032713	CG17323
FBgn0053138	CG33138
FBgn0027073	CG4302
FBgn0035978	CG4347
FBgn0031907	CG5171
FBgn0004507	Glycogen phosphorylase
FBgn0003076	Phosphogluconate mutase
FBgn0038293	Putative glycogen (starch) synthase
FBgn0010851	sugarless

Table 2.2.2 Genes involved in stress response upregulated under starved conditions in the fat body.

Flybase ID	Gene Symbol
FBgn0034366	Autophagy-specific gene 7
FBgn0038035	DNA ligase III
FBgn0028434	CG10215
FBgn0014037	CG32217
FBgn0026751	CG4208
FBgn0031309	CG5041
FBgn0025832	Flap endonuclease 1
FBgn0013277	Heat-shock-protein-70Ba
FBgn0031950	Homocysteine-induced endoplasmic reticulum protein
FBgn0051354	Major heat shock 70 kDa protein Bbb
FBgn0031848	Non-structural maintenance of chromosomes element 1 homolog
FBgn0014020	Ras-like GTP-binding protein Rho1
FBgn0014018	Relish
FBgn0003462	Superoxide dismutase
FBgn0004436	Ubiquitin conjugating enzyme
FBgn0000097	anterior open
FBgn0000229	basket
FBgn0004638	downstream of receptor kinase
FBgn0033483	eiger
FBgn0260817	glaikit
FBgn0243512	puckered
FBgn0003479	spindle A

et al. , 2004) (Table 2.2.3), and several signalling pathways that have not been previously explored in the fat body, such as MAP kinase pathway (Table 2.2.4), TGF-beta (Table 2.2.5), and Wnt signalling (Table 2.2.6).

In summary, TaDa transcriptional profiling identified genes that are differentially transcribed under fed or starved conditions in the fat body during the first 24 hours after larval hatching. The observed patterns of differential gene expression are consistent with known functions of the fat body.

Table 2.2.3 Genes involved in JAK/STAT signalling pathway upregulated under starved conditions in the fat body.

Flybase ID	Gene Symbol
FBgn0010379	RAC serine/threonine-protein kinase
FBgn0016917	Signal-transducer and activator of transcription protein at 92E
FBgn0041184	Suppressor of cytokine signaling at 36E
FBgn0004638	downstream of receptor kinase

Table 2.2.4 Genes involved in MAP kinase signalling pathway upregulated under starved conditions in the fat body.

Flybase ID	Gene Symbol
FBgn0003205	Ras oncogene at 85D
FBgn0000097	anterior open
FBgn0004638	downstream of receptor kinase
FBgn0001137	gurken
FBgn0003079	pole hole

Table 2.2.5 Genes involved in TGF-beta signalling pathway upregulated under starved conditions in the fat body.

Flybase ID	Gene Symbol
FBgn0020493	Daughters against dpp
FBgn0025637	CG16983
FBgn0260439, FBgn0005776	Protein phosphatase 2A at 29B
FBgn0014020	Ras-like GTP-binding protein Rho1
FBgn0025800	Smad on X
FBgn0000575	extra macrochaetae

Table 2.2.6 Genes involved in Wnt signalling pathway upregulated under starved conditions in the fat body.

Flybase ID	Gene Symbol
FBgn0020496	C-terminal Binding Protein
FBgn0030505	CG11172
FBgn0025637	CG16983
FBgn0260439	Protein phosphatase 2A at 29B
FBgn0014020	Ras-like GTP-binding protein Rho1
FBgn0025800	Smad on X
FBgn0000229	basket
FBgn0000499	dishevelled
FBgn0003371	shaggy
FBgn0003390	shifted

2.3 Collagen IV Is an Important Regulator of CNS Development

Since NSCs are only able to reactivate when the larvae are fed essential amino acids, I hypothesised that the fat body derived growth signals would be upregulated under fed conditions. Among the 150 genes upregulated under fed conditions, I decided to first concentrate on the genes encoding secreted proteins. Signal P and Secretome P programs (Bendtsen *et al.* , 2004) predicted 61 genes encoding proteins that could be secreted via either classical Golgi-dependent pathway (Signal P) or Golgi-independent pathway (Secretome P). The symbols of these genes, as well as their biological processes and cellular localisations as predicted by GO, are listed in the Appendix. Subsequently, I knocked down the secreted proteins in the fat body by expressing RNA interference (RNAi) constructs using Lpp-GAL4, and assessed their requirement for neural development by examining the size of third instar larval CNS (Dietzl *et al.* , 2007). Two RNAi libraries were available from the VDRC (Vienna Drosophila Resource Centre), including the older GD library and the newer KK library. The GD library was generated by P element–mediated transformation of short hairpin RNA (shRNA) constructs into the fly genome (Groth *et al.* , 2004), a technique susceptible to insertional mutagenesis (false positive results) and insertion into transcriptionally silent regions in the genome (false negative results). In comparison, the KK collection used a two-step transformation strategy so that gene-specific shRNA sequences could be inserted into defined regions in the genome (Dietzl *et al.* , 2007). This strategy was thought to minimise the risk of insertional mutagenesis. Thus, although the KK library also has its own

limitations such as causing a number of dominant phenotypic effects as discovered recently (Green *et al.* , 2014), it was chosen as my preferred method of knockdown because it was the best available RNAi library at the time of the study. In addition, when I decided to perform fat body RNAi screen, the KK library was incomplete and did not contain RNAi constructs against all the genes that I planned to knock down. Therefore, I used RNAi lines from the GD library for these genes. Gene symbols and VDRC stock numbers for my fat body RNAi screen are listed in the Appendix.

The functional RNAi screen identified a total of 10 genes that are required in the fat body for neural development out of the 61 genes initially screened. When knocked down in the fat body, 6 of the 10 candidates showed severe systemic growth defects: larval growth was significantly impaired as larvae were noticeably smaller in size and they were all arrested at early second instar stage until death (Figure 2.3.1). All of these genes are involved in translational regulation, which include 5 ribosome associated proteins and one translation elongation factor (Figure 2.3.1). In the fat body, TOR signalling functions as a sensor of amino acids (Colombani *et al.* , 2003). It has a well known function to regulate protein synthesis downstream of amino acid sensing via post-translational modification of the translational machinery (e.g. S6K and 4E-BP) (Andersen *et al.* , 2013). Studies showed that TOR signalling can also control the expression of components of the translational machinery, consistent with my findings: recent work demonstrated a specific role for RNA polymerase III and tRNA synthesis, as well as for ribosomal biogenesis downstream of TOR signalling in the control of systemic growth by fat body cells (Elizabeth J Rideout, 2012; Killip & Grewal, 2012; Marshall *et al.* , 2012). It was initially surprising that ribosomal proteins were identified as candidates of secreted fat body signals. Ribosomes can exit in either free (in cytosol) or membrane-bound (in endoplasmic reticulum) states (Woolford & Baserga, 2013). The SignalP program determines whether a protein is secreted or not by the presence or absence of a signal peptide in its amino acid sequence. Ribosomal subunits associated with the endoplasmic reticulum contain signal peptides, which is probably why they were identified as secreted proteins by the SignalP program. On the other hand, a recent study showed that it is indeed possible for ribosomal proteins to be secreted extracellularly. The ribosomal protein S3 (rpS3) is homodimerised and secreted from several human and mouse cancer cell lines such as human fibrosarcoma and mouse plasmacytoma (Kim *et al.* , 2013). The level of secreted rpS3 appeared to correlate with the degree of cancer malignancy. It remains to be investigated whether other ribosomal proteins can also be secreted, and whether this occurs under normal homeostatic conditions.

In contrast, fat body knockdown of the remaining 4 candidates, including *collagen IV*^{vkg},

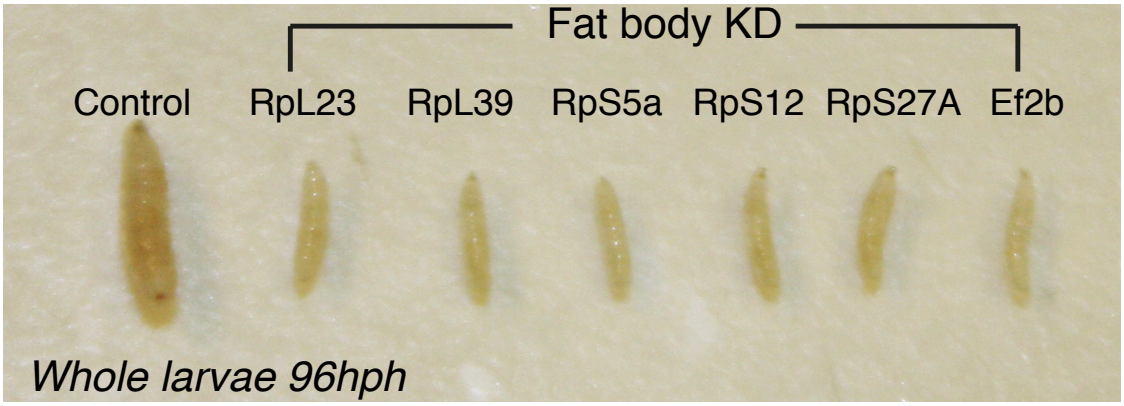

Fig. 2.3.1 Fat body factors are required for systemic larval growth. Knockdown of a number of fat body genes upregulated under fed conditions led to significant impairment of larval growth. Most of these genes are associated with the ribosome and translation machinery.

collagen IV^{cg25C}, *hsc70-C* and *CG13900*, led to viable third instar larvae. These larvae showed mild systemic growth defects compared to control, but their CNS were reduced in size. This indicates that these fat body-secreted proteins are important for neural development during larval stages. In addition to the secreted proteins, I also carried out a functional analysis of the remaining 89 upregulated fat body genes via an RNAi screen. All genes which are required in the fat body for organismal, and especially neural development, are summarised in Table 2.3.1. This includes a total of 9 predicted secreted proteins and a total of 9 non-secreted proteins.

Table 2.3.1 Summary of all genes upregulated under fed conditions whose knockdown led to larval growth defects in the fat body.

CG Number	Gene symbol	Secreted	Comments	Reduction in body size	GO_BIOLOGICAL_PROCESS
CG4145	Cg25C	yes	high penetrance,elongated VNC	moderate	dorsal closure
CG16858	Vkg	yes	high penetrance, elongated VNC	moderate	skeletal muscle tissue development; Malpighian tubule morphogenesis
CG13900	–	yes	high penetrance	moderate	nuclear mRNA splicing, via spliceosome
CG4147	Hsc70-3	yes	–	moderate	sleep ; response to heat
CG3661	RpL23	yes	arrested at 2nd instar	severe	translation; mitotic spindle elongation
CG3997	RpL39	yes	arrested at 2nd instar	severe	translation; mitotic spindle elongation
CG8922	RpS5a	yes	arrested at 2nd instar	severe	translation; mitotic spindle elongation
CG11271	RpS12	yes	arrested at 2nd instar	severe	translation
CG5271	RpS27A	yes	arrested at 2nd instar	severe	translation
CG13360	–	no	high penetrance	moderate	-
CG12101	Hsp60	no	high penetrance	moderate	response to heat ; protein folding
CG1242	Hsp83	no	high penetrance	moderate	spermatogenesis ; centrosome cycle ; regulation of circadian cycle
CG10798	dMyc	no	low penetrance	moderate	cell competition; cell proliferation; positive regulation of cell growth
CG12885	–	no	low penetrance	moderate	-
CG6425	–	no	high penetrance, elongated VNC	moderate	-
CG8280	Ef1alpha48D	no	–	moderate	translational elongation
CG15554	RpII215	no	–	moderate	transcription
CG2238	Ef2b	no	arrested at 2nd instar	severe	DNA damage checkpoint translational elongation

As a starting point to investigate the role of fat body derived growth signals on NSC reactivation, I decided to focus on Collagen IV. This is because the two Collagen IV subunits, Collagen IV^{Vkg} and Collagen IV^{Cg25C}, are the only proven secreted proteins. I will also discuss my preliminary investigation of the other two candidates, Hsc70–3 and CG13900, in Chapter 5.

Collagen IV is an ECM protein and an important component of the basement membrane. Basement membranes are layered polymers of ECM proteins lining the epithelia. They surround organs, including muscles, fat, endothelium, and nervous tissue. Collagen IV is the most abundant component of the basement membrane, comprising 50% of its proteins (Kalluri, 2003). Collagen IV molecules consist of a chains bound in long helical trimers that assemble into a network through lateral and end-domain interactions (Yurchenco & Ruben, 1987). Collagen IV molecules are divided into two subfamilies, the α1 like subunits and α2 like subunits (Aouacheria *et al.* , 2006). The most broadly distributed isoform of collagen IV is a hetero-trimer consisting of two α1 and one α2 chain, designated as α1(IV)2α2(IV) (Pöschl *et al.* , 2004). In the *Drosophila* genome, two genes encode α1-like subunits, named *viking* (*vkg*) and *collagen-at–25C* (*Cg25C*), hereby referred to as *collagen IV^{vkg}* and *collagen IV^{cg25C}*, respectively (Rodriguez *et al.* , 1996; Yasothornsrikul *et al.* , 1997). *collagen IV^{vkg}* and *collagen IV^{cg25C}* are located head-to-head adjacent to each other in the genome, an arrangement conserved in the α1-like pair of Collagen IV genes in mammals (Rodriguez *et al.* , 1996). Levels of Pol II binding across *collagen IV^{vkg}* and *collagen IV^{cg25C}* loci are significantly higher under fed conditions as compared to starved conditions in the fat body (Figure 2.3.2).

Collagen IV is highly conserved from *Drosophila* to humans. Recent work in *Drosophila* revealed its direct role in growth factor signalling (Bunt *et al.* , 2010; Sawala *et al.* , 2012). The most well-characterised signalling pathway mediated by Collagen IV is BMP signalling. Wang et al first demonstrated that interaction between Dpp (Decapentaplegic, a *Drosophila* BMP ligand) and Collagen IV^{Vkg} is essential for the development of the *Drosophila* germarium and in early embryos (Wang *et al.* , 2008). In addition, Collagen IV-dependent BMP signalling has been shown to regulate renal tubule morphogenesis (Bunt *et al.* , 2010) and midgut stem cell proliferation (Tian & Jiang, 2014). Recently, Sawala et al showed that Collagen IV^{Vkg} facilitates Dpp gradient formation by physically binding to Dpp (Sawala *et al.* , 2012). In vertebrates, Collagen IV binds BMP4 and has been suggested to potentiate signalling in cultured cells (Wang *et al.* , 2008). These results suggest that Collagen IV can affect BMP signalling in both invertebrate and vertebrate development.

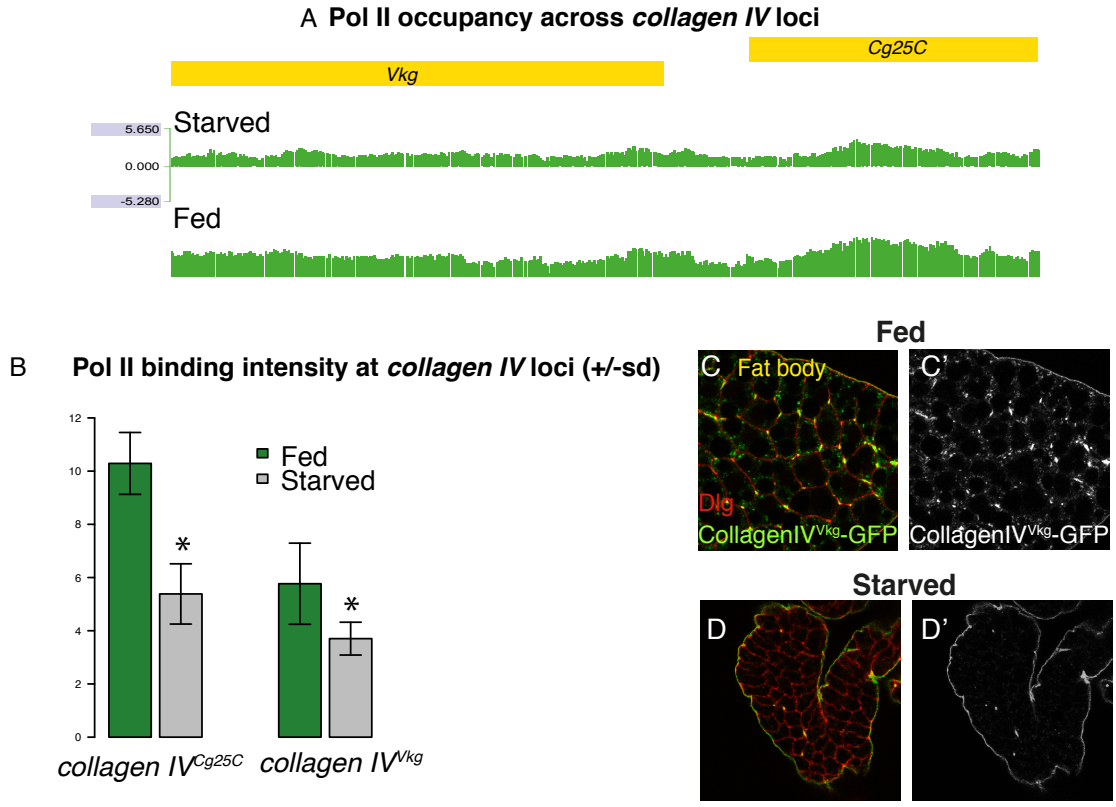

Fig. 2.3.2 Collagen IV Alpha–1 subunits are upregulated under fed conditions in the fat body. (A) RNA Pol II occupancy across *collagen IV^{vkg}* and *collagen IV^{cg25C}* loci from fat body TaDa transcriptional profiling (Log2 scale). The experiment was performed 0–24 hph, under fed and starved conditions. (B) Pol II binding intensities on natural scale were quantified for both *collagen IV* subunits. (C-D) Collagen IV^{Vkg}-GFP protein trap shows higher Collagen IV^{Vkg} expression in the fat body under fed conditions (C) as compared to starved (D) conditions (30 hph.)

Taking advantage of a Collagen^{Vkg}-GFP protein trap line (Morin *et al.* , 2001), I verified the upregulation of Collagen IV^{Vkg} protein in the fat body cells under fed conditions compared to starvation (Figure 2.3.2). To test whether Collagen IV^{Vkg} is required for CNS development, I knocked down *collagen IV^{vkg}* in the fat body using a small hairpin-based microRNA (Ni *et al.* , 2009, 2011) (hereby referred to as "shmiR", as compared to "RNAi") against *collagen IV^{vkg}*. This resulted in reduced brain size in third instar larvae but moderately reduced larval size (Figure 2.3.3), developmental delay and pupal lethality when the experiments were conducted at 25 ºC.

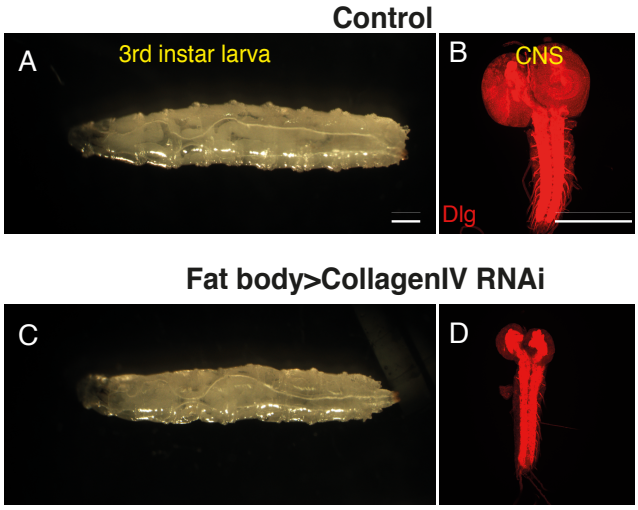

Fig. 2.3.3 Fat body *Collagen IV^{Vkg}* knockdown led to CNS underdevelopment and mild systemic growth defect. (A-B) Third instar whole larvae and larval CNS (72 hph) under control condition (w1118 X UAS-*collagen IV^{vkg}* shmiR). (C-D) Third instar whole larvae and larval CNS in fat body-specific knockdown of Collagen IV^{Vkg} (Lpp-GAL4>UAS-*collagen IV^{vkg}* shmiR). Dlg in red labels neuronal membranes. This experiment was performed at 25 ºC.

2.4 Chapter Summary

In order to investigate fat body secreted proteins regulating NSC reactivation, I performed fat body transcriptional profiling using the TaDa technique, during the time window of NSC reactivation. A subsequent functional RNAi screen of genes upregulated under fed conditions identified a number of candidates, including *collagen IV^{cg25C}* and *collagen IV^{vkg}*, whose knockdown in the fat body results in CNS underdevelopment. I verified the upregulation of Collagen IV^{Vkg} protein under fed conditions using a Collagen IV^{Vkg}-GFP protein trap construct.

Chapter 3

Fat Body and Glia Secreted ECM Proteins Regulate Nutrient-Sensitive NSC Reactivation

3.1 Fat Body Derived Collagen IV Is Deposited on the Brain Surface and Controls NSC Reactivation

3.1.1 Fat Body Derived Collagen IV Is Necessary for NSC Reactivation

After a functional RNAi screen of fat body signal candidates, I decided to focus on *collagen IV^{vkg}* because its knockdown in the fat body resulted in an underdeveloped CNS and a moderate organismal growth defect. Decrease in the CNS size can be caused by a variety of factors, including death of neurons, glia, or NSCs, impaired NSC reactivation, or a disruption of NSC proliferation at later stages of larval development. I examined first instar larval CNS when *collagen IV^{vkg}* was knocked down in the fat body in order to distinguish among these possibilities. Since shmiR knockdown of *collagen IV^{vkg}* showed stronger phenotypes than knockdown with RNAi, and that knockdown at 29 ºC showed stronger phenotypes than at 25 ºC, all subsequent *collagen IV^{vkg}* knockdown experiments were performed using the shmiR strategy at 29 ºC. To further maximise knockdown efficiency, I used a fat body driver combination of Cg-GAL4 and Lpp-GAL4 (two copies of fat body GAL4). In addition, I decided to focus on *collagen IV^{vkg}* instead of *collagen IV^{cg25C}* for the analysis of Collagen IV's role in neural development. This is because the availability of *collagen IV^{vkg}* shmiR and protein trap constructs allowed for in-depth characterisation of Collagen IV.

I confirmed that fat body secreted Collagen IV^{Vkg} is required for NSC reactivation. Reactivation of quiescent NSCs starts with cell growth (enlargement), followed by mitosis. When *collagen IV^{vkg}* was knocked down in fat body using Cg-GAL4; Lpp-GAL4, NSCs failed to enlarge at 24 hph, similar to under starved conditions (Figure 3.1.1). Phosphohistone3 (PH3) marks mitosis, and showed no staining in VNC NSCs, indicating that no NSCs divided in the absence of fat body derived Collagen IV^{Vkg}. However, the numbers of NSCs in the VNC were normal compared to controls, which suggests that Collagen IV^{Vkg} controls NSC reactivation without affecting their survival.

In third instar larval brains, some NSCs in *collagen IV^{vkg}* knockdown larvae eventually reactivated but CNS underdevelopment was permanent. At 72 hph, NSCs from fat body *collagen IV^{vkg}* knockdown larvae remained small, and the number of dividing NSCs remained low (Figure 3.1.2). Because NSCs in the brain lobes and VNC were affected to similar degrees, I concentrated on the VNC for all subsequent analyses of Collagen IV^{Vkg}-dependent NSC reactivation. This is because the proximity of NSCs to the VNC surface makes them easier to quantify than their counterparts in the brain lobes.

To confirm the requirement of Collagen IV^{Vkg} for NSC reactivation, I examined a hypomorphic mutant of *collagen IV^{vkg}* that survives past the time window of NSC reactivation. The hypomorphic *collagen IV^{vkgK197}* line was generated by P-element insertion into the intronic region of the *collagen IV^{vkg}* locus (Yasothornsrikul *et al.* , 1997). As expected, the hypomorphic *collagen IV^{vkgK197}* showed severely reduced brain size and impaired NSC reactivation similar to fat body *collagen IV^{vkg}* knockdown conditions (Figure 3.1.3).

Previous studies showed that glial cells in the CNS serve as a NSC niche. They play a role in NSC reactivation by secreting local DIlps (*Drosophila* insulin-like peptides) (Chell & Brand, 2010; Sousa-Nunes *et al.* , 2011). To assess if there is any glial contribution of Collagen IV during NSC reactivation, I examined NSC enlargement and proliferation when *collagen IV^{vkg}* was knocked down in glial cells. NSC reactivation was unaffected (Figure 3.1.1). Therefore, these results suggest that Collagen IV from the fat body, but not from the glial cells, is required for NSC reactivation. This is consistent with a previous study showing that Collagen IV^{Vkg} in *Drosophila* is secreted centrally in the fat body and transported to peripheral organs (Pastor-Pareja & Xu, 2011).

Next, I tested whether fat body secreted Collagen IV is sufficient for rescuing NSC reactivation defects observed in the hypomorphic *collagen IV^{vkgK197}* mutants. Indeed, fat body specific mis-expression of Collagen IV^{Vkg} protein in the mutant larvae could partially rescue NSC enlargement and proliferation (Figure 3.1.3). Interestingly, Collagen IV^{Vkg} mis-expression in other tissues, including the glial cells (Repo-GAL4) and wing discs (Hh-

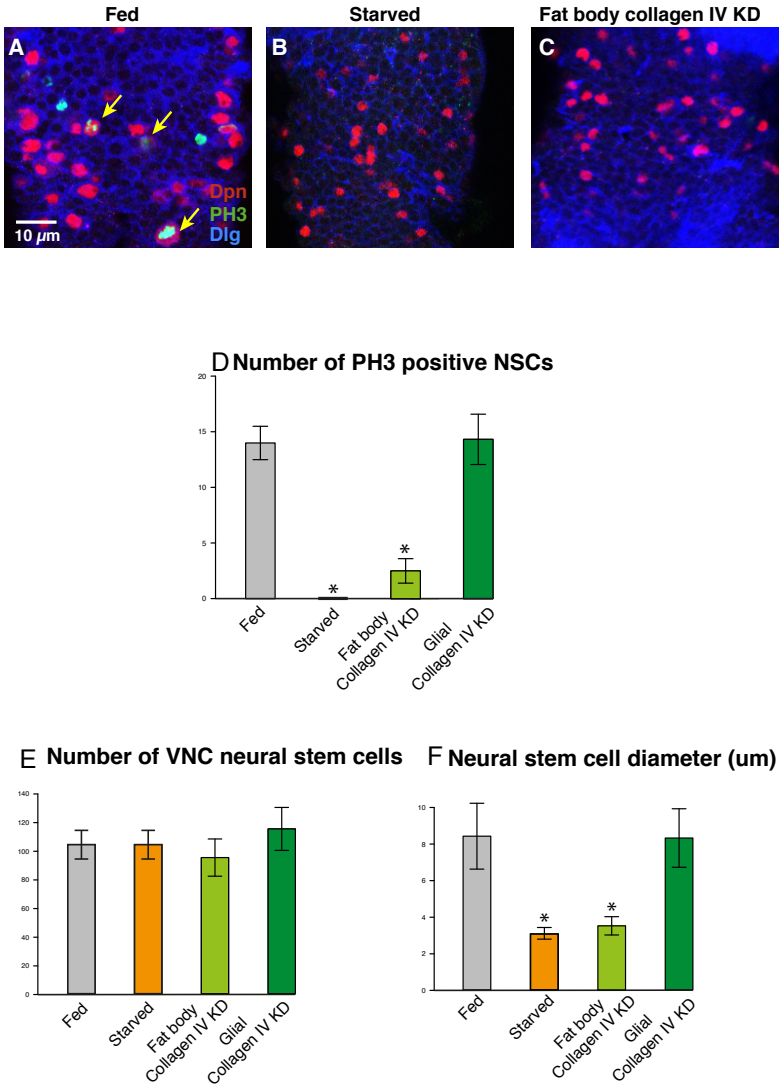

Fig. 3.1.1 Fat body-secreted Collagen IV is required for NSC reactivation. (A-C) Confocal images of NSC enlargement and proliferation under fed conditions (A), starved conditions (B), and fat body-specific knockdown of *collagen IV*^{vkg} (C, Cg-GAL4;Lpp-GAL4>UAS-*collagen IV*^{Vkg} shmiR). CNS were dissected 24–30 hph. Dpn in red marks NSC nuclei and PH3 in green marks mitotic M phase. Yellow arrows point to enlarged and dividing NSCs. (D) Quantification of NSC proliferation (number of PH3 positive NSCs in VNC +/- sd) under fed conditions, starved conditions, fat body knockdown of *collagen IV*^{vkg}, glial knockdown of *collagen IV*^{vkg} 24 hph (*P<0.05). (E-F) Quantification of NSC number and enlargement of above mentioned conditions. All experiments here and onwards that assess NSC reactivation defects at first instar stage were performed at 29 ºC

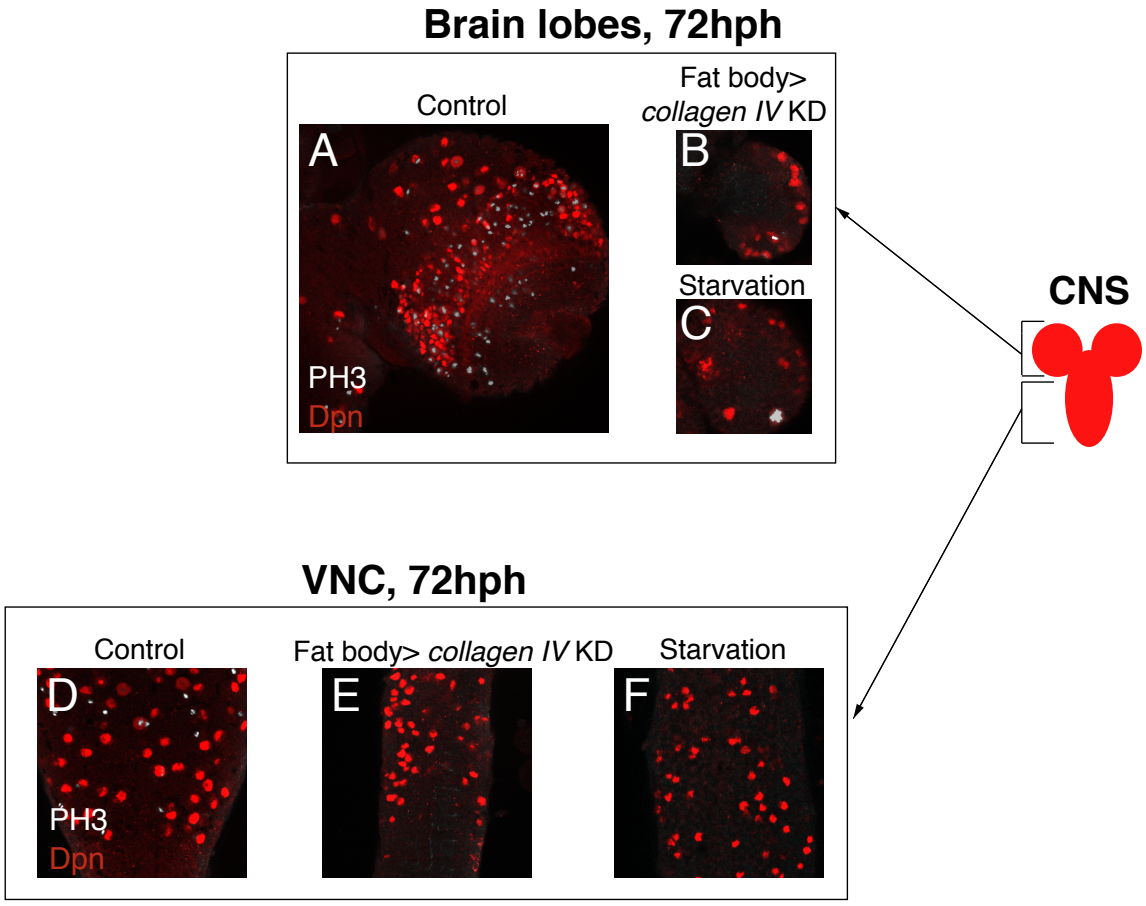

Fig. 3.1.2 Loss of Collagen IV^{Vkg} has a permanent impact on larval neurogenesis. (A-C) NSC proliferation in the brain lobes are severely impaired under fat body *collagen IV^{vkg}* knockdown conditions in third instar larvae. (D-F) Likewise, NSC proliferation in the VNC are also severely impaired.

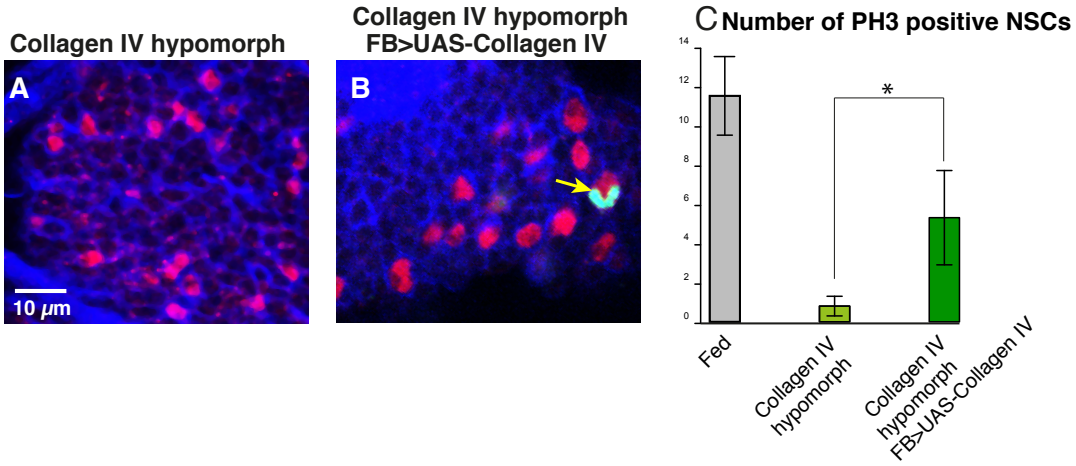

Fig. 3.1.3 Fat body secreted Collagen IV^{Vkg} can partially rescue NSC reactivation defects. (A-B) Confocal images of NSC proliferation in CNS from hypomorphic *collagen IV^{vkgK197}* mutant larvae (A) and in CNS from hypomorphic *collagen IV^{vkgK197}* mutant larvae in which *collagen IV^{vkg}* was mis-expressed in the fat body (B). Yellow arrows point to enlarged and dividing NSCs. (C) Quantification of NSC proliferation in VNC from hypomorphic *collagen IV^{vkgK197}* mutant larvae and in CNS from hypomorphic *collagen IV^{vkgK197}* mutant larvae in which Collagen IV^{Vkg} was mis-expressed in the fat body (*P$<$0.05).

GAL4), could not rescue NSC reactivation defects in *collagen IV^{vkgK197}* mutants (data not shown). In addition, I examined whether fat body Collagen IV^{Vkg} mis-expression under starved conditions could induce ectopic NSC reactivation. I expressed either Collagen IV^{Vkg} or Collagen IV^{Cg25C} alone, or the two together, in the fat body of starved larvae. I did not observe NSC reactivation under these circumstances, but fat body Collagen IV mis-expression led to elongated VNC (Figure 3.1.4). This in part resulted from increased neuronal volume as measured by the volume of Elav (a neuronal marker) staining using Volocity, but it remains to be examined whether this was due to increased neuronal survival or other factors (Figure 3.1.4).

Collagen IV is an important basement membrane component essential for maintaining tissue integrity. Therefore, one may suspect that NSC reactivation phenotype observed in fat body *collagen IV^{vkg}* knockdown conditions may result from a disruption of fat body cells and loss of fat body tissue. However, *collagen IV^{vkg}* knockdown in the fat body did not cause severe anatomical disruption of the fat body. Lipid droplets are still present, although they tend to be smaller than under wildtype conditions (Figure 3.1.5). Similar to starved conditions, fat body knockdown of *collagen IV^{vkg}* resulted in smaller fat body cells, but did not disrupt the integrity of fat body cells as shown by Phalloidin (a marker for F-actin) and

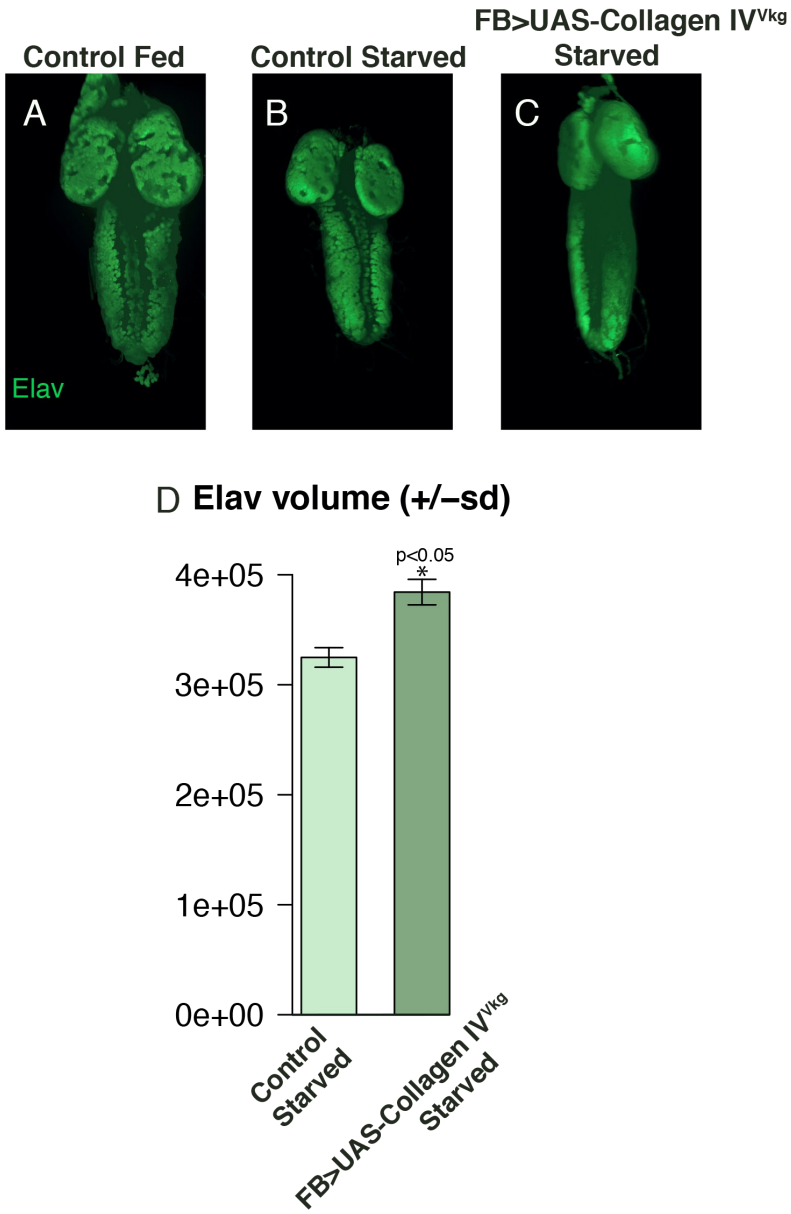

Fig. 3.1.4 Fat body misexpression of Collagen IV in starved larvae increased neuronal volume without causing ectopic NSC reactivation. (A-C) Confocal images of fed WT larvae, starved WT larvae, and starved WT larvae in which Collagen IV^{Vkg} protein was misexpressed in the fat body. Elav: neuronal marker. (D) Quantification CNS neuronal volume in starved WT larvae and starved WT larvae in which Collagen IV^{Vkg} was misexpressed in the fat body.

DAPI (a DNA marker) staining (Figure 3.1.5). I did not detect any difference in the shapes of either the cells or nuclei under the two conditions.

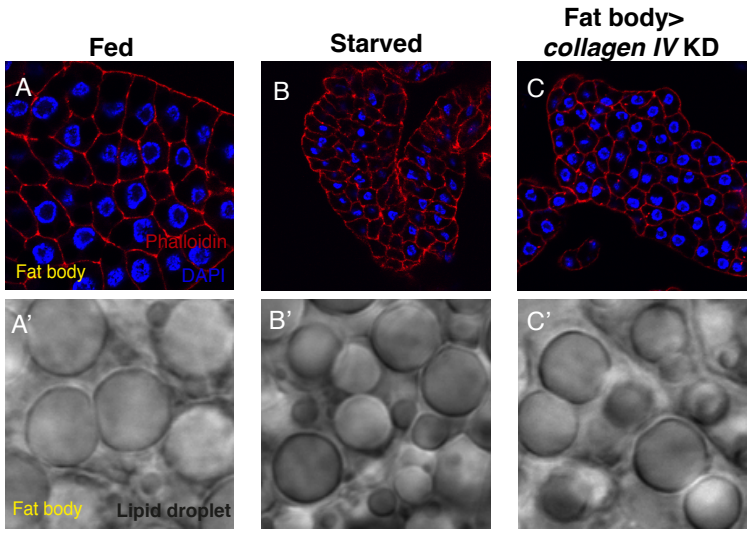

Fig. 3.1.5 Fat body *collagen IV^{vkg}* knockdown did not disrupt fat body tissue structure. (A-C) Membrane (Phalloidin) and DNA (DAPI) staining of fat body cells under fed (A), starved (B), and fat body *collagen IV^{vkg}* knockdown (C, Cg-GAL4; Lpp-GAL4> UAS-*collagen IV^{vkg}* shmiR) conditions. (A'-C') DIC images of lipid droplets in fat body cells under fed (A'), starved (B'), and fat body *collagen IV^{vkg}* knockdown (C', Cg-GAL4; Lpp-GAL4> UAS-*collagen IV^{vkg}* shmiR) conditions.

To verify that fat body Collagen IV expression is downstream of dietary amino acids intake, I disrupted Slif-TOR signalling in the fat body, which has been shown to mediate amino acid sensing in the fat body (Colombani *et al.* , 2003). The TSC complex serves as a negative modulator of TOR signalling pathway and may function via direct interactions with TOR or by blocking the access of TOR to their downstream target proteins (Abraham, 2002). In fat bodies expressing TSC1/2, Collagen IV^{Vkg} protein level was severely reduced as shown by diminished Collagen IV^{Vkg}-GFP staining (Figure 3.1.6).

Taken together, these results show that fat body secreted Collagen IV^{Vkg} is downstream of fat body amino acid sensing pathway, and it is necessary for NSC reactivation.

3.1.2 Collagen IV Could Travel From the Fat Body to the Brain and Its CNS Deposition Is Developmentally Regulated

The key regulator of NSC reactivation, *dIlp6*, shows strong transcriptional upregulation in the first 24 hph (Chell & Brand, 2010). I hypothesised that if Collagen IV^{Vkg} is indispensable for NSC reactivation, its deposition on the CNS surface may also increase during this

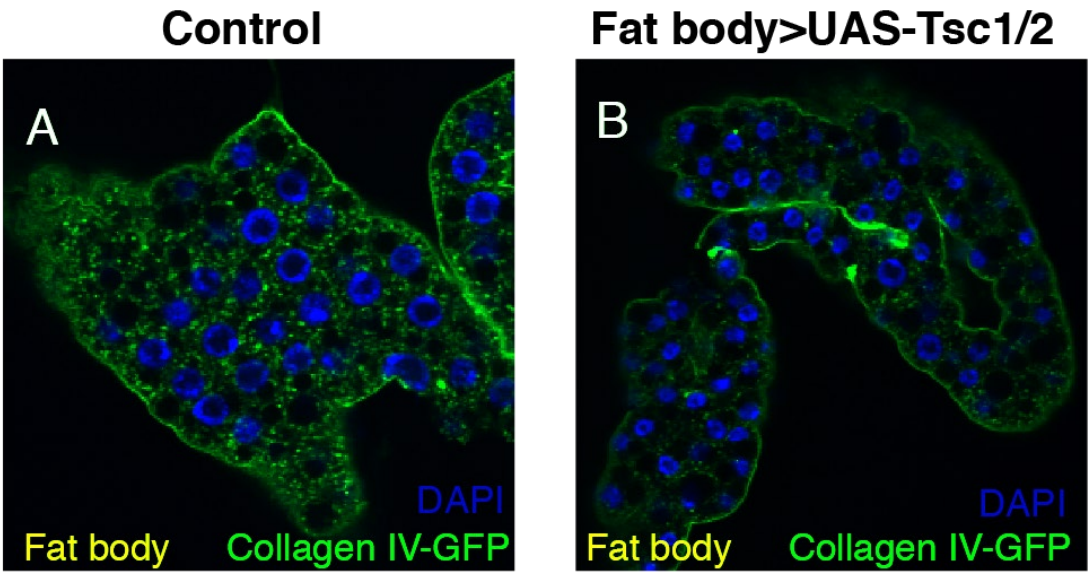

Fig. 3.1.6 Fat body Collagen IV^{Vkg} expression is mediated by Slif-TOR nutrient sensing pathway. (A-B) Collagen IV^{Vkg}-GFP and DNA (DAPI) staining in control fat body (A) and in fat body expressing TSC1/2 (B, Cg-GAL4; Lpp-GAL4>UAS-TSC1/2).

critical time window. Indeed, brains from newly hatched larvae showed very low level of Collagen IV^{Vkg} on their surface (Collagen IV^{Vkg} –GFP protein trap) (Figure 3.1.7). Collagen IV^{Vkg} protein level on the CNS increased rapidly after larval hatching, and at 24 hph, Collagen IV^{Vkg} formed a dense meshwork around the CNS (Figure 3.1.7). However, under starved conditions, Collagen IV^{Vkg} deposition on the brain was dramatically reduced. Therefore, the abundance of Collagen IV^{Vkg} on the brain surface also depends on dietary amino acid intake.

Since fat body secretes Collagen IV^{Vkg} (Pastor-Pareja & Xu, 2011), I decided to test if Collagen IV^{Vkg} directly travels to, and deposits on the CNS, or whether it requires the aid of other modulators from the hemolymph (e.g. hemocytes) as suggested by a previous study (Pastor-Pareja & Xu, 2011). To distinguish between these two possibilities, I performed *ex vivo* tissue co-culture experiment of larval CNS and fat body explants to visualise the deposition of Collagen IV^{Vkg} on the CNS (Figure 3.1.7). Wildtype CNS from newly hatched larvae were co-cultured with fat body from third instar Collagen IV^{Vkg}-GFP larvae that were fed a normal diet. Since the fat body tends to float on the surface of the culture medium and larval CNS tends to sink, there was minimal physical contact between the two tissues during the co-culture experiment. In addition, fat bodies were rinsed in PBS to minimise the contamination with other hemolymph factors, in particular the hemocytes. Collagen IV^{Vkg} -GFP could be detected on the brain surface 24 hours post-culture. This suggests that

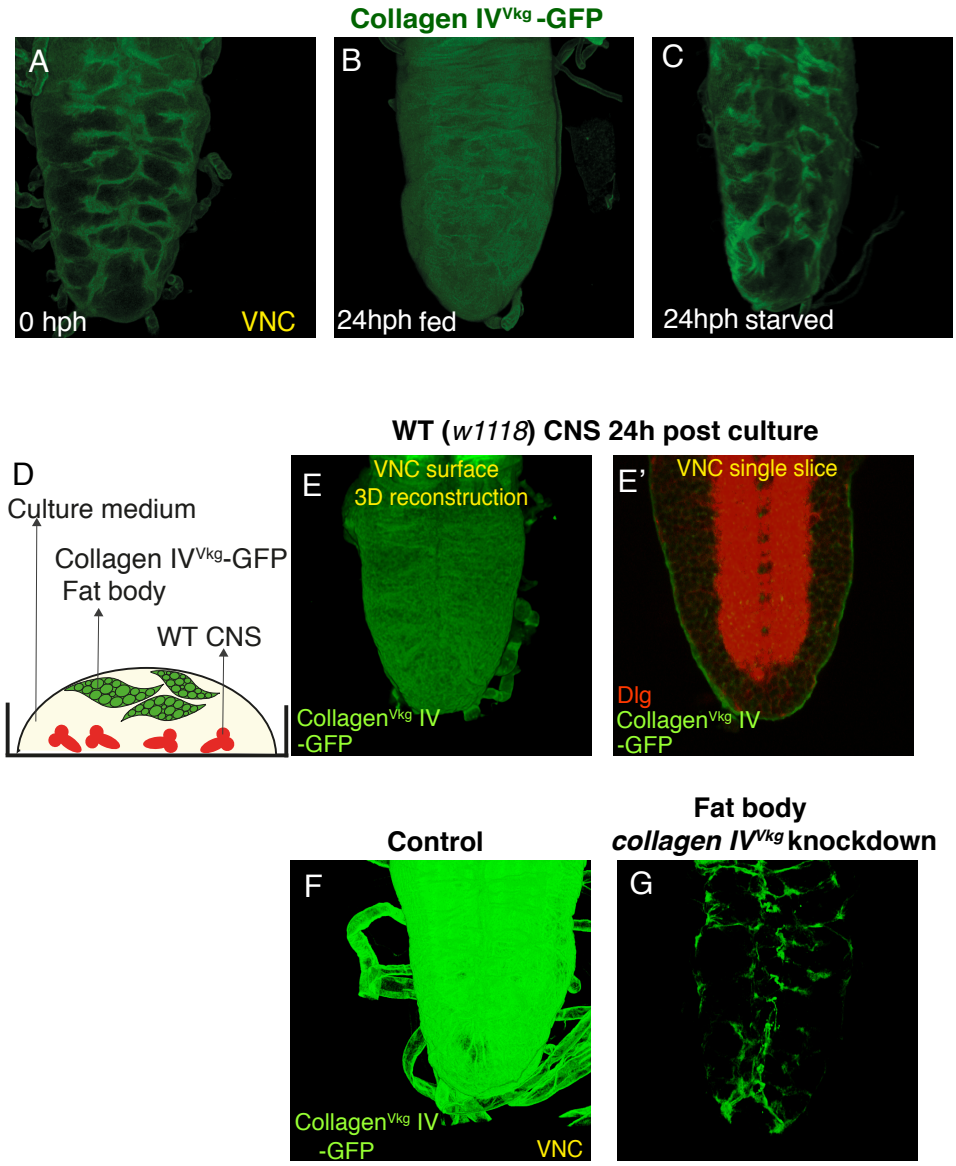

Fig. 3.1.7 Collagen IV deposition on the CNS is developmentally regulated and it acts as a direct humoral link between the fat body and the CNS. (A-C) Collagen IV^{Vkg} deposition on the CNS surface (Collagen IV^{Vkg}-GFP VNC surface staining 3D reconstruction) just after larval hatching (A), 24 hph under fed conditions (B), and 24 hph under starved conditions (C). (D-E) A explant culture system was set up to investigate whether Collagen IV^{Vkg} from the fat body can travel to and deposit on the CNS surface. CNS from just hatched wild type larvae (no endogenous Collagen IV^{Vkg}-GFP expression) were co-cultured with fat body isolated from wandering third instar Collagen IV^{Vkg}-GFP protein trap larvae in supplemented Schneider medium (D). Fat bodies were rinsed in PBS to minimise the presence of other hemolymph factors in the culture. Anti-GFP staining on wild type CNS were visualised 24 hours post culture. Both Collagen IV^{Vkg}-GFP VNC surface 3D reconstruction (E) and single VNC slice (E') show accumulation of GFP on the CNS surface. (F-G) Anti-GFP 3D reconstruction of Collagen IV^{Vkg}-GFP VNC (F), and of VNC from a Collagen IV^{Vkg}-GFP larvae in which Collagen IV^{Vkg} was knocked down in the fat body (G).

Collagen IV^{Vkg} deposition onto the CNS surface can be direct, and it either does not require, or requires minimal assistance of hemolymph factors.

Glial subtype TaDa transcriptional profiling showed that *collagen IV^{vkg}* is also transcribed by the perineurial glia during the time window of NSC reactivation (see Chapter 6, Figure 6.2.9). In order to confirm that fat body makes the major contribution to Collagen IV^{Vkg} proteins on the CNS surface, I examined Collagen IV^{Vkg} deposition *in vivo*. When *collagen IV^{vkg}* was knocked down in the fat body using shmiR in a Collagen IV^{Vkg}-GFP protein trap larvae, I observed a dramatic reduction of Collagen IV^{Vkg}-GFP on the brain surface. This experiment showed that the Collagen IV^{Vkg} on the CNS surface predominantly originates from the fat body. Moreover, this experiment validated that the shmiR construct against *collagen IV^{vkg}* is highly effective (Figure 3.1.7).

Earlier, I showed that fat body Collagen IV^{Vkg} expression is downstream of amino acid-sensitive Slif-TOR signalling. Does impairment of fat body Slif-TOR signalling directly affect the abundance of Collagen IV^{Vkg} protein on the CNS surface? Indeed, Collagen IV^{Vkg} deposition on the CNS was substantially reduced when TSC1/2 was expressed in the fat body (Figure 3.1.8).

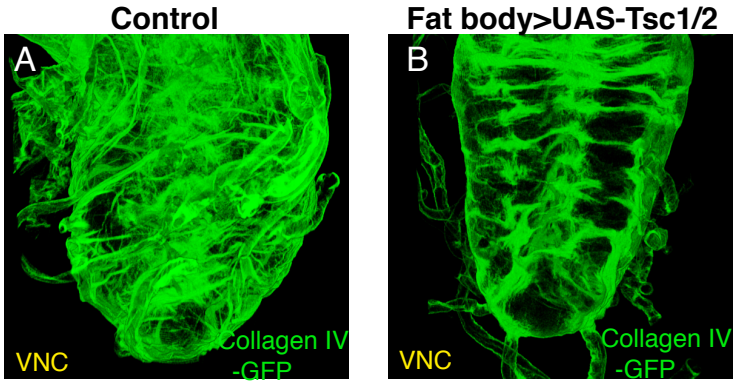

Fig. 3.1.8 CNS Collagen IV deposition is sensitive to Slif-TOR nutrient sensing pathway in the fat body. (A-B) Anti-GFP VNC surface 3D reconstruction of Collagen IV^{Vkg}-GFP CNS (C) and of Collagen IV^{Vkg}-GFP CNS from larvae mis-expressing TSC1/2 in the fat body (D, Cg-GAL4; Lpp-GAL4>UAS-TSC1/2).

Taken together, Collagen IV^{Vkg} is required for NSC reactivation as *collagen IV^{vkg}* knockdown in the fat body led to impaired NSC enlargement and division. Furthermore, Collagen IV^{Vkg} deposition on the CNS is strongly upregulated during the time window of NSC reactivation. *In vitro* tissue co-culture experiment confirmed that Collagen IV acts as a direct humoral link between the fat body and the brain.

3.1.3 Collagen IV Deposition on the CNS Is Responsive to Nutritional Fluctuation During Larval Life Beyond NSC Reactivation Context

My data showed that the secretion and deposition of Collagen IV on the CNS surface are tightly regulated during development and in response to nutrition. This raises the question of whether Collagen IV secretion/deposition remains sensitive to nutritional inputs during later larval development. For example, although Collagen IV deposition on the CNS after larval hatching depends on the organism's amino acid intake, it is not clear whether this dependence is only relevant for the time window of NSC reactivation, or whether it holds true during later stages of development past the reactivation time window. To address this question, I first fed larvae for 24 hours on a normal diet so that the majority of NSCs started to reactivate, and subsequently transferred them to sucrose solution. I wanted to examine that once Collagen IV deposited on the brain surface after feeding, whether this process could still respond to nutritional alterations, or whether Collagen IV continues to deposit on the CNS irrespective of nutrition once the critical time window of NSC reactivation has passed.

In larvae that were initially fed standard laboratory food, NSCs fully enlarged and Collagen IV^{Vkg} coated the most of the brain's surface area. However, there were still areas that were visibly deficient in Collagen IV^{Vkg} coating, especially in the abdominal part of the VNC. If larvae continued to feed, brain surface Collagen IV^{Vkg} deposition would have continued to increase and Collagen IV^{Vkg} would have covered the entire VNC after another approximately 12 hours. However, after larvae were transferred to starvation medium, no further deposition was observed beyond the level already achieved during the first 24 hours of feeding. This indicates that Collagen IV^{Vkg} deposition halted in response to starvation.

In the second experiment, I wanted to assess whether larvae that are starved for a prolonged period of time retain their ability to secrete Collagen IV^{Vkg} and reactivate their NSCs in response to feeding. I first starved larvae for 72 hours immediately after larval hatching, and then transferred them back to standard laboratory food. NSCs remained small and Collagen IV^{Vkg} covered only a small portion of the CNS surface after 72 hours of starvation. When larvae were transferred to standard laboratory food, I observed visible increase in Collagen IV^{Vkg} deposition after 24 hours of re-feeding. After 48 hours of feeding, Collagen IV^{Vkg} completely covered the CNS surface. NSCs also started to reactivate: after 48 hours of feeding, NSCs fully enlarged. Therefore, prolonged starvation for as long as 3 days after larval hatching did not impair the larvae's ability to secreted/deposit Collagen IV^{Vkg} onto

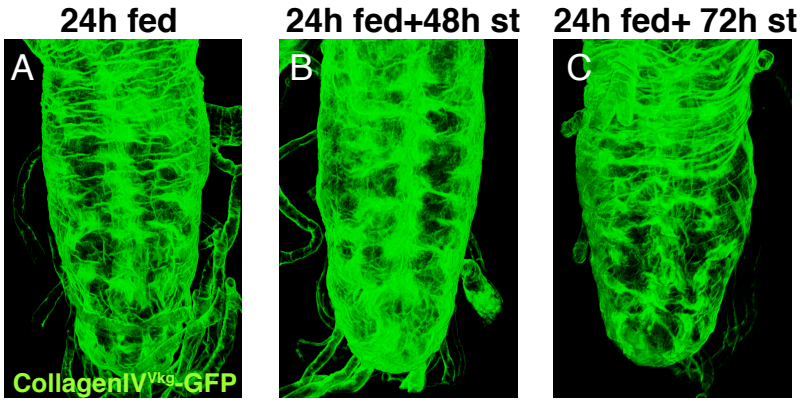

Fig. 3.1.9 Collagen IV deposition is responsive to nutritional fluctuation past the NSC reactivation time window. (A-C) Collagen IV^{Vkg} deposition on the VNC (Collagen IV^{Vkg}-GFP protein trap) in larvae fed a normal diet for 24 hours, and in larvae initially fed for 24 hours but suffered prolonged starvation afterwards.

the CNS surface and reactivate their NSCs.

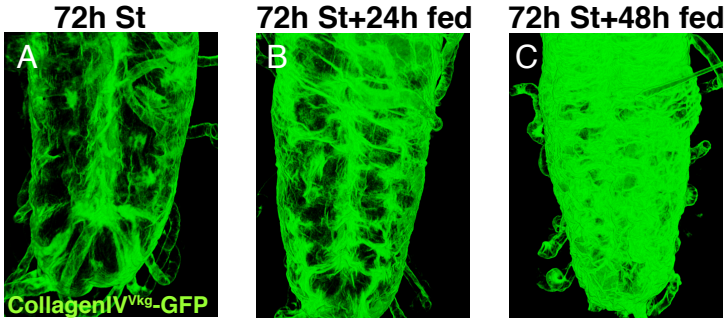

Fig. 3.1.10 Prolonged starvation does not impair fat body's ability to deposit Collagen IV on the CNS. (A-C) Collagen IV^{Vkg} deposition on the VNC (Collagen IV^{Vkg}-GFP protein trap) in larvae starved for 72 hours, and in larvae initially starved for 72 hours but fed a normal diet afterwards.

Taken together, I have shown that fat body secreted Collagen IV is necessary for NSC reactivation. Collagen IV can travel directly from the fat body to deposit on the CNS surface, both *in vitro* and *in vivo*. The deposition is highly sensitive to nutritional inputs both during and beyond the time window of NSC reactivation.

3.2 The ECM Protein, Perlecan^{Trol} From BBB Glia, Is Required for NSC Reactivation

3.2.1 CNS Deposition of Perlecan^{Trol} Is Nutrition-Dependent, and It Follows Spatial Temporal Pattern as Collagen IV^{Vkg}

So far, I uncovered a novel role of fat body derived ECM protein, Collagen IV, in regulating nutrient-sensitive NSC reactivation. This discovery led me to examine another ECM protein, Perlecan^{Trol}. *Perlecan^{trol}* encodes a heparan sulfate proteoglycan (HSPG) and is highly conserved in *Drosophila* and mammals (Park *et al.* , 2003; Voigt *et al.* , 2002). It is an important component of the ECM that interacts with other ECM proteins, growth factors and receptors, to regulate cellular signalling (Lin, 2004a). In *perlecan^{trol}* null mutants, NSC reactivation is severely impaired: NSCs enlarge, but never enter their first S phase (Datta, 1995). Null mutations in *hedgehog* (*hh*) and *branchless* (*bnl*, an FGF homologue) dominantly enhance the impairment in NSC proliferation in a sensitised *perlecan^{trol}* mutant background, suggesting that Perlecan^{Trol} may regulate NSC reactivation by modulating Hh and FGF signalling pathways (Park *et al.* , 2003). Since there is evidence that Collagen IV^{Vkg} and Perlecan^{Trol} can function antagonistically to maintain organ shape in *Drosophila* (Pastor-Pareja & Xu, 2011), I investigated whether the two ECM proteins also interact in the context of NSC reactivation.

I first characterised the temporal expression pattern of Perlecan^{Trol} using a Perlecan^{Trol}-GFP protein trap line (Medioni & Noselli, 2005). I found that similar to Collagen IV^{Vkg}, Perlecan^{Trol} deposition on the CNS also increased significantly after larval hatching, during the time window of NSC reactivation. By 30 hph, Perlecan^{Trol}-GFP formed a dense meshwork around the CNS surface (Figure 3.2.1). Interestingly, when larvae were deprived of dietary amino acids, Perlecan^{Trol}-GFP deposition was reduced, in a fashion similar to Collagen IV^{Vkg}.

3.2.2 CNS Perlecan^{Trol} Predominantly Derives From the Glial Cells

Prior to the present study, it is unclear where Perlecan^{Trol} on the CNS originates from and whether its expression is downstream of dietary amino acid intake (Britton & Edgar, 1998). A previous study suggested that Perlecan^{Trol} is produced in the fat body and deposits on peripheral tissues (Pastor-Pareja & Xu, 2011). In support of this, Perlecan^{Trol} has been found to circulate in the hemolymph (Handke *et al.* , 2013). Other studies speculated glial

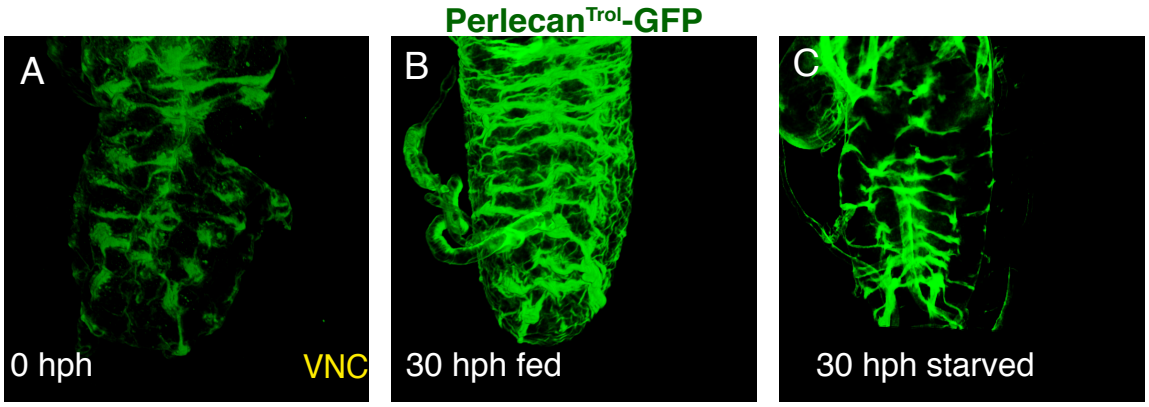

Fig. 3.2.1 Perlecan^{Trol} deposition on the CNS follows similar spatial-temporal pattern as Collagen IV^{Vkg}. (A-C) Confocal images of Perlecan^{Trol} deposition on the CNS surface (Perlecan^{Trol}-GFP protein trap CNS surface staining 3D reconstruction) just after larval hatching (A), 30 hph under fed conditions (B), and 30 hph under starved condition (C).

cells are the source of CNS Perlecan^{Trol} (Lindner *et al.* , 2007). Interestingly, the TaDa transcriptional profiling in glia and fat body showed strong *perlecan^{trol}* transcription in both tissues during the time window of NSC reactivation (Table 3.2.1). Therefore, similar to the DIlps, Perlecan^{Trol} also exists as part of a systemic and a local pool.

To examine the origin of Perlecan^{Trol} on the CNS, I knocked down the expression of the Perlecan^{Trol}-GFP protein trap by targeted RNAi against GFP (iGFPi) (Pastor-Pareja & Xu, 2011) (Figure 3.2.2). Whereas iGFPi driven in the gut (Esg-GAL4) and imaginal discs (Hh-GAL4) did not affect Perlecan^{Trol}-GFP levels on the CNS surface (data not shown), iGFPi in the glial cells (Repo-GAL4) resulted in a severe reduction, and iGFPi in the fat body caused a moderate reduction (Figure 3.2.2). I also confirmed *perlecan^{trol}* transcription in the CNS using Q-PCR. *perlecan^{trol}* transcription showed a strong peak immediately after larval hatching, and sustained transcription throughout larval life (Figure 3.2.3).

Next, I assessed whether Perlecan^{Trol} originating from the glial cells is essential for NSC reactivation. When *perlecan^{trol}* was knocked down in the fat body, NSCs enlarged and entered mitosis as normal (wildtype number of PH3-positive NSCs; Figure 3.2.4). However, when *perlecan^{trol}* was knocked down in glial cells, NSC cell cycle re-entry was delayed (Figure 3.2.4), although NSC enlargement was normal as was the number of NSCs. Therefore, Perlecan^{Trol} produced by glial cells is necessary for efficient reactivation of NSCs, whereas fat body-derived Perlecan^{Trol} is not.

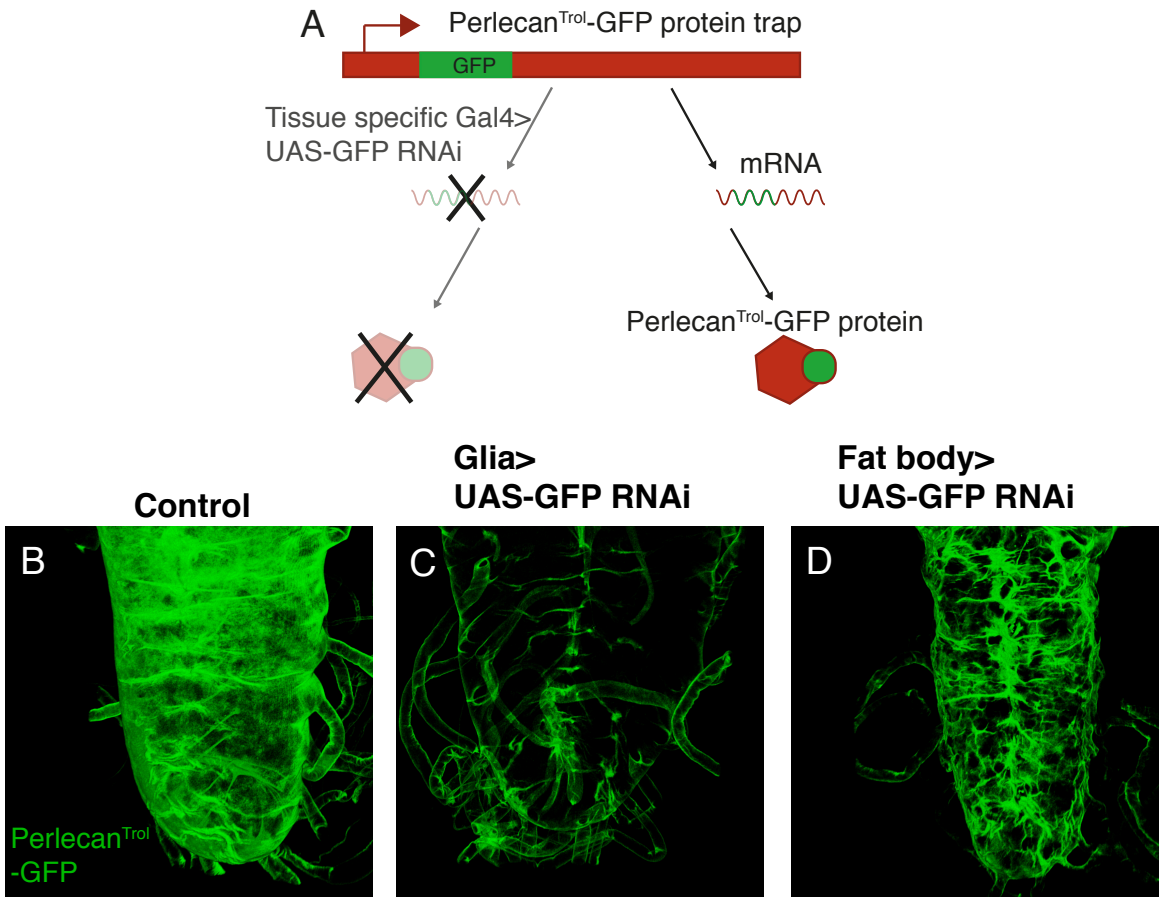

Fig. 3.2.2 Investigation of the origin of CNS Perlecan^{Trol} using iGFPi method. (A) A schematic of iGFPi (*in vivo* GFP interference) method (Pastor-Pareja and Xu, 2011) for determining the source of Perlecan^{Trol} on CNS surface in first instar larvae. A GFP protein trap inserted into the Perlecan^{Trol} locus produces a functional and GFP-tagged Perlecan^{Trol}. Tissue-specific contribution of CNS surface Perlecan^{Trol} can be assessed by knocking down GFP (UAS-GFP RNAi) under tissue-specific GAL4 drivers and subsequently examining the reduction of GFP intensity on the CNS surface. (B-D) Perlecan^{Trol} deposition on the CNS when iGFPi was driven in the glia or fat body.

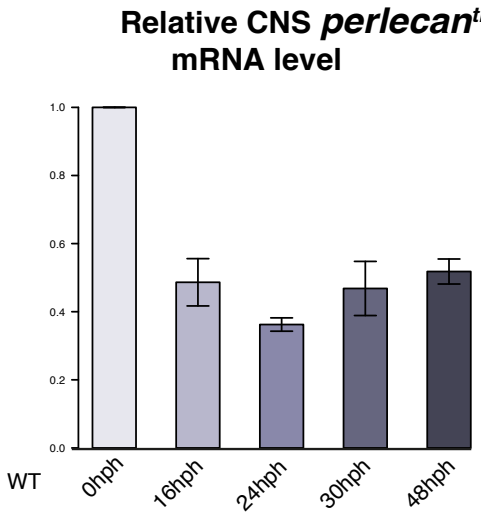

Fig. 3.2.3 Transcription of CNS *perlecan^{trol}* in first and second instar larvae. Q-PCR analysis of CNS *perlecan^{trol}* transcripts level in wild type larvae under fed conditions. Q-PCR was performed on RNA extracted from CNS of wild type (w1118) larvae at 0, 16, 24, 30,and 48 hph at 25 ºC. Values are normalised to 0 hph condition. Error bar=sd, *P$<$0.05.

3.2.3 Perlecan^{Trol} Is Required From the Perineurial Glia and Its Transcription Is Controlled by Nutrition

NSCs are isolated from the hemolymph by the BBB, which is comprised of two glial cell populations: the subperineurial glia (inner layer) and the perineurial glia (outer layer) (Figure 3.2.5) (Stork *et al.* , 2012). Septate junctions form between subperineurial glial cells creating a physical barrier. The outermost perineurial glia are less well characterised, but are hypothesised to mediate signalling from the hemolymph to the CNS due to their location at the interface between the two (Stork *et al.* , 2008). The third population of glial cells, the cortex glia, are located between NSCs, beneath the BBB. Cortex glia have a similar structure to mammalian astrocytes and may provide trophic support for the surrounding NSCs (Freeman & Doherty, 2006b).

To identify which of these glial subtypes secretes Perlecan^{Trol}, I first performed TaDa transcriptional profiling (Southall *et al.* , 2013), of the different glial subtypes using subtype-specific GAL4 drivers (see Chapter 8 for GAL4 drivers used). I found that *perlecan^{trol}* is transcribed in the perineurial glia during NSC reactivation, but not in the subperineurial or cortex glia (Figure 3.2.6). In addition, expression of Perlecan^{Trol}-GFP protein trap and a membrane marker under a subperineurial glia specific GAL4 driver revealed that the

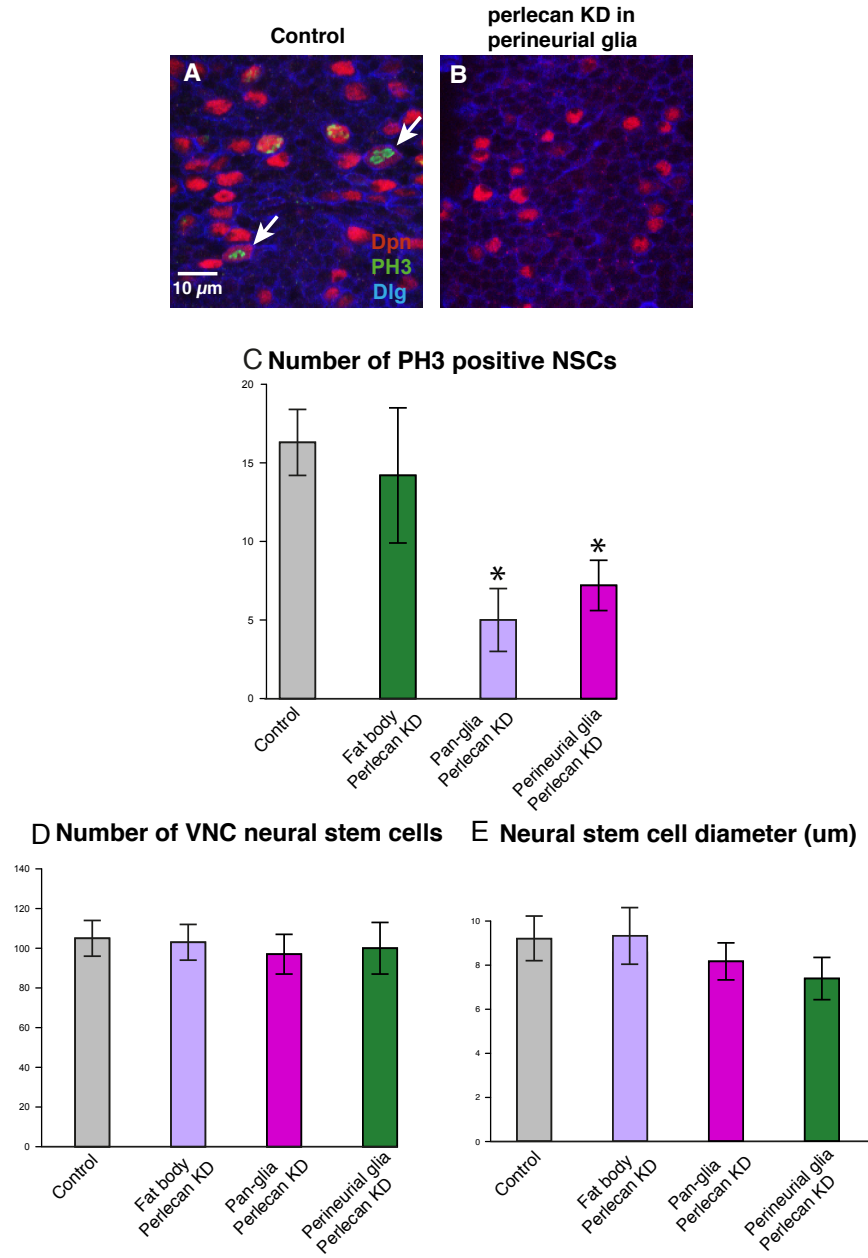

Fig. 3.2.4 BBB glia-derived Perlecan^{Trol} regulates NSC reactivation. (A-D) Confocal images of NSC enlargement and proliferation under fed conditions (A), fat body knockdown of *perlecan^{trol}* (B, Cg-GAL4; Lpp-GAL4> UAS-*perlecan^{trol}* shmiR), pan-glial knockdown of *perlecan^{trol}* (C, Repo-GAL4>UAS-*perlecan^{trol}* shmiR), and perineurial glia knockdown (D, NP6293-GAL4>UAS-*perlecan^{trol}* shmiR) 24 hph. Dpn in red marks NSC nuclei and PH3 in green marks mitotic M phase. Yellow arrows point to dividing NSCs. (E) Quantification of NSC proliferation (number of PH3 positive NSCs in VNC +/- sd) under above mentioned (A-D) conditions ($P<0.05$). (F-G) Quantification of NSC number and diamter under above mentioned (A-D) conditions.

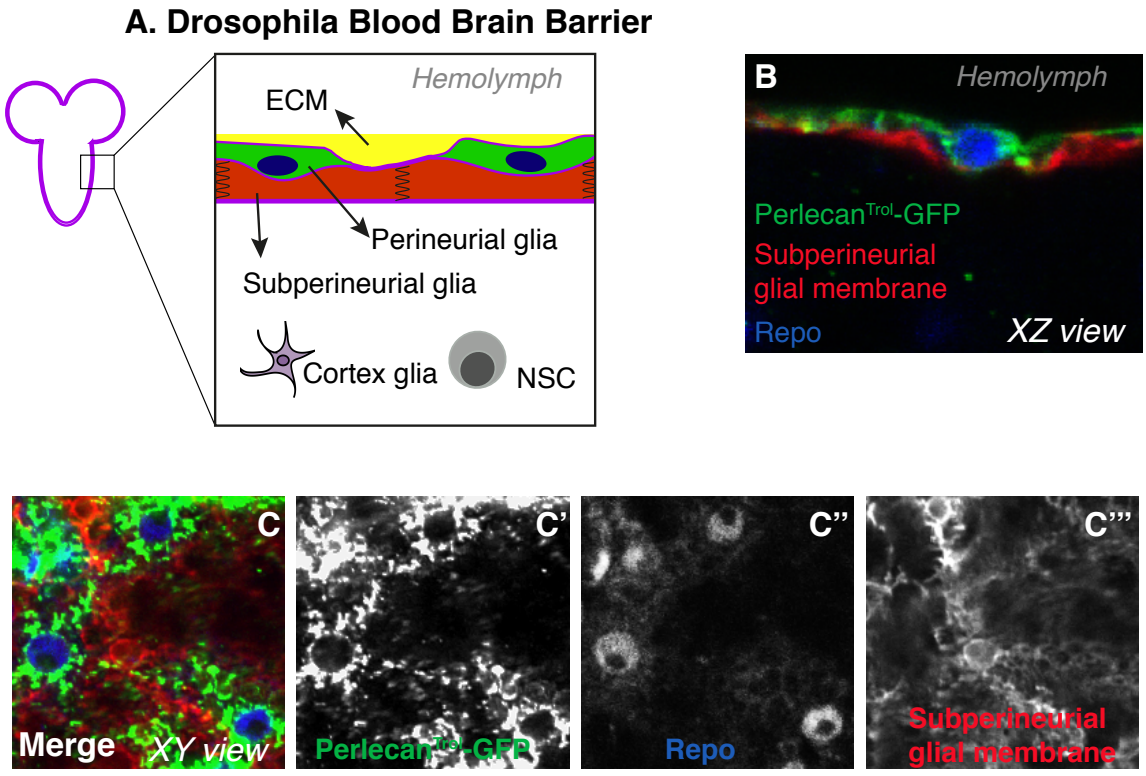

Fig. 3.2.5 Perlecan^{Trol}-GFP protein trap reveals Perlecan expression by the perineurial glia. (A) Cross-section schematic of VNC shows the NSCs and their glial niche, including the cortex glia, subperineurial glia, perineurial glia, and the extracellular matrix. The *Drosophila* BBB consists of perineurial and subperineurial glia. (B) XZ view of a confocal image of a single perineurial glia cell expressing Perlecan^{Trol}. Perlecan^{Trol}-GFP is in green and the underlying subperineurial glia membrane (Moody-GAL4>UAS-mCD8 RFP) is in red. Repo in blue marks glial nuclei. (C) XY view of a confocal image of perineurial glia cells expressing Perlecan^{Trol}, as visualised by Perlecan^{Trol}-GFP protein trap.

Perlecan-expressing glial cells are on the CNS surface (Figure 3.2.5, see XY view) above the subperineurial glia layer (Figure 3.2.5, see XZ view). Since perineurial glial cells are the only cell type apical to the subperineurial glia, the identity of this population of Perlecan^{Trol}-expressing glial cells can be ascertained to be perineurial glia.

Furthermore, glial transcription of *perlecan^{trol}* is dependent on nutrition: *perlecan^{trol}* transcription is down regulated in starved larvae in glial cells but not in fat body (Figure 3.2.7 and Table 3.2.1). Q-PCR analysis of brain extracts from fed and starved animals confirmed the nutritional dependence of *perlecan^{trol}* transcription (Figure 3.2.7). Next, I knocked down *perlecan^{trol}* specifically in perineurial glia. This resulted in a delay of cell cycle re-entry without affecting NSC enlargement or survival (Figure 3.2.4). Taken together our results show that, whereas both the fat body and glial cells secrete Perlecan^{Trol} that can be deposited on the CNS surface, perineurial glia-derived Perlecan^{Trol} is responsible for regulating nutrition-dependent NSC reactivation.

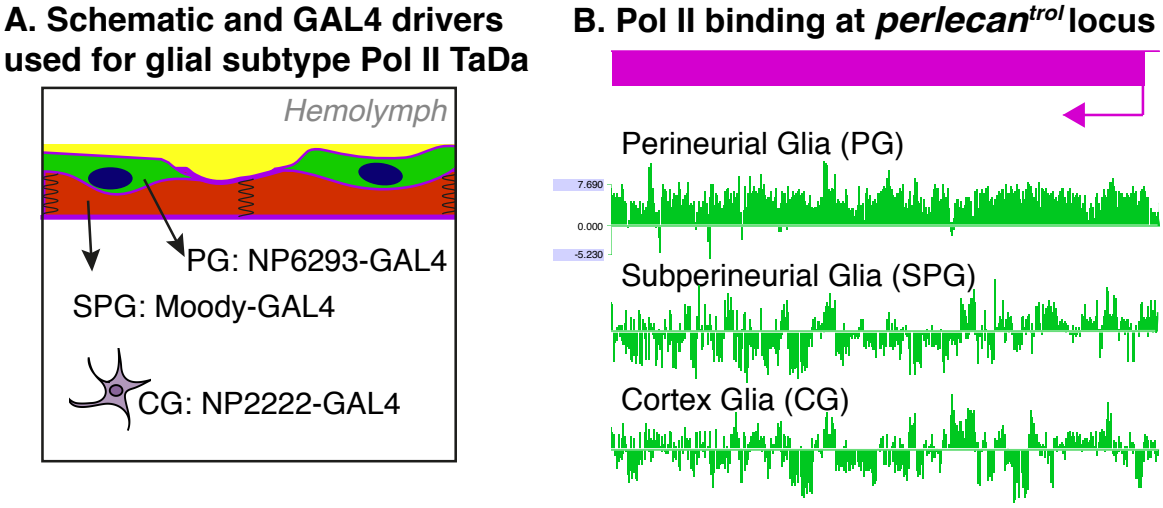

Fig. 3.2.6 Glial subytpe TaDa transcriptional profiling confirmed perineurial glial origin of Perlecan^{Trol}. (A) Glial subtype GAL4 drivers used for TaDa transcriptional profiling experiments. (B) Pol II occupancy traces across *perlecan^{trol}* locus in the three glial subtypes.

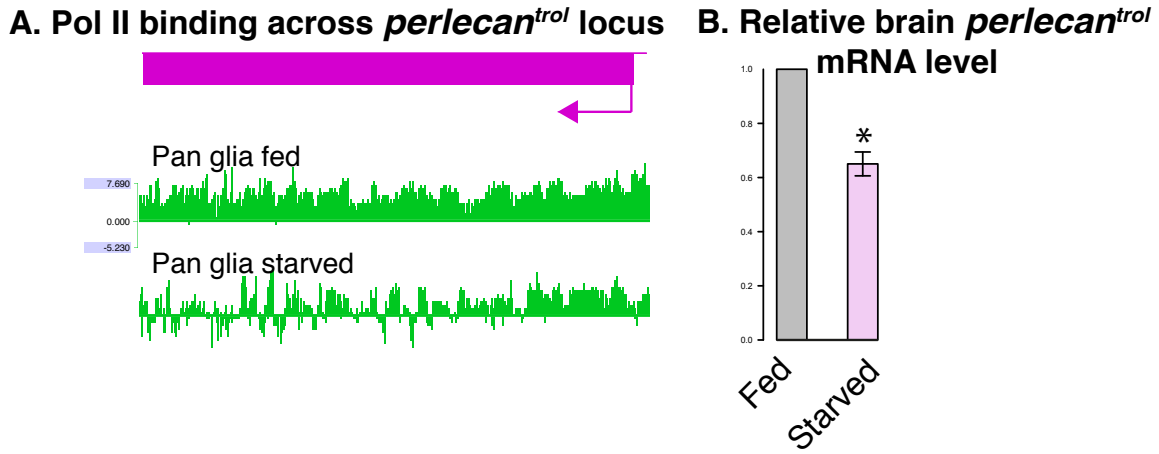

Fig. 3.2.7 Transcription of *perlecan*^{trol} is regulated by nutrition. (A) Pan-glial Pol II occupancy traces across *perlecan*^{trol} locus under fed and starved conditions. (B) Q-PCR experiment confirmed the transcriptional regulation of *perlecan*^{trol} by nutrition.

Table 3.2.1 Summary of Pol II binding intensity (Log2 scale) at Perlecan locus in glia and fat body, under fed and starved conditions

Condition	Glia_Log2 Ratio	Fat body_Log2 Ratio
Fed	1.35	1.96
Starved	0.32	1.48

3.3 Collagen IV Co-Localises With Perlecan^{Trol} and Recruits Perlecan^{Trol} to the CNS Surface

3.3.1 ECM Proteins Interact With Both Populations of the BBB Glia

Previously, I showed that both Collagen IV^{Vkg} and Perlecan^{Trol} are important for dietary amino acid-dependent NSC reactivation, and they both deposit on the BBB. I decided to further characterise their relationship with each other and their interaction with the glial niche in order to gain insights into the mechanisms by which the ECM proteins regulate NSC proliferation.

The BBB consists of two glial subtypes of perineurial glia and subperineurial glia. Which glial subtype is responsible for transducing signals from the hemolymph to the interior of the brain via interaction with ECM proteins? In order to observe ECM proteins' deposition on the BBB, I took advantage of DeltaVision-OMX super resolution imaging system (Applied Precision), which has a XY resolution of 120 nm and Z resolution of 300 nm (http://api.gehealthcare.com/api/deltavision-omx.asp).

The outermost layer of perineurial glia may seem a more feasible glial cell type for direct ECM interaction. However, a closer investigation of the CNS surface structure during early larval life revealed that subperineurial glia may also participate in ECM binding. From 0 to 24 hph (time window of NSC reactivation), perineurial glia undergoes rapid proliferation, but their membranes are only able to partially cover the CNS by 24 hph, leaving patches of the subperineurial glia apical surface directly exposed to the ECM and hemolymph during the NSC reactivation time window (Figure 3.3.1). Perineurial glia completely seal the CNS surface at about 40 hph. Interestingly, although perineurial glia proliferation was observed in the first 24 hph under starvation conditions, the sealing would not occur if larvae were starved (Figure 3.3.1). I hypothesise that the exposure of both perineurial glial and subperineurial glial apical surface to ECM proteins may be functionally important for glial insulin expression/secretion, which will be discussed in detail in Chapter 3.4.

OMX images showed that subperineurial glia are closely associated with the ECM layer (Figure 3.3.2). Some parts of subperineurial glia's apical membrane clearly abuts Collagen IV^{Vkg}, whereas in other places considerable gaps were observed between the subperineurial glia membrane and Collagen IV^{Vkg} (Figure 3.3.2). The gaps are most likely due to the presence of perineurial glia situated in between ECM and the subperineurial glia. OMX images of peirneurial glia membrane and Collagen IV^{Vkg}-GFP showed that Collagen IV^{Vkg} directly abuts the apical surface of the perineurial glia (Figure 3.3.3). No Collagen IV^{Vkg}

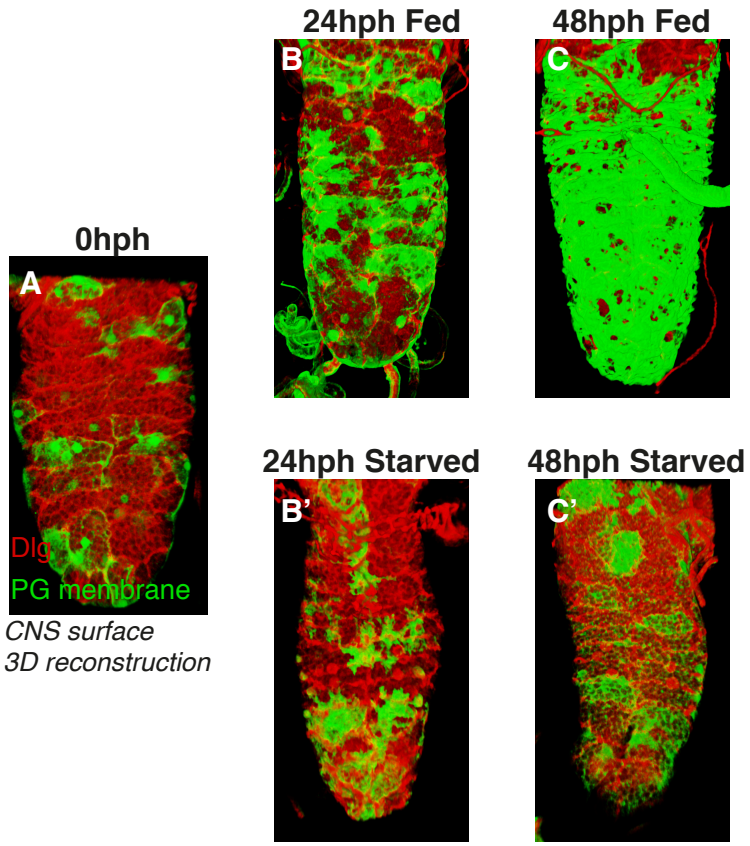

Fig. 3.3.1 Temporal pattern and nutritional dependence of perineurial glia proliferation. (A) Limited CNS enwrapment of perineurial glia immediately after larval hatching. (B-C) Gradual increase of CNS perineurial glia coverage if larvae were fed dietary amino acids. (B'-C') Impaired CNS perineurial glia coverage if larvae were starved.

staining was observed to cross the BBB, or to exist between the two glial layers (i.e. on the basal side of the perineurial glia membrane). I observed the same patterns at the VNC channels which are the invaginations formed by the apical surface of the BBB glia along the midline of VNC.

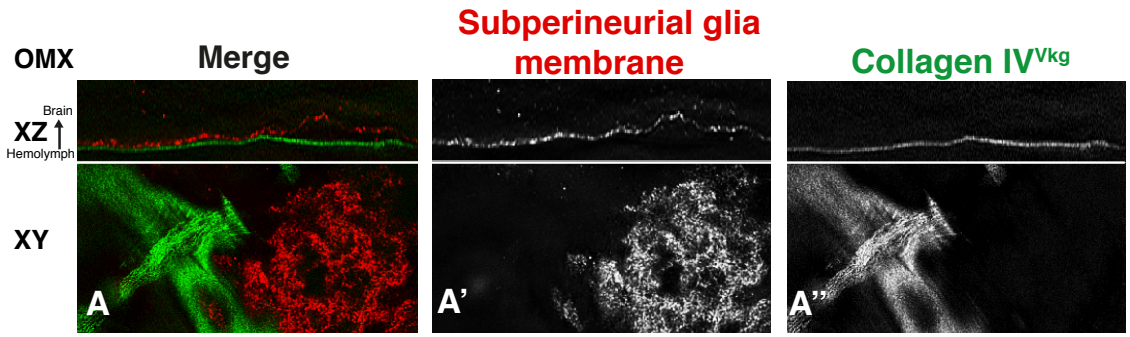

Fig. 3.3.2 Localisation of Collagen IV^{Vkg} with respect to subperineurial glia. (A) DeltaVision-OMX images (both XY and XZ view) of Collagen IV^{Vkg} (Collagen IV^{Vkg} –GFP protein trap) and subperineurial glia membrane.

3.3.2 Collagen IV^{Vkg} and Perlecan^{Trol} Co-Localise at the BBB

Perlecan^{Trol} is produced locally by the perineurial glia and Collagen IV^{Vkg} is produced remotely by the fat body. How are they deposited with respect to each other on the BBB? OMX image revealed close co-localisation of Collagen IV^{Vkg} and Perlecan^{Trol}. Surprisingly, the locally derived Perlecan^{Trol} was deposited further apically (further away from the CNS surface) than Collagen IV^{Vkg}, albeit following the same spatial patterns (Figure 3.3.4).

3.3.3 Collagen IV Recruits Perlecan^{Trol} to the CNS Surface

Given the co-localisation between the two ECM proteins, I decided to examine whether Perlecan^{Trol} and Collagen IV^{Vkg} interact to regulate NSC reactivation. A previous study showed that Collagen IV^{Vkg} recruits Perlecan^{Trol} in the wing discs (Pastor-Pareja & Xu, 2011). In either a *collagen IV^{vkgK197}* hypomorphic mutant or fat body knockdown of *collagen IV^{vkg}*, the level of CNS Perlecan^{Trol} protein was dramatically reduced (Figure 3.3.5). Collagen IV^{Vkg} may be either required for the transcription of *perlecan^{trol}* and/or the translation of the protein from the perineurial glia, or it may recruit Perlecan^{Trol} protein to CNS surface. Q-PCR analysis on *perlecan^{trol}* with mRNA extracted from CNS under fat body *collagen IV^{vkg}* knockdown conditions shows that loss of Collagen IV^{Vkg} did not reduce CNS

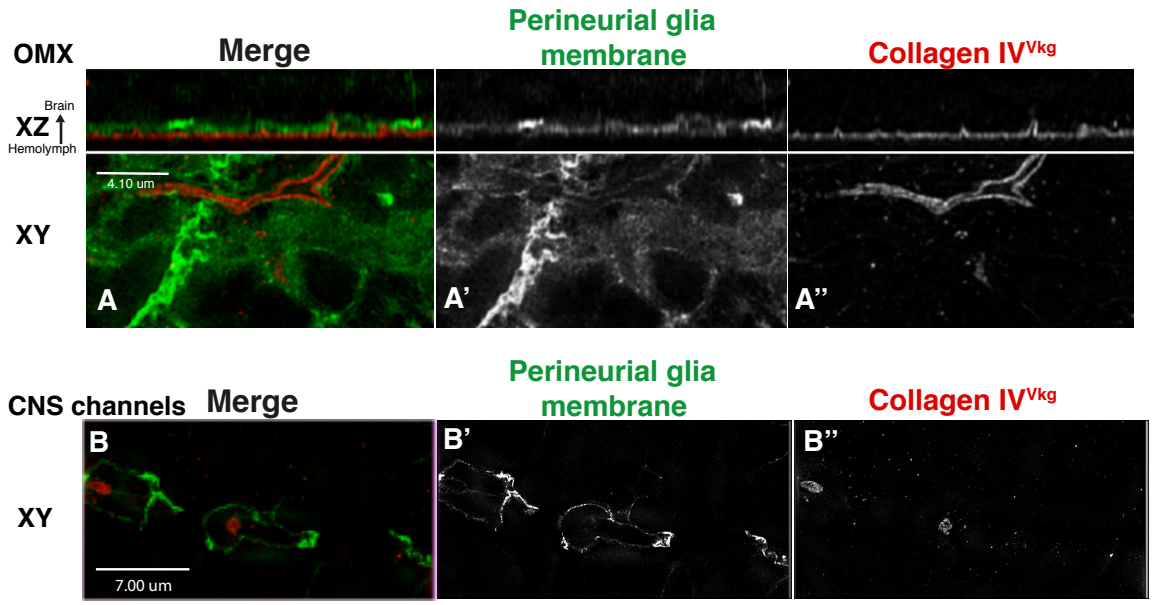

Fig. 3.3.3 Localisation of Collagen IV^{Vkg} with respect to perineurial glia. (A) DeltaVision-OMX images (both XY and XZ view) of Collagen IV^{Vkg} and perineurial glia membrane. (B) DeltaVision-OMX images (both XY and XZ view) of Collagen IV^{Vkg} (Collagen IV^{Vkg} –GFP protein trap) and perineurial glia membrane at the VNC channels.

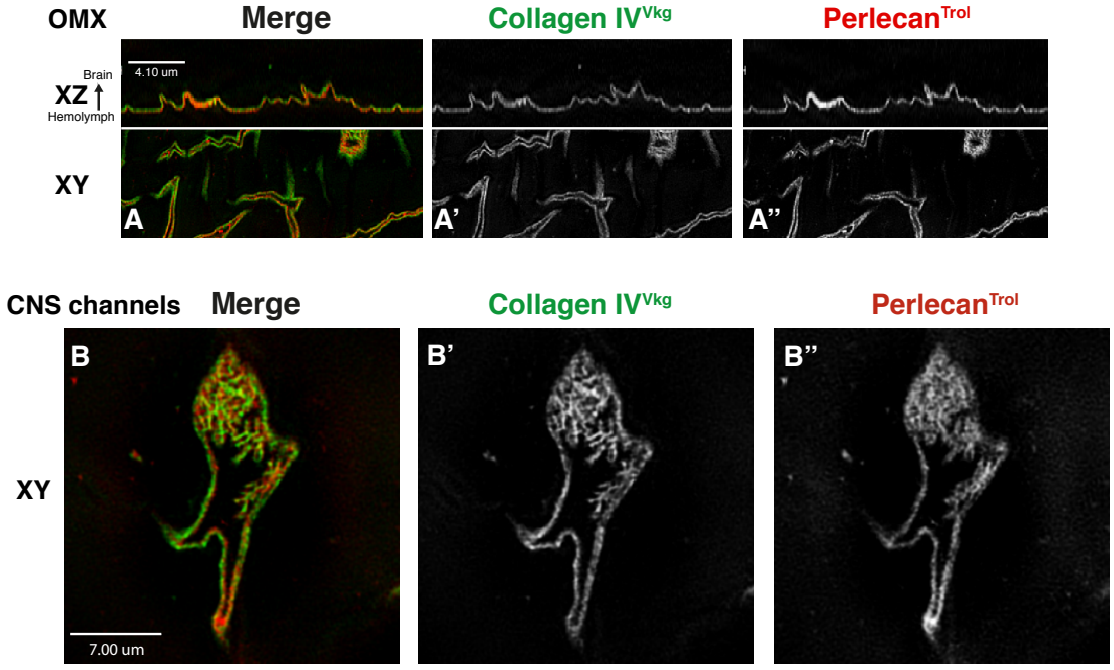

Fig. 3.3.4 Perlecan^{Trol} and Collagen IV^{Vkg} closely co-localise at CNS surface. DeltaVision-OMX super-resolution imaging shows the co-localisation of Collagen IV^{Vkg} (protein trap) and Perlecan^{Trol} (antibody staining) on the surface of VNC (A) and at the VNC channels (B).

perlecan^{trol} transcription, suggesting that it is more likely for Collagen IV to serve as a scaffold upon which Perlecan^{Trol} can deposit (Figure 3.3.5). Interestingly, the requirement of Collagen IV for the deposition of Perlecan^{Trol} is "one-sided": Collagen IV deposition on the CNS does not require Perlecan^{Trol}, as CNS from Perlecan^{Trol} null mutant larvae showed similar level of Collagen IV^{Cg25C} protein on the CNS surface (Figure 3.3.6). In this experiment, I only assessed Collagen IV^{Cg25C} protein level because the only available Collagen IV antibody was produced against Collagen IV^{Cg25C} subunit. Since a functional Collagen IV protein hetero-trimer consists of both Collagen IV^{Cg25C} and Collagen IV^{Vkg} subunits, one can expect that the levels of Collagen IV^{Cg25C} serve as a reasonable read-out of the abundance of functional Collagen IV trimers on the CNS surface.

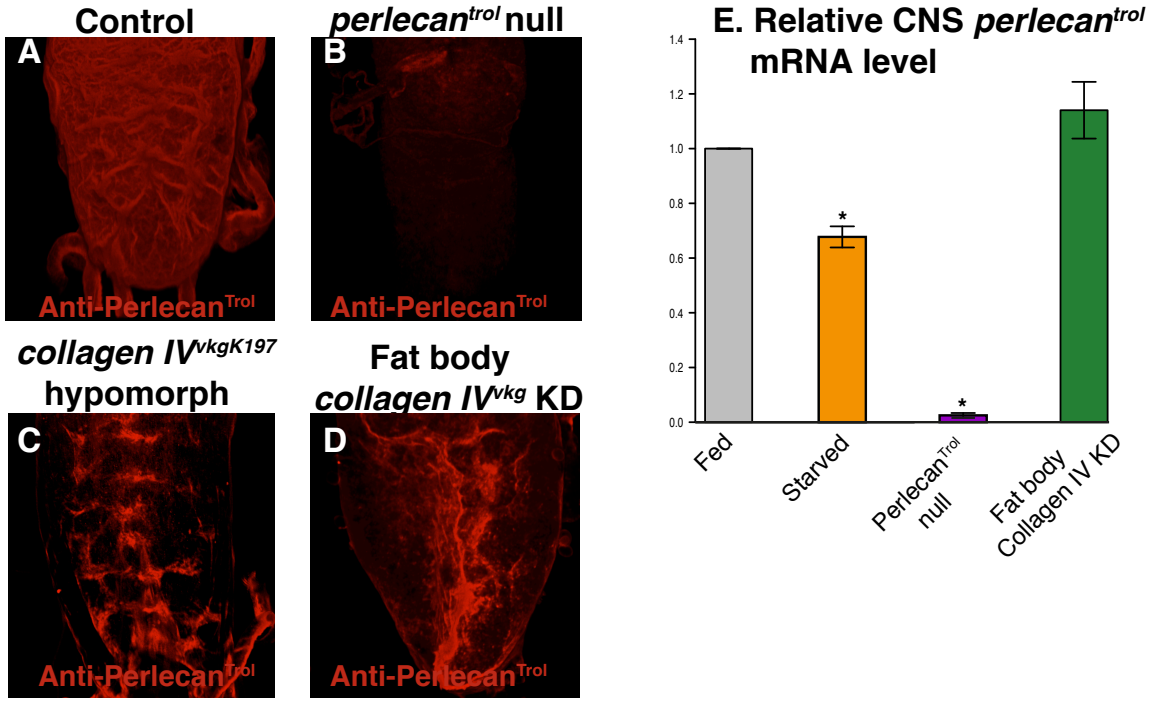

Fig. 3.3.5 Perlecan^{Trol} CNS deposition, but not transcription, depends on The presence of Collagen IV^{Vkg}. (A-D) Levels of Perlecan^{Trol} deposition on the CNS surface (Anti-PerlecanTrol staining 3D reconstruction) in control (A), Perlecan^{Trol} null (B), hypomorphic mutant *collagen IV*^{vkgK197} (C) and fat body *collagen IV*^{vkg} knockdown (D, Cg-GAL4; Lpp-GAL4> UAS-Vkg shimR) conditions 24 hph. (E) Q-PCR analysis of CNS *perlecan*^{trol} transcripts under fed, starved, *perlecan*^{trol} null, and fat body *collagen IV*^{vkg} knockdown conditions.

In summary, DeltaVision-OMX super resolution microscopy revealed that Collagen IV^{Vkg}, Perlecan^{Trol}, and the BBB glia are closely associated with one another. Furthermore, although perineurial glia expression of Perlecan^{Trol} does not require Collagen IV, Collagen

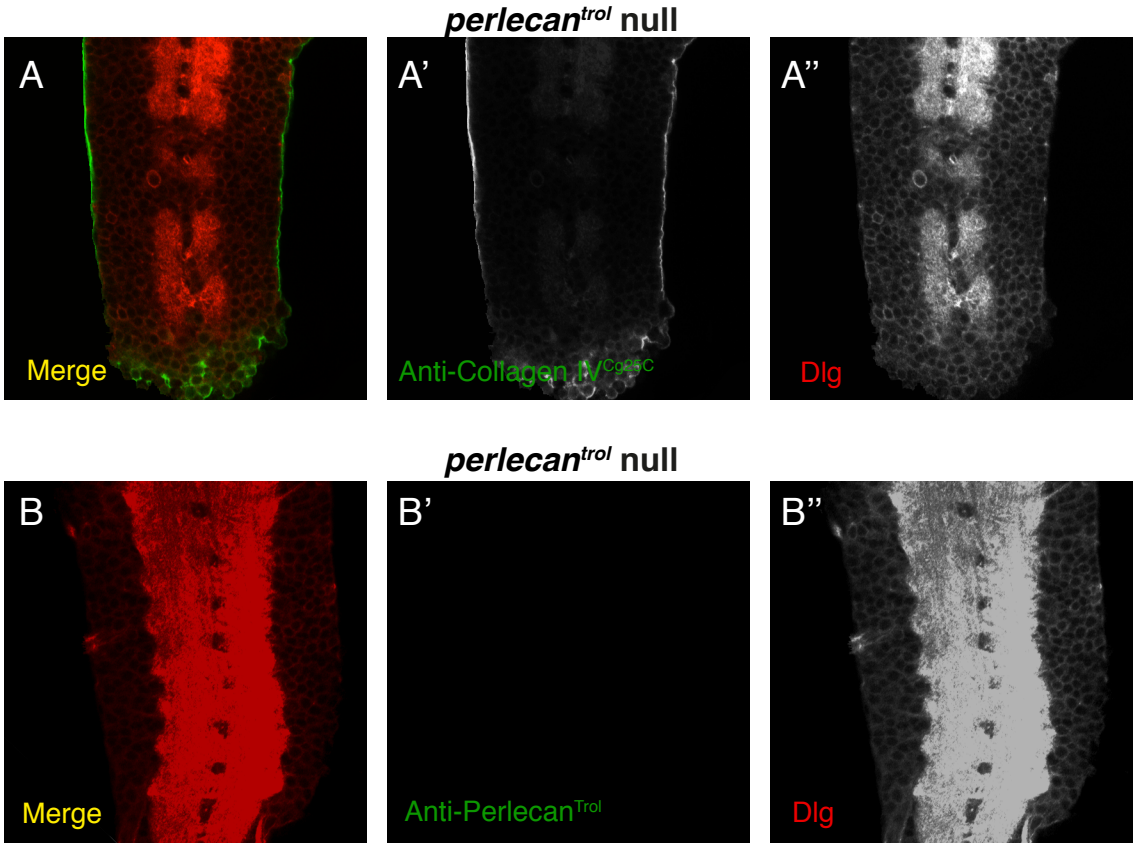

Fig. 3.3.6 Loss of Perlecan^{Trol} does not affect the deposition of Collagen IV on the CNS surface. Snapshot of *perlecan^{trol}* null VNC shows a complete loss of Perlecan^{Trol} protein (B) but normal deposition of Collagen IV^{Cg25C} on the CNS surface (A). Dlg, red; anti-Collagen^{Cg25C}, green; anti-Perlecan^{Trol}, green.

IV is required to recruit Perlecan^{Trol} to anchor at the CNS surface.

3.4 Collagen IV^{Vkg} and Perlecan^{Trol} Promote *dILP6* Transcription in the BBB Glia

3.4.1 BBB Glia Transcribes *dIlp6* in Response to Dietary Amino Acids

NSCs reactivate in response to insulin signalling from the BBB glia, which act as a stem cell niche (Chell & Brand, 2010; Sousa-Nunes *et al.* , 2011). Perlecan^{Trol} and Collagen IV^{Vkg} may stimulate NSC reactivation via the regulation of insulin secretion by the underlying BBB glia (Chell & Brand, 2010). First, I confirmed that the BBB glia (subperineurial and perineurial glia), but not the cortex glia, express *dIlp6* during the time window of NSC reactivation (glial subtype TaDa transcriptional profiling; Figure 3.4.1). TaDa transcriptional profiling also verified the upregulation of *dIlp6* transcription after feeding (Figure 3.4.1, Table 3.4.1). I found no evidence for the involvement of other *dIlp*s, including *dIlp2*, which had been proposed to regulate NSC reactivation (Sousa-Nunes *et al.* , 2011): there is no significant transcription of these *dIlp*s 0–36 hph (Figure 3.4.1, Table 3.4.1).

Table 3.4.1 Summary Of pan-glial TaDa Pol II binding intensity (Log2 scale) across all 8 dIlp loci under fed and starved conditions.

Gene symbol	Log2 ratio_Fed	FDR_Fed	Log2 ratio_Starved	FDR_Starved
dIlp1	-1.30	552.37	-0.17	28.68
dIlp2	-0.09	1.72	0.09	0.66
dIlp3	-1.30	918.76	-0.98	55002.07
dIlp4	-1.27	418.49	-0.40	326.59
dIlp5	-1.49	95.13	-0.05	1.25
dIlp6	1.59	0.00	1.09	2.03E-05
dIlp7	-0.13	1.68	-0.17	8.17
dIlp8	0.69	0.00	0.46	4.00

The transcription of *dIlp6* in BBB glia but not cortex glia was confirmed with *dIlp6* Fluorescence in situ hybridisation (FISH). Bright punctation of *dIlp6* FISH signals were observed on the CNS surface, co-localising with either subperineurial glia or perineurial glia membrane (Figure 3.4.2).

These data indicate that the BBB glia but not cortex glia, serve as a nutrition-responsive NSC niche during NSC reactivation. Indeed, disrupting vesicle trafficking using a dominant negative Dynamin (Shi^{DN}) in BBB glia, but not cortex glia, resulted in NSC reactivation defects (see Chapter 6 for experimental details).

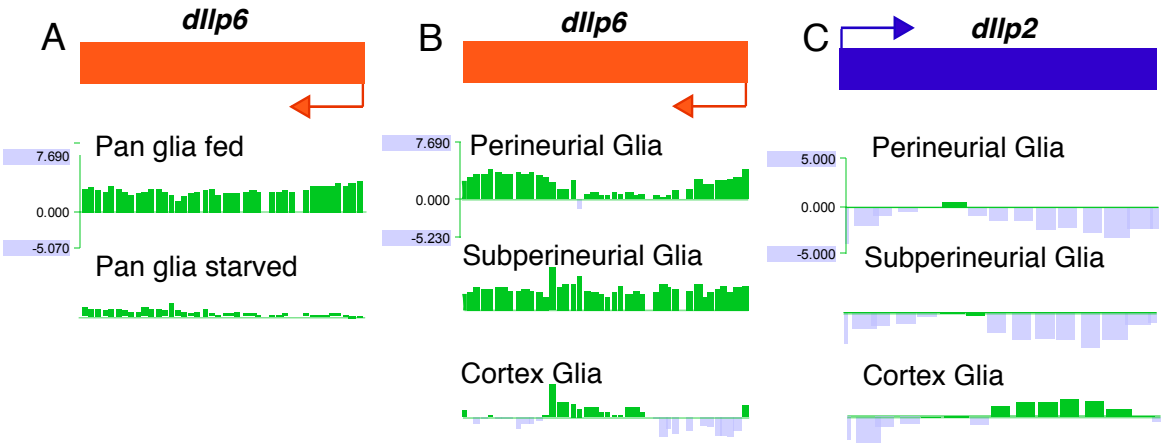

Fig. 3.4.1 Glial subtype transcription of *dIlp*s according to TaDa transcriptional profiling. (A) Pan-glial RNA Pol II occupancy across *dIlp6* locus under fed and starved conditions. (B-C) RNA Pol II occupancy across *dIlp6* (C) and *dIlp2* (D) loci in each glial subtype from DamID RNA Pol II transcriptional profiling with glial subtype-specific GAL4 drivers. Perineurial glia driver: NP6293-GAL4; subperineurial glia driver: moody-GAL4; cortex glia driver: NP2222-GAL4.

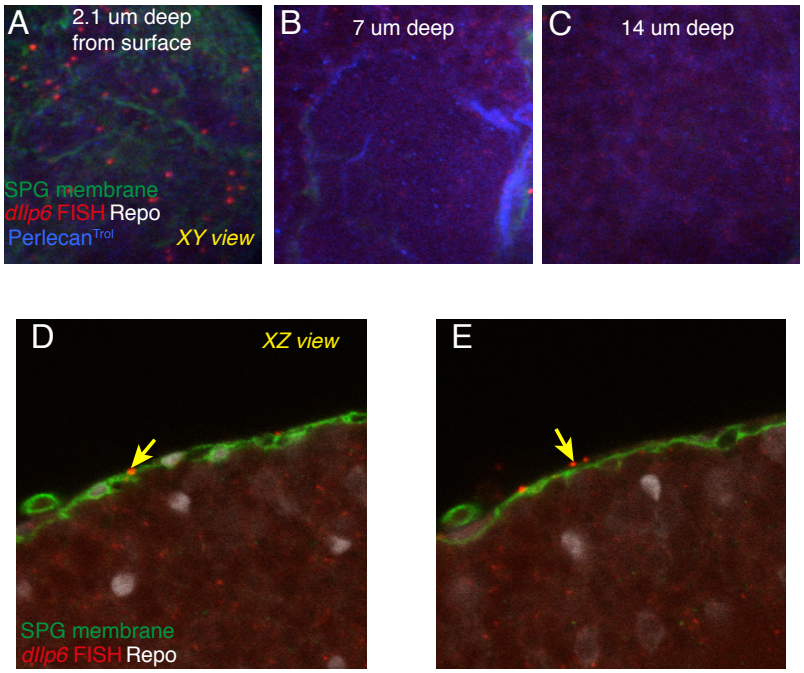

Fig. 3.4.2 Fluorescence in situ hybridisation (FISH) confirmed the localisation of *dIlp6* transcripts in BBB glia. (A-C) XY view of *dIlp6* FISH signals at the CNS surface (A), and deeper into the CNS (B-C). (D-E) XZ view of *dIlp6* FISH signals at the BBB.

3.4.2 Collagen IV^{Vkg} and Perlecan^{Trol} Regulate NSC Reactivation via Glial Insulin Signalling

Perlecan^{Trol} and Collagen IV^{Vkg} deposit at the apical surface of the BBB glia, which are the source of local DIlp6. Thus, I hypothesised that the ECM proteins may regulate NSC reactivation via insulin signalling from the underlying BBB glia. To test this, I extracted mRNA from the brains of fed and starved larvae, *perlecan^{trol}* null mutant larvae, and larvae in which *collagen IV^{vkg}* was knocked down in the fat body. Compared to controls, loss of Perlecan^{Trol} resulted in a mild but significant decrease in *dIlp6* transcription, while loss of Collagen IV^{Vkg} in the fat body resulted in a further decrease, giving a level similar to that seen upon starvation (Figure 3.4.3).

Next, I examined whether forced expression of DIlp6 in glial cells could rescue NSC reactivation in *perlecan^{trol}* and *collagen IV^{vkg}* mutant larvae. In *perlecan^{trol}* null larvae, NSCs can enlarge to a certain extent but fail to enter mitosis. Forced glial DIlp6 expression was able to rescue NSC reactivation, driving NSCs into mitosis ($>$ 50% of wildtype; Figure 3.4.4). *collagen IV^{vkgK197}* mutants could also be rescued, but to a lesser extent (Figure 3.4.4). Taken together, the data suggest that Collagen IV^{Vkg} and Perlecan^{Trol} control NSC reactivation through upregulation of *dIlp6* transcription in the BBB glia. In addition, I could partially rescue NSC reactivation in *perlecan^{trol}* null or *collagen IV^{vkgK197}* hypomorphic larvae by expressing a constitutively active form of Akt/PKB (a downstream effector of insulin signalling) in the NSCs (data not shown).

3.4.3 Chapter Summary

In this chapter, I characterised fat body derived Collagen IV^{Vkg} and its role in regulating nutrient-sensitive NSC reactivation. Collagen IV^{Vkg} travels from the fat body and deposits on the brain surface. It recruits perineurial glia-derived Perlecan^{Trol} to anchor at the BBB. Glial subtype TaDa transcriptional profiling identified DIlp6 from the BBB glia as the main reactivation signal from the glial niche. Furthermore, ECM binding on the BBB upregulates *dilp6* transcription from the BBB glia, leading to NSC reactivation.

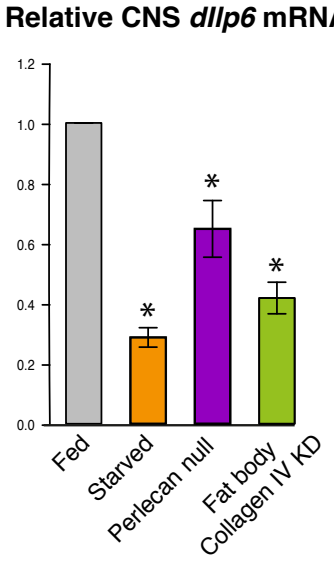

Fig. 3.4.3 Loss Of ECM proteins on the CNS surface impairs CNS *dIlp6* transcription. Q-PCR analysis of CNS *dIlp6* performed on mRNA extracted from brains under fed conditions, starved conditions, *perlecan*^{trol} null, fat body *collagen IV*^{vkg} knockdown (Cg-GAL4; Lpp-GAL4> UAS-*collagen IV*^{vkg} shimR) conditions. CNS were dissected 24 hph. Error bar=sd, *P<0.05.

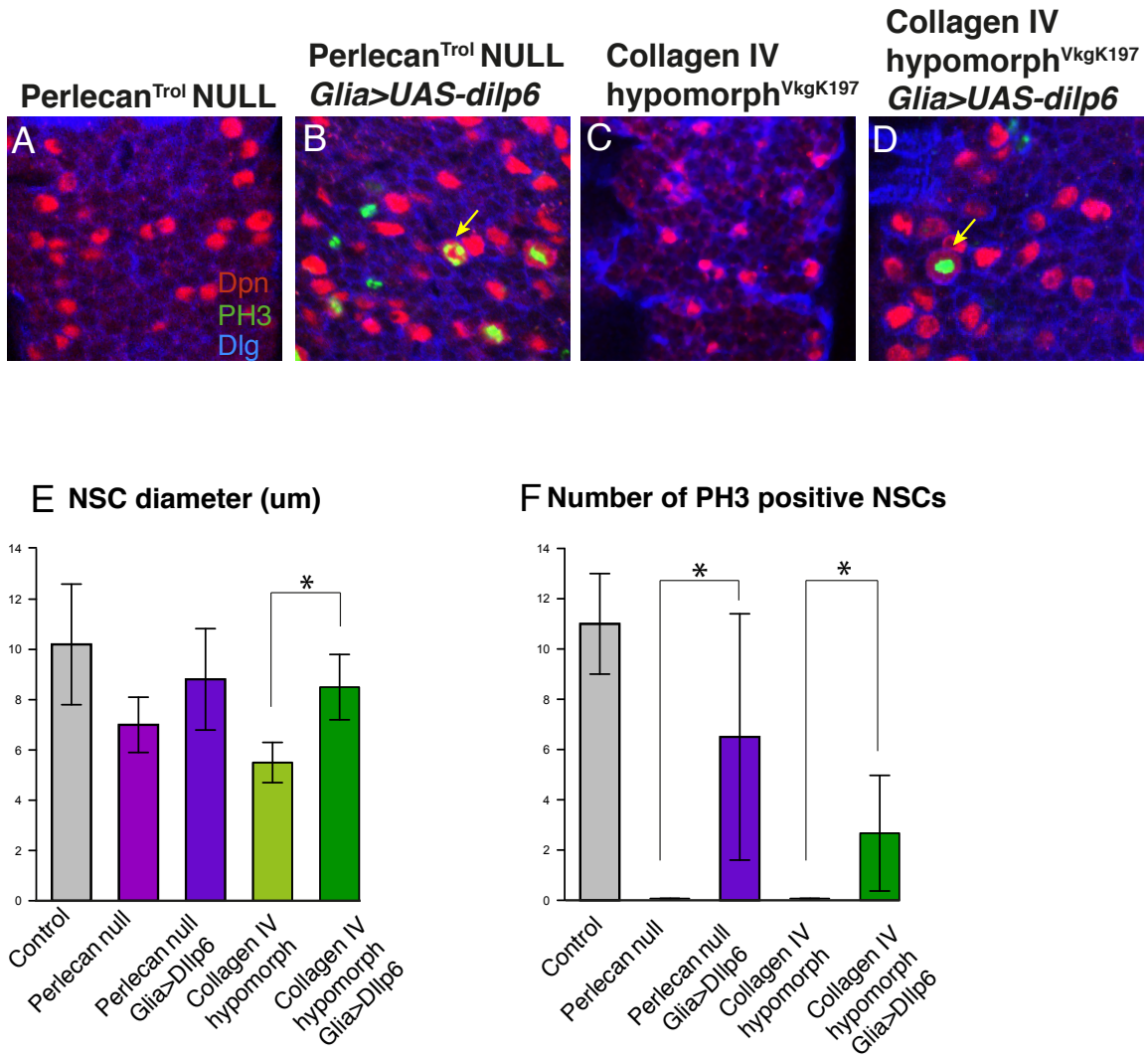

Fig. 3.4.4 Both Collagen IV^{Vkg} and Perlecan^{Trol} regulate NSC reactivation via glial insulin signalling. (A-D) Confocal images of NSC enlargement and proliferation in *perlecan^{trol}* null CNS (A), CNS with glial mis-expression of DIlp6 (Repo-GAL4> UAS-DIlp6) in *perlecan^{trol}* null larvae (B), hypomorphic mutant *collagen IV^{vkgK197}* CNS (C), and CNS with glial mis-expression of DIlp6 under *collagen IV^{vkg}* mutant background (D) 48 hph at 25 ºC. Dpn in red marks NSC nuclei and PH3 in green marks mitotic M phase. The yellow arrows point to dividing NSCs. (E-F) Quantification of NSC enlargement (E, VNC NSC diameter in µm +/- sd) and proliferation (F, number of PH3 positive NSCs in VNC +/- sd) under above mentioned conditions *P<0.05.

Chapter 4

Exploring ECM-Receptor Interaction on the CNS Surface and ECM Regulation of Systemic Larval Growth

4.1 Glial Integrin Receptors Mediate ECM Binding to the CNS Surface and NSC Reactivation

4.1.1 Glial βPS Integrin^{Mys} and αPS2 Integrin^{if} Are Required for Proper CNS Development

Since the fat body is the main source of Collagen IV for the whole the organism (Pastor-Pareja & Xu, 2011), *collagen IV^{vkg}* knockdown in the fat body leads to systemic Collagen IV deficiency. Other organs besides the CNS may require Collagen IV for their normal functions, and some of these functions may be intertwined with CNS development. For example, I observed Collagen IV^{Vkg} to coat the surface of the ring gland, which secretes ecdysone that regulates larval growth including the CNS. Although fat body *collagen IV^{vkg}* knockdown using RNAi led to only a moderate systemic growth defect, knockdown using shmiR led to severe growth retardation (see Appendix for RNAi lines used and Chapter 8 for shmiR lines used), raising the possibility that NSC reactivation defects may be a secondary consequence of global growth arrest. The difference is likely due to a higher knockdown efficiency of the shmiR construct compared to RNAi. A recent study undertook a systematic approach to compare the RNAi knockdown strategy, which uses a long double-stranded hairpin RNA, with shmiR, which is modelled on an endogenous micro-RNA (Ni *et al.* ,

2011). This study concluded that shmiR generally led to higher efficiency compared to RNAi, consistent with my observation (Ni *et al.* , 2011).

Due to the concerns that systemic Collagen IV deficiency may cause secondary CNS growth retardation, I sought to disrupt Collagen IV^{Vkg} binding on the CNS surface locally without affecting Collagen IV^{Vkg} binding to other organs. To accomplish this, I first needed to identify Collagen IV receptors on the CNS surface. Previous work on other organ systems (e.g. wing discs) suggested that the βPS Integrin, Myospheroid (Mys), can act as a Collagen IV receptor. However, ECM proteins can bind to different receptors depending on tissue type and developmental context. For example, the mammalian Collagen IV is known to bind to a variety of integrin receptors, including Integrin $\alpha1\beta1$ and Integrin $\alpha10\beta1$, as well as DDR1 (Discoidin domain receptor family, member 1) (Leitinger & Hohenester, 2007). Thus, even if βPS Integrin^{Mys} also binds to Collagen IV at the CNS surface, it may not be the only receptor. To search for all potential ECM receptors that mediate Collagen IV binding at the BBB and regulate NSC reactivation, I used glial subtype TaDa transcriptional profiling data to examine the expression of ECM protein receptors during the time window of NSC reactivation. Using a Log2 ratio threshold of 0.58 and FDR rate cut-off of 0.01, I found that many ECM receptors are transcribed by the glial cells. In particular, ECM receptor transcription is most active in the two BBB glial subtypes compared to cortical glia (Table 4.1.1). Next, I carried out an RNAi screen against all known *Drosophila* ECM receptors using a pan glial driver (Repo-GAL4), assessing for brain size at third instar larval stage. For candidates that led to CNS undergrowth when knocked down in glia, a secondary screen was conducted to assess for NSC reactivation defects at first instar stage. Table 4.1.2 summarises the result of the RNAi/shmiR screens. RNAi and shmiR lines used for this experiment are listed in Appendix.

When knocked down in all glia, *αPS2 integrin^{if}* and *βPS integrin^{mys}* exhibited NSC reactivation defects (Table 4.1.2). *Myospheroid* (*mys*) encodes the only βPS Integrin in *Drosophila*, whereas several αPS Integrins exist, including the αPS2 Integrin, encoded by *inflated* (*if*). Integrin receptors function by forming dimers between a βPS submit and αPS submit. Given the similarity in their knockdown phenotypes, it appears that the αPS2 and βPS integrin complex is functionally important for CNS development. Since the two integrins showed similar NSC reactivation phenotypes when knocked down in glia (normal enlargement but reduced proliferation), I will present results regarding only βPS *integrin^{mys}* knockdown in the rest of the chapter.

Antibody staining was used to confirm βPS Integrin^{Mys} expression at the CNS surface in the first instar larvae (courtesy of N. Brown lab). Bright punctae of βPS Integrin^{Mys}

Table 4.1.1 Transcription of ECM protein receptors and matrix metalloproteinases in glial subtypes based on glial TaDa transcriptional profiling.

Gene Symbol	Gene Name	Pan glia	SPG	PG	CG
mew	alphaPSi integrin	y	y	n	y
if	alphaPS2 integrin	y	y	y	n
scb	alphaPS3 integrin	y	y	n	n
alphaPS4	alphaPS4 integrin	n	y	n	n
alphaPS5	alphaPS5 integrin	n	n	n	n
mys	betaPS integrin	y	y	n	n
betaInt_v	betaV integrin	n	n	n	n
Dg	dystroglycan	n	n	n	n
dally	glypican5	y	y	n	n
dlp	dally-like(glypican 4)	y	y	y	n
sdc	syndecan 1	y	n	n	n

Table 4.1.2 An RNAi screen of all Drosophila ECM receptors for roles in CNS development.

Gene Symbol	Gene name	NSC reactivation defect when KD in glia
mew	alphaPSi integrin	N
if	alphaPS2 integrin	Y
scb	alphaPS3 integrin	N
alphaPS4	alphaPS4 integrin	N
alphaPS5	alphaPS5 integrin	N
mys	betaPS integrin	Y
betaInt_v	betaV integrin	N
Dg	dystroglycan	N
dally	glypican5	N
dlp	dally-like(glypican 4)	N
sdc	syndecan 1	N

were observed throughout the CNS 24 hph, and they are particularly concentrated at the CNS surface and channels, corresponding to the localisation of the BBB glia (Figure 4.1.1). Punctated βPS Integrin^{Mys} has been previously described at the surface of wing imaginal discs (Brown *et al.* , 2002) and lamellocytes (Xavier & Williams, 2011). Interestingly, like Perlecan^{Trol}, glial expression of βPS Integrin^{Mys} also depends on nutrition. I did not detect any difference in CNS βPS Integrin^{Mys} staining at 24 hph. However, at 48 hph, a higher level of surface βPS Integrin^{Mys} protein was observed in fed larvae as compared to starved larvae (Figure 4.1.1).

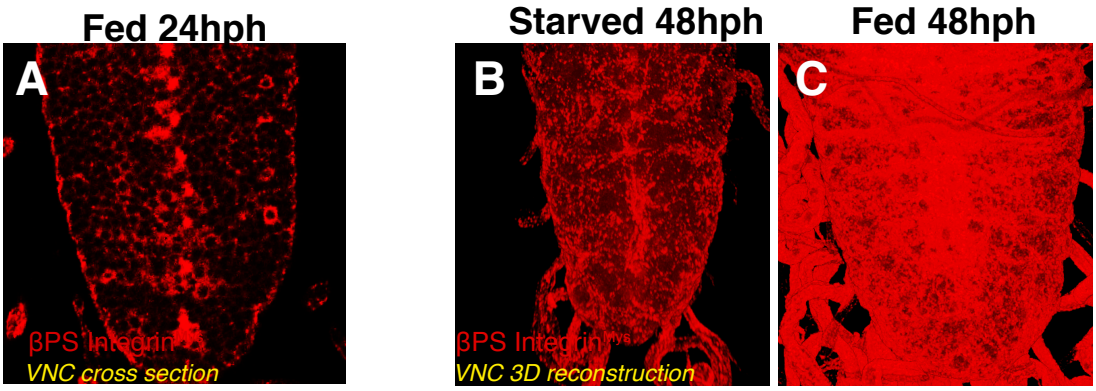

Fig. 4.1.1 βPS Integrin^{Mys} localises to the BBB and its CNS protein level is nutrition dependent. (A) A single cross section slice of VNC βPS Integrin^{Mys} antibody staining. (B-C) βPS Integrin^{Mys} VNC 3D reconstruction in fed and starved larvae.

4.1.2 Super Resolution Microscopy Reveals Distinct βPS Integrin^{Mys} Organisation in the Two BBB Glial Subtypes

Glial subtype TaDa transcriptional profiling suggests that the subperineurial glia (SPG) transcribe *βPS integrin^{mys}* during the time window of NSC reactivation. Confocal microscopy is unable to resolve whether βPS Integrin^{Mys} protein is localised to the SPG or perineurial glia (PG) membranes and how closely integrin receptors are associated with Collagen IV and Perlecan^{Trol}. Therefore, I took advantage of the DeltaVision OMX super resolution imaging system to examine the co-localisation between integrin receptors, ECM proteins and the BBB glial membranes. The OMX imaging system has a resolution of 120 nm in XY direction and 300 nm in Z direction. The PG membrane is approximately 1000 nm thick based on electron microscopy (Yager *et al.* , 2001). Although the thickness of SPGl membrane has not been measured, one can expect it to be similar to that of PG because both of the glial subtypes co-establish the BBB and exhibit a flattened morphology. The length

of an individual integrin is approximately 10 nm (Comisar *et al.* , 2011), which cannot be resolved by OMX imaging system. However, integrin complexes tend to organise in clusters in biological systems, and the intermediate length of integrin clusters is approximately 50 to 500 nm (Comisar *et al.* , 2011). This means that although the smaller clusters cannot be resolved, integrin clusters bigger than 120 nm can be resolved in XY direction and the ones bigger than 300 nm can be resolved in the Z direction. Is OMX capable of resolving the ECM layer (i.e. Collagen IV and Perlecan)? The thickness of ECM at the *Drosophila* BBB has not been measured, but it is known that ECM layer at the surface of *Drosophila* eye discs is approximately 400 nm thick (Schiller *et al*, 2013). Therefore, assuming that ECM at the BBB has a comparable thickness, it can be resolved by OMX imaging in both XY direction and Z direction.

βPS Integrin^{Mys} has been shown to act as a Collagen IV receptor in *Drosophila* (Pastor-Pareja & Xu, 2011), but it remains unclear whether it binds to Perlecan^{Trol}. OMX images reveal that βPS Integrin^{Mys} is closely associated with both Collagen IV^{Vkg} and Perlecan^{Trol} (Figure 4.1.2). Integrin^{Mys} punctae often partially overlap with Collagen IV^{Vkg}-GFP (yellow arrowheads), whereas they are mostly separated from Perlecan^{Trol}. In a few instances, Integrin^{Mys} punctae partially overlap with Perlecan^{Trol}. Whether the overlap between ECM ligands and βPS Integrin^{Mys} punctae indicates physical binding and whether their associations are functionally relevant await further investigation, such as biochemical assays of protein interaction.

How is integrin localised with respect to the BBB glial membrane? OMX imaging reveals co-localisation between βPS Integrin^{Mys} and membranes of both BBB glial subtypes (Figure 4.1.3). βPS Integrin^{Mys} punctae are often observed to overlap with the BBB glial membrane, which is visualised by driving the expression of mCD8GFP under glial subtype-specific GAL4 (see figure legends for GAL4 drivers used). This further supports the hypothesis that both of the BBB glial subtypes can directly interact with the ECM. Initially, it was puzzling that the TaDa glial subtype transcriptional profiling experiment showed βPS Integrin^{Mys} transcription in only SPG 0–24 hph, but βPS Integrin^{Mys} protein was detected in both PG and SPG at 24 hph. It is possible that βPS Integrin^{Mys} is transcribed in PG prior to larval hatching, and its protein is inserted into the PG membrane after embryogenesis.

Although βPS Integrin^{Mys} proteins were found in both SPG and PG, the integrin protein complex exhibits different patterns of organisation in the two BBB glial subtypes. In the SPG membrane (approximately 2–4 um from the brain surface), βPS Integrin^{Mys} forms hollow, ring-like structures that are 0.2–0.5 μm in diameter (Figure 4.1.4). The ring-like structures completely disappear 4 μm deep from the surface below the SPG membrane

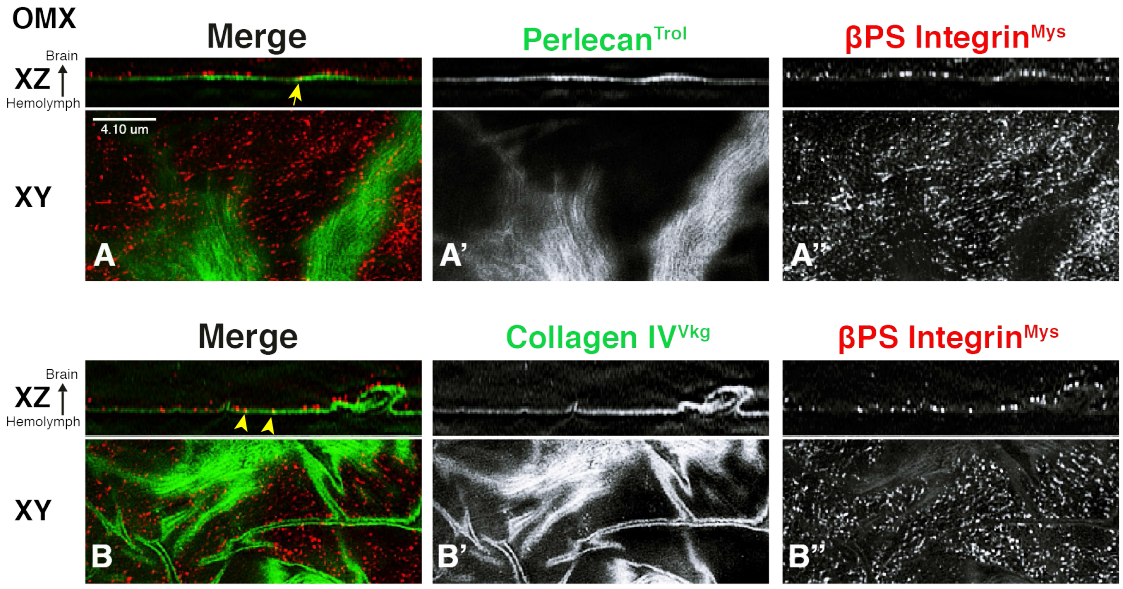

Fig. 4.1.2 Perlecan^{Trol} and Collagen IV^{Vkg} closely co-localise with integrin receptors. (A) DeltaVision-OMX images (both XY and XZ view) of βPS Integrin^{Mys} (antibody staining) and Perlecan^{Trol} (antibody staining). (B) DeltaVision-OMX images (both XY and XZ view) of βPS Integrin^{Mys} (antibody staining) and Collagen IV^{Vkg} (Collagen IV^{Vkg} –GFP protein trap).

(Figure 4.1.4). βPS Integrin^{Mys} punctae also co-localise with the PG membrane (approximately 0–2 um from the brain surface), but the integrin staining pattern appears as solid dots instead of ring-like structures. These ring-like structures are visible from approximately 2 μm basal from the PG layer into the SPG layer (Figure 4.1.4). Therefore, βPS Integrin^{Mys} is present in both PG and SPG membranes, but the ring-like structures are only in the SPG membrane.

What are these βPS Integrin^{Mys} ring structures? Since they are exclusively in the SPG membrane, they may either mediate adhesion/communication between the two BBB glial populations or ECM binding to the SPG surface where PG have not sealed on top. The rings are not present right after larval hatching, and they can be observed in abundance at 24 hph (data not shown). The formation of Integrin^{Mys} ring structures during the time window when the majority of NSCs reactivate indicates that glial Integrin^{Mys} complexes may play a role in NSC reactivation. At 48 hph, the rings have enlarged in size, and sometimes bigger rings appear to be the result of fusion between several smaller ones (Figure 4.1.5). Further experiments are required to determine the functional significance of these SPG specific βPS Integrin^{Mys} ring structures.

Integrin^{Mys} rings have not been described in the *Drosophila* CNS, but they are certainly not unique to the BBB: they are also present in the basal membranes of *Drosophila* wing

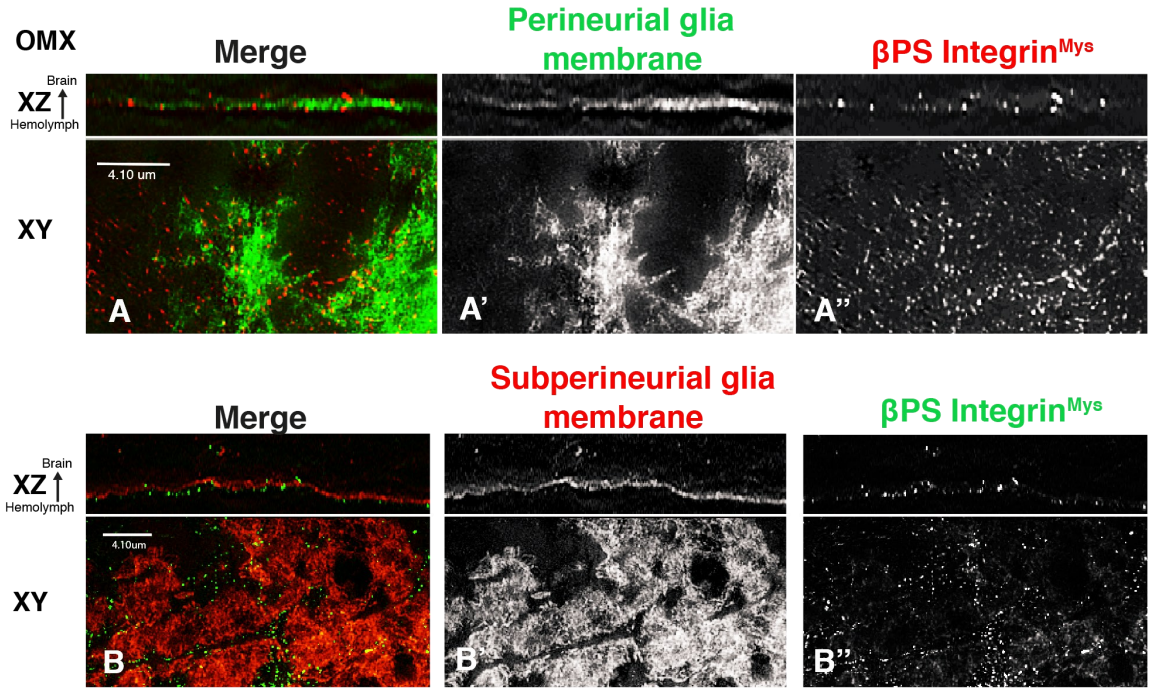

Fig. 4.1.3 Co-localisation of Collagen IV^{Vkg} and βPS Integrin^{Mys} with subperineurial glia and perineurial glia. (A) DeltaVision-OMX images (both XY and XZ view) of integrin (antibody staining) and perineurial glia membrane (NP6293-GAL4>UAS-mCD8RFP). (B) DeltaVision-OMX images (both XY and XZ view) of integrin and subperineurial glia membrane (moody-GAL4>UAS-mCD8RFP).

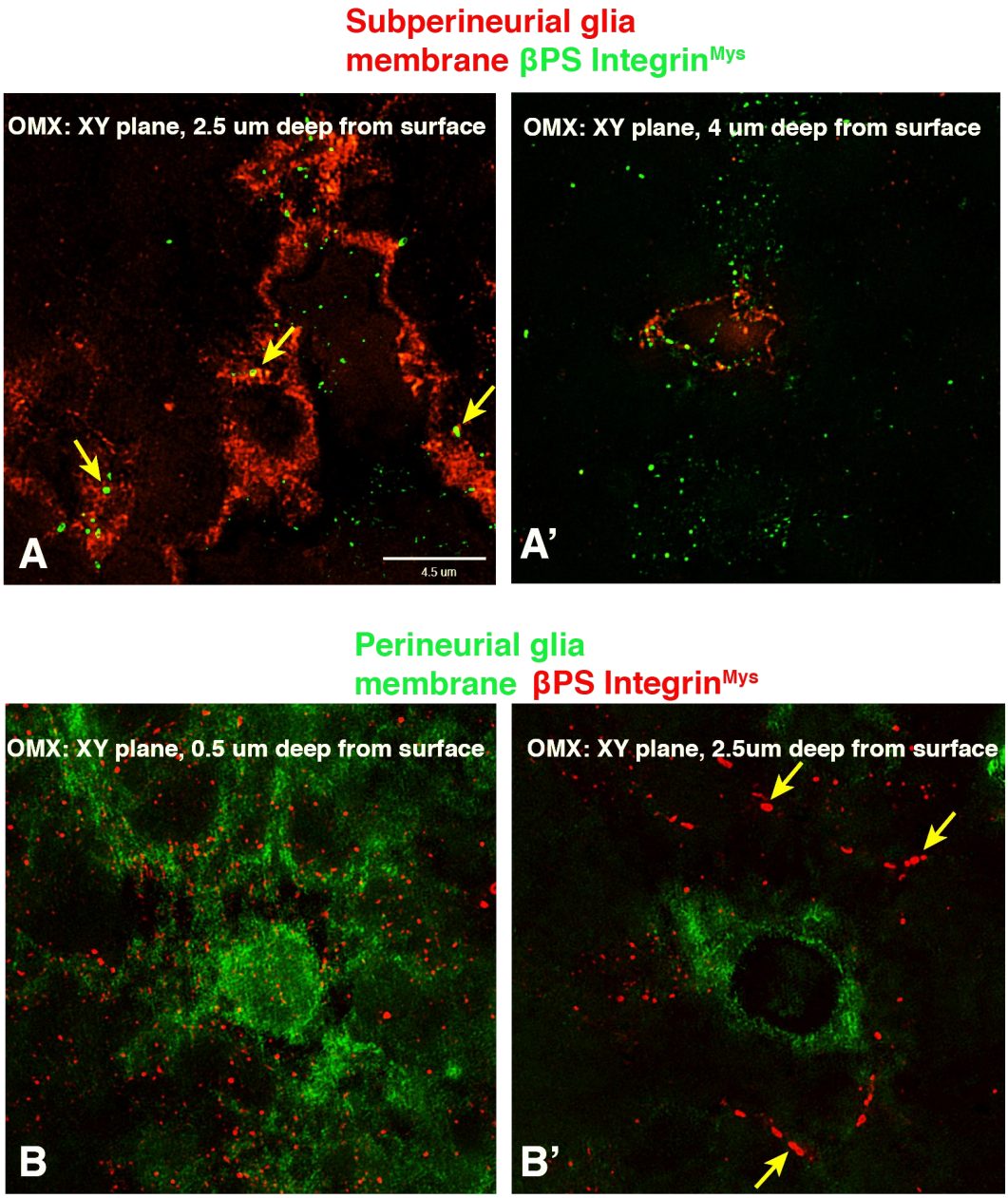

Fig. 4.1.4 Integrin rings co-localise with the subperineurial glia membrane but not perineurial glial membrane. (A-A‘) DeltaVision-OMX images showed that integrin rings are localised to the subperineurial glia membranes approximately 2–4 μm beneath the CNS surface (A, yellow arrows), and were not observed at or below 4 μm beneath the CNS surface (A’). (B-B‘) DeltaVision-OMX images showed that integrin rings are not localised to the perineurial glia membranes approximately 0–2 μm beneath the CNS surface (B, yellow arrows), but appeared at 2.5 μm beneath the CNS surface at the level of subperineurial glia membrane (B’, yellow arrows).

discs and are hypothesised to be the sites of focal adhesion (personal communication with Benjamin Klapholz, Nicolas Brown lab). Preliminary investigation showed that the hollow space between the rings contains F-Actin, as shown by co-staining with Phalloidin (Figure 4.1.5). In addition, integrin rings, but not dots, are closely associated with gap junctions (Figure 4.1.6). Gap junctions are encoded by the *connexin* gene family in mammals (Segretain & Falk, 2004) and the *innexin* gene family in *Drosophila* (Phelan, 2005). A recent study identified Innexins from the *Drosophila* BBB as an important regulator of NSC reactivation (Speder and Brand, 2014, in press): Innexins are required to translate metabolic signals into synchronised calcium pulses and coordinated insulin secretion from the BBB glia. Is the association between integrins and gap junctions observed with OMX imaging functionally relevant? Interestingly, another recent study showed that the human $\alpha 5 \beta 1$ integrin interacts directly with Connexin 43 and that this interaction is required for mechanical stimulation-induced opening of the Connexin hemichannels in a human osteocytic cell line (Nidhi Batra, 2012). Further work should address whether βPS Integrin^{Mys} also interacts with Innexins to regulate coordinated insulin secretion from *Drosophila* BBB glia.

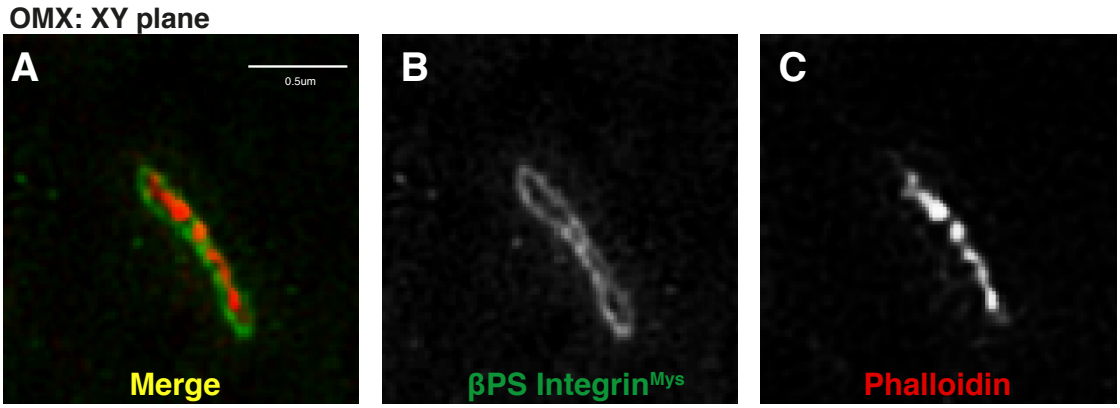

Fig. 4.1.5 Integrin ring structures co-localise with F-actin. (A) Anti-βPS Integrin^{Mys} and Phalloidin merged. (B) Anti-βPS Integrin^{Mys} only. (C) Phalloidin only.

4.1.3 Glial *βPS Integrin^{Mys}* Knockdown Impairs NSC Reactivation and Glial Insulin Transcription

Is integrin required for ECM-mediated NSC reactivation? Q-PCR experiments showed downregulation of *dIlp6* transcripts in the CNS when *βPS integrin^{mys}* was knocked down

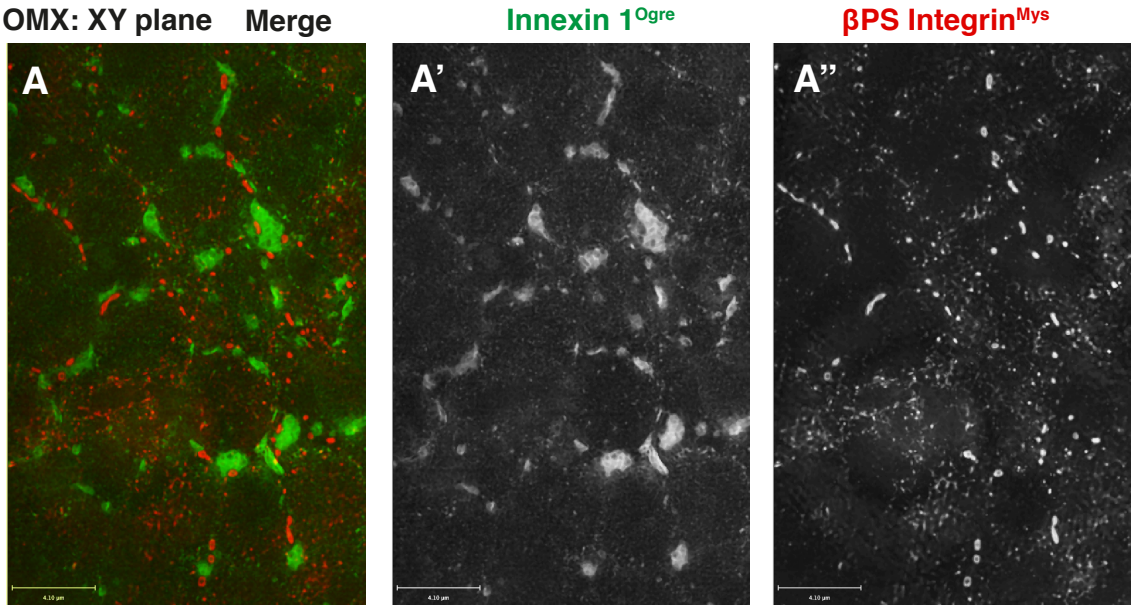

Fig. 4.1.6 Integrin ring structures are associated with gap junction. (A) Anti-βPS Integrin^{Mys} and anti-Innexin^{Ogre} merged. (A') Anti-Innexin^{Ogre} only. (A") Anti-βPS Integrin^{Mys} only.

in the glial cells, to level comparable to fat body *collagen IV*^{vkg} knockdown (Figure 4.1.7). Next, I checked if knockdown of *βPS integrin*^{mys} recapitulates the NSC reactivation phenotype observed with fat body *collagen IV*^{vkg} knockdown. CNS surface βPS Integrin^{Mys} levels were significantly reduced by pan-glial knockdown, validating the efficiency of the RNAi construct (data not shown). Although NSCs were able to enlarge, fewer proliferating NSCs were observed by 24 hph as compared to control (Figure 4.1.7).

βPS Integrin^{Mys} is transcribed in SPG but its proteins can be detected in both SPG and PG. Which population of integrins is important for NSC reactivation? To address this question, I performed knockdown of βPS Integrin^{Mys} in each glial subtype by expressing an RNAi and shmiR construct simultaneously from the start of embryogenesis (UAS-*βPS integrin*^{mys} RNAi; UAS-*βPS integrin*^{mys} shmiR). That way, I could maximise knockdown efficiency during both embryonic and larval stages. Knockdown of *βPS integrin*^{mys} in the PG did not lead to NSC reactivation defects. NSCs enlarged and proliferated normally at 24 hph (Figure 4.1.8). On the other hand, knockdown of *βPS integrin*^{mys} in SPG resulted in impaired NSC reactivation. Although most NSCs enlarged, no NSC proliferation was observed by 24 hph (Figure 4.1.8). In addition, βPS Integrin^{Mys} antibody staining revealed that the SPG knockdown resulted in a much stronger reduction of βPS Integrin^{Mys} protein level on the CNS surface.

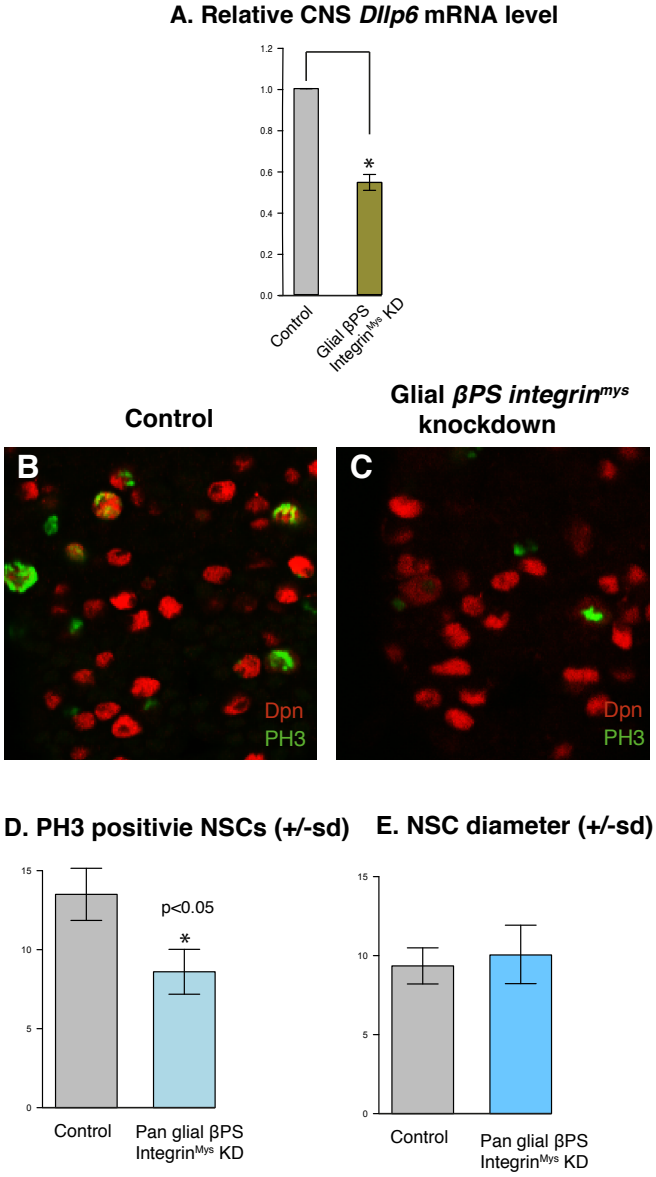

Fig. 4.1.7 Glial integrin receptors mediate ECM dependent NSC reactivation. (A) Q-PCR analysis of CNS *dIlp6* performed on mRNA extracted from brains under control condition (B, w1118X UAS-$\beta PS\ integrin^{mys}$ RNAi; UAS-$\beta PS\ integrin^{mys}$ shmiR) and pan-glial $\beta PS\ integrin^{mys}$ KD conditions (Repo-GAL4; UAS-DicerII X UAS-$\beta PS\ integrin^{mys}$ RNAi; UAS-$\beta PS\ integrin^{mys}$ shmiR). CNS were dissected 24 hph. Error bar=sd, $P<0.05$. (B-C) Confocal images of NSC reactivation under control condition and glial integrin knockdown condition. CNS were dissected 24 hph. Dpn in red marks NSC nuclei and PH3 in green marks mitotic M phase. (D-E) Quantification of PH3 positive NSCs +/- sd and NSC diameters +/- sd in the VNC under control condition and glial knockdown of $\beta PS\ integrin^{mys}$ 24 hph $P<0.05$.

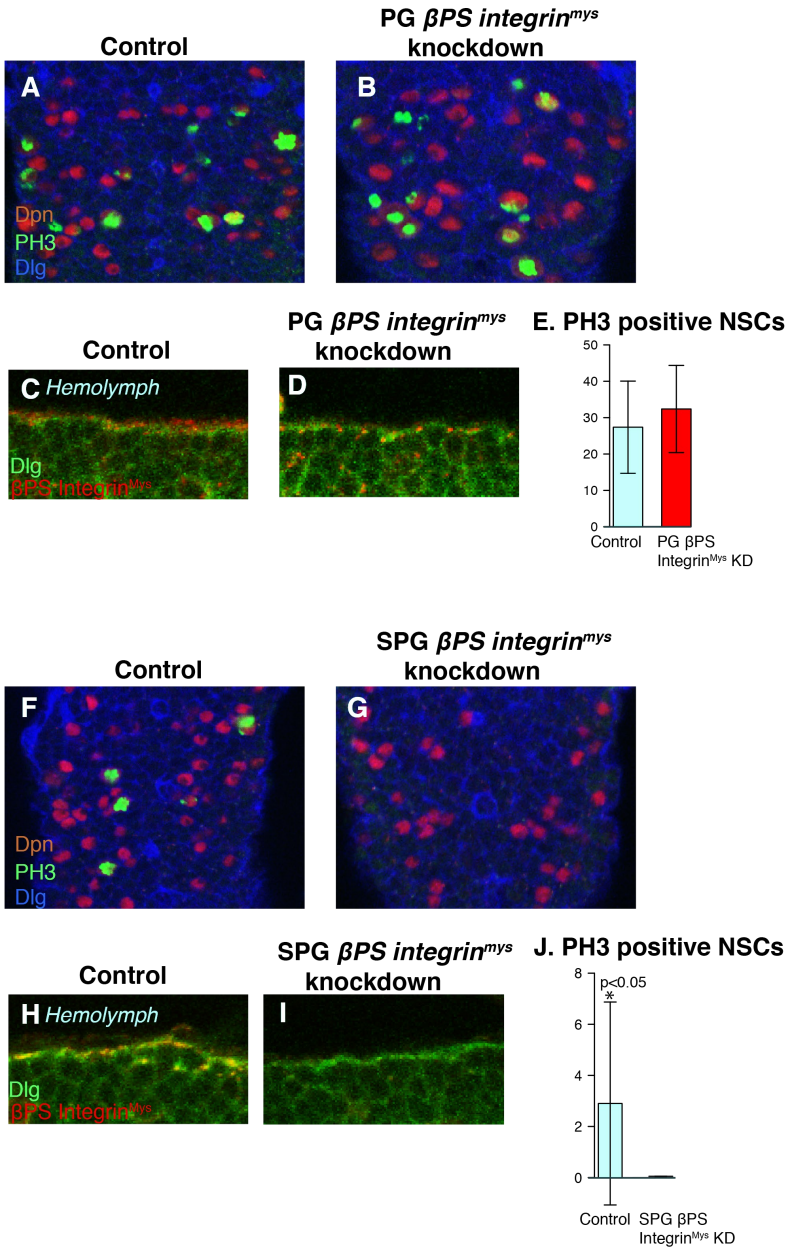

Fig. 4.1.8 Integrin receptors expressed by the subperineurial glia mediate ECM and nutrition-dependent NSC reactivation. (A-B) Confocal images of NSC reactivation in controls (C, w1118X UAS-$\beta PS\ integrin^{mys}$ RNAi; UAS-$\beta PS\ integrin^{mys}$ shmiR) and perineurial glial integrin knockdown (D, NP6293-GAL4; UAS-DicerII X UAS-$\beta PS\ integrin^{mys}$ RNAi; UAS-$\beta PS\ integrin^{mys}$ shmiR). (C-D) Confocal images of anti Dlg and anti βPS Integrin^{Mys} staining at the BBB in controls (C, w1118X UAS-$\beta PS\ integrin^{mys}$ RNAi; UAS-$\beta PS\ integrin^{mys}$ shmiR) and perineurial glial integrin knockdown condition (D, NP6293-GAL4; UAS-DicerII X UAS-$\beta PS\ integrin^{mys}$ RNAi; UAS-$\beta PS\ integrin^{mys}$ shmiR). (E) Quantification of PH3 positive NSCs +/- sd in the VNC in controls and perineurial glia knockdown of $\beta PS\ integrin^{mys}$ 24 hph ($P<0.05$). (F-J) Confocal images of NSC reactivation (F-G), anti dlg and anti-integrin staining at BBB (H-I) and quantification of the number of PH3 positive NSCs (J) in controls and subperineurial glial knockdown of $\beta PS\ integrin^{mys}$ (Moody-GAL4>).

4.1.4 Investigating the Roles of Integrin-Associated Proteins in Larval Neurogenesis

Integrin-dependent adhesion and cellular signalling are mediated by a number of integrin associated proteins. Paxillin (Pax), Talin (encoded by *rhea* in *Drosophila*), Focal adhesion kinase (FAK) and integrin-linked kinase (Ilk) are among the most important proteins associated with integrin functions (Harburger & Calderwood, 2009). An increasing number of recent studies suggest that integrin-dependent cellular processes are important for many aspects of CNS growth and homeostasis in mammals (Mobley & McCarty, 2011; Wojcik-Stanaszek *et al.* , 2011). To check the CNS expression patterns of these integrin-associated proteins, I first examined Ilk-GFP and Pax-GFP protein trap expression. Ilk and Pax are highly expressed in the BBB in first instar larvae, in a pattern similar to βPS Integrin^{Mys} (Figure 4.1.9).

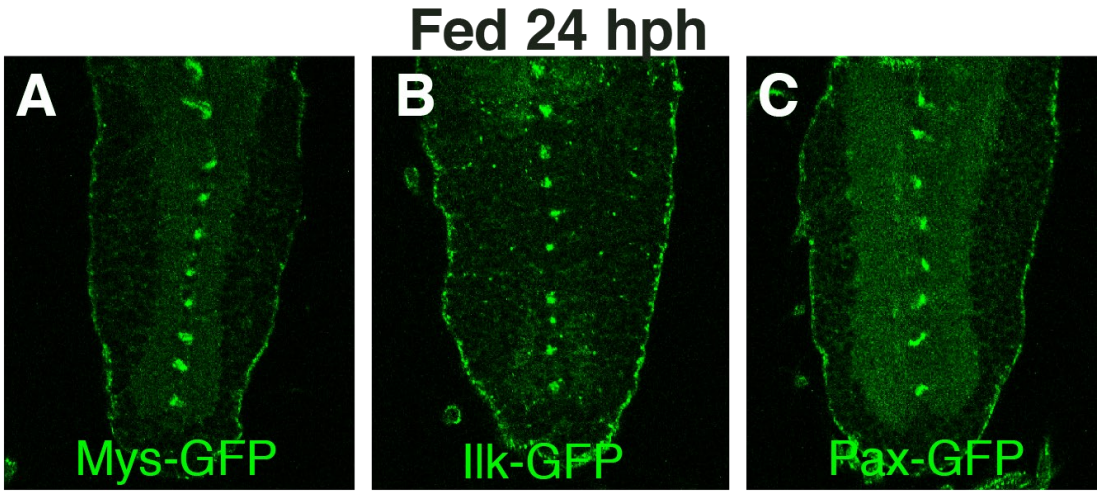

Fig. 4.1.9 GFP protein trap expression patterns of integrin-associated proteins. VNC expression pattern of Mys (A), Ilk (B) and Pax (C). Larval brains were dissected after 24 hph.

Next, I carried out an RNAi/shmiR knockdown experiment using a pan-glial driver, in order to find out which of these integrin-associated proteins are required in glia during larval CNS development. I assessed CNS size and shape at third instar stage and pupal lethality. Since the null mutant of FAK is viable, it is highly unlikely that FAK is indispensable for CNS growth. Thus I did not perform knockdown of FAK. For all the other candidates, only *talin^{rhea}* showed elongated VNC, brain size reduction, and pupal lethality similar to the phenotypes observed with *βPS integrin^{mys}* knockdown in the 3rd instar larvae (Table 4.1.3). Talin^{Rhea} was originally identified in *Drosophila* in a differential embryonic head cDNA screen, and was found to be expressed in a subset of CNS neurons (Brody *et al.*

, 2002). Consistent with my results, embryos deficient in *talin^{rhea}* also showed similar phenotypes to *βPS integrin^{mys}* mutant, such as failure in germ band retraction and muscle detachment (Brown *et al.* , 2002). Interestingly, no CNS-specific phenotype was detected in *talin^{rhea}* mutant embryos, as assayed by glial and neuronal markers (Brown *et al.* , 2002). Talin^{Rhea}'s role in CNS development has not been assessed post-embryonically, and it is possible that Talin^{Rhea} is required during larval, but not embryonic, neurogenesis. It is slightly worrisome that only one out of three Talin^{Rhea} shmiR knockdown resulted in CNS developmental phenotypes. To ascertain that the phenotype did not result from mere off-target effects, I would like to verify the phenotype with additional RNAi lines.

If Talin^{Rhea} can be confirmed to play a role in larval CNS development, future experiments need to investigate whether *talin^{rhea}* knockdown also impairs NSC reactivation. If so, I would like to investigate whether Talin^{Rhea} and βPS Integrin^{Mys} function in the same pathway to regulate NSC reactivation. To assess this question, I would examine glial knockdown of both *talin^{rhea}* and *βPS integrin^{mys}* to see if this enhances CNS growth/NSC reactivation defects in the knockdown of *βPS integrin^{mys}* alone.

Table 4.1.3 An RNAi screen of integrin-associated proteins for roles in CNS development

Gene Symbol	Gene name	BL stock NO.	3rd instar CNS phenotype when KD	Pupal lethality
rhea	Talin	32999 shmiR	NA	NO
		33913 shmiR	elongated&smaller	Yes
		28950 dsRNAi	NA	NO
Pax	Paxillin	42614 shmiR	NA	NO
		28695 dsRNAi	NA	NO
Ilk	Integrin linked kinase	35374 shmiR	NA	NO

In summary, I identified a role for βPS Integrin^{Mys} and αPS2 Integrin^{If} in mediating NSC reactivation. *βPS integrin^{mys}* is transcribed in PG but βPS Integrin^{Mys} protein is present in both PG and SPG. The distinct ring-like integrin structures observed with DeltaVision-OMX imaging are only present in the SPG membrane. Most importantly, integrins in the SPG appear to be functionally important for NSC reactivation: knockdown of *βPS integrin^{mys}* in the SPG, but not in the PG, caused NSC reactivation defects. The identification of the integrin receptors allows me to impair nutrient-sensitive and ECM-mediated NSC reactivation without causing a systemic growth defect in the whole larvae.

4.2 ECM Protein Deficiencies Cause Systemic Growth Defect Potentially by Disrupting the Functions of IPCs and Systemic Insulin Signalling

In both *perlecan*^{trol} null mutant larvae and fat body *collagen IV*^{vkg} knockdown larvae, overall larval growth was significantly impaired. To a large extent, larval growth is coordinated by circulating DIlps (Rulifson *et al.* , 2002). They are secreted into the hemolymph from the IPCs (insulin-producing cells, pancreas equivalent) in the brain. As a starting point to understand the systemic growth arrest phenotype of *perlecan*^{trol} null and *collagen IV*^{vkg} knockdown larvae, we examined if there is a disruption of the IPCs and their DIlp secretion. In wildtype larvae, IPCs are clustered symmetrically into two groups, one on either side of the brain. The IPCs, marked with DIlp2 antibody, are situated right beneath the BBB (Yellow arrows, Figure 4.2.1).

The clustering of IPCs may be important for coordinated systemic DIlp secretion, and their close proximity to the BBB/ECM may also be functionally relevant. Indeed, in *perlecan*^{trol} null mutant larval brains, the IPCs lost their characteristic clustering, and instead formed two or three smaller clusters on either side of the brain (yellow arrowheads, Figure 4.2.1). In addition, the smaller clusters are no longer located close to the BBB and they have moved towards the more interior parts of the brain. These phenotypes are unique to *perlecan*^{trol} null mutant larvae, and are not observed in fat body *collagen IV*^{vkg} knockdown (Figure 4.2.1) or glia *perlecan*^{trol} knockdown condition (data not shown). Future work needs to address how the loss of Perlecan$^{\mathrm{Trol}}$ on the BBB leads to dissociation of the underlying clusters of IPCs. Given the close proximity between the IPC clusters and the BBB, it is possible that ECM-dependent signalling from the BBB glia is required for instructing proper formation of IPC clusters during embryogenesis. It is also possible that ECM-dependent signalling is essential for maintaining the structural integrity of the IPC clusters: the IPCs clusters may have formed by default in the beginning, but an ECM deficiency may have led to IPCs' dissociation from one another later on. In order to distinguish between these two possibilities, I need to track IPC morphology throughout embryogenesis and early larval stage in *perlecan*^{trol} null animal. Furthermore, it would be interesting to investigate whether the dissociation of IPCs impairs coordinated secretion of systemic DIlps from the IPCs.

What happens to DIlp secretion from IPCs in ECM-deficient larvae? The IPCs are known to express a number of DIlps, including DIlp2 (Nässel *et al.* , 2013). The IPCs project their axons into the larval endocrine gland and on the aorta, from which DIlp2 can

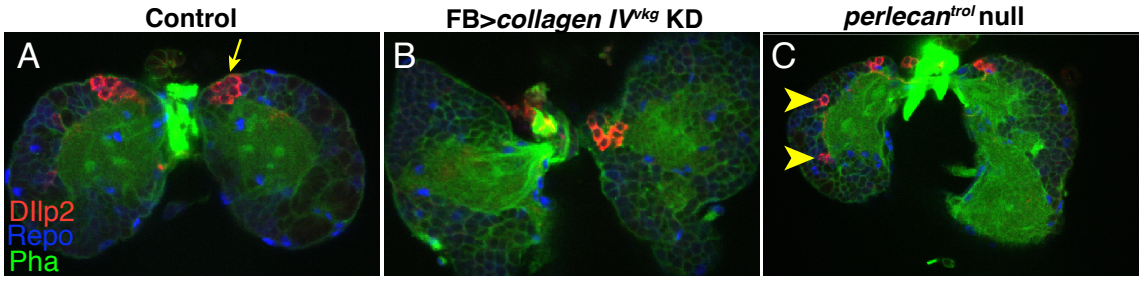

Fig. 4.2.1 Loss of ECM proteins on the CNS surface disrupts the organisation of insulin producing cells (IPCs) in the brain. Organisation of IPCs in control (W1118) larval brains (A), in brains where *collagen IV*^{vkg} was knocked down in the fat body (B), and in *perlecan*^{trol} null larvae (C). DIlp2 antibody marks the cell bodies of the IPCs; Repo marks glial nuclei, and Phalloidin (Pha) marks cellular membranes.

be released into the circulating hemolymph (Ikeya *et al.* , 2002). In fed wildtype brains, DIlp2 can be detected in both the IPC cell bodies and within their extensive axonal networks (Figure 4.2.2, yellow arrows). Previous work showed that DIlp2 transcription remains unchanged under starvation. However, DIlp2 is retained in the IPC cell body and as a result, its secretion into the hemolymph is impaired (Ikeya *et al.* , 2002). Consistent with this observation, I also found a high level of DIlp2 antibody staining in the cell bodies of starved IPCs, but DIlp2 staining was significantly reduced in axonal tracks compared to control conditions. Similar to starvation, under both fat body *collagen IV*^{vkg} knockdown and *perlecan*^{trol} null conditions, DIlp2 staining was strong in the IPC cell body but weak in the axons, indicating that there may be cell body retention of DIlp2 and impaired DIlp2 secretion (Figure 4.2.2). Further work is required to address whether there is a causal relationship between IPC DIlp2 retention and arrested larval growth in ECM deficient larvae.

Apart from regulating NSC reactivation, ECM proteins appear to play multifaceted roles during larval development. I provided some preliminary evidence for their role in maintaining proper CNS architecture and promoting neuronal survival. In addition, they are important for systemic growth potentially by regulating the organisation and potentially secretory functions of IPCs, which are located immediately beneath the ECM-covered BBB.

4.2.1 Chapter Summary

In this chapter, I briefly characterised the roles of integrin receptors in mediating ECM-dependent NSC reactivation. I identified βPS Integrin^{Mys} and αPS2 Integrin^{If} as the ECM receptors important for NSC reactivation. βPS Integrin^{Mys} is expressed by both perineurial

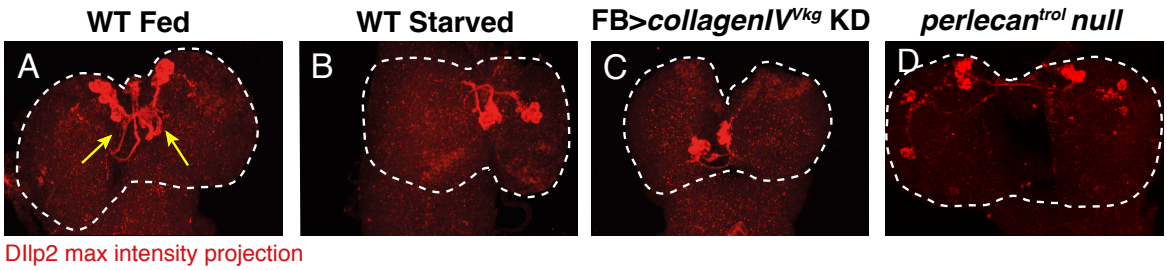

Fig. 4.2.2 Loss of ECM proteins on the CNS surface potentially impairs DIlp2 secretion from the IPCs. Maximum projection of DIlp2 staining in the IPCs in fed control (W1118) larval brains (A), in starved control larval brains (B), in brains where *collagen IV*^{Vkg} was knocked down in the fat body (C), and in *perlecan*^{trol} null larvae (D).

glia and subperineurial glia, but the distinct ring-like integrin structures are only present in the subperineurial glia membrane. Most importantly, integrins in the subperineurial glia appear to be functionally important for reactivation. The identification of the integrin receptors allowed me to impair ECM-dependent NSC reactivation without causing a systemic growth defect in the whole animal.

In addition, I explored other roles of Collagen IV, Perlecan^{Trol} and integrin receptors on CNS development beyond the context of NSC reactivation. Loss of ECM ligands or integrin receptors led to severe disruption in CNS organisation both internally and externally. ECM deficiency also caused neuronal death and systemic growth retardation, which could be caused by morphological abnormalities of the IPCs and impaired systemic insulin secretion.

Chapter 5

Nutrient Sensitive Fat Body Candidates

5.1 The Fat Body Proteins Hsc70–3 and CG13900 Are Required for CNS Development

5.1.1 Fat Body RNAi Screen Identified Hsc70–3 and CG13900 as Potential Regulators of CNS Growth

An RNAi screen was carried out on genes encoding potentially secreted proteins that are upregulated under fed conditions. *collagen IV*^{vkg} and *collagen IV*^{cg25C} were among of the four promising candidates whose knockdown in the fat body resulted in CNS underdevelopment with mild systemic growth defect. The other two candidates were *hsc70–3* and *CG13900* (Figure 5.1.1).

Hsc70–3 is a highly conserved heat shock cognate protein. It is predicted to have ATPase activity and has been shown to be involved in a variety of functions, including centrosome duplication, RNA interference, sleep regulation, and response to heat (Cirelli, 2003; Dorner *et al.* , 2006; Müller *et al.* , 2010). Hsc70–3 encodes a signal peptide in its protein sequence, and a recent study on the characterisation of the hemolymph proteome detected Hsc70–3 protein in the third instar *Drosophila* larval hemolymph (Handke *et al.* , 2013). Interestingly, Hsc70–3 protein levels in the hemolymph were upregulated under fed conditions as compared to starved conditions, although the difference did not reach a statistically significant level. In addition, the mammalian Hsc70 protein was found to be secreted in a variety of cells (Evdokimovskaya *et al.* , 2013; Vega *et al.* , 2008). Given Hsc70–3's role in protein folding, Hsc70–3 is more likely to serve as a post-translational regulator of other fat body-derived growth signals (e.g. Collagen IV), instead of acting as a direct fat body signal

itself.

CG13900 is the *Drosophila* ortholog of the mammalian splicing factor 3b subunit (SF3b). It is highly conserved in chordates: the *Drosophila* and human orthologs share approximately 75% amino acid conservation. Apart from its role in alternative splicing, the mammalian SF3b is also involved in damaged DNA binding, mitotic spindle organization, mRNA splicing and neurogenesis (Herold *et al.* , 2008; Mount, 2000; Neumüller *et al.* , 2011). Recently, the mammalian SF3b has been identified as the target of potent anti-tumour chemicals pladienolide and FR901464 and SF3b-regulated alternative splicing has emerged as an important regulator of tumour growth (Webb *et al.* , 2013). 15% of the most downregulated genes in patients with SF3b1 mutations have a role in mitochondrial function (Papaemmanuil *et al.* , 2011). The identities and functions of genes alternatively spliced by SF3b are just beginning to be understood (Bonnal *et al.* , 2012). Although CG13900 is predicted by SecretomeP program to be secreted via a non-classical pathway, its secretion seems unlikely given its function. In addition, CG13900 protein was not detected in third instar *Drosophila* larval proteome (Handke *et al.* , 2013). It is possible that CG13900 acts as a post-transcriptional regulator of other fat body derived growth signals that are destined for secretion.

5.1.2 CNS Development and NSC Morphology Are Impaired by Knockdown of Fat Body *hsc70–3* and *CG13900*

When *CG13900* or *hsc70–3* were knocked down in the fat body, CNS size was severely reduced, but unlike glial *perlecan*^{trol} or fat body *collagen IV* knockdown, the CNS retained its normal shape.

However, in both knockdown conditions, NSCs in the ventral nerve cord showed abnormal elongated slit-like morphology (Figure 5.1.2, yellow arrows), which was rarely observed in controls. NSCs and their nuclei are normally rounded in shape (Figure 5.1.2, white arrows). Interestingly, the abnormal NSC morphology phenotype was only observed in the ventral nerve cord but not in the brain lobes, despite the brain lobes showing a reduction in size compared to control brains (Figure 5.1.2).

In addition to Collagen IV, Hsc70–3 and CG13900 play an important role in nutrient-sensitive CNS growth based on a functional RNAi screen. Both proteins are unlikely to serve as direct growth-promoting signals, but they may be important post-transcriptional and post-translational regulators of other fat body proteins via alternative splicing and promoting proper protein folding. They are poorly characterised in *Drosophila*, and more experiments

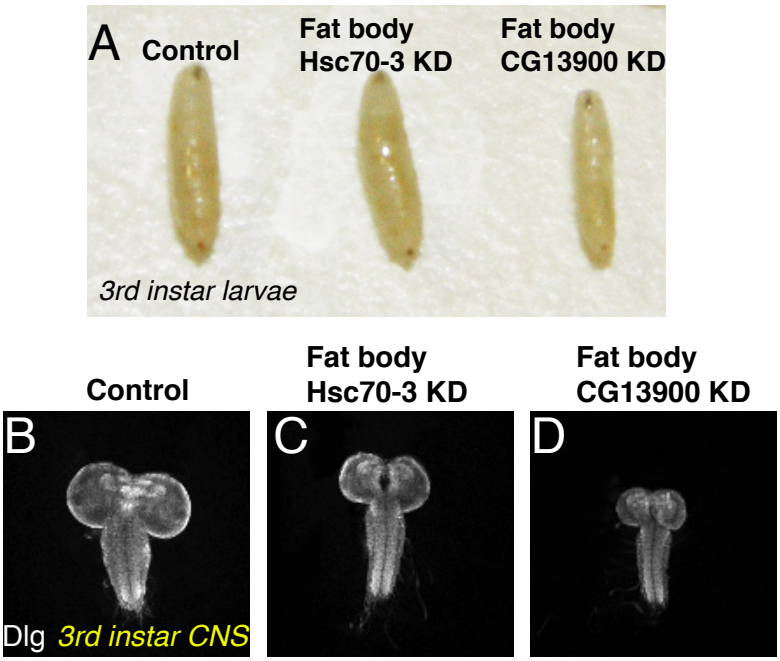

Fig. 5.1.1 Fat body knockdown of *hsc70–3* and *CG13900* led to CNS underdevelopment without causing significant systemic growth defects. (A) Whole third instar images of control larvae (Lpp-GAL4>UAS-mCD8GFP), fat body *hsc70–3* knockdown (Lpp-GAL4>UAS-*hsc70–3* RNAi) and fat body CG13900 knockdown (Lpp-GAL4>UAS-*CG13900* RNAi). (B-D) Whole brain images (anti-Dlg) of control larvae, fat body *hsc70–3* knockdown and fat body *CG13900* knockdown.

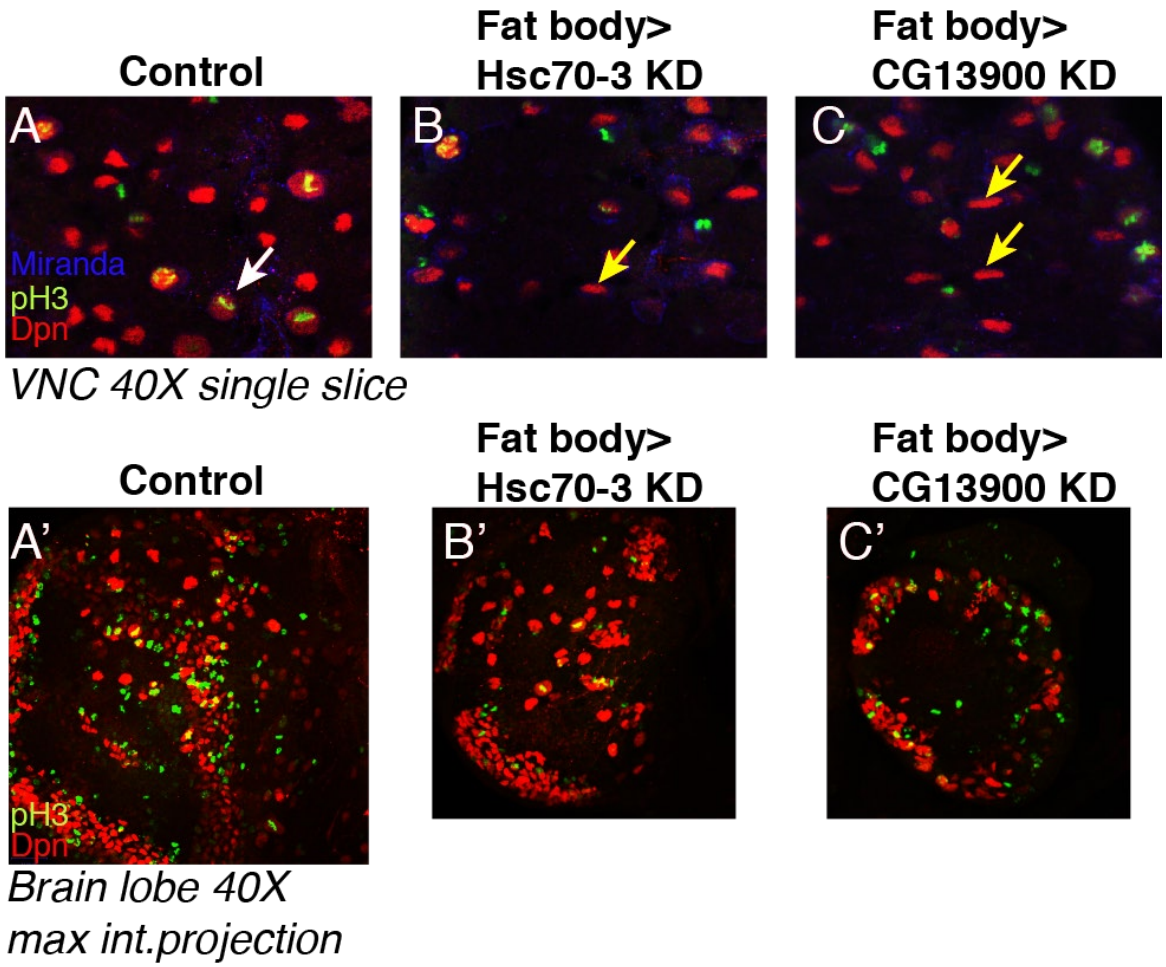

Fig. 5.1.2 Impaired NSC proliferation and abnormal NSC morphology in fat body *hsc70–3* and *CG13900* knockdown Conditions. (A-C) Single plane of VNC images of control larvae (Lpp-GAL4>UAS-mCD8GFP), fat body hsc70–3 knockdown larvae (Lpp-GAL4>UAS-*hsc70–3* RNAi) and fat body *CG13900* knockdown larvae (Lpp-GAL4>UAS-*CG13900* RNAi). White arrow points to a normally shaped NSC. Yellow arrows point to slit-like NSC nuclei morphology. (A'-C') Maximum intensity projection brain lobe images of control larvae, fat body *hsc70–3* knockdown larvae and fat body *CG13900* knockdown larvae. Dpn marks NSC nuclei and PH3 marks mitotic M phase.

are required to elucidate their functions in the context of CNS development.

5.2 Investigating the Role of CG13900 in NSC Reactivation

5.2.1 *CG13900* Transcription Is Nutrient-Sensitive in Multiple Tissues

CG13900 transcription is highly upregulated under fed conditions in the fat body (Figure 5.2.1). To determine the expression of *CG13900* in the brain, I examined *CG13900* expression in glia of fed vs. starved animals (in collaboration with Pauline Speder and Jessie Van Buggenum, Brand lab). I also examined CG13900 expression in NSCs based on a NSC TaDa transcriptional profiling experiment performed by Seth Cheetham (Brand lab). It was somewhat surprising that *CG13900* is transcribed in both glia and NSCs, in addition to fat body (Log2 ratio>=0.58 and FDR<=0.01, Figure 5.2.2). Furthermore, *CG13900* transcription is highly upregulated in glia under fed conditions, and moderately upregulated in VNC NSCs under fed conditions (Figure 5.2.2).

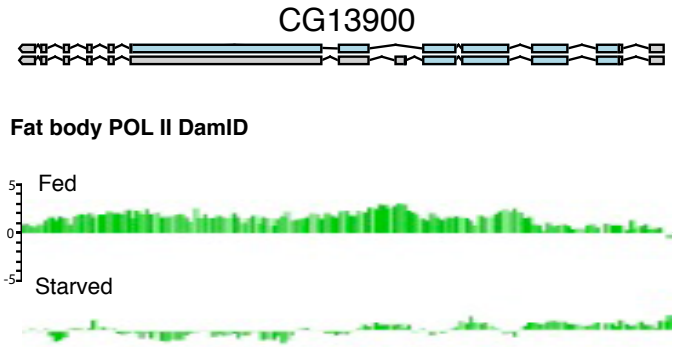

Fig. 5.2.1 RNA Pol II occupancy across *CG13900* locus under fed and starved conditions in fat body. The traces were obtained from fat body TaDa transcriptional profiling (Lpp-GAL4>UAS-Lt2-Dam-Pol II). The experiment was performed 0–24 hph, under fed and starved conditions.

The upregulation of *CG13900* under fed conditions in all three tissues led to the hypothesis that *CG13900* may be a global nutrient-responsive gene. In support of this idea, Zinke et al performed microarray using whole larvae extracts and identified *CG13900* as one of the 19 genes that are transcriptionally down-regulated under both complete starvation and sugar-only-diet in comparison to larvae fed a normal diet at 48 hph (Zinke *et al.* , 2002). CG13900-regulated alternative splicing events and other functions may be nutrient dependent as well.

Glial subtype transcriptional profiling showed that *CG13900* is only transcribed in subperineurial glia (Figure 5.2.2), but not in perineurial glia or cortex glia (data not shown).

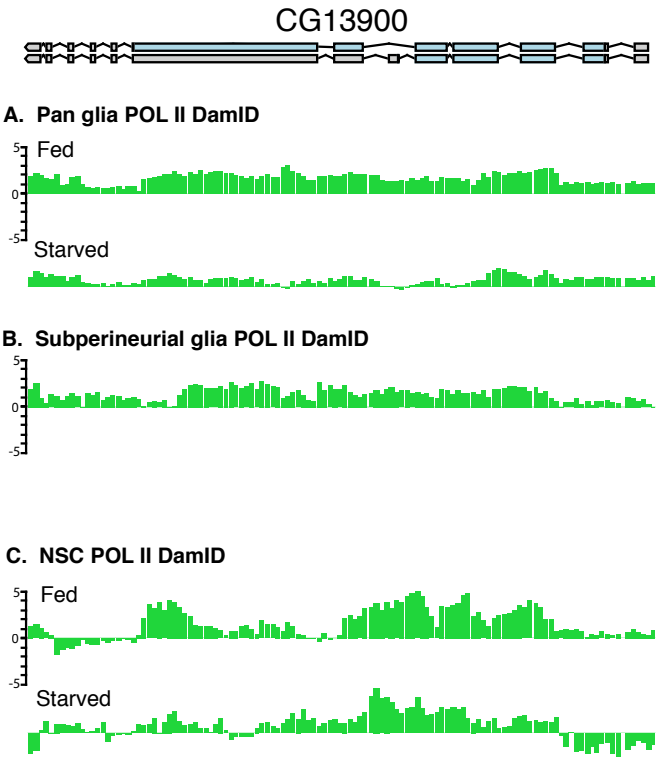

Fig. 5.2.2 RNA Pol II occupancy across *CG13900* locus under fed and starved conditions in glia and NSCs. Traces A were obtained from pan-glia TaDa transcriptional profiling (Repo-GAL4>UAS-Lt2-Dam-Pol II) under fed and starved conditions 12–36 hph. Trace B was obtained with subperineurial glia TaDa transcriptional profiling (Moody-GAL4>UAS-Lt2-Dam-Pol II) under fed conditions 0–24hph (in collaboration with Pauline Speder and Jessie Van Buggenum, Brand lab). Traces C were obtained from NSC TaDa transcriptional profiling (Insc-GAL4>UAS-Lt2-Dam-POL II) under fed and starved conditions 12–36 hph in the VNC (courtesy of Seth Cheetham, Brand lab).

The subperineurial glia are an essential component of the NSC niche: they are the source of DIlp6 and abut the NSCs. Interestingly, the mammalian homologue of *CG13900*, *SF3b3*, is enriched in the mouse BBB, suggesting SF3b-mediated alternative splicing may be important for both invertebrate and vertebrate CNS development (Daneman *et al.* , 2010).

5.2.2 CG13900 May Act as a General Regulator of Growth and Proliferation

CG13900 is transcribed in a variety of tissues, including the fat body, glia and NSCs. I wanted to determine if *CG13900* is required for NSC reactivation, and if so from which tissue(s). *CG13900* knockdown in the fat body impaired NSC reactivation at 24 hph (Figure 5.2.3). NSCs showed significantly reduced proliferation. In addition to affecting NSC proliferation, *CG13900* is also important for maintaining proper fat body architecture. Knockdown of *CG13900* resulted in shrinkage as well as a change in the texture of fat body tissue (data not shown). Therefore, the NSC reactivation defects may be a secondary effect of fat body impairment.

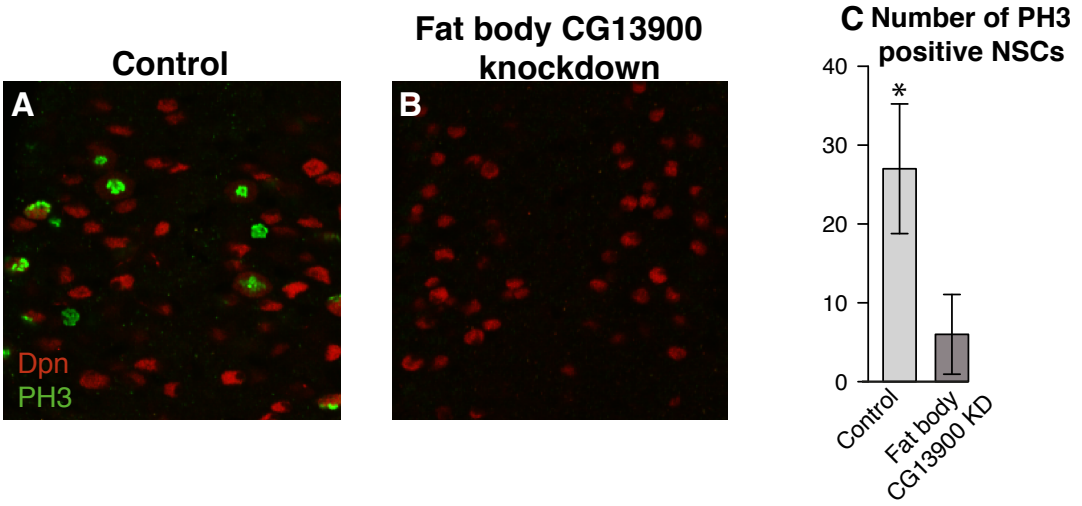

Fig. 5.2.3 Fat body derived CG13900 is required for NSC reactivation. (A-B) Confocal images of NSC enlargement and proliferation under control condition and fat body-specific knockdown of *CG13900*. CNS were dissected 24–30 hph. Dpn in red marks NSC nuclei and PH3 in green marks mitotic M phase. (C) Quantification of NSC proliferation (number of PH3 positive NSCs in VNC +/- sd) under above-mentioned conditions *P<0.05.

Interestingly, *CG13900* knockdown in subperineurial glia also impaired NSC reactivation (Figure 5.2.4). Similar to the fat body knockdown, NSCs enlarged but failed to enter mitotic cell cycle properly.

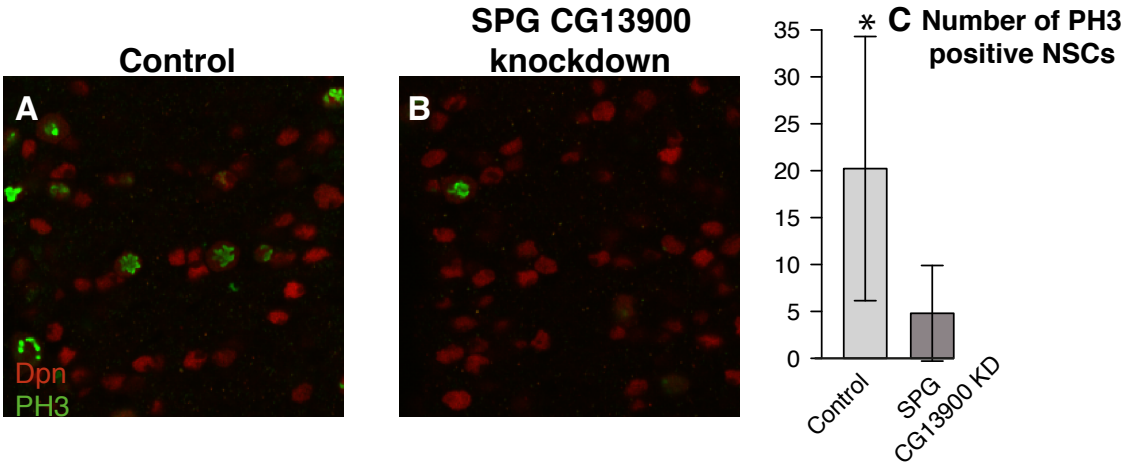

Fig. 5.2.4 Subperineurial glia derived CG13900 is required for NSC reactivation. (A-B) Confocal images of NSC enlargement and proliferation under control condition and subperineurial glia-specific knockdown of *CG13900*. CNS were dissected 24–30 hph. Dpn in red marks NSC nuclei and PH3 in green marks mitotic M phase. (C) Quantification of NSC proliferation (number of PH3 positive NSCs in VNC +/- sd) under above-mentioned conditions *P<0.05.

Since *CG13900* is transcribed by the reactivating NSCs, *CG13900* may be required cell autonomously for NSC reactivation. A previous study (Neumüller *et al.* , 2011) showed that knockdown of *CG13900* with a NSC GAL4 driver (Insc-GAL4) results in larval lethality and NSC under-proliferation at third instar stage. This study, which performed genome-wide RNAi analysis, identified regulators of alternative splicing as a major enriched gene cluster affecting NSC asymmetric cell division and self-renewal in a cell autonomous manner (Neumüller *et al.* , 2011). It remains to be tested whether and how CG13900-mediated alternative splicing affects NSC reactivation. Recently, a number of studies began to investigate the role of alternative splicing in mammalian brain development. The splicing factor TRA2B has been shown to be expressed in murine cortical neural progenitors, and its deletion in neural progenitors results in death and disorganisation of the cortical plate. (Roberts *et al.* , 2014).

Splicing factor 3B subunit 3, a protein in humans that is encoded by the SF3B3 gene, has been shown to perform a variety of roles. Although little attention was paid to the *Drosophila* ortholog, SF3B3's role in mammalian alternative splicing has been well characterised. Splicing factor 3b forms the U2 small nuclear ribonucleoproteins complex (Us snRNP) together with splicing factor 3a and a 12S RNA unit (Will, 2002). In addition, splicing factor 3b is part of the minor U12-type spliceosome (Biplab K Das, 1999). U12-

type introns represent less than 1% of all introns in human, but many of the genes have essential functions. Only a small number of *Drosophila* genes are predicted to be spliced by the U12 minor spliceosome. To investigate if CG13900's involvement in U12 splicing is important for its function in the fat body, I conducted a functional RNAi screen on genes predicted to contain U12-type introns. None of these knockdowns resulted in phenotypes comparable to what was observed with *CG13900* knockdown. Therefore, the fat body genes important for regulating NSC reactivation are mostly likely spliced via the U2 spliceosome.

Splicing factor 3B Subunit 3 has also been identified as part of the STAGA (SPT3-TAF(II)31-GCN5L acetylase) transcription co-activator-HAT (histone acetyltransferase) complex, and the TFTC (TATA-binding-protein-free TAF(II)-containing complex) (Martinez *et al.* , 2001). Therefore, CG13900/SF3B3 may be involved in a diverse array of other functions such as transcription, DNA repair, and chromatin modification.

Another notable function of CG13900 is its potential role as a snoRNA (small nuclear RNA) host gene. CG13900 encodes 9 snoRNAs in its intron region, including Psi18S–110, Me28S-C788b, Me28S-C788a, Me28S-G3113b, Me28S-G3113b, Me5.8S-G74, Me28S-A771, Psi28S–3308, and Psi18S–1086. Despite the common assumption that snoRNAs only have cellular housekeeping functions, in the past few years, studies using diverse strategies have con- verged in implicating snoRNAs in the control of cell fate and oncogenesis in mammals, as reviewed in (Williams & Farzaneh, 2012). In addition, the CG13900 locus encodes a long non-coding RNA, CR45184 (Figure 5.2.5)(http://flybase.org/cgi-bin/gbrowse/dmel/?Search=1;name=FBgn0035162). Long non-coding RNA also recently emerged as important regulators during mammalian neural development and pathogenesis, as reviewed in (Brian S Clark, 2014). Can snoRNAs and CR45184 contribute to the observed phenotypes of CG13900 knockdown? The RNAi construct maps to exon 7 of the CG13900 transcript as well as exon 1 of CR45184. Therefore, further investigation is required to determine whether knockdown of CG13900 or CR45184 led to impaired NSC reactivation.

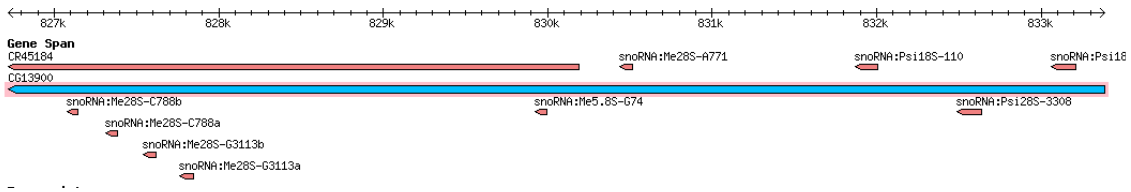

Fig. 5.2.5 CG13900 is a host gene of snoRNAs and a long non-coding RNA. Image was obtained from Flybase.org.

5.2.3 Chapter Summary

In this chapter, I briefly explored the role of two other fat body proteins, Hsc70–3 and CG13900, in CNS development. They are both upregulated in the fat body under fed conditions and are predicted to be secreted. Fat body knockdown of CG13900 or Hsc70–3 led to NSC reactivation defects and abnormal NSC morphology. Interestingly, CG13900 is also required in glia and NSCs for NSC reactivation/proliferation.

Due to the complex nature of the *CG13900* locus, further work is required to elucidate which one(s) of its potential roles are relevant in the context of *Drosophila* NSC regulation, and in which tissue(s). Since pre-mRNA splicing occurs in close proximity with the template DNA, and concurrently with transcription (Jiménez-García & Spector, 1993; Zhang *et al.* , 1994), the TaDa technique (Southall *et al.* , 2013) may be a useful tool to assess binding sites of CG13900 and alternative splicing events mediated by it in a tissue specific manner. TaDa technique has never been adopted to study splicing factors, so it might be important to first test the technique with a known *Drosophila* splicing factor whose regulatory sites have been mapped.

Chapter 6

Investigating Glial Subtypes' Transcriptional Responses to Changes in Systemic Energy Metabolism

6.1 Response of Glial Subtypes to Changes in Metabolism

The main effort of my PhD project was to study how nutrient-sensitive fat body signals regulate NSC reactivation and CNS development. After the discovery that ECM proteins' binding to their receptors on the glial surface induces glial *dIlp6* transcription, I wanted to know what signal molecules interact with ECM proteins at the BBB and operate upstream of Dilp6 production. In mammals, ECM ligands and their receptors participate in a wide array of signalling pathways, including FGFs, HGF (Hepatocyte growth factor), VEGF, BMP (Bone morphogenetic protein), TGF-beta (Transforming growth factor beta), EGF (Epidermal growth factor receptor), PDGF (Platelet-derived growth factor) and IL–3 (Interleukin 3), as reviewed in (Brizzi *et al.* , 2012). In *Drosophila*, ECM proteins' are also known to regulate a few signalling pathways, including BMP (Bunt *et al.* , 2010; Sawala *et al.* , 2012; Wang & Su, 2011), FGF (Park *et al.* , 2003) and Hedgehog (Barrett *et al.* , 2008). I decided to take a systematic approach to examine glial cells' transcriptional responses to starvation in order to identify downstream effectors of signalling pathways mediated by the ECM.

In a collaboration with three other colleagues in the Brand lab (Pauline Speder, Jessie Van Buggenum and Jorge Buendia-Buendia), we analysed the glial transcriptional response to changes in nutritional intake using the glial subtype RNA Polymerase II (Pol II) Targeted DamID (TaDa) transcriptional profiling data (Southall *et al.* , 2013). In this collabora-

tive project, Pauline Speder, Jessie Van Buggenum and myself performed brain dissection, DNA sample preparation and microarray. Jorge Buendia-Buendia and myself performed data analysis. We expected that our data would yield insights regarding the specific glial signalling pathways mediated by ECM proteins at the BBB-hemolymph interface. The analysis would also help to address a number of other outstanding questions, such as which glial subtypes are most sensitive to systemic nutritional fluctuations and how do glial cells sense such fluctuations. Furthermore, while DIlp6 is a key glial signal to induce NSC reactivation, DIlp6 alone is unable to fully rescue the NSC reactivation defect under starved conditions (Chell & Brand, 2010). Glial expression of DIlp6 in starved larvae led to full rescue of NSC enlargement but only partial rescue of proliferation. This means that other signals, perhaps in parallel with DIlp6, are responsible for modulating the scale and/or timing of NSC reactivation and are yet to be identified. It is possible that some of these signals may be secreted from the glial cells and our analysis of the glial transcriptome could lead to the identification of these signals.

6.2 CNS Glial Cells' Transcriptional Response to Starvation

6.2.1 Pan-Glial TaDa Transcriptional Profiling Reveals Significant Changes in Glial Transcriptional Profiles in Response to Starvation

As discussed in previous chapters, quiescent NSCs reactivate when larvae are fed a normal diet containing essential amino acids after larval hatching, but remain quiescent when larvae are starved. The reactivating NSCs are surrounded by glial cell (Figure 6.2.1), which secrete mitogenic DIlp6 in response to feeding. Therefore, it was hypothesised that the CNS glia serve as a nutrient sensitive NSC niche (Chell & Brand, 2010). As a starting point to investigate the glial cells' transcriptional response to amino acid starvation, I performed transcriptional profiling experiment in the glial cells under fed and starved conditions in collaboration with Pauline Speder and Jessie Van Buggenum. Taking advantage of the Pol II TaDa technique (Southall *et al.* , 2013), we were able to map Pol II binding across the entire *Drosophila* genome in all the CNS glial cells from 12 hph to 36 hph, a time window closely coinciding with NSC reactivation (Figure 6.2.2). We used Repo-GAL4 as the CNS glial driver, which has a highly specific expression pattern in all glial cells except for midline glia (Figure 6.2.3). Importantly, Repo-GAL4 shows comparable driver strengths in CNS of both fed and starved larvae, which should allow for comparable expression of Pol II-Dam fusion protein and DNA methylation under the two experimental conditions (Figure 6.2.1 and Figure 6.2.3).

A threshold of Log2 ratio>=0.58 and FDR <= 0.01 was used to determine significantly transcribed genes. Genome-wide transcription patterns differ substantially between fed and starved conditions (Figure 6.2.4). There appears to be global transcriptional downregulation in the glial cells under starvation: starting with comparable amounts of genomic DNA, starved glial cells contain significantly lower level of Pol II bound sequences compared to glial cells from fed larvae (Figure 6.2.5). 4823 genes are transcribed in the glial cells under fed conditions, whereas only 2517 genes are transcribed under starved conditions. This difference cannot be explained by a change in the number of glial cells (quantified with glial nuclei staining) or overall expression levels of Repo-GAL4 (quantified using UAS-MyrRFP), as neither of them changed significantly between the two experimental conditions (Figure 6.2.3). A significant proportion of genes are transcribed in both fed and starved conditions (2318 in total), which are probably essential for glial development and function regardless of nutritional states (Figure 6.2.5). Using a medium stringency threshold (log2

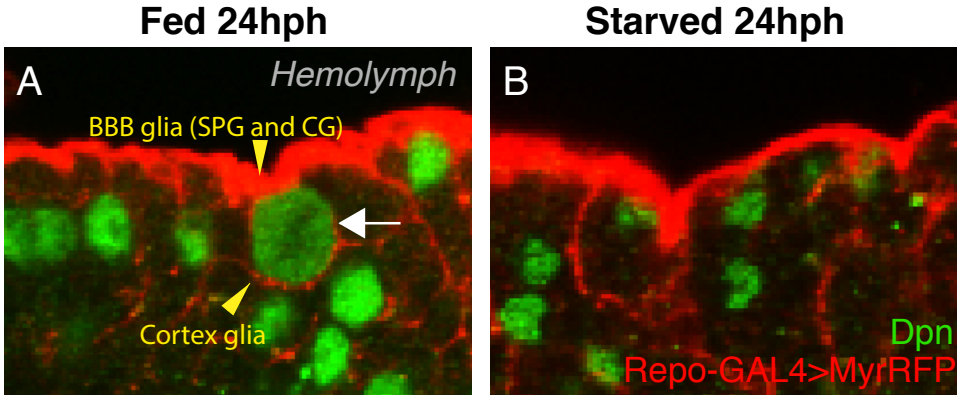

Fig. 6.2.1 Reactivating NSCs are surrounded by glial processes. Confocal images of NSCs (marked by Dpn in green) surrounded by glial processes (Repo-GAL4>UAS-MyrRFP) in CNS from fed and starved larvae. NSCs enlarge and enter mitosis under fed conditions. Under starved conditions, NSC nuclei do not enlarge. White arrow points to an enlarged NSC. Yellow arrow heads point to BBB glia and cortex glia that are associated with NSCs.

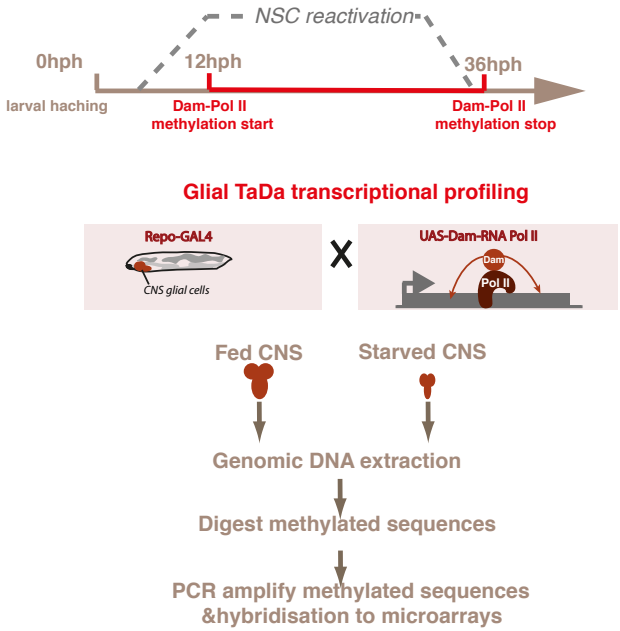

Fig. 6.2.2 Schematic of glial Pol II TaDa transcriptional profiling in fed and starved first instar larvae, 12 hph to 36 hph. A schematic of workflow for pan-glial transcriptional profiling, which was performed between 12–36 hph, a time window closely associated with NSC reactivation. Repo-GAL4 was used as a pan-glial driver. 220–250 CNS from fed larvae, and 250–300 CNS from starved larvae were dissected. Tubulin-GAL80^{ts} was used to allow temporal expression of GAL4.

ratio>=0.58, FDR<=0.01), I found that 2094 genes were upregulated under fed conditions as compared to starved conditions, whereas only 37 genes are upregulated under starved conditions. The symbols of differentially transcribed genes, their Log2 ratios and FDR can be found in my thesis' data deposition folder (see Chapter 8). I found that genes known to be upregulated under fed conditions in glial cells, such as *dIlp6* (Chell & Brand, 2010) and *perlecan*^{trol}, are represented in our data. The top 40 most highly upregulated genes under fed conditions are summarised in Appendix.

Very little is known about glial genes transcriptionally upregulated under starved conditions. However, among the only 37 genes upregulated under starved conditions, 2 encode proteins with known functions associated with the glial cells. *CG6398* encodes a membrane-associated protein which is predicted to be a *Drosophila* homolog of Claudin based on sequence similarities (http://www.ebi.ac.uk/interpro/). Claudins are a family of proteins that are the most important components of tight junctions, where they establish a barrier that controls the flow of molecules between cells of an epithelium (Furuse, 1998). CG6398 has been shown to play a role in establishing glial septate junction (*Drosophila* equivalent of tight junction) at the *Drosophila* BBB (Stork *et al.* , 2008). *jeb* (jelly belly) encodes a transmembrane tyrosine receptor kinase which is expressed in glial cells surrounding NSCs (Cheng *et al.* , 2011). Interestingly, *jeb* plays a role in brain sparing (i.e. privileged brain growth) during starvation in late larval stages (Cheng *et al.* , 2011). Jeb binds to its Alk (anaplastic lymphoma kinase) receptors on the surface of NSCs, and activates PI3K signalling to promote proliferation of NSCs when larvae are deprived of nutrition. Many other glial genes upregulated in starved conditions have been shown to be involved in CNS function and development based on Gene Ontology. Gene symbols and GO biological functions of all 37 genes upregulated under starved conditions are summarised in the Appendix.

I hypothesised that glial niche factors important for NSC activation are likely to be transcriptionally upregulated under fed conditions. Therefore, I decided to focus on these genes. First of all, I analysed enriched GO biological processes via DAVID (Database for Annotation, Visualisation and Integrated Discovery) (Huang *et al.* , 2009). Using a fold enrichment cutoff of 1, p value cutoff of 0.05, and GO level of 3, I found that 117 biological processes are enriched among the glial genes transcriptionally upregulated under fed conditions (Figure 6.2.6). After grouping these terms into broad categories, I found that three categories are most highly represented compared to others, including metabolic processes, organismal development, and morphogenesis.

GO terms associated with the category "metabolic processes" are highly diverse and encompass not only amino acid/protein metabolism, but also cofactor, lipid, sugar and nu-

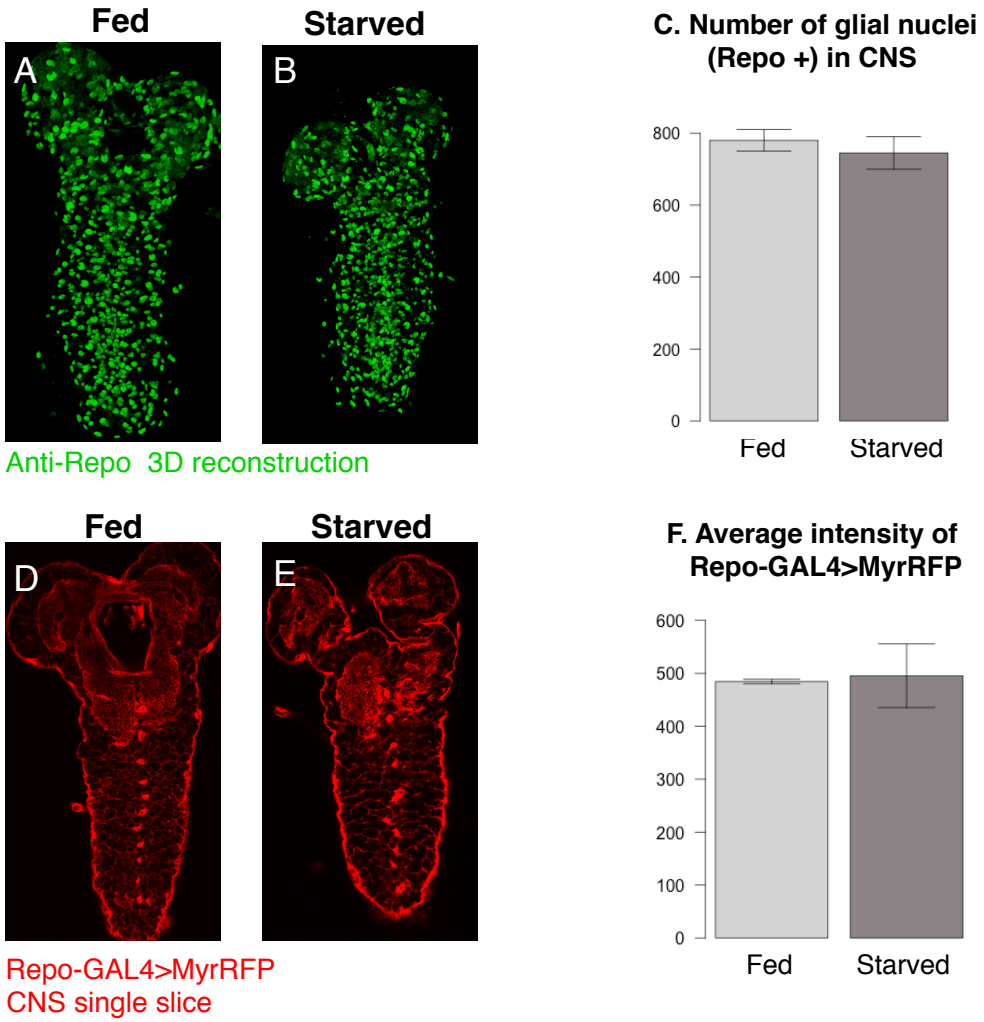

Fig. 6.2.3 Repo-GAL4 driver strength and numbers of glial cells in fed and starved first instar CNS. (A-B) Maximum Z-projection of confocal images showing all glial nuclei (anti-Repo in green) in CNS from fed and starved larvae. (C) Quantification of Repo-positive nuclei under fed and starved conditions. No significant difference was detected between the two conditions. (D-E) Single plane of confocal images showing membrane RFP (Myr-RFP) driven by Repo-GAL4 under fed and starved. (F) Quantification of endogenous Myr-RFP average intensity.

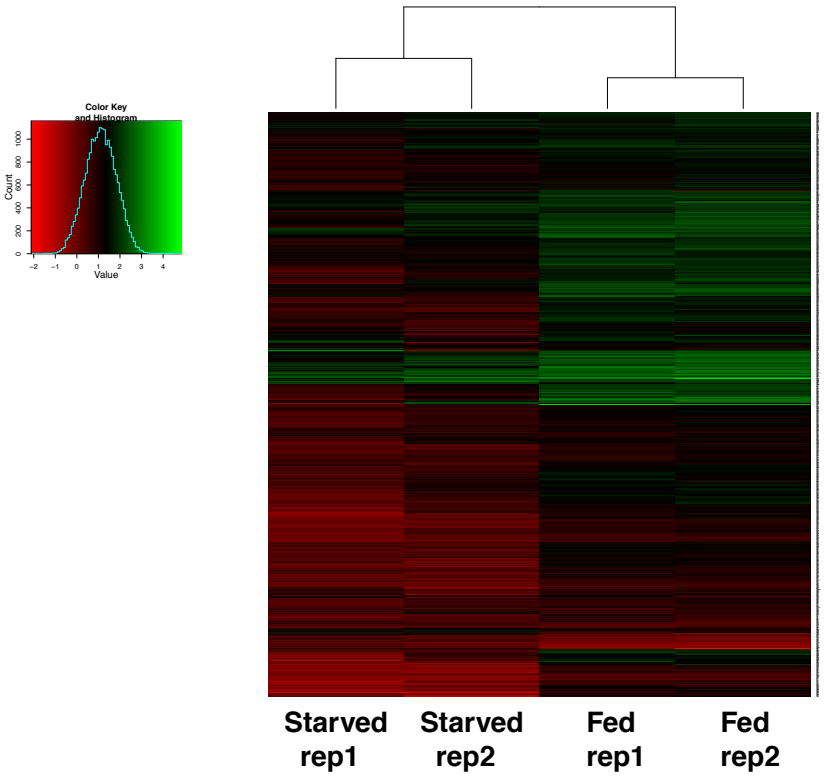

Fig. 6.2.4 Pan-glial TaDa Pol II transcriptional profiles under fed and starved conditions. Heat maps are generated from pan-glial TaDa transcriptional profiling experiments under fed and starved conditions. Log2 ratio of all genes with FDR<=0.01 from each replicate were calculated and plotted.

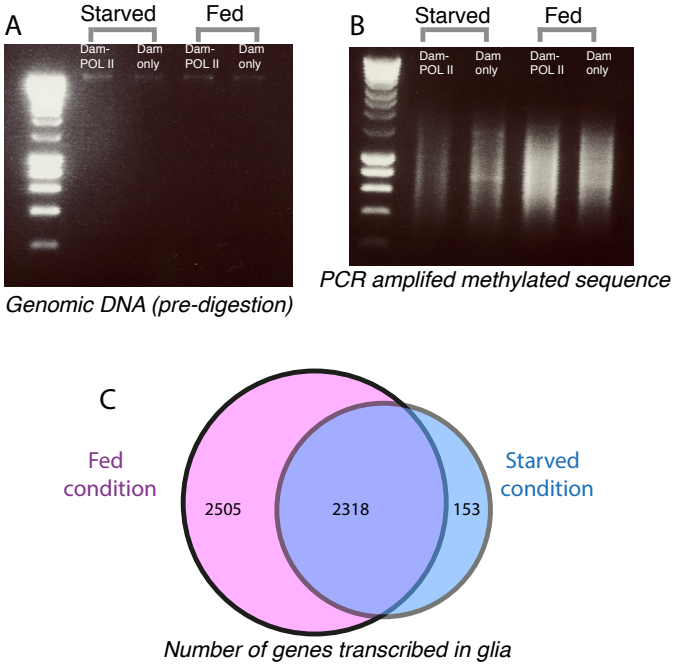

Fig. 6.2.5 Global glial transcriptional down-regulation in starved larvae. (A) Agarose gel of total genomic DNA extracted from larval CNS under fed and starved conditions. (B) Agarose gel of PCR-amplified methylated DNA sequences under fed and starved conditions. (C) Venn diagram showing numbers of transcribed genes in glial cells under fed and starved conditions. Log2 ratio>=0.58 and FDR<=0.01.

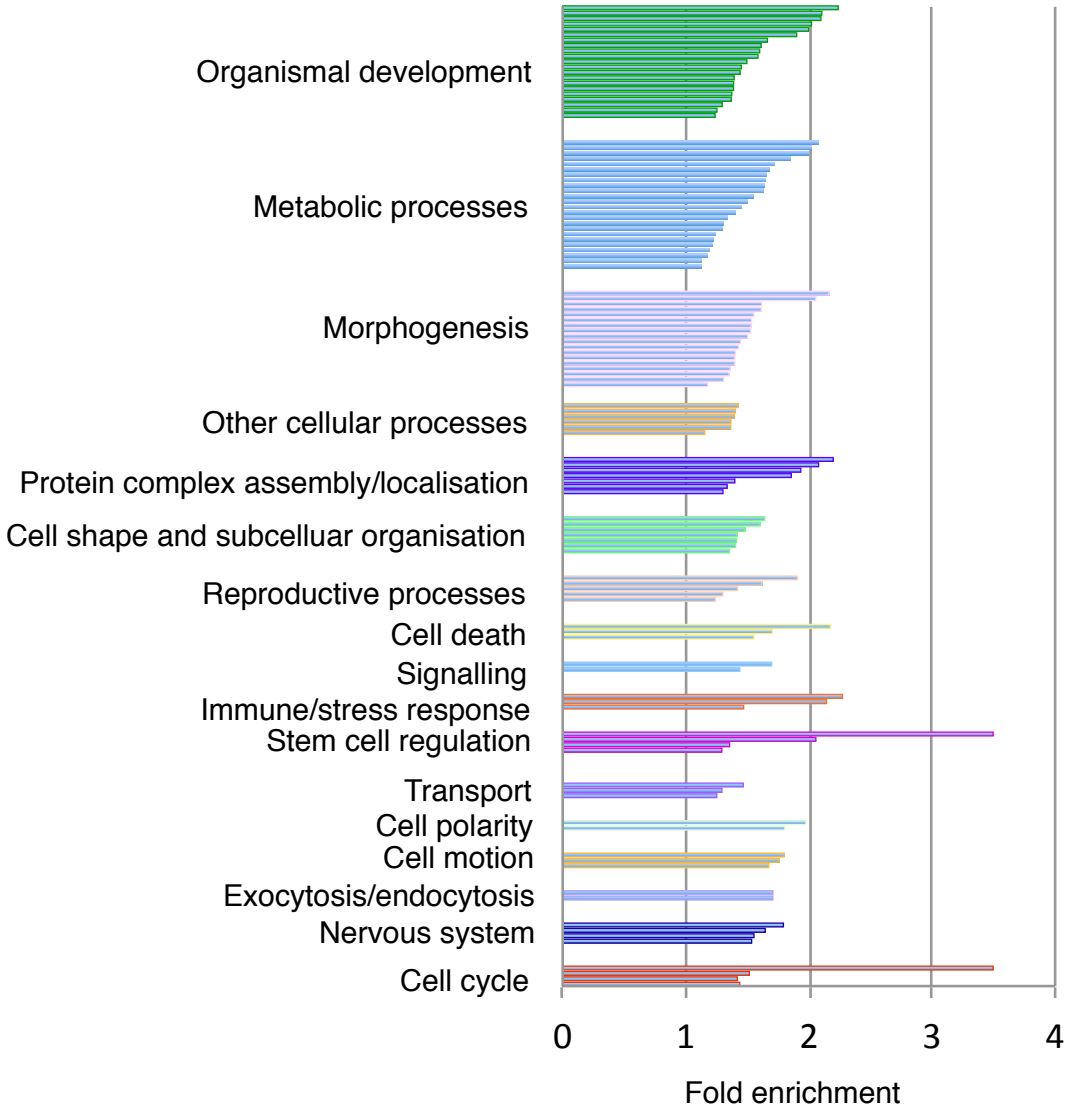

Fig. 6.2.6 GO biological processes enriched in genes upregulated under fed conditions. 128 highly significantly enriched biological processes (P value<=0.05, GO_BP level=3) were identified among glial genes upregulated under fed conditions, using Gene Ontology algorithms. Each horizontal bar represents a specific GO term. All enriched GO terms were clustered into 17 broader functional categories, shown in the graph.

Table 6.2.1 Gene Ontology (GO) terms associated with metabolic processes enriched in glial genes upregulated under fed conditions

GO terms related to metabolic processes	Fold change
sulfur metabolic process	2.07
lipid catabolic process	2.01
carbohydrate biosynthetic process	1.99
cell redox homeostasis	1.84
cellular lipid metabolic process	1.71
organic acid metabolic process	1.68
monosaccharide metabolic process	1.65
cofactor metabolic process	1.64
homeostatic process	1.63
cellular ketone metabolic process	1.63
generation of precursor metabolites and energy	1.54
cellular carbohydrate metabolic process	1.49
lipid metabolic process	1.45
cellular amino acid and derivative metabolic process	1.40
regulation of metabolic process	1.12
regulation of macromolecule metabolic process	1.13
macromolecule biosynthetic process	1.17
cellular macromolecule metabolic process	1.19
cellular biosynthetic process	1.21
nucleobase, nucleoside, nucleotide and nucleic acid metabolic process	1.22
cellular nitrogen compound metabolic process	1.24
cellular catabolic process	1.29
phosphorus metabolic process	1.30
heterocycle metabolic process	1.33

cleotide metabolic processes (Table 6.2.1). In addition, other processes that one would expect to be associated with glial cells are also represented in the GO biological processes enrichment analysis, such as “nervous system regulation”, “stem cell regulation”, “stress response”, and “endocytosis/exocytosis”. I next sought to examine which pathways are enriched among genes upregulated under fed conditions using KEGG (Kyoto Encyclopedia of Genes and Genomes) algorithm via DAIVD (Huang *et al.* , 2009). Using a fold enrichment cutoff of 1, and KEGG p value cutoff of 0.1, I found that 8 pathways are enriched in the glial cells under fed conditions (Table 6.2.2). The majority of these pathways are related to amino acid and fatty acids metabolism. Under fed conditions, larvae were provided with a well-rounded diet containing protein, lipid and sugar, whereas larvae under starved conditions were fed only sugar. Therefore, the upregulation of pathways involved in amino acid and lipid metabolism under fed conditions is perhaps unsurprising.

In conclusion, pan-glial Pol II TaDa transcriptional profiling experiments showed that CNS glial cells exhibit profound transcriptional changes in response to feeding as compared to starvation. GO and KEGG analyses highlighted metabolic pathways expected to be upregulated under fed conditions, validating the transcriptome data for further analyses.

Table 6.2.2 KEGG pathways enriched in glial genes upregulated under fed conditions

KEGG pathway terms	Fold Enrichment
Fatty acid elongation in mitochondria	3.55
beta-Alanine metabolism	2.35
Propanoate metabolism	2.27
Cysteine and methionine metabolism	2.23
Fatty acid metabolism	2.15
Valine, leucine and isoleucine degradation	2.10
Ribosome	2.09
Citrate cycle (TCA cycle)	1.69

6.2.2 Pan-Glial TaDa Transcriptional Profiling Across Different Time Windows Shows Temporal Shifts in Glial Starvation Response

I also performed a similar experiment at an earlier developmental time window together with Pauline Speder. This time window should capture glial transcription before NSC reaction and during the early phase of NSC reactivation, from 4 hours before hatching (hbh) to 16 hph (Figure 6.2.7). This experiment was also performed for brains from both starved and

fed larvae. Combining the two experiments, I was able to explore the glial transcriptional response to systemic metabolic changes over time.

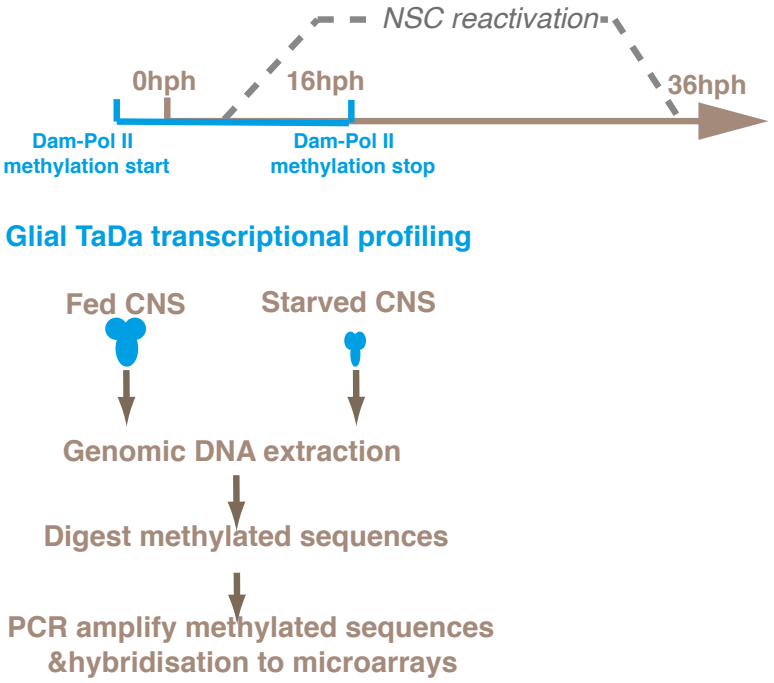

Fig. 6.2.7 Schematics of glial Pol II TaDa transcriptional profiling in fed and starved first instar larvae 4 hbh to 16 hph. A schematic of workflow for pan-glial transcriptional profiling, which was performed between 4 hbh and 16 hph, a time window closely associated with NSC reactivation. Repo-GAL4 was used as a pan-glial driver.

During the 4 hbh to 16 hph time window, glial cells' transcriptional response to feeding is far less dramatic compared to the slightly later time window at 12–36 hph. A global transcriptional profile heat map was generated with log2 ratio of fed over starved conditions for all genes that pass an FDR threshold of 0.01, across the two time windows analysed (Figure 6.2.8). More genes showed transcriptional upregulation under fed vs. starved conditions during the later time window. For example, both *dIlp6* and *perlecan*^{trol} transcription was unchanged between fed and starved conditions during the earlier time window, but were significantly upregulated during the later time window. This is consistent with a a previous study showing that CNS *dIlp6* transcript level exhibited only moderate increase (approximately 0.5 fold) at 12 hph, but increased nearly 8 fold at 24 hph under fed condition, compared to 0 hph (Chell & Brand, 2010).

Using a medium stringency level cut off (log2 ratio>=0.58 or >=1.5 fold change, FDR<=0.01), only 92 genes are upregulated under fed conditions between 4 hbh and 16 hph, in contrast to 2094 genes that are upregulated under fed conditions between 12 hph and 36 hph. Pro-

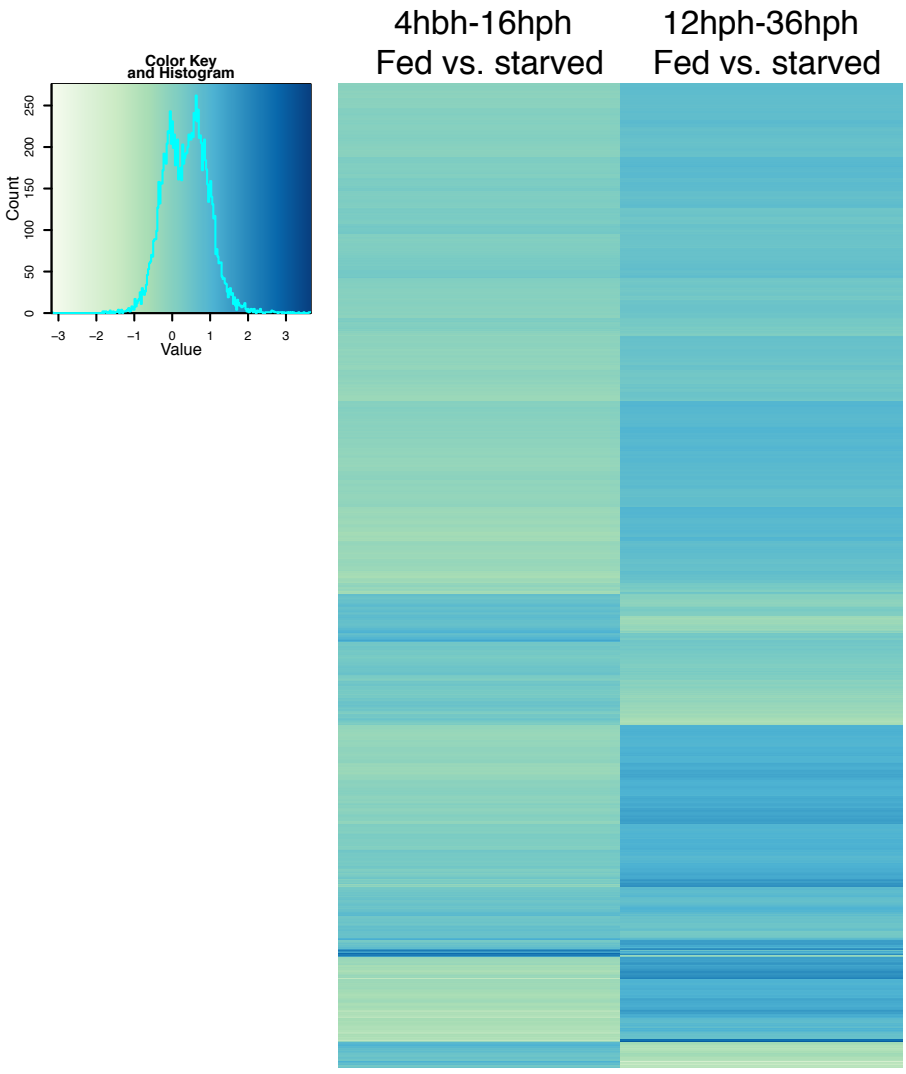

Fig. 6.2.8 Transcriptional responses to starvation in CNS glial over time. Heat maps are generated from pan-glial TaDa transcriptional profiling experiments under fed and starved conditions over two time windows (4hbh–16hph, 12hph–36hph). Log2 ratio between fed and starved conditions for all genes with FDR<=0.01 were calculated and plotted across two time windows.

teins encoded by these 92 genes form a dense interaction network according to known and predicted protein interactions, based on STRING functional protein association network analysis (Franceschini *et al.* , 2013; von Mering *et al.* , 2005). Enriched clusters of interaction include "translation","RNA processing","fatty acid biosynthesis","citric acid cycle" and "extracellular matrix proteins" (Figure 6.2.9). Interestingly, the "extracellular matrix proteins" cluster includes both Collagen IV^{Cg25C} and Collagen IV^{Vkg}, which have previously been shown to travel from the fat body and deposit on the CNS surface. Although glial TaDa transcriptional profiling indicates that glial cells may be capable of expressing their own Collagen IV protein locally, I confirmed that the majority of Collagen IV protein on the CNS surface originate from the fat body and that only fat body derived Collagen IV is required for NSC reactivation (see Chapter 3 for details).

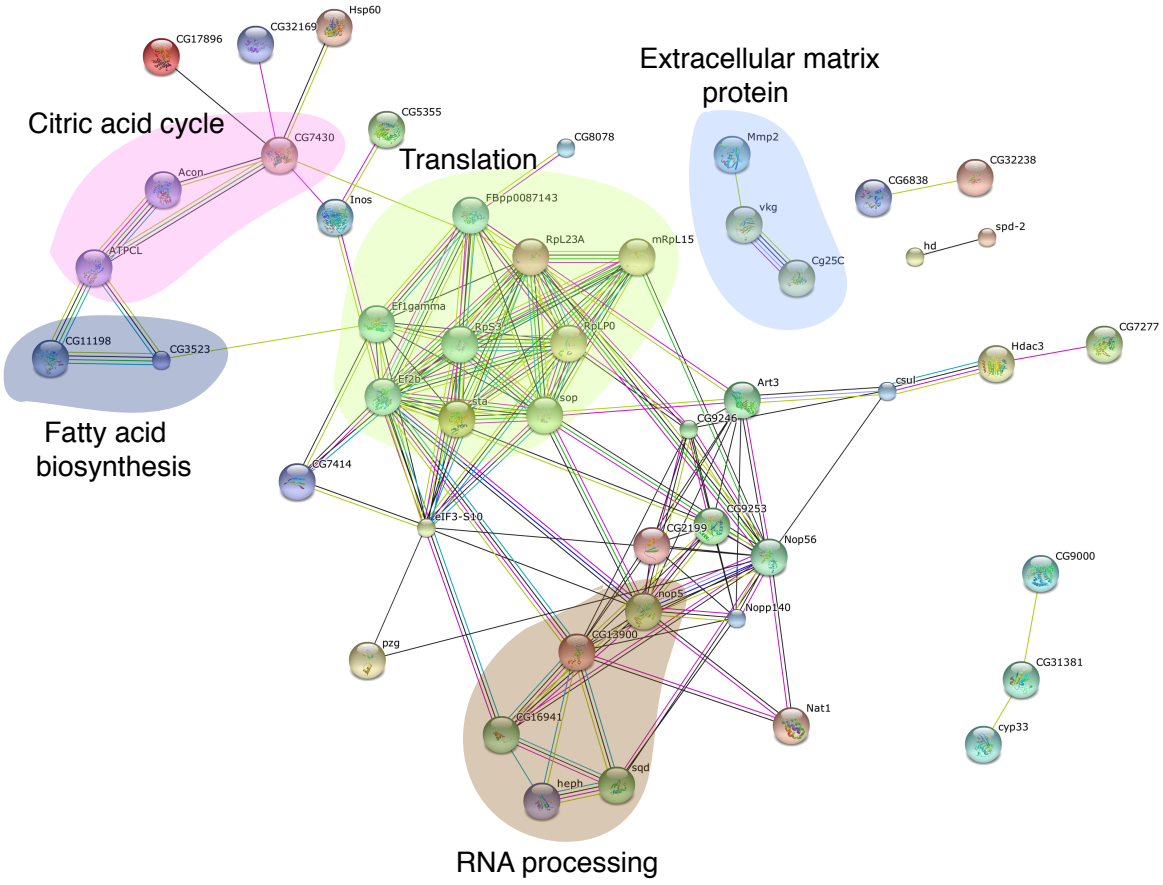

Fig. 6.2.9 Known and predicted interactions between the products of 92 genes upregulated in the glia under fed conditions. Analysis was performed using STRING with a medium confidence score of 0.4 and all interaction methods available. Clusters representing selected pathways and processes are highlighted. Single nodes are not displayed

6.3 Components of the Glial Niche Show Distinct Transcriptional Signatures

6.3.1 CG, PG and SPG Undergo Extensive Transcriptional Activities During the Time Window of NSC Reactivation

The glial niche associated with NSCs consists of three major glial subtypes: subperineurial glia (SPG), perineurial glia (PG), and cortex glia (CG). Studies so far have not reached a consensus regarding the relative contributions of glial subtypes to NSC reactivation. Whereas Chell and Brand suggest that the "surface glia" (PG and/or SPG) are the most important components of the glial niche (Chell & Brand, 2010), another study argues for a prominent role of the cortex glia (Sousa-Nunes *et al.* , 2011). Due to the technical difficulty of isolating individual glial subtypes, it has not been feasible to systematically assess the contribution of individual glial subtype to NSC reactivation. Taking advantage of the availability of glial subtype specific GAL4 drivers and the TaDa technique (Southall *et al.* , 2013), we undertook the first systematic approach to examine the transcriptomes of each glial subtype during the critical time window of NSC reactivation (Figure 6.3.1).

The TaDa transcriptional profiling experiment revealed extensive transcriptional activities and distinct transcriptional signatures among the three glial niche components (Figure 6.3.2). SPG showed the highest level of transcriptional activity. Using a medium stringency level of Log2 ratio>=0.58 and FDR<=0.01, I found 2997, 1214 and 848 genes are transcribed in SPG, PG and CG, respectively during the first 24 hours post larval hatching. The transcriptomes and enriched pathways in the three glial subtypes showed extensive overlaps (Figure 6.3.3). Interestingly, among the 308 genes transcribed in all glial subtypes, KEGG pathways related to "glycolysis/gluconeogenesis" are enriched, indicating that carbohydrate metabolism/homeostasis is a shared and essential function of CNS glial cells (Figure 6.3.3). The role of glial carbohydrate metabolism as energy conduits for neurons and NSCs are conserved in flies and mammals. For example, astrocytes in the mammalian BBB localise glucose transporters at their endfeet, which project into the surrounding brain capillaries to take up glucose from the circulation. The astrocytes store glucose in the form of glycogen and release glucose to fuel neuronal activities when needed. For a review of mammalian glial niche's role in carbohydrate metabolism of the CNS, see (Freeman & Doherty, 2006a). In *Drosophila*, the main energy supply of the brain is provided by trehalose in the hemolymph (Wyatt & KALE, 1957). Trehalose is a disaccharide, which is taken up and broken down to either monosaccharide or C3 metabolites by specialised glial cells, which is then supplied to

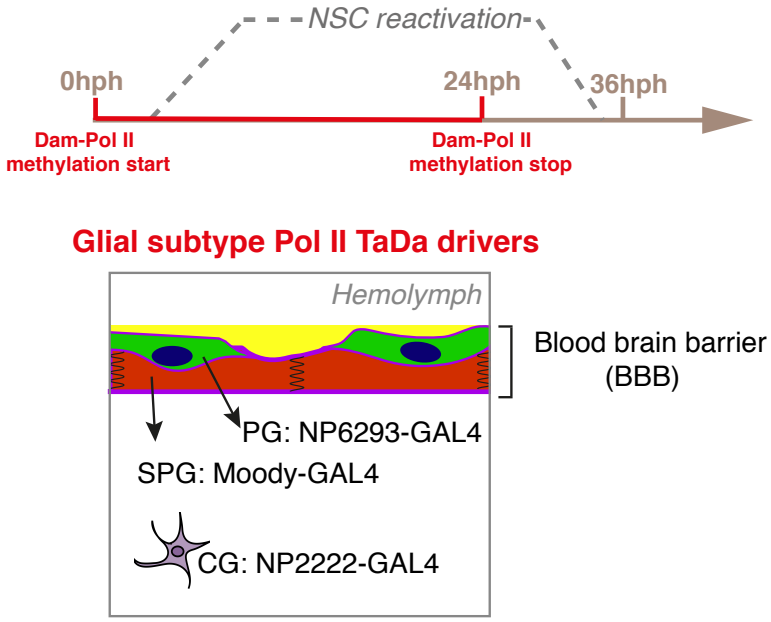

Fig. 6.3.1 Schematics of glial subtype TaDa transcriptional profiling. Glial subtype transcriptional profiling was performed between 0–24 hph, a time window closely associated with NSC reactivation. Glial subtype specific GAL4 drivers used: NP6293-GAL4 for PG, Moody-GAL4 for SPG, and NP2222-GAL4 for CG.

neurons (personal communication with Stefanie Limmer, Christian Klambt lab, University of Munster).

The two BBB glia, SPG and PG, shared "oxidative phosphorylation" and "pentose phosphate pathway" as enriched pathways in addition to the two mentioned earlier. Interestingly, the two BBB glia showed distinct enrichment in different amino acid metabolism: whereas metabolism of the non-essential alanine, glutamate and aspartate are enriched in PG, metabolism of three essential amino acids, valine, leucine and isoleucine, are enriched in SPG. This may indicate cooperation or "division of labor" between the two BBB glial cell types in the complex process of amino acid/protein metabolism.

Interestingly, lipid metabolism pathways are enriched in both BBB glial subtypes. It should be noted that sphingolipid metabolism is highly enriched only in the PG. Sphingolipid is a class of lipid known to participate in cellular signalling, such as MAPK (Mitogen-activated protein kinase) and JNK (c-Jun N-terminal kinases) signalling, as well as play a role in nutrient response. For a review of sphingolipids in flies, see (Kraut, 2011). Recent studies revealed a novel role of sphingolipid in regulating exocytosis (Darios *et al.* , 2009), which is particularly relevant to the function of the glial niche. CNS glia is known to secrete factors important for NSC reactivation, such as DIlp6, Perlecan^{Trol} and Anachronism. Therefore, exocytosis plays an essential part in the glial regulation of CNS development. Exocytosis occurs when vesicles loaded with secretory particles such as neurotransmitters fuse with the plasma membrane, causing release of their content. Neuronal exocytosis requires three SNARE (soluble-N-ethylmaleimide sensitive factor attachment protein receptor) proteins: synaptobrevin–2 (also known as VAMP–2) on the synaptic vesicle, and syntaxin–1 with SNAP–25 (Synaptosomal-associated protein 25) on the plasma membrane (Jahn & Scheller, 2006). The formation of SNARE complex by the three proteins is an essential step toward membrane fusion and exocytosis. Sphingosine allows for the release of synaptobrevin from its phospholipid anchorage so that SNARE complex can be formed together with syntaxin/SNAP–25. It would be interesting to investigate whether sphingolipids play similar roles to facilitate exocytosis from the perineurial glia, and whether sphingolipid-mediated secretion/signalling are important for NSC reactivation.

The *Drosophila* CNS glial cells were considered to perform the function of a NSC niche mainly based on the prominent roles of several glial factors, including DIlp6, Anachronism, and Perlecan^{Trol}. However, the precise sources of these key glial factors (i.e. which glial subtype do they come from) were previously unknown or ambiguous. For example, whereas one study showed that DIlp6 is secreted by "surface glia" (PG and/or SPG) (Chell & Brand, 2010), another argued that DIlp6 is expressed by the cortex glia (Sousa-Nunes *et al.* , 2011).

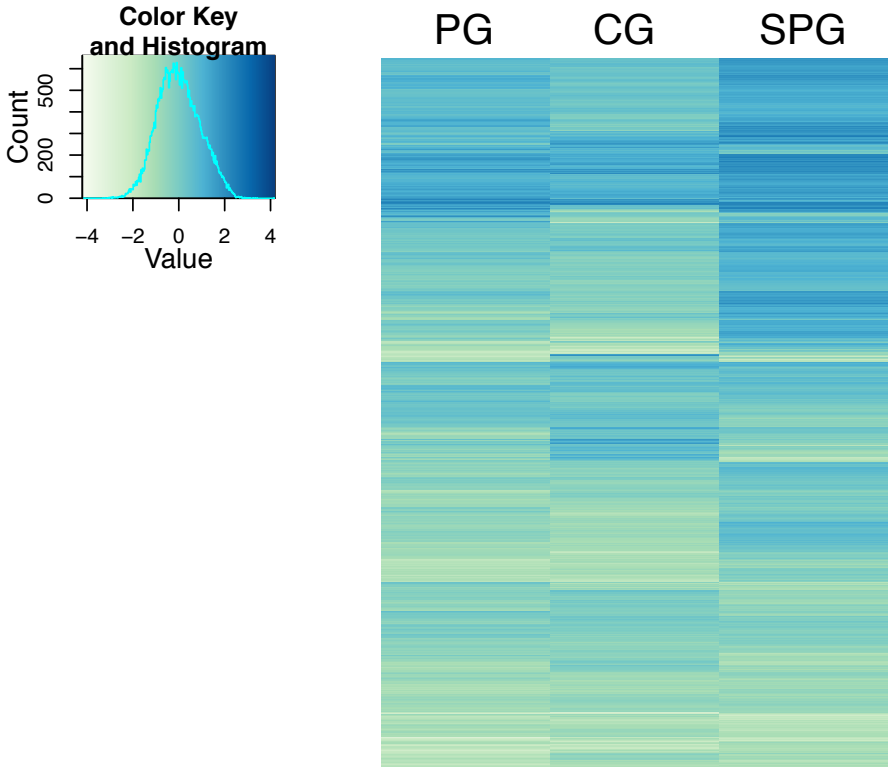

Fig. 6.3.2 Glial subtypes exhibit distinct transcriptional signatures. Heat maps are generated with Log2 ratios of all genes from glial subtype TaDa transcriptional profiling experiments in three glial subtypes (CG, PG and SPG).

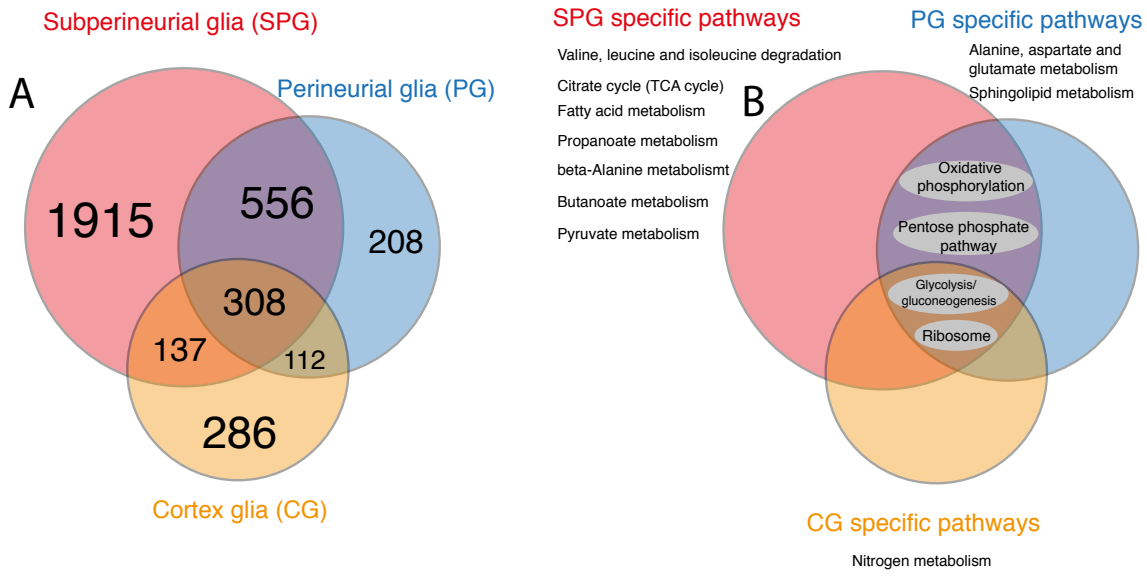

Fig. 6.3.3 Overlaps of transcribed genes and enriched pathways in the glial subtypes. (A) Venn diagram shows the numbers of genes transcribed in and shared between three glial subtype. (B) Venn diagram shows biological pathways enriched in and share between three glial subtypes.

Whereas Ebens et al showed that anachronism proteins are associated with the cortex glia (Ebens *et al.* , 1993), a more recent study suggests that NSCs transcribe *anachronism*, which is suppressed by a microRNA to enable proper NSC proliferation (Weng & Cohen, 2012). Our glial transcriptome analysis was able to trace these factors to their subtype origin: SPG and PG both transcribe *dIlp6*, PG transcribes *perlecan*^{trol}, and CG transcribes *anachronism* (Figure 6.3.4). *dIlp6* has 3 transcription start sites which result in 4 mRNA isoforms that encode proteins with the same amino acid sequences. Based on Pol II binding patterns, transcription of *dIlp6* initiates at different sites in the two BBB glia subtypes (Figure 6.3.4). In CG, an abrupt peak of Pol II binding coincides with a transcription start site in the middle of the *dIlp6* locus, suggesting Pol II pausing. As discussed previously, *perlecan*^{trol} is transcribed exclusively in the perineurial glia. In addition, the current study revealed many other glial subtype-specific factors that potentially contribute to the development of the CNS and NSC proliferation/differentiation. 73 genes, most of which are transcribed specifically in the SPG, have been implicated in neurogenesis according to analysis of GO biological processes (see Appendix).

Our data suggest that many glial genes are conserved between flies and human. Some of these glial subtype-specific genes have human orthologs which have been implicated in

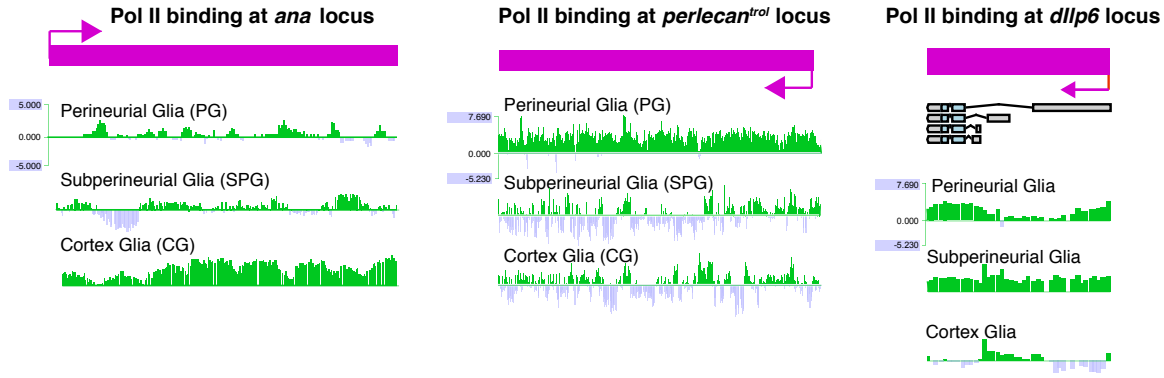

Fig. 6.3.4 Pol II binding at *ana*, *trol* and *dIlp6* loci in three glial subtypes. Three known regulators of NSC reactivation, *ana*, *trol* and *dIlp6* are transcribed by different glial subtypes during the time window of NSC reactivation. *ana* is transcribed by CG only, *trol* is transcribed by PG only, and *dIlp6* is transcribed by SPG and PG.

CNS pathologies, from Alzheimer's to neuroblastoma (Table 6.3.1). In mammalian CNS, glial cells greatly outnumber neurons, and the majority of malignant brain tumours are derived from glial cells or their progenitors, as reviewed in (Jessen, 2004). Although many neurodegenerative diseases were initially thought to be neuronal pathologies, increasing evidence points to the contributions of glial cells (Dong *et al.* , 2010; Nagele *et al.* , 2004; Shie *et al.* , 2009). For example, astrocytes contribute to the development of amyloid plaque in Alzheimer's (Nagele *et al.* , 2004). Due to technical and ethical constraints, it is often difficult to study the functions of genes involved in human CNS pathogenesis and to dissect their functions in human glial cells. The identification of these conserved genes means that *Drosophila* can serve as a useful model system to study human CNS diseases. With its powerful genetics, *Drosophila* could advance our mechanistic understanding of glial biology, which could help to elucidate how different types of glial cells participate in the pathogenesis of the brain, such as during ageing and tumour formation.

6.3.2 Analysis of Global Transcriptional Profiles Revealed Closer Clustering Between the Two BBB Glial Cell Types

Both SPG and PG are located at the surface of the CNS and have been proposed to form the *Drosophila* BBB (Stork *et al.* , 2008). However, efforts investigating the *Drosophila* BBB function has focused predominantly on the SPG, to an almost total exclusion of PG. Key functions such as septate junction (equivalent to mammalian tight junction) formation and clearance of toxic agents are associated with the SPG (DeSalvo *et al.* , 2011), but virtually

nothing is known about the function of PG. The hypothesis that PG forms the BBB was purely based on the localisation of PG rather than any molecular evidence. I hypothesised that if indeed PG and SPG form the BBB, their molecular functions may be intertwined, and thus their transcriptional profiles may show greater similarity with each other than with the CG. Indeed, I have shown earlier that a significant number of genes are co-expressed in PG and SPG (Figure 6.3.3). Next, I decided to investigate the relationship of the three glial subtypes' transcription profiles in a more quantitative manner. A scatterplot matrix of Log2 ratios of all *Drosophila* genes was created for all available pairs of glial transcriptomes (CG vs. PG, CG vs. SPG, PG vs. SPG, CG vs. pan-glia, PG vs. pan-glia, and SPG vs. pan-glia). Correlations between all pairs of expression profiles are visualised in Figure 6.3.5 and summarised in Table 6.3.2. Colours indicate the degrees of correlation, with red representing the strongest correlation and yellow representing the weakest (Figure 6.3.5). The clustering diagram on the left-hand side of Figure 6.3.5 was again computed based on correlations between each pair of transcriptional profiles. The correlation coefficient is highest between SPG and pan-glia, followed by SPG and PG, whereas the correlation coefficients between SPG and CG or PG and CG are low in comparison. This suggests that global Pol II binding profiles between the two BBB glia is the closest among the three glial subtypes.

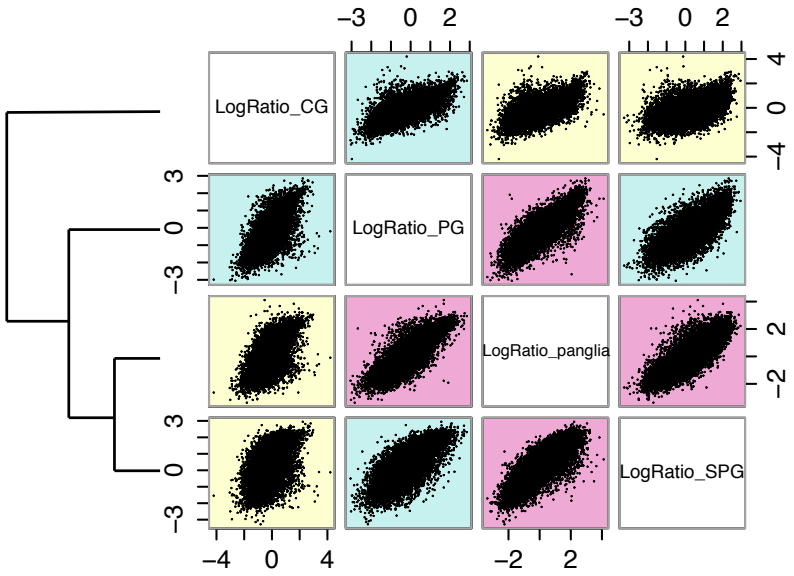

Fig. 6.3.5 Matrix and clustering of global Pol II binding profile scatterplots for pan-glial and glial subtype transcriptomes. A scatterplot matrix of Log2 ratios of all *Drosophila* genes were created for all available pairs of glial transcriptomes (CG and PG, CG and SPG, PG and SPG, CG and pan-glia, PG and pan-glia, and SPG and pan-glia). Colours indicate the strength of association (decreasing level of association from red to yellow to blue).

Table 6.3.2 Correlation table of Pol II binding profiles in individual glia subtype

	LogRatio_SPG	**LogRatio_PG**	**LogRatio_CG**	**LogRatio_Pan-glia**
LogRatio_SPG	1	0.73	0.47	0.81
LogRatio_PG	0.73	1	0.68	0.82
LogRatio_CG	0.47	0.68	1	0.62
LogRatio_panglia	0.81	0.82	0.62	1

Using an alternative approach, Jorge Buendia-Buendia investigated gene expression clustering by comparing the on/off states of transcription for all genes which pass a FDR threshold of 0.01, among three glial subtypes. Again, we found closer clustering between PG and SPG (data not shown).

6.3.3 The *Drosophila* BBB Glial Transcriptional Profiles Share Remarkable Similarity With the Mammalian BBB

Although recent years have seen exciting advances in the investigation of the mammalian BBB, our understanding of the BBB remains rudimentary. BBB has been implicated in a variety of CNS diseases, including multiple sclerosis, stroke, and cancer, as reviewed in (Stork *et al.* , 2008). However, pathogenic mechanisms of these diseases still remain elusive. In addition, scientists and clinicians have long been frustrated by the obstacle that the BBB poses to pharmacologic intervention of the brain. Previously, several parallels have been drawn between the *Drosophila* and mammalian BBB. Do *Drosophila* and mammalian BBBs share conserved functions on a larger scale? Can the *Drosophila* BBB help to advance our understanding of basic mechanisms governing mammalian BBB development and homeostasis? Comparing the published mammalian BBB transcriptome (Daneman *et al.* , 2010) with our BBB glial transcriptome (PG + SPG), we were able to compare invertebrate and vertebrate BBB gene expression, biological functions and signalling pathway enrichment, on a genome-wide scale.

A mouse BBB transcriptome of both adult and post-natal animals has recently been published (Daneman *et al.* , 2010). I decided to first compare our BBB glial transcriptional profiling with post-natal mouse BBB. The mouse BBB consist of pericytes, astrocytic end-feet, and endothelial cells. In the Daneman et al study, both post-natal pericytes and endothelial cells are marked by Tie2GFP, which were FACS sorted into one combined category (Daneman et al did not publish the post-natal astrocyte transcriptome). Ideally, it would be interesting to compare the SPG transcriptome with the endothelial cell transcriptome, because the septate junction-forming *Drosophila* SPG are proposed to be the functional equivalent of the tight junction-forming mammalian endothelial cells. Likewise, the PG, which form a loosely fenestrated network around the brain, show morphological similarities to the pericytes and/or astrocytes. However, since Daneman et al did not separate post-natal endothelial cells from pericytes when performing their transcriptome analysis, I decided to compare their merged BBB transcriptome (containing both endothelial cells and pericytes) with our BBB transcriptome (containing both SPG and PG).

In order to compare the *Drosophila* and mammalian transcriptional data, I first identified known or predicted mammalian orthologs of the *Drosophila* genes of interest through the online DRSC Integrative Ortholog Prediction Tool (Drosophila RNAi Screening Center) website (http://www.flyrnai.org/diopt) (Hu *et al.* , 2011). This tool integrates all existing approaches to facilitate identification of vertebrate othologs of *Drosophila* genes. All pre-

diction settings were left to default, except that the "exclude low score" filter was selected. The converted *Drosophila*-to-mouse ortholog gene list was then compared to the mouse BBB transcriptome. Approximately half of genes transcribed by larval *Drosophila* PG and SPG are also transcribed by the post-natal mouse BBB (Table 6.3.3).

In addition to serving as a physical barrier between the brain and the blood/hemolymph, the BBB in both vertebrates and flies plays an active role in the clearance of foreign and toxic substances, therefore serving as a chemical barrier and detoxification centre for the brain, as reviewed in (Stork *et al.* , 2008). The conserved BBB genes show enriched KEGG pathways related to these roles, such as "drug metabolism" and "metabolism of xenobiotics by cytochrome P450" (Table 6.3.4). Genes and their molecular functions associated with drug metabolism are shown in Table 6.3.5. In addition, several metabolic pathways related to both essential and non-essential amino acids, lipids and aerobic respiration as previously observed to be enriched in genes transcribed by PG and SPG, are also enriched in the conserved gene list.

Interestingly, our analysis highlighted an enrichment of "retinol metabolism" among conserved BBB genes. This finding is consistent with a recent discovery that retinoic acid is secreted from the NSCs (radial glial cells) to induce BBB formation in the mouse fetal brain, and expression of retinoid acid as well as its receptors are highly enriched in human fetal BBB, although their mechanism of action are unclear (Mizee *et al.* , 2013). The current study provides the first indication that retinol-signalling may be a conserved pathway that regulates BBB development and homeostasis in invertebrates and vertebrates. Genes and their molecular functions associated with retinol metabolism are shown in Table 6.3.6.

Next, I identified and clustered enriched biological processes among the conserved gene list using Gene Ontology. GO terms associated with metabolism, developmental processes and morphogenesis are most prevalent, but processes related to "transport and exo/endo-cytosis", "regulation of growth" and "cell/tissue size", and "cell cycle" are also highly enriched (Figure 6.3.6). Interestingly, "amino acid transport" was found under the "transport and exo/endo-cytosis" cluster. If toxic molecules cannot penetrate the brain, then nutrients and metabolites have similar difficulty in passing the BBB to reach and nourish cells within the brain (DeSalvo *et al.* , 2011). Recent years have seen growing interest in understanding the transport and delivery of nutrients such as amino acids in mammalian brain. Several specific amino acid transporters have been identified in mammalian CNS, but little is known about BBB-dependent nutrient homeostasis in *Drosophila* (Freeman *et al.* , 2003; Stork *et al.* , 2008). Therefore, our study identified potential players of amino acid transport in the BBB and provided a starting point to investigate how the *Drosophila* BBB regulates

CNS amino acid metabolism, which will allow for more meaningful cross-comparison with the vertebrate BBB. Another point of interest about BBB mediated amino acid transport is its potential role during NSC reactivation. Existing evidence suggests that fat body is the key systemic amino acid sensor in *Drosophila* (Britton & Edgar, 1998; Sousa-Nunes *et al.* , 2011). In response to dietary amino acids, it secretes circulating factors to instruct the BBB glia to produce DIlps, which in turn reactivates the NSCs. However, it cannot be ruled out that the BBB glia possess intrinsic amino acid sensing capacity, which signals directly upstream of TOR and DIlp production in parallel or independently of fat body factors. In support of this idea, a recent study showed that when the amino acid-sensitive PI3K/TOR signalling components were disrupted in CNS glia, NSCs fail to reactivate efficiently even though fat body signals were undisturbed (Sousa-Nunes *et al.* , 2011). The current glial transcriptome analysis provides evidence for the existence of a diverse array of conserved amino acid transporters/sensors in the BBB. Some of these transporters, such as the proton-assisted amino acid transporter family (Slc36/path), have been shown to play dual transporter and sensor functions, directly impinging on downstream TOR signalling, as reviewed in (Reynolds *et al.* , 2007). Genes and their molecular functions associated with amino acid transport/sensing are shown in Table 6.3.7.

Thus, the GO analysis not only confirmed known biological processes of the BBB, such as metabolism, response to external stimulus/stress response, and cellular junction formation, but also highlighted potential novel processes worthy of further investigation such as direct amino acid sensing by BBB glia.

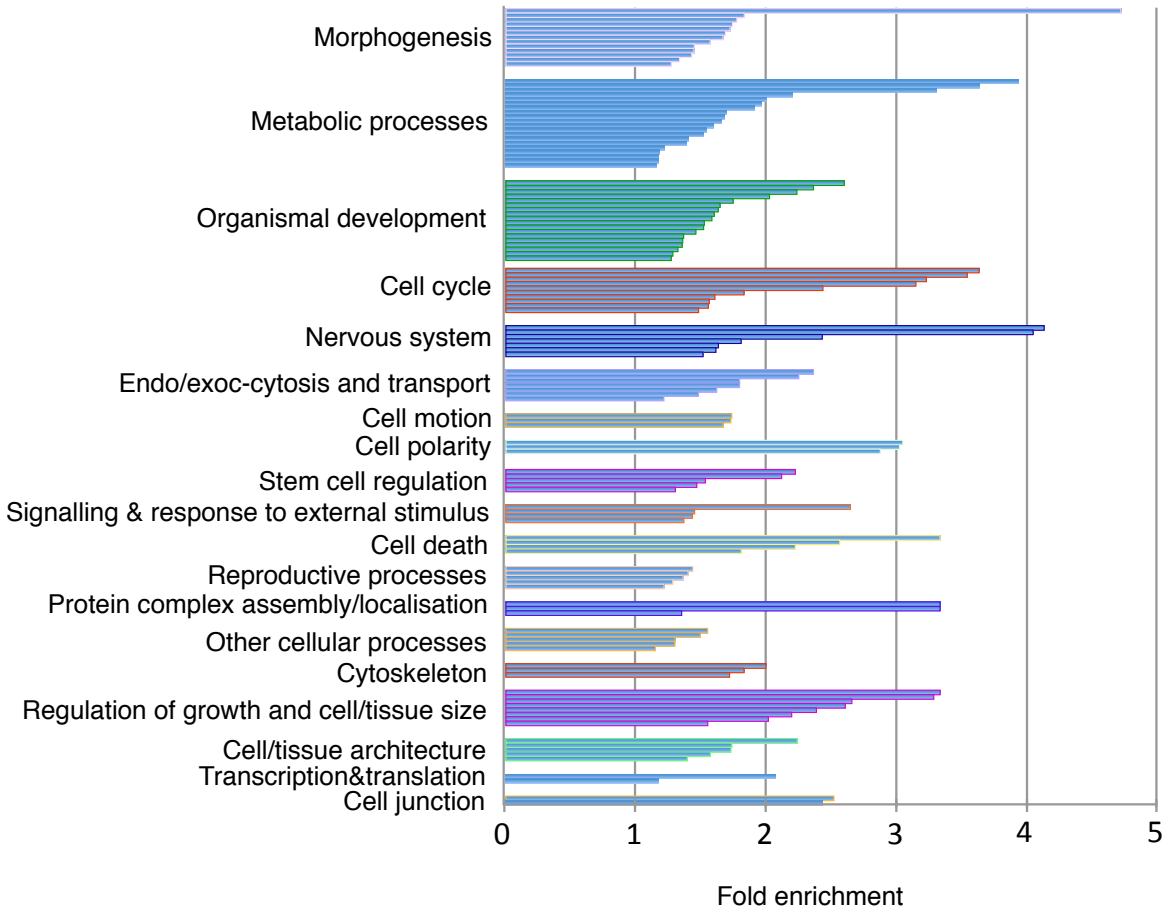

Fig. 6.3.6 Clustered GO biological processes among conserved BBB genes. 126 significantly enriched biological processes (P value<=0.05, GO_BP level=3) were identified among genes transcribed in both *Drosophila* and mammalian BBB, using Gene Ontology algorithms. These were clustered into 19 broader functional categories, shown in the graph.

Table 6.3.1 Glial subtype specific genes whose human orthologs play roles in human CNS diseases

Fly gene symbol	Glial subtype	Human gene symbol	Nervous system diseases
mRpL10	SPG	MRPL10	Alzheimer's disease (cognitive decline)
Got2	SPG	GOT1	Aspartate aminotransferase
Bem46	SPG	ABHD13	Attention deficit hyperactivity disorder and conduct disorder
gkt	SPG	TDP1	Spinocerebellar ataxia, autosomal recessive with axonal neuropathy
Wdr82	SPG	WDR82	Bipolar disorder
fy	SPG	FUZ	Neural tube defects
Npc1a	SPG	NPC1	Niemann-Pick disease, type C1
Myo31DF	SPG	MYO1D	Hypertension risk in short sleep duration
Tap42	SPG	IGBP1	Agenesis of Corpus callosum, with mental retardation
cenG1A	SPG	AGAP1	Schizophrenia
VhaSFD	SPG	ATP6V1H	Bipolar disorder (mood-incongruent)
fbp	SPG	FBP1	Fructose-1,6-bidphosphatase deficiency
Arpc2	SPG	ARPC2	Inflammatory bowel disease
Acon	SPG	ACO2	Infantile cerebellar-retinal degeneration
Uba1	SPG	UBA1	Spinal muscular atrophy, X-linked 2, infantile
park	CG	PARK2	Disc degeneration (lumbar)
toy	CG	PAX6	Coloboma of optic nerve
hoe1	CG	OCA2	Parkinson's disease (age of onset)
esg	CG	SNAI2	Waardenburg syndrome, type 2D
dac	CG	DACH1	Obsessive-compulsive disorder
Lim3	CG	LHX3	Pituitary hormone deficiency
trh	CG	NPAS3	Schizophrenia, bipolar disorder and depression (combined)
btl	CG	FGFR1	Jackson-Weiss syndrome
Eaat2	CG	SLC1A2	Essential tremor
salm	CG	SALL1	Townes-Brocks syndrome
Blimp-1	CG	PRDM1	Crohn's disease
Csas	CG	CMAS	Entorhinal cortical thickness
peb	CG	RREB1	Multiple sclerosis
Sp1	CG	SP8	Bipolar disorder
SoxN	CG	SOX2	Microphthalmia, syndromic 3
Cg25C	PG	COL4A5	Alport syndrome
Dh44-R2	PG	CRHR1	Intracranial volume
Sema-5c	PG	SEMA5A	Autism
htl	PG	FGFR3	Crouzon syndrome with acanthosis nigricans
Dys	PG	DMD	Response to antidepressant treatment
trol	PG	HSPG2	Schwartz-Jampel syndrome, type 1
dnc	PG	PDE4D	Neuroticism
Spred	PG	SPRED2	Inflammatory bowel disease
lin-28	PG	LIN28B	Neuroblastoma
LpR1	PG	VLDLR	Alzheimer's disease (age of onset)
Syb	PG	VAMP3	Periodontal microbiota
Dys	PG	NPAS4	Bipolar disorder
Slc45-1	PG	SLC45A2	Oculocutaneous albinism, type IV
Ac78C	PG	ADCY8	Total ventricular volume
plx	PG	TBC1D1	Crohn's disease

Table 6.3.3 Overlap between Drosophila and mouse BBB gene expression

Glial Subtype	NO. of transcribed genes	NO. of transcribed genes whose orthologs are transcribed in mouse BBB	Percentage of transcribed genes whose orthologs are transcribed in mouse BBB
SPG	2914	1413	48
PG	1184	562	47

Table 6.3.4 KEGG pathways enriched in BBB genes expressed in both Drosophila and mouse

Kegg pathway terms	Fold Enrichment
Cysteine and methionine metabolism	2.83
beta-Alanine metabolism	2.65
Propanoate metabolism	2.62
Valine, leucine and isoleucine degradation	2.48
Fatty acid metabolism	2.38
Ribosome	2.07
Retinol metabolism	1.92
Glycerolipid metabolism	1.86
Pentose and glucuronate interconversions	1.89
Drug metabolism	1.81
Metabolism of xenobiotics by cytochrome P450	1.77
Citrate cycle (TCA cycle)	1.71

Table 6.3.5 Conserved BBB genes involved in drug metabolism

Fly gene symbol	Mouse gene symbol	Molecular function	Prediction derived from
Cyp9f2	Cyp3a59	electron carrier activity	Homologene, Inparanoid, orthoMCL
GlcAT-S	B3gat1	galactosylgalactosylxylosylprotein 3-beta-glucuronosyltransferase activity	Compara, OrthoDB
Ugt86Dd	Ugt2b37	glucuronosyltransferase activity	Inparanoid, Isobase
CG15661	Ugt2b38	glucuronosyltransferase activity	Inparanoid, Phylome
CG4302	Ugt2b36	glucuronosyltransferase activity	Homologene, Inparanoid, OMA, orthoMCL, Phylome
Ugt36Bc	Ugt3a2	glucuronosyltransferase activity	Compara
Ugt86Di	Ugt2a3	glucuronosyltransferase activity	Inparanoid, Isobase
Ugt35a	Ugt8a	glucuronosyltransferase activity	Compara, Inparanoid, orthoMCL
GstD1	Gstt2	glutathione transferase activity	Compara, OrthoDB
gfzf	Gsto2	glutathione transferase activity	Isobase
GstE1	Gstt2	glutathione transferase activity	Compara, OrthoDB, orthoMCL
GstE6	Gstt3	glutathione transferase activity	Compara, orthoMCL
GstE7	Gstt3	glutathione transferase activity	Compara, orthoMCL
GstE9	Gstt2	glutathione transferase activity	Compara, OrthoDB, orthoMCL
GstE3	Gstt2	glutathione transferase activity	Compara, OrthoDB, orthoMCL
GstE2	Gstt3	glutathione transferase activity	Compara, orthoMCL
Fmo-1	Gm4847	monooxygenase activity	Inparanoid, orthoMCL, RoundUp
Adhr	Hpgd	NAD binding, alcohol dehydrogenase (NAD) activity	Compara, OrthoDB, orthoMCL, Phylome, Treefam
Aldh-III	1700055N04Rik	oxidoreductase activity, acting on the aldehyde or oxo group of donors, NAD or NADP as acceptor	Compara, OrthoDB, RoundUp, Treefam

Table 6.3.6 Conserved BBB genes involved in retinol metabolism

Fly gene symbol	Mouse gene symbol	Molecular function	Prediction derived from
mdy	Dgat1	diacylglycerol O-acyltransferase activity	Compara, Homologene, Inparanoid, Isobase, OMA, OrthoDB, orthoMCL, Phylome, RoundUp, Treefam
CG4302	Ugt2b36	glucuronosyltransferase activity	Homologene, Inparanoid, OMA, orthoMCL, Phylome
GlcAT-S	B3gat3	galactosylgalactosylxylosylprotein 3-beta-glucuronosyltransferase activity	Compara, OrthoDB
Adhr	Hpgd	alcohol dehydrogenase (NAD) activity	Compara, OrthoDB, orthoMCL, Phylome, Treefam
Ugt35a	Ugt2b35	glucuronosyltransferase activity	Inparanoid, OMA, orthoMCL
Cyp9f2	Cyp3a11	electron carrier activity	Inparanoid, Isobase, orthoMCL, Phylome, RoundUp
Ugt86Dd	Ugt1a6b	glucuronosyltransferase activity	Inparanoid, OMA
CG15661	Ugt2b35	glucuronosyltransferase activity	Homologene, Inparanoid, Isobase, Phylome
CG10673	Dhrs4	oxidoreductase activity, acting on CH-OH group of donors	Compara, Homologene, Inparanoid, Isobase, OrthoDB, orthoMCL, Phylome, RoundUp, Treefam
Ugt36Bc	Ugt1a6b	glucuronosyltransferase activity	OMA
Ugt86Di	Ugt8a	glucuronosyltransferase activity	Compara, Inparanoid, OMA

Table 6.3.7 Conserved BBB genes involved in amino acid transport

Fly gene symbol	Mouse gene symbol	Molecular function	Prediction derived from
CG30394	Slc38a10	amino acid transmembrane transporter activity	Compara, Homologene, Inparanoid, Isobase, OrthoDB, orthoMCL, Phylome, RoundUp, Treefam
CG7888	Slc36a1	amino acid transmembrane transporter activity	Compara, Phylome
colt	Slc25a20	carnitine:acyl carnitine antiporter activity	Compara, Homologene, Inparanoid, Isobase, OMA, OrthoDB, orthoMCL, Phylome, RoundUp, Treefam
CD98hc	Slc3a2	cation binding	Compara, Isobase, Phylome, Treefam
path	Slc36a3	amino acid transmembrane transporter activity	Compara, Phylome
mnd	Slc7a10	amino acid transmembrane transporter activity	Isobase, orthoMCL
Ncc69	Slc12a3	sodium:chloride symporter activity	Inparanoid, OrthoDB, orthoMCL, Phylome, RoundUp, Treefam
Eaat1	Slc1a5	glutamate:sodium symporter activity	OrthoDB, orthoMCL, Treefam
VGAT	Slc32a1	gamma-aminobutyric acid:hydrogen symporter activity	Compara, Homologene, Inparanoid, Isobase, OrthoDB, orthoMCL, Phylome, RoundUp, Treefam
JhI-21	Slc7a10	amino acid transmembrane transporter activity	Compara, orthoMCL, Phylome

6.4 BBB Glia Constitute a Nutrition-Sensitive NSC Niche

6.4.1 Analysis of Glial Subtype Transcriptional Profiles Under Different Nutrient Conditions

In order to interrogate each glial subtype's response to nutrition and advance our understanding of each subtype's role during NSC reactivation, Jorge Beundia-Buendia and I analysed glial subtype transcriptional profiles in conjunction with pan-glial transcriptional profiles under fed and starved conditions. This comprehensive analysis combining the two experiments allowed me to identify glial subtype-specific genes that are differentially transcribed under different nutritional conditions.

First, I wanted to compare the three glial subtypes' sensitivity to amino acid starvation. Among all genes upregulated under fed conditions, 1055 genes are SPG specific, 354 genes are transcribed in both SPG and PG, 79 are PG specific, whereas only 43 are CG specific (Figure 6.4.1). Based on numbers of genes affected by nutritional states, the BBB glial subtypes, especially SPG, appear to be the most sensitive to dietary amino acid deprivation, compared to the other glial subtypes.

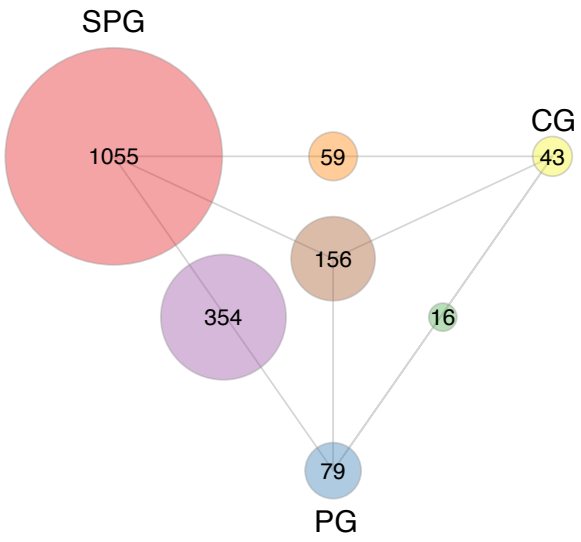

Fig. 6.4.1 SPG and PG contain higher numbers of nutrient-responsive genes than CG. A modified Venn Diagram showing numbers of genes upregulated under fed conditions in individual glial subtypes.

However, nutrient-sensitive gene numbers may be biased, because the SPG Pol II TaDa transcriptome contained higher number of total transcribed genes compared to other glial subtypes whereas CG contained the lowest number of total transcribed genes to start with.

In order to address such bias, I interrogated proportions of genes that are differentially expressed under different nutrient conditions, within each glial subtype. I hypothesised that if the SPG is indeed the most nutrient-sensitive glial subtype, a greater percentage of SPG genes would be differentially transcribed under different nutrient conditions as compared to other glial subtypes. Indeed, this is true when analyses were performed on total genes transcribed in each glial subtype (Figure 6.4.2 and Table 6.4.1), and on genes that are specific to each glial subtype (Figure 6.4.3 and Table 6.4.2). Proportions of genes upregulated under starved conditions are low in all glial subtypes.

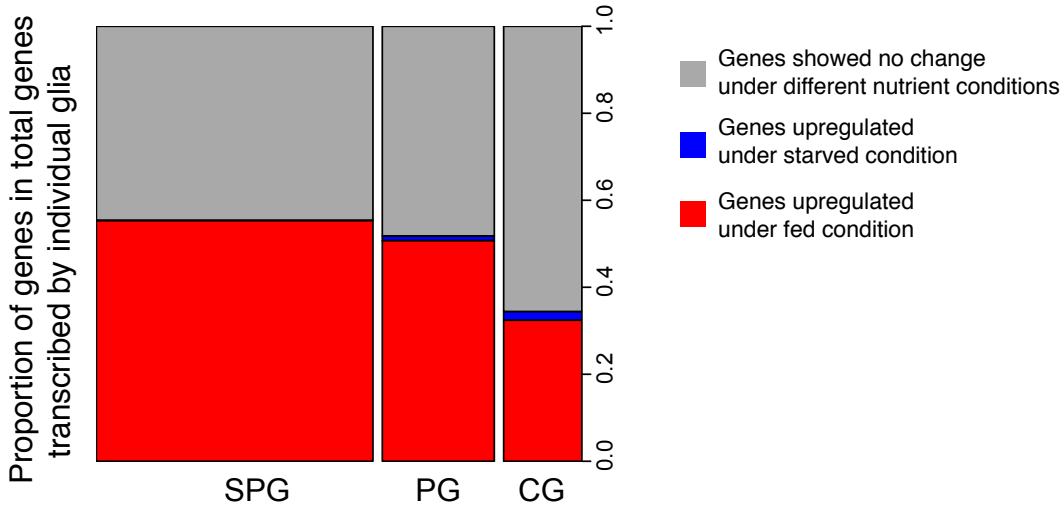

Fig. 6.4.2 BBB glial subtypes, especially SPG, transcribe higher proportions of nutrient-responsive genes than CG. The spine plots show the proportions of genes upregulated under fed conditions, genes upregulated under starved conditions, and genes unchanged under different nutrient conditions, among all transcribed genes within each glial subtype. Area of spine plots are proportional to total number of genes in different glial subtypes.

Table 6.4.1 Percentage of nutrient-responsive genes expressed by glial subtypes

Glial subtype	Total expressed genes(%)	Up in fed (%)	Up in starved(%)	No change(%)
SPG	100	55.33	0.10	44.56
PG	100	50.74	1.07	48.18
CG	100	32.42	2.00	65.56

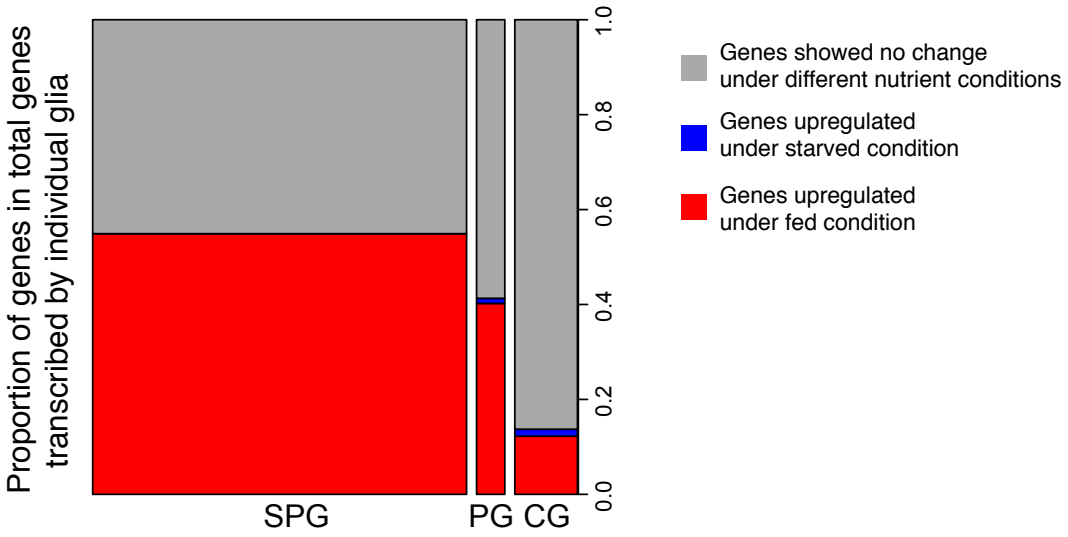

Fig. 6.4.3 BBB glial subtypes, especially SPG, contain higher proportions of nutrient-responsive subtype-specific genes than CG. The spine plots show the proportions of genes upregulated under fed conditions, genes upregulated under starved conditions, and genes unchanged under different nutrient conditions, among genes that are specific to each glial subtype. Area of spine plots are proportional to total number of genes in different glial subtypes.

Table 6.4.2 Percentage of nutrient-responsive genes specific to glial subtypes

Glial subtype	Total specific genes (%)	Up in fed (%)	Up in starved (%)	No change (%)
SPG	100	54.92	0	45.07
PG	100	40.21	1.08	58.69
CG	100	12.25	1.47	86.27

6.4.2 Disruption of Vesicle Trafficking in BBB Glia Impairs NSC Reactivation

SPG is most sensitive to nutritional fluctuation, and is also one of the sources of a key NSC reactivation signal, DIlp6. Thus, I hypothesised that SPG is the most important glial subtypes contributing to nutrition-dependent NSC reactivation. To test this hypothesis, I sought to disrupt vesicle trafficking in individual glial subtypes using a dominant negative Dynamin (Shi^{DN}), and assessed the outcome of NSC reactivation. Indeed, disrupting vesicle trafficking in SPG resulted in the strongest NSC reactivation defects, followed by PG and CG (Figure 6.4.4). At 24 hph, NSCs enlarged and started to proliferate in control larvae

and in larvae where a Shi^{DN} was expressed in the cortex glia. When Shi^{DN} was expressed by the subperineurial glia, NSCs failed to enlarge. When Shi^{DN} was expressed by the perineurial glia, NSCs enlarged but showed impaired proliferation. Quantifications of NSC enlargement and proliferation (numbers of PH3 positive NSCs) are shown in Figure 6.4.5.

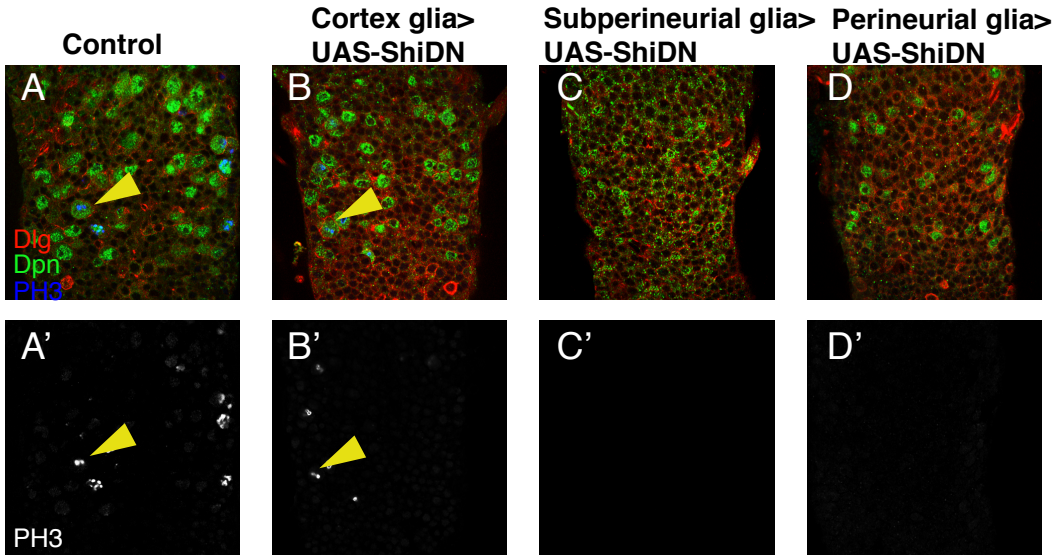

Fig. 6.4.4 Disruption of vesicle trafficking in BBB glia impairs NSC reactivation. Glial trafficking was disrupted by expressing dominant negative Dynamin (UAS-ShiDN;UAS-ShiDN) in different subtypes of glial cells after larval latching. GAL80^{ts} was used to suppress GAL4 expression during embryogenesis. NSC enlargement and reactivation was assessed 24 hours post hatching with Dlg, Dpn, and PH3 staining. (A-A‘) In control larvae (w1118 X UAS-ShiDN;UAS-ShiDN), NSCs enlarged (A) and started to proliferate (A’) by 24 hph. (B-B’) Disruption of cortical glia did not impair NSC enlargement, and only mildly affected proliferation. See Figure 6.4.5 for quantification. (C-C’) Disruption of subperineurial glia vesicle trafficking led to complete impairment of reactivation. NSCs were unable to enlarge and no proliferation was observed. (D) Disruption of perineurial glia led to moderate impairment of both enlargement and proliferation. See Figure 6.4.5 for quantification.

6.4.3 Exploration of Signalling Pathways in BBB Glia Regulating NSC Reactivation

A simplified model for NSC reactivation states that upon receipt of fat body signals, the BBB glia secrete DIlps, which in turn drives the NSCs into mitosis. However, little is known about the upstream regulators of DIlp6 production from the BBB. In addition, mis-

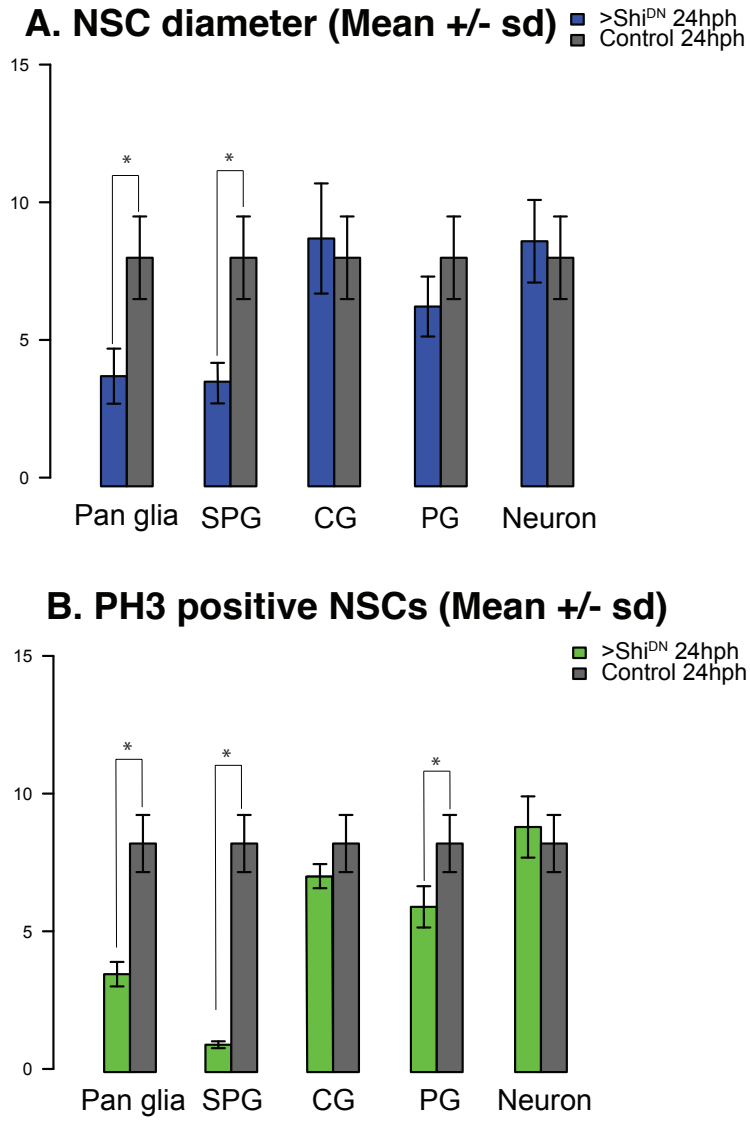

Fig. 6.4.5 Quantification Of NSC reactivation defects when vesicle trafficking was disrupted in glial subtypes. (A) NSC enlargement in the VNC was assessed by measuring the longest diameter of Dpn positive cells using Dlg to determine cell membrane boundaries. NSC enlargement was examined at 24 hph. Brains from control (w1118 X UAS-ShiDN; UAS-ShiDN) progeny were used as controls. Students' t test was conducted between control and experimental condition for each GAL4 driver at each time point. n=6. * $P<0.05$. (B) NSC proliferation in the VNC was assessed by measuring the number of PH3 positive and Dpn positive cells at 24 hph. Students' t test was conducted between control and experimental condition for each GAL4 driver at each time point. * $P<0.05$.

expression of DIlp6 alone was able to rescue NSC enlargement completely, but was not able to rescue NSC proliferation to the full extent (Chell & Brand, 2010). Thus, it is probable that other signalling pathways in the BBB glia may act in parallel with DIlp6 to instruct NSC reactivation. To identify these unknown pathways upstream of, or in parallel with, DIlp6, I searched for enriched signalling pathways among SPG specific genes that are upregulated under fed conditions using KEGG algorithm via DAIVD (Huang *et al.* , 2009). Using a medium stringency level, fold enrichment cutoff of 1, and p value cutoff of 0.1, I found that 6 pathways are enriched in the dataset (Table 6.4.3). TGF-beta pathway is the only enriched signalling pathway, with 7 components enriched in the SPG under fed conditions (Table 6.4.4). Interestingly, another report demonstrated a role for TGF-beta signalling in controlling NSC proliferation during a later stage of larval neurogenesis in *Drosophila* (Zhu *et al.* , 2008). Zhu et al showed the involvement of glial cells in this process, as Activin, a TGF-beta ligand, was expressed in the glia. However, the authors did not investigate the contribution of glial subtypes or delved into further mechanistic details.

Ongoing experiments aim to address whether and how TGF-beta signalling mediate nutrition-dependent NSC reactivation, and most importantly, whether ECM proteins regulate NSC reactivation via TGF-beta signalling pathway. Existing evidence suggests that Collagen IV may act as a co-receptor to recruit signalling ligands. The most well-characterised signalling pathway mediated by Collagen IV in *Drosophila* is BMP signalling (Bunt *et al.* , 2010; Sawala *et al.* , 2012; Tian & Jiang, 2014; Wang *et al.* , 2008), which belongs to the TGF-beta superfamily signalling pathway. Although the interaction between Collagen IV and TGF-beta ligands in *Drosophila* (including Activin-beta, Dawdle, Myoglianin and Maverick) has not been investigated, Collagen IV was shown to bind to TGF-beta1 ligands in vertebrates (Paralkar *et al.* , 1991). Since the BBB glia transcribe multiple TGF-beta ligands and downstream effectors during the time window of NSC reactivation (data not shown), I hypothesise that an autocrine/paracrine TGF-beta signalling may mediate NSC reactivation via ECM-ligand interaction at the CNS surface.

6.4.4 Chapter Summary

In collaboration with Pauline Speder, Jessie Van Buggenum and Jorge Buendia-Buendia (Andrea Brand lab), I performed a systematic analysis of the glial niche' responses to starvation, during two sequential time windows. I showed that CNS glia are highly responsive to nutrient-deprivation after approximately 12 hph, with each glial subtype exhibiting distinct transcriptional signatures. Glial subtype transcriptome analyses reveal that the BBB

glia's transcriptional activity is most sensitive to changes in nutritional intake, and many genes involved in neurogenesis and multiple metabolic/signalling pathways are upregulated upon feeding. These analyses may serve as a starting point for identifying signalling pathways acting in parallel with or upstream of glial *dIlp6* transcription. They may also aid in elucidating the molecular mechanisms underlying ECM binding to the CNS and its role in glial insulin production.

Many glial genes are conserved between flies and human. Some glial subtype-specific genes have human orthologs which have been implicated in human CNS pathologies. In addition, a comparison between mammalian and *Drosophila* BBB transcriptomes revealed high degree of overlap. Therefore, with its powerful genetics, *Drosophila* can serve as a useful model system to study glial contribution to human CNS development, homeostasis, and diseases. In particular, further mechanistic investigation of these genes may help to elucidate how different types of glial cells, especially BBB glia, participate in the pathogenesis of the brain, such as during ageing and tumour formation. Some novel/important BBB glial functions highlighted in our analysis that await further investigation include sphingolipid signalling, retinoid acid signalling, amino acids sensing, and TGF-beta signalling. In particular, TGF-beta signalling may hold the key to understanding how ECM proteins regulate NSC reactivation at the BBB.

Table 6.4.3 KEGG pathways enriched in SPG-specific genes upregulated under fed conditions

KEGG Pathway Terms	Fold Enrichment
Glyoxylate and dicarboxylate metabolism	4.28
Valine, leucine and isoleucine degradation	3.53
Propanoate metabolism	3.03
Citrate cycle (TCA cycle)	2.65
TGF-beta signaling pathway	2.57
Ubiquitin mediated proteolysis	1.95

Table 6.4.4 SPG specific genes involved in TGF-beta signalling pathway

Gene Symbol	Gene Name
Pp2A-29B	Protein phosphatase 2A at 29B
S6k	RPS6-p70-protein kinase
Rbf	Retinoblastoma-family protein
dpp	decapentaplegic
lack	lethal with a checkpoint kinase
lin19	lin-19-like
Daw	Dawdle

Chapter 7

Discussion

7.1 Summary of Main Findings

Nutrient intake affects the development and homeostasis of the brain in both vertebrates and invertebrates. The fat body acts as a systemic metabolic sensor and coordinates organismal growth with nutrient availability. Using an unbiased approach of fat body transcriptional profiling, I identified genes upregulated in the fat body under fed conditions as compared to starved conditions. I focused on Collagen IV, which is secreted from the fat body and released into the hemolymph where it regulates NSCs' exit from quiescence. Collagen IV is deposited onto the CNS surface and this in turn is required for the proper deposition of BBB glia derived Perlecan^{Trol}. Furthermore, both Collagen IV and Perlecan^{Trol} are critically required for NSC reactivation at least in part via integrin receptors and the induction of insulin signalling from the BBB glia. I showed that ECM components are key factors that mediate inter-organ communication in the context of NSC reactivation. A schematic of the ECM and insulin signalling mediated fat body-glia-NSC reactivation relay is summarised in Figure 7.1.1. In addition to ECM proteins' roles in NSC reactivation, I also briefly explored their functions in other aspects of larval development, including their role in systemic larval growth and insulin secretion from the IPCs.

In parallel to the investigation of fat body signals, I also took part in a collaborative effort to systematically investigate the glial niche's response to nutritional fluctuation based on glial TaDa transcriptional profiling experiments. The aim of this analysis was to identify candidate signalling pathways that are active in the glial niche and are mediated by ECM proteins at the brain surface. Bioinformatics and *in vivo* analyses revealed BBB glia as a nutrient-sensitive NSC niche, and highlighted important niche factors and signalling pathways, such as BMP/TGF-beta signalling, in mediating glia's nutrient response.

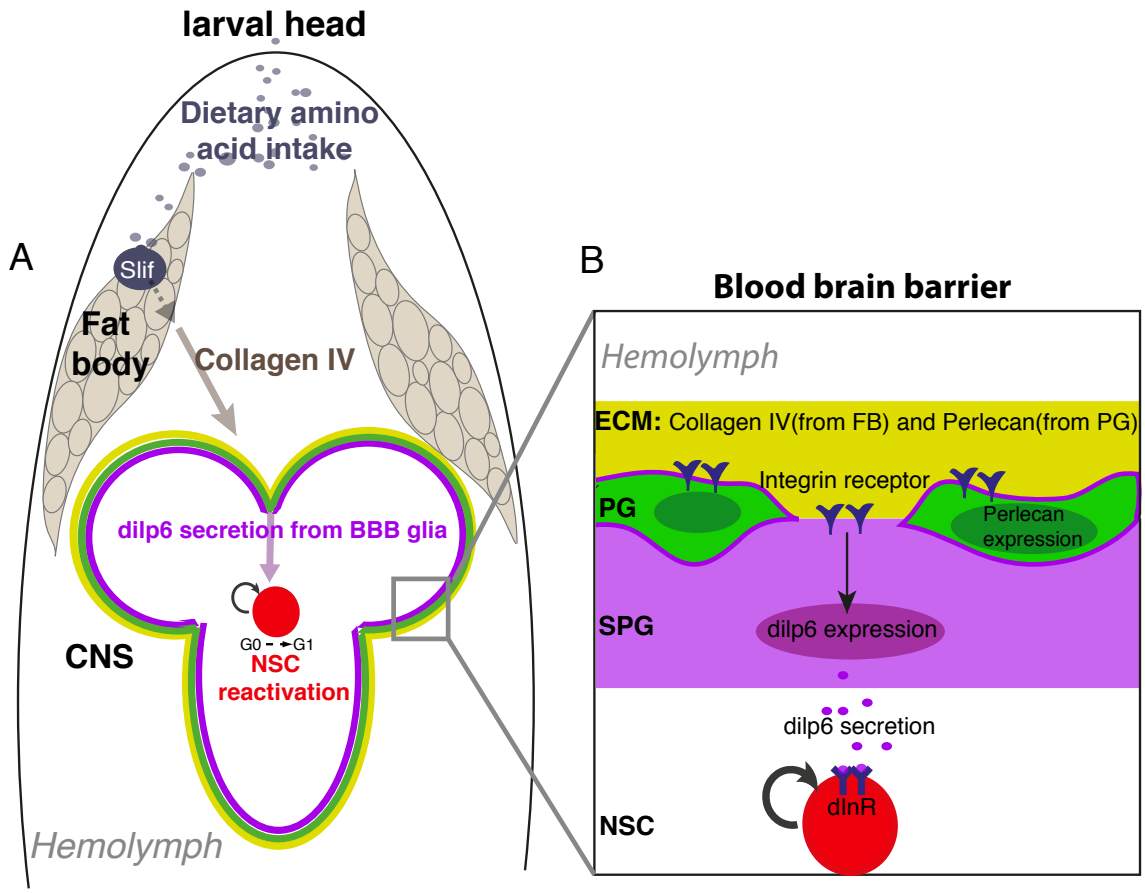

Fig. 7.1.1 ECM proteins and insulin-signalling dependent fat body-glia relay regulates NSC reactivation. (A) A relay model of amino acid dependent NSC reactivation via fat body secreted Collagen IV and glial insulin signalling. Upon sensing dietary amino acids and activation of Slif-TOR amino acid sensing pathway, the fat body secretes Collagen IV, which travels to and coats the CNS surface. (B) Collagen IV recruits perineurial glia-derived Perlecan^{Trol}, a known requirement for NSC reactivation, to the BBB and the vicinity of NSCs. Upon binding to integrin receptors on glial cells, the two ECM proteins induces glial insulin/IGF signalling from the BBB glia, which in turn triggers NSC reactivation. See text for more details.

7.2 ECM Is Important for Neurogenesis and NSC Behaviour

Many ECM components are highly conserved between vertebrates and *Drosophila* (Kazanis, 2011). A flurry of recent vertebrate studies has uncovered the crucial functions of ECM proteins in the development and homeostasis of the CNS. In particular, ECM proteins control NSC proliferation, differentiation, and migration (Ariza *et al.* , 2010; Kazanis & ffrench Constant, 2011; Kazanis *et al.* , 2010; Schlaepfer *et al.* , 2000; Schneller *et al.* , 1997). Notably, the NSC microenvironment in the neurogenic subependymal zone of adult mammalian brain is associated with distinct ECM signatures in its quiescent and reactivated state, respectively (Kazanis *et al.* , 2010). ECM proteins including laminins and their integrin receptors are implicated in regulating NSCs' transition from quiescence to reactivation (Kazanis *et al.* , 2010). Whereas the mammalian studies revealed a requirement of ECM proteins for a variety of NSC behaviours, the current study aimed at investigating the mechanisms and signalling pathways mediated by ECM during neurogenesis. Importantly, I uncovered a novel involvement of insulin signalling downstream of Collagen IV and Perlecan binding at the BBB.

Both Collagen IV and Perlecan may have conserved roles in vertebrate and invertebrate neurogenesis. A transcriptome analysis of neurogenic regions of human and mouse fetal neocortex suggests that ECM proteins may be involved in neuronal progenitor self-renewal (Simone A Fietz, 2012). In this study, transcripts of *perlecan* were highly enriched in the germinal zones consisting of neuronal progenitors compared to the cortical plates consisting of mature neurons. *collagen IV*^{vkg} transcripts were exclusively present in the germinal zone and absent from the cortical plate.

In flies and mammals alike, ECM proteins are important for early CNS development, including NSC proliferation. CNS Perlecan^{Trol} expression can be detected in both *Drosophila* and mammals. Loss of Perlecan^{Trol} led to microcephaly in mouse, as well as impaired CNS development in flies. However, although *collagen IV* expression was detected in the CNS, the consequences of Collagen IV-deficiency during CNS development have not been described in mammalian systems before. It remains unclear whether mammalian Collagen IV is also required for Perlecan^{Trol} deposition. It should be noted that the source of CNS Collagen IV may be different in mammals and flies: the current study and work of others (Pastor-Pareja & Xu, 2011) showed that Collagen IV at the *Drosophila* BBB originates exclusively from the fat body. I did not detect local Collagen IV expression in the *Drosophila* CNS based on glial TaDa transcriptional profiling. However, the mammalian fetal brain is capable of producing its own Collagen IV locally (Simone A Fietz, 2012).

Although Perlecan^{Trol} deposition on the CNS surface is downstream of Collagen IV deposition, I believe that Collagen IV's role in NSC reactivation only in part functions through Perlecan^{Trol}. This is because deprivation of Collagen IV^{Vkg} led to much stronger phenotypes compared to deprivation of Perlecan^{Trol}: whereas loss of Perlecan^{Trol} only resulted in moderate (app. 30%) reduction of CNS *dIlp6* transcription and impaired proliferation without affecting NSC enlargement, fat body knockdown of Collagen IV^{Vkg} resulted in a striking 60% reduction of *dIlp6* transcription (similar to starvation conditions). Both NSC enlargement and proliferation were abolished. Therefore, levels of *dIlp6* transcripts in the CNS appear to correlate with various degrees of NSC reactivation. It is possible that a lower threshold of DIlp6 level is required for NSC enlargement, but CNS DIlp6 needs to reach a higher level to drive NSCs into mitosis.

7.3 Collagen IV Plays a Fat Body Specific Role in Regulating Amino Acid Dependent NSC Reactivation, Potentially via BMP/TGF-Beta Signalling

Prior to the present study, very little was known about the identity and mechanism of fat body factors involved in NSC reactivation. This is in part due to technical constraints, as the fat body in the first instar larvae is difficult to isolate in its entirety. With TaDa transcriptional profiling, I eliminated the need for dissection, and was able to map the transcriptome of first instar larval fat body *in vivo*.

Collagen IV is a main component of basement membrane and it has recently been shown to play key signalling roles in both human and in flies (Bunt *et al.* , 2010; Kaido *et al.* , 2004; Sawala *et al.* , 2012). Although previous studies showed that hemocytes are required for Collagen IV diffusion during embryogenesis (Bunt *et al.* , 2010), I found that Collagen IV^{Vkg} can travel to the larval CNS surface without or with minimal aid of hemolymph factors, at least *in vitro*. How does Collagen IV on the brain surface regulate CNS development? Existing evidence suggests that Collagen IV may act as a co-receptor to recruit signalling ligands. Whereas little is known about Collagen IV's participation in cellular signalling in mammalian systems, studies in *Drosophila* started to uncover Collagen IV's involvement in BMP signalling both *in vivo* and *in vitro*. Wang et al first demonstrated that interaction between Dpp and Collagen IV^{Vkg} is essential for correct signalling in the *Drosophila* germarium and early embryo. This study suggests that Dpp secreted from the germline stem cell niche binds to Collagen IV^{Vkg}, which restricts the spreading of extracellular Dpp from

the source. In *collagen IV^{Vkg}* mutant germaria, less Dpp would be bound, resulting in an increased Dpp signalling range and increased germline stem cell number (Wang *et al.* , 2008). The formation of a BMP morphogen gradient in *Drosophila* embryos requires transport of a heterodimer of the BMPs Dpp and Scw in protein shuttling complexes. Recently, Sawala et al provided mechanistic insights that Collagen IV facilitates such gradient formation by physically binding to Dpp: Collagen IV functions as a scaffold to promote the assembly of the shuttling complexes in a multistep process to restrict the range of BMP signalling in embryos (Sawala *et al.* , 2012). This study also attempted to map the binding sites of BMP ligands on Collagen IV and identified Dpp as the only BMP ligand that physically binds to Collagen IV. In addition, Collagen IV-dependent BMP signalling has been shown to be important in other developmental contexts such as renal tubule morphogenesis (Bunt *et al.* , 2010) and midgut stem cell proliferation (Tian & Jiang, 2014). In the latter, Dpp and Gbb, two BMP ligands, are produced by enterocytes and act in a paracrine fashion to promote intestinal stem cell (ISC) self-renewal in the niche (Tian & Jiang, 2014). In vertebrates, Collagen IV has also been found to bind BMP4 and has been suggested to potentiate signalling in cultured cells (Wang *et al.* , 2008). Collagen IV was also shown to be able to bind to TGF-beta1 ligands in an osteoblast cell line (Paralkar *et al.* , 1991). These results suggest that Collagen IV can affect BMP/TGF-beta signalling during vertebrate development.

Could BMP/TGF-beta signalling play a role at the NSC niche to regulate NSC reactivation, similar to what has been previously reported for the ISC niche (Tian & Jiang, 2014)? Encouragingly, bioinformatic analysis identified TGF-beta signalling as the only nutrient-sensitive signalling pathway enriched in BBB glia. Ongoing experiments are underway to test a potential role for autocrine/paracrine BMP/TGF-beta signalling at the BBB upstream of insulin production by the glial cells. Glial transcriptional profiling shows that a number of BMP/TGF-beta ligands, including Dpp, Daw and Myo, are transcribed in BBB glia during the time window of NSC reactivation (data not shown). When a Dpp-GFP fusion protein is expressed by the glial cells, GFP is detected exclusively at the apical surface of the BBB and co-localises with the ECM. Furthermore, perturbing glial BMP/TGF-beta signalling by over-expression of ligands or expression of constitutively-active receptors (Tkv and Babo), led to abnormal NSC reactivation (data not shown).

It remains to be tested whether BMP/TGF-beta signalling is disrupted when the BBB is deprived of ECM, and whether glial insulin transcription/secretion is impaired upon disruption of BMP/TGF-beta signalling at the BBB. Interestingly, a few recent studies in both vertebrates and flies showed evidence of cross-talk between BMP/TGF-beta and insulin signalling pathways. Lin et al showed that TGF-beta/Smad3 signalling regulates insulin gene

transcription in pancreatic beta-cells, and Smad3 occupies the promoter region of the insulin gene (Lin *et al.* , 2009). Furthermore, expression profiling of the *Drosophila* larval CNS showed *dIlp2* as one of the 101 down-regulated genes in *wit* (*wishful thinking*, shared BMP/ TGF-beta Type II receptor) mutants (Kim & Marqués, 2010). *dIlp6* transcripts were not affected in *wit* mutants. However, this study examined late third instar larvae. It remains to be examined whether *dIlp6* is transcriptionally regulated by *wit* and BMP/TGF-beta signalling during the first instar stage.

7.4 Perlecan Participates in a Diverse Array of Signalling Pathways

In vertebrates, Perlecan has been well characterised in the growth and morphogenesis of the skeleton and vascular system, and it is involved in FGF, PDGF, and VEGF signalling (Melrose *et al.* , 2008; Segev *et al.* , 2004; Whitelock *et al.* , 2008). Recent studies also revealed its participation in BMP signalling (DeCarlo *et al.* , 2012), and TGF-beta signalling by interacting with the prodomains of TGF-beta ligands (Sengle *et al.* , 2011). Its involvement in a diverse array of signalling pathways could be at least partly responsible for its essential roles in many aspects of brain functions. For example, Perlecan is required for mammalian neurogenesis (Girós *et al.* , 2007), promotes regeneration from ischemic stroke (Roberts *et al.* , 2012), and protects the brain from βamyloid fibre-induced neurotoxicity (Parham *et al.* , 2013).

In *Drosophila*, early studies on Perlecan$^{\mathrm{Trol}}$ focused on its role on NSC reactivation. Null mutations in *hedgehog* (*hh*) and *branchless* (*bnl*, an FGF homologue) dominantly enhance the impairment in NSC proliferation in a sensitised *perlecan^{trol}* mutant background, suggesting that Perlecan$^{\mathrm{Trol}}$ may modulate Hh and FGF signalling activities (Park *et al.* , 2003). A recent study supported Perlecan$^{\mathrm{Trol}}$'s role in Hh signalling in a different context. *perlecan^{trol}* mutant lymph glands showed disrupted architecture and premature stem cell differentiation, and overexpression of hh in Perlecan$^{\mathrm{Trol}}$ mutants was able to rescue the premature differentiation phenotype (Grigorian *et al.* , 2013). Another study revealed a novel role of Perlecan$^{\mathrm{Trol}}$ in Wnt signalling. At the *Drosophila* neuromuscular junction (NMJ), Wnt/Wingless (Wg) regulates the formation of both pre- and postsynaptic structures. Mutation in *perlecan^{trol}* resulted in diverse postsynaptic defects and overproduction of synaptic boutons at the NMJ. The postsynaptic defects of *perlecan^{trol}* mutants could be rescued by the postsynaptic activation of the Wnt pathway (Kamimura *et al.* , 2013). Whether Perlecan$^{\mathrm{Trol}}$

is also involved in BMP/TGF-beta signalling in *Drosophila*, and especially in the context of NSC reactivation, awaits further investigation.

7.5 Collagen IV and Perlecan Regulate NSC Reactivation at Least in Part via Integrin Receptors

ECM proteins can either mediate signalling and NSC reactivation indirectly by sequestering ligands close to the BBB, or they may act as direct signals to induce insulin secretion via binding to their integrin receptors, or by a combination of both. The present study provided evidence that the integrin receptors, including βPS Integrin^{Mys} and αPS2 Integrin^{If}, at the BBB are at least in part responsible for the role of Collagen IV and Perlecan^{Trol} in NSC reactivation.

In vertebrates, integrins can be bound by many ECM ligands, including Collagen IV and Perlecan. *In vitro* biochemical assays confirmed human Collagen IV-Integrin binding. Purified $\alpha1\beta1$ and $\alpha2\beta1$ integrin complexes can directly bind Collagen IV, with $\alpha1\beta1$ showing higher binding affinity, as reviewed in (Tuckwell & Humphries, 1996). However, in *Drosophila*, only a small number of ECM proteins have been confirmed as integrin ligands, which includes two laminins (Henchcliffe *et al.* , 1993; Martin, 1999), tiggrin (Fogerty *et al.* , 1994), thrombospondin (Subramanian *et al.* , 2007) and tenectin (Fraichard *et al.* , 2010). Other ECM proteins, such as Collagen IV (Le Parco *et al.* , 1986) and tenascin (Graner *et al.* , 1998) and Perlecan (Friedrich *et al.* , 2000) are important in *Drosophila* but they have not been confirmed to be integrin ligands with biochemical assays. OMX images in my study showed close association and partial co-localisation between Collagen IV^{Vkg} and βPS Integrin^{Mys}. In addition, a number of recent *in vivo* studies in different developmental contexts support the idea that Collagen IV can exert its functions via its association with integrin receptors.

Vanderploeg et al showed that the accumulation of integrins (βPS1 Integrin^{Mys} and αPS3 Integrin^{Scb}) is required for the migration of cardioblasts and the establishment of the luminal domain during the formation of *Drosophila* heart (Vanderploeg *et al.* , 2012). In an effort to search for factors acting in the same or in a converging pathway with integrin during this process, Vanderploeg et al explored genetic interaction between α*PS3 integrin*^{scb} and other genes, including genes encoding various ECM ligand proteins. Whereas heterozygous mutant α*PS3 integrin*^{scb} embryos were not affected in their cardioblast migration, homozygous mutant α*PS3 integrin*^{scb} embryos exhibited dramatic defects in this process. Embryos

simultaneously heterozygous for *αPS3 integrin^{scb}* and *collagen IV^{vkg}* showed similar phenotypes to *αPS3 integrin^{scb}* homozygous mutants. This indicates that αPS3 Integrin^{Scb} and Collagen IV^{Vkg} regulate heart formation in the same or in a converging pathway, raising the possibility that the ECM ligand-receptor interaction may account for the convergence of their functions (Vanderploeg *et al.* , 2012).

Haigo and Bilder showed that *Drosophila* oocytes undergo stereotypical rotation when transforming from a sphere to an ellipsoid shape during oogenesis (Haigo & Bilder, 2011). Follicle epithelia mutant for either integrin or Collagen IV^{Vkg} showed nearly identical phenotypes: eggs fail to rotate and elongate which resulted in round shapes. These results again point to the possibility that the interaction between integrin receptors and Collagen IV at follicle epithelia promotes egg rotation.

Finally, a study by Pastor-Pareja and Xu provides good *in vivo* evidence for Collagen IV^{Vkg} binding to integrin receptors. They created wing discs clones of cells mutant for *βPS1 integrin^{mys}* in the genetic background of a Collagen IV^{Vkg}-GFP protein trap (Pastor-Pareja & Xu, 2011). Loss of βPS1 Integrin^{Mys} led to "scars" in the wing disc basement membrane, where Collagen IV^{Vkg}-GFP was absent. This shows that integrins are involved in the capture of Collagen IV from hemolymph.

Collagen IV-integrin receptor interactions alone are likely to be necessary but not sufficient for NSC reactivation: misexpression of Collagen IV^{Vkg} and Collagen IV^{Cg25C} in the fat body under starved conditions could not rescue NSC reactivation. On the other hand, it is difficult to assess the extent to which functional Collagen IV proteins were produced under the misexpression condition. This is because components involved in Collagen IV secretion, such as the chaperone protein *SPARC* (Martinek *et al.* , 2008; Pastor-Pareja & Xu, 2011), and components required for the assembly of Collagen IV trimers, such as Prolyl–4-Hydroxylase (*PH4alphaNE3*) (Abrams & Andrew, 2002) were simultaneously downregulated transcriptionally in the fat body during starvation according to the fat body TaDa transcriptional profiling (data not shown). In addition, glial transcription of *perlecan^{trol}* and the *βPS integrin^{mys}* receptor is also downregulated under starvation conditions (data not shown). Thus, even if abundant functional Collagen IV protein were over-expressed in the fat body, it could not deposit on the CNS. In order to fully recapitulate the conditions under fed conditions, it would require the co-misexpression of Collagen IV, SPARC, PH4alphaNE3 from the fat body, as well as Perlecan^{Trol} and βPS Integrin^{Mys} from glia. This experiment is technically difficult and therefore has not been performed.

A recent study showed the requirement for integrin-dependent adhesion and signalling in stem cell proliferation and homeostasis of another *Drosophila* stem cell niche, the ISC

niche of the midgut (Lin *et al.* , 2013). Integrin-mediated cell adhesion facilitates ISC anchorage to the basement membrane. Specifically, the αPS1 Integrin^{Mew}, αPS3 Integrin^{Scb} and βPS^{Mys} are expressed by ISCs and are required for their maintenance: integrin mutant ISCs are less proliferative, and genetic interaction studies suggest that Ilk (integrin-linked kinase)-dependent integrin signalling is required for ISC proliferation in response to various proliferative signals. Whereas this study did not identify ECM ligands, it shows that integrin-mediated signalling may be a conserved mechanism of regulating cell proliferation in different stem cell niches.

OMX images in my study showed that Perlecan^{Trol} is also closely associated with βPS Integrin^{Mys}. Similar to Collagen IV, Perlecan's interaction with integrin receptors are better characterised in mammals compared to *Drosophila*. Perlecan protein has five domains, and its domain V consists of an array of three laminin G-type (LG) modules and four epidermal growth factor-like (EG) modules. The LG and EG modules have been shown to bind to βPS Integrin receptors both *in vivo* and *in vitro* in mammalian systems (Bix *et al.* , 2006, 2004; Brown *et al.* , 1997). Interestingly, a recent study showed that Perlecan-Integrin interaction can protect neuronal cells from neurotoxicity caused by amyloid fibres during the pathogenesis of Alzheimer's disease (Wright *et al.* , 2012). The amino acid sequence of Perlecan domain V is highly conserved between *Drosophila* and mammals, including the LG and EG repeats (Friedrich *et al.* , 2000). Therefore, *Drosophila* Perlecan^{Trol} is also capable of binding to integrin receptors, but their physical interaction awaits precise biochemical assays (Friedrich *et al.* , 2000). A recent study provided the first and only *in vivo* evidence of *Drosophila* Perlecan^{Trol}'s interaction with integrin receptors. Perlecan^{Trol} plays a cell-autonomous role in anchoring intestinal stem cells (ISCs) to their niche and is required for ISC proliferation (You *et al.* , 2014). Whereas ISC anchorage does not depend on integrins, Perlecan^{Trol}-mediated ISC proliferation is partially dependent on βPS Integrin^{Mys}. Ectopic expression of βPS Integrin^{Mys} in Perlecan^{Trol} null mutant ISC clones can partially rescue ISC proliferation defects observed in Perlecan^{Trol} null ISCs (You *et al.* , 2014).

7.6 Matrix-Integrin Interaction Controls Insulin Signalling *in Vivo*

The present study presents an interesting parallel between invertebrate and mammalian regulation of insulin signalling by ECM proteins. RT-PCR analyses showed that in the absence

of Collagen IV^{Vkg} and Perlecan^{Trol} on the CNS surface, glial *dIlp6* transcription is downregulated. Forced expression of DIlp6 can partially drive NSC reactivation in the *collagen IV^{vkg}* and *perlecan^{trol}* mutant. Therefore, whereas Collagen IV and Perlecan^{Trol} act antagonistically in the process of maintaining organ shape (stretching vs. constricting) (Pastor-Pareja & Xu, 2011), they function cooperatively upstream of insulin signalling during the regulation of NSC reactivation.

Strikingly, glial knockdown of the ECM receptor, *βPS integrin^{mys}*, resulted in nearly 50% decrease of CNS *dIlp6* transcript level, on a par with fat body-specific *collagen IV^{vkg}* knockdown or starvation. However, knocking down *βPS integrin^{mys}* using a either PG specific or SPG specific GAL4 driver was not able to recapitulate the phenotype. It is possible that the pan-glia driver, Repo-GAL4, may have stronger expression and earlier onset of expression in the BBB glia than the subtype specific drivers themselves. In addition, βPS Integrin^{Mys}-mediated *dIlp6* transcription may occur in both perineurial glia and subperineurial glia (both glial subtypes express *βPS integrin^{mys}* and *dIlp6*). Therefore, there may be some degree of functional redundancy and compensation between the two glial subtypes with regards to their regulation of insulin signalling. Therefore, one may need to knockdown integrin receptors in both glial populations simultaneously in order to efficiently block *dIlp6* transcription in the BBB.

ECM-mediated insulin signalling from the *Drosophila* BBB is consistent with studies showing that key ECM components such as Collagen IV can directly regulate glucose-dependent insulin secretion in human pancreatic beta cells (Kaido *et al.* , 2004; Weber *et al.* , 2008). However, whereas the mammalian evidence comes from isolated pancreatic tissue in culture, the present study provided the first *in vivo* evidence of ECM regulation of insulin transcription. Although it is very likely that Collagen IV and Perlecan^{Trol} regulate glial insulin signalling indirectly by harnessing other signalling molecules at the BBB, decreased *dIlp6* transcription and impaired NSC reactivation under glial integrin knockdown condition suggest that binding of ECM proteins to their receptors itself is at least partially responsible for the transcription of glial insulin. Indeed, integrins are known as critical regulators of β cell survival and function. They have been shown to protect against cell death and promote glucose-induced insulin expression and secretion in both rodent and human islet cells *in vitro* (Krishnamurthy *et al.* , 2008; Rondas *et al.* , 2012). A recent study also provided convincing *in vivo* evidence that conditional knockout of *βPS1 integrin* in pancreatic islet cells led to impaired glucose tolerance in mice, with a significant decrease in pancreatic insulin content (Riopel *et al.* , 2011).

7.7 Alteration in Nutrition and Systemic Metabolism Selectively Affect Relevant ECM Protein Expression

The present study identified key nutrient-sensitive ECM components in invertebrates. The expression of *collagen IV^{vkg}* and *collagen IV^{cg25C}* depend on the availability of dietary amino acids. Dietary amino acids not only regulate glial *perlecan^{trol}* transcriptionally, they also regulate Perlecan^{Trol} protein deposition on the CNS via Collagen IV. To our initial surprise, Q-PCR reveals peak CNS transcription of *perlecan^{trol}* just after larval hatching before the larvae are even exposed to food. This is followed by rapid Perlecan^{Trol} protein deposition, which can be observed a few hours after larval hatching. The high level of *perlecan^{trol}* transcription immediately after larval hatching perhaps allows for fast and immediate CNS deposition of Perlecan^{Trol} protein in response to nutrient-availability. In this way, the animal can coordinate its ECM deposition with the fastest proliferative phase of the NSCs in the first 24 hours of larval life. Later on, glial *perlecan^{trol}* transcription becomes sensitive to nutrition starting from approximately 12 hph, as suggested by pan-glial transcriptional profiling under fed and starved conditions in two time windows (4hbh–16hph vs. 12–36hph).

Similar to what I observed in *Drosophila* larvae, alterations in nutritional status can affect the production and deposition of ECM proteins in mammals as well (Alcantara *et al.* , 2011; Farhadian *et al.* , 2012; Groos *et al.* , 2003; Guerra *et al.* , 2009; Higami *et al.* , 2006). This may lead to systemic physiological responses such as autophagy and organ remodelling. In particular, Higami et al showed that dietary restriction in mice led to down regulation of a number of ECM proteins, including Collagen IV, in the white adipose tissue (Higami *et al.* , 2006). Although future research is needed to address the physiological significance of this down-regulation, this study indicates that the regulation of Collagen IV in vertebrate and invertebrate fat tissue by nutrition may be conserved. It remains to be tested whether Collagen IV or other mammalian ECM proteins have tissue non-autonomous functions, and whether insulin signalling plays a role downstream of Collagen IV deficiency when altering nutritional state in mammalian systems.

7.8 Dissecting the Interaction Between Systemic Signals and Local Niche in Regulating NSC Behaviour

Using the powerful genetic tools of *Drosophila*, we are starting to dissect the mechanisms of how NSCs are regulated by their systemic environment and local niche, as well as how the

two interact. In *Drosophila*, the fat body serves as a systemic energy sensor to coordinate organismal growth with food availability. Another fat body-secreted factor, Unpaired2, was shown to regulate body growth in response to dietary lipid and sugar in adult flies (Rajan & Perrimon, 2012). It acts by binding to its receptor on the surface of GABAergic neurons which in turn synapse on the insulin producing cells in the brain (Rajan & Perrimon, 2012). I wondered whether Collagen IV could interact with Unpaired2 in regulating NSC reactivation, but I did not observe Unpaired2 transcription in the first instar larval fat body in our transcriptome data (data not shown). In addition, Unpaired2 receptor *dome* is not transcribed by either SPG or PG during the time window of NSC reactivation based on TaDa transcriptional profiling (data not shown). Disrupting Unpaired2 signalling in the BBB glia by expressing an RNAi construct against *dome* had no effect on CNS development (data not shown). As a systemic energy sensor throughout fly life, the fat body is likely to produce multiple factors in response to different nutritional inputs such as sugar, lipids, and amino acids, and at different developmental stages.

How are systemic signals transduced to NSCs, which do not have access to the hemolymph (blood equivalent)? CNS glial cells secrete local insulin to reactivate NSCs under feeding conditions (Chell & Brand, 2010; Sousa-Nunes *et al.* , 2011) upon ECM binding. Therefore, the present study confirmed the BBB's role as a NSC niche, and illustrated one potential mechanism through which systemic fat body signals can be relayed to NSCs via the glial niche. The novel discovery that Perlecan^{Trol} is expressed exclusively by perineurial glia highlights the essential role of the BBB in modulating the ECM environment of the CNS during neurogenesis. The source of CNS DIlp6 was a matter of contention among previous studies. One study showed that "surface glia" are responsible for producing DIlp6 based on expression pattern of a promoter fusion *dIlp6*-GAL4 (Chell & Brand, 2010). Another study suggested that the cortex glia may be the source based on the expression pattern of another enhancer trapped Ilp6-GAL4 lines (Sousa-Nunes *et al.* , 2011), where GAL4 insertion is upstream of *dIlp6* gene but within the coding region of another gene, *phl*. Our TaDa transcriptional profiling confirmed Chell and Brand's observation that the BBB glia transcribe *dIlp6* during the time window of NSC reactivation. This makes sense anatomically, as the BBB is situated at the interface between the hemolymph and the NSCs: both fat body secreted Collagen IV and glial derived Perlecan^{Trol} deposit on the BBB, and the reactivating NSCs are located below. Signalling through the BBB glia would therefore be the most efficient way for systemic regulation of NSC behaviour.

Therefore, the BBB is not just a physical barrier separating neuronal tissues from the systemic environment. The present study provided convincing evidence that the BBB is in

fact an active regulator of neurogenesis by modulating the ECM environment and secreting neurogenic factors such as DIlp6 and Perlecan^{Trol} to promote NSC reactivation. Future studies should strive to further characterise the interaction between the systemic regulation and the local NSC niche, in particular, how ECM molecules induce insulin signalling from the BBB glia. Interestingly, a recent study identified Betatrophin, a novel peptide hormone secreted by the mammalian liver and adipose tissue, in controlling glucose-dependent insulin secretion from the pancreatic beta cells *in vivo* (Yi *et al.* , 2013). This suggests that the systemic regulatory function of the invertebrate fat body or vertebrate liver/adipose tissue on insulin production may be conserved.

7.9 BBB: a Nutrient Sensitive NSC Niche

Since the discovery that astrocytes induce neurogenesis from adult NSCs, it has been proposed that glial cells act as a NSC niche (Song *et al.* , 2002). In the past ten years, little has been understood about the mechanistic details of glial cells' actions as well as upstream regulators of the glial niche factors, partly due to the difficulty in manipulating mammalian glial cells *in vivo*. The powerful genetic tools of *Drosophila* make it an attractive system to help elucidate these intriguing questions. The *Drosophila* glial cells, especially the flat and thin BBB glial subtypes, are difficult to isolate due to their position and morphology. This is part of the reason why individual glial subtype's roles have not been investigated systematically (i.e. with RNA seq or microarray). Taking advantage of the TaDa transcriptional profiling transcriptional profiling technique, we were able to map glial subtype transcriptional profiles *in vivo* in intact glial cells without isolation and cell sorting, during early larval stages. Combining glial subtype transcriptional profiles with pan-glial transcriptional profiles under fed and starved conditions from a similar time window, we helped to elucidate signalling networks governing early glial development, glial subtypes' response to nutrition, and discover novel glial signalling pathways mediating nutrition-sensitive NSC reactivation.

The present study highlighted that although DIlp6 is the key factor regulating NSC reactivation, other glial factors may act to fine tune nutrient-dependent NSC reactivation. Glial subtype transcriptome analyses reveal that the BBB glia's transcriptional activity is highly sensitive to changes in nutritional intake, and many genes involved in neurogenesis and multiple metabolic/signalling pathways are upregulated upon feeding. These analyses may serve as a starting point to identify signalling pathways acting in parallel with or upstream of glial *dIlp6* transcription. Furthermore, they may aid in elucidating the molecular mecha-

nisms underlying ECM binding to the CNS and its role in glial insulin production.

Of particular interest is the BMP/TGF-beta signalling pathway, which shows upregulation in the BBB upon feeding. Many of the components in this pathway, including ligands, receptors, and downstream effectors, are enriched in the BBB glia. Collagen IV has been shown to play an important role in BMP signalling in other developmental contexts in *Drosophila*. It remains to be examined whether Perlecan^{Trol} also plays a role in BMP signalling in *Drosophila*. Encouragingly, closely related heperan sulphate proteoglycans such as Dally and Dlp have established roles in BMP signalling in vertebrates (Yan & Lin, 2009). A recent study showed that Perlecan can augment BMP–2 activity during osteogenesis in a human cell line (DeCarlo *et al.* , 2012). Current efforts aim to investigate whether both Collagen IV and Perlecan regulate BMP/TGF-beta signalling, and whether glial BMP/TGF-beta signalling regulates NSC reactivation upstream of insulin signalling.

Chapter 8

Experimental Procedures

8.1 Statement of Collaboration

Chapter 6 was carried out in collaboration with Pauline Speder, a postdoc in the Brand lab, Jessie Van Buggenum, a Master's student in the Brand lab, and Jorge Buendia-Buendia, another Master's student in the Brand lab. Pauline Speder and I dissected brains for pan-glial TaDa transcriptional profiling under fed and starved conditions. I dissected samples for glial subtype TaDa transcriptional profiling together with Pauline Speder and Jessie Van Buggenum: I was in charge of dissection and microarray for perineurial glia TaDa transcriptional profiling, whereas Pauline Speder and Jessie Van Buggenum were in charge of pan glia, subperineurial glia, and cortex glia samples. Data analysis of chapter 6 was performed in collaboration with Jorge Buendia-Buendia, where Jorge generated all heat map figures and I generated all the rest of the figures.

8.2 Fly Husbandry and Strains

Flies were raised at 25 °C on standard *Drosophila* cornmeal-molasses-agar medium vials or bottles. For temperature shift experiments using temperature sensitive GAL80 (tub-GAL80^{ts}), flies were kept at 18 °C, the permissive temperature for GAL80^{ts}, and transferred to 29 °C to inactivate GAL80^{ts}. In addition, all knockdown experiments were performed at 29 °C.

The following fly strains were used: w1118 and OrR were used as wild-type controls; the fat body drivers cg-GAL4 (H Asha, 2003) and lpp-GAL4 (Brankatschk & Eaton, 2010); pan-glial driver repo-GAL4 (Sepp, 2001); perineurial glia driver NP6293-GAL4

(DGRC, Kyoto); subperineurial glia driver moody-GAL4 (gift from Takeshi Awasaki); cortex glia driver NP2222-GAL4 and NP0577-GAL4(DGRC, Kyoto); gut driver esg-GAL4 (DGRC); imaginal discs driver hh-GAL4 (Tanimoto *et al.* , 2000); NSC driver ase-GAL4 (Zhu *et al.* , 2006); Collagen IV^{Vkg}-GFP (Morin *et al.* , 2001); hypomorphic Collagen IV^{Vkg} K1672 (gift from Hilary Ashe); hypomorphic Collagen IV^{Vkg} k197 (gift from Hilary Ashe); UAS-Collagen IV^{Vkg}; UAS-Collagen IV^{Cg25C} ; $Perlecan^{Trol}$-GFP (gift from Stephan Noselli); $Perlecan^{Trol}$ null (Voigt *et al.* , 2002); UAS-$Perlecan^{Trol}$ ShmiR (Bloomington 38298); UAS-$Collagen^{Vkg}$ ShmiR (Bloomington 50895); UAS-dIlp6 (Ikeya *et al.* , 2002); UAS-Tsc1/2 (Tapon *et al.* , 2001); UAS-Mys RNAi (VDRC 103704); UAS-Mys shmiR (BL33642); UAS-$Slif^{anti}$ (Colombani *et al.* , 2003); Mdr65-GAL4 (Arnim Jenett, 2012); βPS $Integrin^{Mys}$-GFP (gift of Nick Brown); Ilk-GFP (gift of Nick Brown); Pax-GFP (gift of Nick Brown); UAS-DicerII (Dietzl *et al.* , 2007); UAS-Tubulin-$GAL80^{ts}$ (McGuire *et al.* , 2003); UAS-LT2-Dam (Southall *et al.* , 2013); UAS-LT2-Dam-PolII (Southall *et al.* , 2013); Worniu-GAL4 (gift from Tony Southall, Brand lab); Insc-GAL4; UAS-Syntaxin5 RNAi (VDRC 3859); FB-GAL4 (gift of Maria Southall); ppl-GAL4 (gift of Pierre Leopold); UAS-shiDN; UAS-shiDN (Bloomington). RNAi lines used in the screen of secreted fat body factors were obtained from VDRC, Vienna, Austria. When available, lines from the KK library were used. In cases where KK lines were unavailable, flies from the GD library were used. Screens of glial ECM receptors, βPS $Integrin^{Mys}$ associated proteins, as well as glial receptors for major signalling pathways involved in neurogenesis were conducted using ShmiR and RNAi lines in the TRiP stock, which are available from the Bloomington Stock Centre. All TRiP and VDRC lines used for screens are listed in Appendix 1.

8.3 Larval Culture

Embryos were laid on a fresh apple juice plate prior to larval hatching. Larvae that hatched within a 30 min window were transferred to fresh yeast plates, and this was called 0 hour post hatching (hph) (referred to as “fed” condition). To deprive larvae of dietary amino acids, larvae were transferred to a solution of 20% sucrose in PBS after hatching instead of fresh yeast (referred to as “starved” condition). Sucrose solution was sterile filtered and kept at 4 ºC prior to use.

8.4 Larval Brain and Fat Body Explant Co-Culture

CNS from just hatched larvae (0 hph) and fat bodies from crawling 3rd instar larvae were dissected for tissue co-culture experiments. Prior to dissection, larvae were washed with 70% ethanol followed by two rinses with sterile water. Fat body and CNS dissections were performed in the culture medium using sterile tools. Culture medium consists of Schneider's medium (Gibco) supplemented with 10% fetal calf serum (Sigma), 2 mM L-glutamine (Gibco) and Pen/Strep 1X (Gibco). The dissected CNS and fat bodies were rinsed in culture medium to minimise contamination of the explant culture by hemolymph factors. These were transferred to Nunclon 4-well dishes containing fresh culture medium, and then placed in a humidified chamber at 25 °C. Hydrogen peroxide was added to the space between the wells to oxygenise the tissue.

8.5 Generation of UAS-Collagen^{Vkg} and UAS-Collagen^{Cg25C} transgenic flies

8.5.1 Primer Design

Primers were designed by submitting the sequence of the gene of interest (5' to 3') to the OligoCalc online tool (http://www.basic.northwestern.edu/biotools/oligocalc.html), using algorithms designed by Kibbe et al (Kibbe, 2007). Primer selection criteria included: primer length between 20 and 25 bp; primers ending with G or C; salt adjusted melting temperature difference between forward and reverse primer of a given gene smaller than 3 ºC. All other parameters were left at default settings.

The following primers were selected for UAS-Collagen^{Vkg} and UAS-Collagen^{Cg25C}:

Collagen^{Cg25C} Forward:ATGTTGCCCTTCTGGAAGCGGCTG

Collagen^{Cg25C} Reverse:CTAGGGGGCGGTGGTGTCC

Collagen^{Vkg} Forward:ATGTTGCCCTTCTGGAAGCGGCTG

Collagen^{Vkg} Reverse:CTACGAGGAGTTCTTCATGCACACC

*Note: these were the primer sequences sufficient for amplifying the genes of interest. Additional sequences were added to the primers in order to create final primer sequences suitable for carrying out Gibson Assembly reactions (see "Cloning with Gibson Assembly" section, below).

8.5.2 PCR Amplification of Collagen^{Vkg} and Collagen^{Cg25C} Transcripts

Full length Collagen^{Vkg} and Collagen^{Cg25C} transcripts were PCR amplified from an embryonic genomic cDNA library generated by Boris Egger (Brand lab). The optimal annealing temperature was determined to be 65 ºC for both Collagen^{Vkg} and Collagen^{Cg25C}.

The PCR reaction mix was prepared using the following recipe:

cDNA template (85ng/μl) 1μl
5X High Fidelity Buffer (New England Biolabs) 10μl
10 mM dNTP mix 1.5μl
10 μM forward primer 1μl
10 μM reverse primer 1μl
dd H2O 35μl
Phusion Polymerase (New England Biolabs) 0.5μl
PCR reaction mix total volume: 50μl

The following PCR programme was used to amplify Collagen^{Vkg} and Collagen^{Cg25C}:

98 ºC 2 min (denaturation of the template)
30 cycles start:
98 ºC 20 sec (denaturation)
65 ºC 20 sec (annealing)
72 ºC 6 min (elongation, approximately 1min/kb)
30 cycles end
72ºC 5 min
hold at 4ºC

8.5.3 Gel Electrophoresis

To check the quality of PCR amplified DNA, 1 to 2 μl of DNA was used for analysis by agarose gel electrophoresis. A 1% agrose gel was made by adding 0.5 g agarose (Invitrogen) to 50 ml 1X Tris/Borate/EDTA (TBE) buffer. DNA was visualised by adding Ethidium Bromide (100ng/ml, Sigma-Aldrich) to the gel mix before it set. DNA was mixed with ddH2O and 5X DNA loading buffer (Bioline) to achieve a final concentration of 1X prior to loading. A Gel Doc 2000 machine (BioRad) was used to image the gel and DNA fragment sizes were determined by comparing to a 200bp–10kb DNA ladder (HyperLadder I, Bioline).

8.5.4 DNA Purification and Quantification

If a single band was detected with agarose gel electrophoresis, PCR products were subsequently purified using Qiaquick PCR Purification kit (Qiagen) using the manufacturer's protocol. If multiple bands were present, the desired band was isolated using agarose gel electrophoresis. The band was excised with a razor blade and purified with Qiaquick Gel Extraction kit (Qiagen).

8.5.5 Cloning with Gibson Assembly

Gibson Assembly was used to sub-clone Collagen^{Vkg} and Collagen^{Cg25C} sequences into the pUAST vector. This method can simultaneously join several DNA fragments based on sequence identity. It requires that the DNA fragments contain 20–40 bp overlap with adjacent DNA fragments. These DNA fragments are mixed with a master solution containing three enzymes: exonuclease, DNA polymerase, and DNA ligase. The exonuclease digests DNA from the 5' end, leaving single-stranded overhang regions on adjacent DNA fragments which anneal to one another. The DNA polymerase subsequently fills in any gaps. In the final steps, DNA ligase covalently joins the DNA of adjacent segments to remove nicks in the DNA (Gibson, 2011; Gibson *et al.* , 2009). The Gibson assembly protocol used in this study was modified by Elizabeth Caygill (Brand lab).

The pUAST vector containing an attB site was created by Tony Southall (Brand lab). The attB site allows for targeted insertion of the desired construct into defined attP docking sites in the embryo's germline during the generation of transgenic flies. The vector contained multiple restriction sites. NotI and XbaI were used to linearise the vector. The final primer sequences used for amplification of Collagen^{Vkg} and Collagen^{Cg25C} cDNA contain a 5' 30bp that overlap with the linearised vector at the insertion site as well as a Cavener/ Kozak consensus sequence to facilitate the translation initiation (Cavener, 1987):
Collagen^{Cg25C} Forward:
*GGGAATTGGGAATTCGTTAACAGATCTGC***AATCAAAA**ATGTTGCCCTTCTGGAAGCGGCTG
Italic: overlapping sequence with vector sequence downstream of NOT I cutting site
Bold: Kozak consensus sequence
Collagen^{Cg25C} Reverse:
*ACAGAAGTAAGGTTCCTTCACAAAGATCCT*CTAGGGGGCGGTGGTGTCC
Italic: overlapping sequence with vector sequence upstream of Xba I cutting site
Collagen^{Vkg} Forward:
*GGGAATTGGGAATTCGTTAACAGATCTGC***AATCAAAA**ATGTTGCCCTTCTGGAAGCGGCTG

Italic: overlapping sequence with vector sequence downstream of NOT I cutting site
Bold: Kozak consensus sequence
Collagen^{Vkg} Reverse:
*ACAGAAGTAAGGTTCCTTCACAAAGATCCT*CTACGAGGAGTTCTTCATGCACACC
Italic: overlapping sequence with vector sequence upstream of Xba I cutting site

Approximately 100 ng of the linearised vector backbone and equimolar amounts of PCR purified Collagen^{Cg25C} or Collagen^{Vkg} cDNA sequences were added to thawed 15 μl Gibson master mix. The solution was topped up to 20 μl with ddH2O. The Gibson assembly reaction was carried out at 50 ºC for 1 hour, and immediately placed on ice. Diagnostic agarose gel electrophoresis was conducted to check successful assembly before transformation.

Gibson assembly master mix (optimised for 20 to 150 bp sequence homology overlaps) contained:
5X ISO Buffer (see recipe below) 320 μl
10 U/μl T5 exonuclease (Epicentre) 0.64 μl
2 U/μl Phusion polymerase (New England Biolabs) 20 μl
40 U/μl Taq ligase (New England Biolabs) 160 μl
add dH20 up to 1.2 ml

5X ISO buffer contained:
1 M Tris-HCl pH 7.5 3 ml
2 M MgCl2 150 μl
100 mM dNTP mix (25 mM each: dGTP, dCTP, dATP, dTTP) 240 μl
1 M DTT 300 μl
PEG–8000 1.5g
100 mM NAD 300 μl
add dH20 up to 6ml

8.5.6 Transformation of *E.Coli*

5 μl of the Gibson Assembly reaction was added to 100 μl of DH5a competent *E.Coli* and incubated for 10 min on ice. The mixture was heat shocked for 45 seconds at 42 ºC. After adding 200 μl LB, the mixture was incubated at 37 ºC for 30 min, with vigorous shaking. The mixture was spread onto agar plates containing ampicillin (50 μl per plate), which were incubated overnight at 37ºC.

8.5.7 DNA Plasmid Preparation and Sequencing

Individual bacteria colonies were picked and cultured in 2 ml LB medium containing ampicillin antibiotic at 37 ºC overnight. Plasmid DNA was isolated using QIAprep Miniprep Kit (Qiagen) according to the manufacturer's protocol. A Thermo Scientific NanoDrop 1000 was used to determine DNA concentration.

Plasmid DNA was sequenced by Cogenics (Beckman Coulter Genomics). Primer sequences used for sequencing are listed below. MacVector software was used to analyse the sequencing results.

AttB primer (used for both Collagen IV^{Cg25C} and Collagen IV^{Vkg} sequencing):

CGATTCATTAATGCAGCTGGC

Collagen IV^{Cg25C}-specific Sequencing primers (10 in total):

AAGTGAACACGTCGCTAAGCG
AAAGCCCGGTCAGCAGGGTCC
CCCAGGAATTTACGATCCTAG
CCCGGGTAGCCATGGAAACCG
TCGTGGCGAAATTGGTGACCGTG
TGGCGAGATCGGAGAGCGTGG
TGGTGATCAAGGACCACGCGG
CATTGTCGGCAGGCAGGGCG
GGCCGCCAGCAGAGCGGTGGG
GTCCAGGGCAGATGCGTCTTC

Collagen IV^{Vkg}-specific Sequencing primers (10 in total):

AAGTGAACACGTCGCTAAGCG
TCCAGGGACCCGCCGGCAATC
CTACAGGACAAAAGGGAGATC
GTCGTCCCGGCACTCCTGGCC
CCGGTAGCTGTGCGCTTGACG
TTGGTCGGCATGCCCGGTAAC
ATTCCTGGTGCTCCCGGAATG
GGAGAGCGTGGTCTCGCCGGC
GCTGCTCTGGACTATCTCACC
GTTCGAGAGGCCACAGCAGCAG

8.5.8 Germline Transformation

Site specific attP-attB mediated transgenesis was accomplished using a protocol from Tony Southall (Brand lab). In short, purified attB plasmid (100 ng/μl) and helper integrase plasmid (400 ng/μl) were injected into embryos carrying either attP2 or attP154 docking sites to ensure that the insertion of the transgenes occurred at the same genomic loci on the third or the second chromosome. Micro-injection was performed by Melanie Cranston (Brand lab) and John Overton (Nick Brown lab). Hatched adults from micro-injected embryos were individually crossed to w1118 flies, and the progeny were examined for eye colour. Flies with non-white eye colour were crossed to balancer flies to establish balanced stocks.

8.6 Dam ID Transcriptional Profiling

The Targeted Dam ID (DNA adenine methyltransferase identification), or "TaDa", protocol was designed by Tony Southall (Southall *et al.* , 2013), modified from van Steensel et al. and Choksi et al (Choksi *et al.* , 2006; van Steensel *et al.* , 2001). This technique involves tagging a DNA or chromatin binding protein with the *E. coli* Dam (DNA adenine methyltransferase). Wherever the Dam fusion protein binds the genome, surrounding DNA sequences are methylated at the A nucleotide of GATC (Figure 8.5.1).

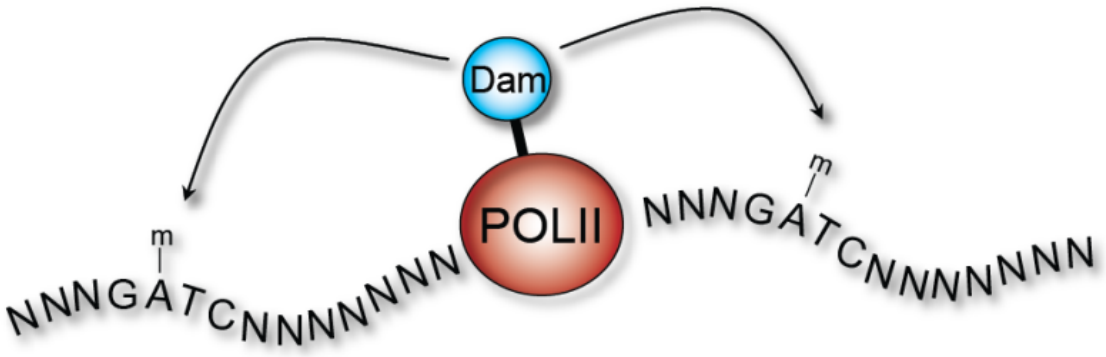

Fig. 8.6.1 Schematic of TaDa technique mechanism. TaDa involves tagging the E. coli Dam (DNA adenine methyltransferase) with a DNA or chromatin binding protein. I used Dam fused with RNA PolII (RNA Polymerase II) subunit for transcriptional profiling. Wherever the Dam-POLII fusion protein binds the genome, surrounding DNA sequences are methylated.

The methylated sequences can be digested with DpnI, PCR amplified, and hybridised to Roche Nimblegen whole genome tiling arrays to determine DNA binding sites. In the present study, I used the TaDa system to express the Dam-RNA POLII fusion protein

in a tissue-specific manner utilising the GAL4/UAS system (Brand & Perrimon, 1993). UAS-Dam was used as a control to account for background methylation by the Dam protein. Temporal control was achieved with a temperature sensitive GAL80, tubulin-GAL80^{ts} (McGuire *et al.* , 2003). A schematic of the fat body specific POLII TaDa experiment was shown in Figure 9.6.2.

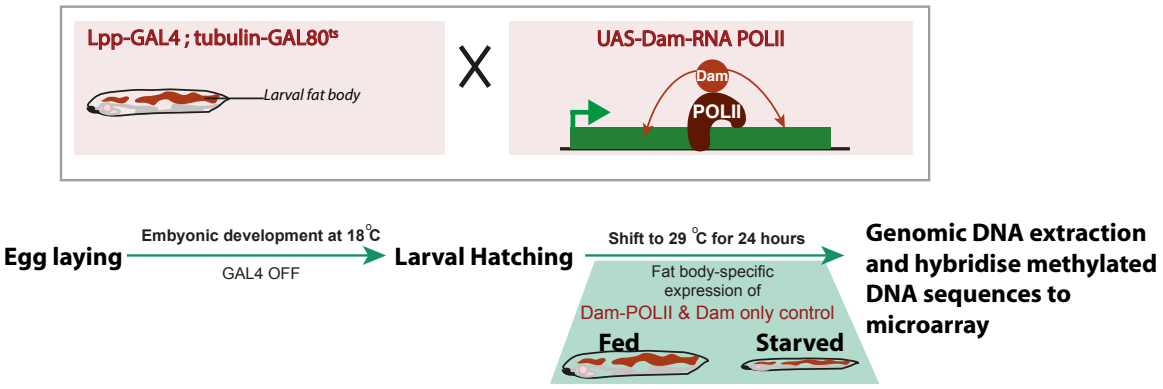

Fig. 8.6.2 Schematic of fat body TaDa transcriptional profiling under fed and starved conditions. A fat body specific GAL4 driver (Lpp-GAL4) drives Dam-POL II fusion protein expression in the fat body. In combination with tubulin-GAL80^{ts}, temporal control of Dam-POL II fusion protein expression can be achieved, so that one can obtain transcriptional profiles during the time window of interest (18 ºC: GAL4 off, 29 ºC: GAL4 on).

8.6.1 Larval CNS Dissection

For glial TaDa experiments, larval CNS were dissected in 1XPBS and kept on ice. Dissection time was limited to less than 1 hour to keep the tissue fresh. The tissue was snap frozen in dry ice and stored at –80 °C. 220–250 CNS from fed larvae, and 250–300 CNS from starved larvae were used for each condition. In total, 880–1000 brains from fed larvae and 1000–1200 brains from starved larvae were used for each glial TaDa transcriptional profiling experiment.

For fat body TaDa experiments, whole larvae were collected and immediately washed 3 times in 1XPBS containing 100 mM EDTA (PH=8). The larvae were snap frozen and stored at –80 °C. 100–120 fed larvae, and 120–150 starved larvae were used for each condition. In total, 400–480 fed larvae, and 480–600 starved larvae were used for each fat body TaDa experiment. It was essential that whole larvae homogenisation was carried out in 100 mM

EDTA in PBS because the EDTA prevented DNAase in the larval gut from shearing the genomic DNA non-specifically.

8.6.2 Genomic DNA Extraction

Genomic DNA was extracted from larval CNS using DNeasy Blood and Tissue kit (Qiagen). Larval brains were thawed from –80 °C and washed with 1XPBS. Samples were homogenised with a sterile pestle. 20 μl DNase free RNase A (12.5 μg/μl, ROCHE) was used to degrade RNA and the samples incubated at room temperature for 20 min. Cells were lysed and proteins were digested by adding 20 μl of proteinase K and 200 μl of buffer AL (DNeasy kit, Qiagen).

Samples were mixed by pipetting up and down gently approximately 50 times. After a quick centrifuge, samples were incubated at 70 °C for 10 min for protease K digestion. DNA was purified according to manufacturer's protocol (Qiagen), and eluted in 2 X 200 μl of AE buffer sequentially (e1=elution1, e2=elution2). Eluted genomic DNA was analysed on an agarose gel by electrophoresis to examine the quality and quantity of genomic DNA. The samples should be a single band on the gel with low mobility. In the case of genomic DNA shearing, a smear pattern would appear in the agarose gel and those samples were discarded. The concentration of genomic DNA was measured with a Thermo Scientific NanoDrop 1000. Elution 1 and elution 2 were combined together to proceed to DNA precipitation.

8.6.3 DNA Precipitation

Approximately 100 μl of ddH2O were added to the total eluted gDNA (e1+e2) to make a total of 500 μl. To precipitate the genomic DNA, 1 ml of 100% ethanol, 50 μl of 3M sodium acetate, and 1 μl of molecular grade glycogen were added. The mixture was incubated at –20 °C for at least 30 min. Genomic DNA was precipitated by centrifugation (16100 x g) at 4 °C for 30 min. The supernatant was removed and the pellets were washed with 500 μl of 70% ethanol and centrifuged again for 10 minute at 4 °C (16100 x g). Ethanol was removed and the DNA was air-dried for approximately 5 min. Care was taken so that DNA was not over-dried.

8.6.4 DpnI Digestion

The air-dried DNA pellets were digested with 50 μl DpnI enzyme (New England Biolabs) in reaction buffer at 37 °C overnight. DpnI was used to cut methylated GATC sequences,

allowing the isolation of sequences that have been methylated by Dam methyltransferase.
DpnI reaction mix was made up with the following recipe.
DpnI (New England Biolabs): 1.5 μl
10X Buffer4 (New England Biolabs): 5 μl
ddH2O: 43.5 μl

To prevent non-specific DNA shearing, the enzyme solution was added to the pellets gently without mixing. The next morning, another 5 U, or 1.5 μl of DpnI was added into the samples, gently mixed with pipet tips, and incubated at 37 °C for one hour to complete the digestion. DpnI enzyme purchased within 6 months was used to ensure maximal enzyme activity.

8.6.5 Adaptor Ligation

DpnI digest was inactivated by incubating the sample at 80 °C for 20 min. Digested samples were purified using a PCR purification kit (Qiagen). Samples were eluted with 30 μl of ddH2O. In order to provide primer sequences for PCR amplification of methylated DNA later on, a double stranded oligonucleotide adaptor was ligated to each of the blunt ends of DNA fragments digested by DpnI. 15 μl of purified DpnI digested genomic DNA was mixed with 5 μl of ligation solution (containing 2 μl of ligation buffer (ROCHE, Rapid Ligation Kit), 1 μl of T4 DNA ligase (ROCHE), 0.8 μl of double strand adaptor oligonucleotide (50 uM) and 1.2 μl ddH2O). The ligation mixtures were incubated at 16 °C for 2 hours. The double stranded adaptor was made by annealing two oligonucleotides (AdRt and AdRb). The sequences of AdRt and AdRb are:
AdRt: 5'-CTAATACGACTCACTATAGGGCAGCGTGGTCGCGGCCGAGGA–3'
AdRb: 5'-TCCTCGGCCG–3'

8.6.6 DpnII Digestion

The ligation mixture was incubated for 10 min at 65 °C to inactivate the T4 DNA ligase. Genomic DNA fragments containing unmethylated GATC sites were digested with DpnII, so that these fragments would not be amplified by PCR. DpnII reaction mix was added to the ligation reaction and incubated at 37 °C for one hour or overnight.
DpnII reaction mix was made with the following recipe.
10X DpnII buffer (New England Biolabs): 8 μl
DpnII (New England Biolabs): 1 μl
ddH2O: 51 μl

8.6.7 PCR Amplification of Methylated DNA Fragments

PCR was used to amplify methylated DNA fragments with the adaptors on both ends.
PCR reaction mix was made up with:
DpnII digested DNA: 20 μl
10 X PCR reaction buffer (Clontech): 8 μl
50 μM AdR PCR primer: 1.25 μl
50 X dNTP mix (Clontech): 1.6 μl
50 X Advantage DNA polymerase mix (Clontech): 1.0 μl
48.15 μl: ddH2O
PCR reaction total volume: 80 μl

3 μl of PCR product was analysed on agarose gel. A smear pattern was observed if methylated DNA fragments were successfully amplified. For successful sample, PCR products were purified using the QIAquick PCR purification kit (Qiagen). 30 μl of ddH2O was used for elution and the concentration was measured with a Thermo scientific NanoDrop ND–1000 spectrophotometer.

8.6.8 Genome-Wide Tiling Microarray

Purified DNA samples were analysed by microarray at the FlyChip facility at the Department of Genetics, University of Cambridge. Samples were hybridised to *Drosophila* whole-genome tiling arrays. The tiling arrays contain 385,000 probes with each probe representing an average 60 bp of the genomic DNA spaced every 300 bp to cover the entire *Drosophila* euchromatic genome (ROCHE Nimblegen). Microarray data were visualised using NimbleScan software. Full details of labelling and hybridisation can be found online: http://www.flychip.org.uk/protocols/chip/NimblegenBioPrime.php. 3 replicates were performed for fat body TaDa transcriptional profiling experiments (fed vs. starved), 2 replicates were performed for pan-glial transcriptional profiling TaDa experiments (fed vs. starved), and 3 replicates were performed for glial subtype TaDa transcriptional profiling. Each experiment contained one dye swap replicate.

8.7 Clarification Regarding Fat Body TaDa Transcriptional Profiling and RNAi Screen

I carried out a functional RNAi screen after I completed two replicates of fat body TaDa Transcriptional Profiling, which yielded 150 genes up in fed conditions. The number of upregulated genes decreased to only 83 after I performed three replicates of fat body TaDa transcriptional profiling. Since all the 83 genes are nested within the original 150 gene list, and my main concern was to avoid false negatives, I reported the screen results based on the original 2 replicate screen. The top candidates, including Collagen IV, CG13900 and Hsc70–3 were retained in the new gene list after analysis of 3 replicates.

8.7.1 Bioinformatics Analysis

An algorithm with false discovery rate (FDR) analysis was developed by Tony Southall (Brand lab) to identify significant Dam-POLII binding sites (Southall *et al.* , 2013). Firstly, log2 ratio files were generated (Dam-Pol II over Dam-only) and median normalised (NimbleScan software) for each replicate. Using *Drosophila* genome annotation release 5.47, the mean ratio change across each annotated transcript was calculated. To assign a FDR value, the frequency of transcripts with a mean ratio over specific values (from 0.1 to 0.75 log2 increase) were calculated within a randomised data set (for each chromosome arm) using 10 iterations and 1,000 sampling events. This was repeated for a range of gene sizes (250 to 2,500 bp). These data were used to model FDR values relative to the Dam-Pol II enrichment across a transcript and gene sizes, enabling extrapolation of FDR values for larger ratio changes and larger transcripts. After being performed for each replicate, each transcript was assigned a mean ratio between the biological replicates and the highest associated FDR. To compare data sets, log2 ratios were subtracted and the data median normalised. The data were analysed as described above to identify genes with significantly different Pol II occupancy. Due to the presence of negative log2 ratios in TaDa transcriptional profiling experiments, these genes were filtered to confirm that any significantly enriched genes were also bound by Pol II in the experiment of interest.

Transcripts with log2 POL II occupancy intensity ratio of 1 or higher and FDR rate of 0.01 or lower were considered significantly transcribed for comparison experiments. Genes with a comparison log2 value (after subtraction) of 1 or higher (equivalent to 2 fold changes between condition A and B) and log2 POL II occupancy binding intensity value of 1 or higher, as well as FDR rate of 0.01 or lower, were considered significantly upregulated

under condition A compared to condition B.

8.8 Quantitative Real-Time PCR (Q-PCR)

8.8.1 Primer Design

Primers for Q-PCR were either taken from published literature or designed using the QuantPrime online primer design tool (http://www.quantprime.de/). Only intron-spanning primers were selected.

The following Q-PCR primers were used:

Perlecan^{Trol}: forward, AACGGAGGAAGCTGCAGTGAAC; reverse, CATTGAAGCCCAGTTGGAGGTG (QuantPrime).

Dilp6 primers: forward, CGATGTATTTCCCAACAGTTTCG; reverse, AAATCGGTTACGTTCTGCAAGTC (Grönke *et al.* , 2010).

GAPDH: forward, ATTTCGCTGAACGATAAGTTCGT; reverse, CGATGACGCGGTTGGAGTA (Chell & Brand, 2010).

Rp49: forward, CCAAGATCGTGAAGAAGCG; reverse, GTTGGGCATCAGATACTGTC (QuantPrime).

Ork1: forward, GCTGTACATCCTCAAAGTGAAGCC; reverse, TTGGAACGTGGCAGTGTGTAGG (QuantPrime).

CG3523: forward,TCGCTGAGCTGATGAGCAATGAG; reverse, ACAGAGTGGCGGATTTCTTGATCG (QuantPrime).

IsoQC: forward, CGTGCAGACAGCTTTGATAGCC; reverse, CGCTGGGATTGTAGGATATCTGTG (QuantPrime).

Sema–5c: forward, CGACAGCGCAGTTGCAACAATC; reverse, AGTTCGTCACTTGGGTGCTGATG (QuantPrime).

CG4476: forward, AGCTTGCTTACCATGCGTCCAC; reverse, CCGATACACACCAACCAACAACTC(QuantPrime).

CG30203: forward, ACATTAGGGAGTGCGAAGAGGTTC; reverse, AGTTGGTCCACTCGTTCCAAGG (QuantPrime).

CG4825: forward, CATCACCTTGCTGGCTGTTTCG; reverse, ACGTTCGCCTCGTTTCTGAC (QuantPrime).

Syx5: forward, ACTGGAGAAGCTCACAATGTTGG; reverse, TGAATCTCCTGCGGTCTGTCATC (QuantPrime).

Cct5: forward, ACGCCTGAGAAACTAGGTGTTGC; reverse, TGTCCTTGGATGTTCC-

GAATGCC (QuantPrime).

8.8.2 RNA Extraction and Preparation of cDNA

For each sample, total mRNA was extracted from approximately 60 first instar CNS. CNS were homogenised with 200 μl Trizol reagent (Invitrogen) in an Eppendorf tube. The homogenised sample was topped to 800 μl with Trizol and incubated for 5 min at room temperature. 160 μl of Chloroform (SigmaAldrich) was added to the Eppendorf tube and the tube was shaken vigorously for 15 seconds. After incubation at room temperature for 3 min, the sample was centrifuged at 11,000 rpm for 15 min at 4 ºC. Separation should occur into a lower phenol-chloroform phase, an interphase, and a colourless upper aqueous phase. The upper phase containing mRNA, was transferred to a fresh tube. To precipitate RNA, 1 μl of molecular grade glycogen (10 μg/μl) and 400 μl isopropanol were added, and the tube was incubated at room temperature for 10 min. The mix was centrifuged at 11,000 rpm at 4 ºC for 10 min. A pellet containing the RNA could be detected at the bottom and was washed with 1 ml of 70% ethanol, followed by centrifugation at 8000 rpm at 4 ºC for 5 min. The pellet was left to dry and re-suspend in 20 μl DEPC water.

cDNA was prepared using the QuantiTect Reverse Transcription Kit according to the manufacturer's protocol (Qiagen).

8.8.3 Q-PCR Reaction and Quantification

A StepOnePlus™ Real-Time PCR System machine (Applied Biosystems) was used with SYBR green (Fast SYBR® Green Master Mix, Qiagen) to perform Q-PCR analysis. Results were calculated using the standard curve method and normalised against the geometric means of two reference genes: GAPDH and Rp49. Three biological replicates per sample type were performed and each with three technical replicates.

8.9 RNA *in Situ* Hybridisation

8.9.1 Primer Design for Riboprobes

The coding region of the gene of interest was found on the Flybase website (flybase.org) and was entered into the NCBI website primer blast online tool (http://www.ncbi.nlm.nih.gov/BLAST/). A product size of 900 to 1200 bp was specified, with a minimal primer size of 19 bp, maximal size of 24 bp, and an optimal size of 22 bp. A minimal anealling temperature

of 55 ºC, maximal temperature of 57 ºC, and an optimal temperature of 60 ºC were selected. A minimal GC content of 40% and a maximal GC content of 60% were selected. The T7 RNA polymerase promoter sequence was then added to the 5´ end of the reverse primer sequence.
T7: CAGTAATACGACTCACTATTA

The following oligonucleotide primers were used for normal and fluorescence *in situ* hybridisation:
Dilp6 forward: TTCTCAAAGTGCCGACGTCCAAAG
Dilp6 reverse: cagtaatacgactcactattaTAGTATACTCTAGGGGACACTGCTGC
Repo forward: AGTAGCAACAGCAGCCCAGTTATG
Repo reverse: cagtaatacgactcactattaGGAGGAACTACTTGGCGGAGTAAC

8.9.2 RNA Probe Generation

cDNA fragments of the gene of interest were amplified by PCR from a *Drosophila* embryonic cDNA library (Boris Egger, Brand lab), purified using the Qiaquick PCR Purification kit (Qiagen), and eluted with DEPC water. These DNA templates were used to synthesise digoxigenin (DIG)-labelled antisense riboprobes using the Roche DIG RNA Labelling kit (Roche).
The reaction mix consisted of:
Purified PCR Product from cDNA template: 1 μg to 2 μg
10X Digoxigenin-labelled ribonucleotide mix: 2 μl
10X Transcription buffer: 2 μl
T7 RNA polymerase: 2 μl
RNase Inhibitor (New England Biolabs): 0.2 μl
DEPC H2O: top the total volume up to 20 μl

The *in vitro* transcription reaction was incubated overnight at 18 ºC. The DNA template was removed by incubation with DNaseI for 30 min at 37 ºC. Before degradation, the volume of purified RNA sample was increased to 30 μl total with DEPC H2O. RNA probes were degraded to an average length of 500 bp by hydrolysis in carbonate buffer in order to increase their penetrance. 30 μl of 2X Carbonate Buffer (60 mM Na2CO3, 40 mM NaHCO3, pH 10.2) was added to the sample and the mixture incubated for approximately 10 min at 60 ºC. The formula for calculating incubation time can be found online (http://www.roche-applied-science.com/sis/lad/lad_docs/ISH_55–57.pdf).

To stop probe degradation, 3.5 μl 10 % acetic acid and 6.5 μl 6 M sodium acetate

were added to the reaction. To precipitate the probe, 250 μl 100 % ethanol was added immediately afterwards and the mixture was incubated for 30 min at –20 ºC. The sample was centrifuged at 13,000 rpm for 15 min at 4 ºC and the resulting pellet was washed with 70 % ethanol. After further centrifugation at 13,000 rpm for 5 min, the pellet was allowed to dry and was resuspended in 10 μl DEPC H2O and 0.2 μl RNase inhibitor (Roche). 1 μl of probe was run on an agarose gel to check the quantity and quality of the RNA probes.

8.9.3 Larval Brain Preparation, Pre-Hybridisation and Hybridisation

Larval CNS were dissected in 1XPBS, and fixed with 4% formaldehyde in PBS containing 0.5mM EGTA and 5mM MgCl2 for 20 min at room temperature. The samples were washed with PBTw (0.1% Tween–20 (Sigma-Aldrich) in PBS) for 5 X 5 min, followed by a 10 min wash in a solution containing 50% PBTw and 50% hybridisation buffer (see recipe below) and a wash in 100% hybridisation buffer for 10 min at room temperature. Afterwards, the samples were pre-hybridised for at least 1 hour in hybridisation buffer at 65 ºC. The samples were hybridised with riboprobes in hybridisation buffer at a concentration of 1:500–1:1000 overnight at 65 ºC.

Hybridisation buffer was made up with the following recipe:

50% deionised formamide (Sigma-Aldrich)
5X SSC (0.75 M NaCl, 0.075 M Na3C6H5O7)
0.1% Tween–20 (Sigma-Aldrich)
100 μg/ml *E. coli* tRNA (stock 25 mg/ml, Sigma-Aldrich)
50 μg/ml heparin (stock 50 mg/ml, Sigma-Aldrich)
The pH of the solution was adjusted to 6.5 using concentrated HCl.

8.9.4 Post Hybridisation and Antibody Detection

Following overnight probe hybridisation, the riboprobes were removed and saved for later re-use. The post-hybridisation washes were carried out at 65 ºC and the washing solutions were all pre-warmed at 65 ºC. The CNS were washed in the following order: 1 X 30 min in hybridisation buffer, 1 X 30 min in 50% hybridisation and 50% PBTw, and 4 X 30 min in PBTw. After the washes were completed, sheep anti-digoxigenin antibody conjugated to alkaline phosphatase (Roche) was diluted 1:2000 in PBTw and incubated with the sample for 2 hours at room temperature.

The antibodies were removed and the samples were washed for 3 X 20 min with PBTw. The samples were then rinsed with alkaline phosphatase (AP) buffer (see recipe below),

and washed for 5 min in fresh AP buffer. The chromogenic antibody detection reaction was carried out with NBT (nitro-blue tetrazolium chloride, Roche) and BCIP (5-bromo–4-chloro–3´-indolyphosphate p-toluidine salt, Roche). These two reagents react with alkaline phosphatase to yield an insoluble dark purple precipitate. CNS were first washed in 300 μl AP buffer and 1.5 μl NBT for 5 min. The solution was then replaced with 300 μl AP buffer, 1.5 μl NBT and 1 μl BCIP. The brains were transferred to a 12-well tissue culture plate (Nunclon). The reaction was allowed to progress until dark purple coloration was clearly detectable under a dissection microscope. The enzymic reaction was stopped by washing for 3 X 5 min in PBTw. After the tissues were mounted, a Zeiss Axioplan microscope was used to view the slides and capture images.

AP buffer was made up with the following recipe:

100 mM Tris pH 9.5

100 mM NaCl

50 mM MgCl2

0.1% Tween–20 (Signma-Aldrich)

8.10 RNA Fluorescence *in Situ* Hybridisation

The procedures for fluorescence *in situ* hybridisation (FISH) were identical to regular *in situ* hybridisation prior to post-hybridisation steps, including primer design. After hybridisation, sample for FISH were washed with PBTw for 15 min at 65 ºC. Endogenous peroxidase activity was blocked with 3% hydrogen peroxide in PBTw for 1 hour at room temperature. This was followed by a number of washes: 3 X 5 in PBTw, 5 min in PBS, and 3 X 5 min in PBSt(0.3% Triton (Sigma-Aldrich) in PBS). Since antibody staining is more effective with Triton compared to Tween–20 detergent, all washes from this point onwards were carried out in PBSt. Samples were washed with 10% NGS in PBSt for 30 min at room temperature to block non specific binding and incubated with primary antibody against digoxigenin, conjugated with horseradish peroxidase (Roche, diluted 1 in 200), overnight at 4 ºC. All other primary antibodies were added at this point. The next morning, samples were washed for 3 X 5 min and 3 X 15 min in PBSt, and were incubated with secondary antibodies for 2 hours at room temperature. After 3 X 5 min and 3 X 15 min washes in PBSt, a tyramide reaction was carried out according to manufacturer's protocol (Life Technologies).

8.11 TUNEL

TUNEL staining was performed with ApopTag Red In Situ Apoptosis Detection Kit (Chemicon). The protocol was modified from manufacturer's recommendations by Pauline Speder (Brand lab). Larval CNS were dissected in 1XPBS and fixed with 4% formaldehyde in PBS containing 0.5mM EGTA and 5mM MgCl2 for 20 mins. This was followed by 3 X 5 min washes with PBSt at room temperature. Post-fixation was carried out with pre-cooled ethanol and PBS (2:1) for 5 mins at –20 ºC, followed by 3 X 5 min washes in PBSt. Afterwards, the sample was pre-treated with 10 mM sodium citrate (pH=6) for 30 min at 70 ºC, followed by 3 X 5 min washes in PBSt. PBSt was removed and the sample was incubated in 75 μl of equilibration buffer for 10 min at room temperature, with shaking. The equilibration buffer was removed and replaced with 50 μl of 30% terminal deoxynucleotidyl transferase (TdT) enzyme in reaction buffer (volume/volume) for 3 hours at 37 ºC. TdT enzyme catalyses a template-independent addition of nucleotide triphosphates to the 3-OH ends of DNA, created by apoptosis-induced double stranded DNA breaks. The incorporated nucleotides were partially conjugated with digoxigenin.

The TdT enzyme reaction was stopped by removing the enzyme solution and washing briefly with 1 ml of 1 X Stop/Wash solution. The sample was incubated in a second volume of 1 X Stop/Wash solution for 10 min at room temperature, followed by 3 X 1 min washes in PBTw. Antibody against digoxigenin, conjugated with rhodamine dye, was diluted to 47% (volume/volume) in blocking solution, so that the final volume per sample would be 100 μl. Other primary antibodies were added to the anti-Dig rhodamine solution at appropriate dilutions. The sample was incubated in the antibody solution overnight at 4 ºC. The next morning, antibody solution was removed and the sample was washed 3 X 5 mins with PBSt. Secondary antibody staining was carried out as normal (see below).

8.12 Immunofluorescence of Larval Tissues

8.12.1 Larval Dissection and Fixation

Larval CNS were dissected in 1X PBS at room temperature and transferred to poly-lysine coated Menzel-Glaser cover glasses. They were fixed with 4% formaldehyde in PBS containing 0.5mM EGTA and 5mM MgCl2 at room temperature for 20 min. Immediately after fixation, CNS were washed in PBSt (0.3% Triton-X100 in PBS) 3 X 5 min each and blocked for 15 min in PBSt containing 10% normal goat serum (Sigma-Aldrich).

8.12.2 Primary and Secondary Antibody Incubation

Incubation with primary antibodies was conducted in blocking buffer at 4 °C overnight. After removing primary antibodies with PBSt washes, fluorophore-conjugated secondary antibodies diluted in PBSt/10% normal goat serum were added and incubated for at least four hours at room temperature. All secondary antibodies (Invitrogen) were used at a dilution of 1 in 200. Secondary antibody was removed by PBSt washes and the larval CNS was mounted in Vectashield (Vector Laboratories) prior to imaging with Olympus Upright FV1000 or DeltaVision OMX microscope.

8.12.3 Antibodies Used

The following antibodies were used: guinea pig anti Deadpan (gift from Jim Skeath) at 1:5000; mouse anti Discs Large (DHSB) at 1:70; chicken anti GFP (Abcam) at 1:2000; rabbit anti Phospho-histone 3 (Upstate) at 1:100; rat anti Phospho-histone 3 (Abcam) at 1:5000; mouse anti Repo (DSHB) at 1: 70; rat anti RFP (Abcam) at 1: 1000; rabbit anti PerlecanTrol (gift of S. Baumgartner) at 1: 1000; rabbit anti Collagen IV^{Cg25C} (gift of John Fessler) at 1:500; mouse anti Elav at 1:20 (DSHB); Phalloidin (546 conjugated) at 1:200 (Invitrogen); rabbit anti Miranda at 1:200 (gift of Nung Jan Yuh); mouse anti Prospero at 1:30 (DSHB); mouse anti βPS Integrin^{Mys} at 1:30 (DSHB); rat anti Dilp2 at 1:100 (gift of Pierre Leopold); guinea pig anti Ogre (Innexin1) at 1:200 (gift of Pauline Speder); DAPI at 1:100 (Life Technologies).

8.13 OMX Imaging

Super resolution imaging was performed using DeltaVision OMX BLAZE V3 (Applied Precision, a GE Healthcare company), a 3D-SIM system equipped with sCMOS cameras. Images were captured using an Olympus 60x 1.515NA oil objective, 405nm, 488nm and 593 nm laser illumination and standard excitation and emission filter sets. 3D-SIM image stacks were sectioned using a 125 nm Z-step size. Raw data was reconstructed using softWoRx 6.0 (Applied Precision, a GE Healthcare company) software. Image capture and analyses were assisted by Nicola Lawrence (Gurdon Institute).

8.14 Data Analysis and Deposition

Images were processed and captured using ImageJ and Volocity. Adobe Illustrator and Photoshop were used to generate figures. R was used to perform statistical analysis.

All raw data (gff files) and analysis files of glial and fat body TaDa transcriptional profiling experiments can be found in Gurdon Institute datastore folder: datastore/brand/Brand group folder/reactivation data share/. Pol II binding profiles in these experiments can be viewed on the Brand Lab Genome Browser at https://gbrowse/.

References

Aberg, Maria A I, Aberg, N David, Palmer, Theo D, Alborn, Ann-Marie, Carlsson-Skwirut, Christine, Bang, Peter, Rosengren, Lars E, Olsson, Torsten, Gage, Fred H, & Eriksson, Peter S. 2003a. IGF-I has a direct proliferative effect in adult hippocampal progenitor cells. *Molecular and cellular neurosciences*, **24**(1), 23–40.

Aberg, N David, Blomstrand, Fredrik, Aberg, Maria A I, Björklund, Ulrika, Carlsson, Björn, Carlsson-Skwirut, Christine, Bang, Peter, Rönnbäck, Lars, & Eriksson, Peter S. 2003b. Insulin-like growth factor-I increases astrocyte intercellular gap junctional communication and connexin43 expression in vitro. *Journal of Neuroscience Research*, **74**(1), 12–22.

Ables, Elizabeth T, & Drummond-Barbosa, Daniela. 2010. The Steroid Hormone Ecdysone Functions with Intrinsic Chromatin Remodeling Factors to Control Female Germline Stem Cells in Drosophila. *Cell Stem Cell*, **7**(5), 581–592.

Abraham, Robert T. 2002. Identification of TOR Signaling Complexes. *Cell*, **111**(1), 9–12.

Abrams, Elliott W, & Andrew, Deborah J. 2002. Prolyl 4-hydroxylase alpha-related proteins in Drosophila melanogaster: tissue-specific embryonic expression of the 99F8-9 cluster. *Mechanisms of Development*, **112**(1-2), 165–171.

Alcantara, Ethel H, Lomeda, Ria-Ann R, Feldmann, Joerg, Nixon, Graeme F, Beattie, John H, & Kwun, In-Sook. 2011. Zinc deprivation inhibits extracellular matrix calcification through decreased synthesis of matrix proteins in osteoblasts. *Molecular nutrition & food research*, **55**(10), 1552–1560.

Alexopoulou, Annika N, Multhaupt, Hinke A B, & Couchman, John R. 2007. Syndecans in wound healing, inflammation and vascular biology. *The International Journal of Biochemistry & Cell Biology*, **39**(3), 505–528.

Alexson, Tania O, Hitoshi, Seiji, Coles, Brenda L, Bernstein, Alan, & van der Kooy, Derek. 2006. Notch Signaling Is Required to Maintain All Neural Stem Cell Populations – Irrespective of Spatial or Temporal Niche. *Developmental Neuroscience*, **28**(1-2), 34–48.

Alvarez-Buylla, Arturo, & Garcia-Verdugo, Jose Manuel. 2002. Neurogenesis in adult subventricular zone. *Journal of Neuroscience*, **22**(3), 629–634.

Andersen, D S, Colombani, J, & Leopold, P. 2013. Coordination of organ growth: principles and outstanding questions from the world of insects. *Trends in Cell Biology*, **23**(7), 336–344.

Andersen, Jimena, Urbán, Noelia, Achimastou, Angeliki, Ito, Ayako, Simic, Milesa, Ullom, Kristy, Martynoga, Ben, Lebel, Mélanie, Göritz, Christian, Frisén, Jonas, Nakafuku, Masato, & Guillemot, Francois. 2014. A Transcriptional Mechanism Integrating Inputs from Extracellular Signals to Activate Hippocampal Stem Cells. *Neuron*, **83**(5), 1085–1097.

Aouacheria, Abdel, Geourjon, Christophe, Aghajari, Nushin, Navratil, Vincent, Deléage, Gilbert, Lethias, Claire, & Exposito, Jean-Yves. 2006. Insights into early extracellular matrix evolution: spongin short chain collagen-related proteins are homologous to basement membrane type IV collagens and form a novel family widely distributed in invertebrates. *Molecular biology and evolution*, **23**(12), 2288–2302.

Arikawa-Hirasawa, E, Watanabe, H, Takami, H, Hassell, J R, & Yamada, Y. 1999. Perlecan is essential for cartilage and cephalic development. *Nature genetics*, **23**(3), 354–358.

Ariza, Carlos Atico, McHugh, Kyle P, White, Steven J, Sakaguchi, Donald S, & Mallapragada, Surya K. 2010. Extracellular matrix proteins and astrocyte-derived soluble factors influence the differentiation and proliferation of adult neural progenitor cells. *Journal of Biomedical Materials Research Part A*, **9999A**, NA–NA.

Arnim Jenett, Gerald M Rubin Teri-T B Ngo David Shepherd Christine Murphy Heather Dionne Barret D Pfeiffer Amanda Cavallaro Donald Hall Jennifer Jeter Nirmala Iyer Dona Fetter Joanna H Hausenfluck Hanchuan Peng Eric T Trautman Rob Svirskas Eugene W Myers Zbigniew R Iwinski Yoshinori Aso Gina M DePasquale Adrianne Enos Phuson Hulamm Shing Chun Benny Lam Hsing-Hsi Li Todd R Laverty Fuhui Long Lei Qu Sean D Murphy Konrad Rokicki Todd Safford Kshiti Shaw Julie H Simpson Allison Sowell Susana Tae Yang Yu Christopher T Zugates. 2012. A GAL4-Driver Line Resource for Drosophila Neurobiology. *Cell reports*, **2**(4), 991–1001.

Arsenijevic, Y, Weiss, S, Schneider, B, & Aebischer, P. 2001. Insulin-like growth factor-I is necessary for neural stem cell proliferation and demonstrates distinct actions of epidermal growth factor and fibroblast growth factor-2. *Journal of Neuroscience*, **21**(18), 7194–7202.

Barczyk, Malgorzata, Carracedo, Sergio, & Gullberg, Donald. 2009. Integrins. *Cell and Tissue Research*, **339**(1), 269–280.

Barrett, A L, Krueger, S, & Datta, S. 2008. Branchless and Hedgehog operate in a positive feedback loop to regulate the initiation of neuroblast division in the Drosophila larval brain. *Developmental Biology*, **317**(1), 234–245.

Bendtsen, Jannick Dyrløv, Nielsen, Henrik, von Heijne, Gunnar, & Brunak, Søren. 2004. Improved prediction of signal peptides: SignalP 3.0. *Journal of molecular biology*, **340**(4), 783–795.

Besse, Florence, Mertel, Sara, Kittel, Robert J, Wichmann, Carolin, Rasse, Tobias M, Sigrist, Stephan J, & Ephrussi, Anne. 2007. The Ig cell adhesion molecule Basigin controls compartmentalization and vesicle release at Drosophila melanogaster synapses. *Journal of Cell Biology*, **177**(5), 843–855.

Beumer, K J, Rohrbough, J, Prokop, A, & Broadie, K. 1999. A role for PS integrins in morphological growth and synaptic function at the postembryonic neuromuscular junction of Drosophila. *Development (Cambridge, England)*, **126**(24), 5833–5846.

Biplab K Das, Ling Xia Leon Palandjian Or Gozani Yung Chyung Robin Reed. 1999. Characterization of a Protein Complex Containing Spliceosomal Proteins SAPs 49, 130, 145, and 155. *Molecular and Cellular Biology*, **19**(10), 6796.

Bix, G, Castello, R, Burrows, M, Zoeller, J J, Weech, M, Iozzo, R A, Cardi, C, Thakur, M L, Barker, C A, Camphausen, K, & Iozzo, R V. 2006. Endorepellin In Vivo: Targeting the Tumor Vasculature and Retarding Cancer Growth and Metabolism. *JNCI Journal of the National Cancer Institute*, **98**(22), 1634–1646.

Bix, Gregory, Fu, Jian, Gonzalez, Eva M, Macro, Laura, Barker, Amy, Campbell, Shelly, Zutter, Mary M, Santoro, Samuel A, Kim, Jiyeun K, Höök, Magnus, Reed, Charles C, & Iozzo, Renato V. 2004. Endorepellin causes endothelial cell disassembly of actin cytoskeleton and focal adhesions through 2 1 integrin. *The Journal of Cell Biology*, **166**(1), 97–109.

Bökel, Christian, & Brown, Nicholas H. 2002. Integrins in development: moving on, responding to, and sticking to the extracellular matrix. *Developmental Cell*, **3**(3), 311–321.

Bonaguidi, Michael A, Peng, Chian-Yu, McGuire, Tammy, Falciglia, Gustave, Gobeske, Kevin T, Czeisler, Catherine, & Kessler, John A. 2008. Noggin expands neural stem cells in the adult hippocampus. *Journal of Neuroscience*, **28**(37), 9194–9204.

Bonaguidi, Michael A, Wheeler, Michael A, Shapiro, Jason S, Stadel, Ryan P, Sun, Gerald J, Ming, Guo-Li, & Song, Hongjun. 2011. In Vivo Clonal Analysis Reveals Self-Renewing and Multipotent Adult Neural Stem Cell Characteristics. *Cell*, **145**(7), 1142–1155.

Bond, Allison M, Peng, Chian-Yu, Meyers, Emily A, McGuire, Tammy, Ewaleifoh, Osefame, & Kessler, John A. 2014. BMP Signaling Regulates the Tempo of Adult Hippocampal Progenitor Maturation at Multiple Stages of the Lineage. *Stem Cells*, **32**(8), 2201–2214.

Bondy, C A. 1991. Transient IGF-I gene expression during the maturation of functionally related central projection neurons. *The Journal of neuroscience : the official journal of the Society for Neuroscience*, **11**(11), 3442–3455.

Bonnal, Sophie, Vigevani, Luisa, & rcel, Juan Valc aacute. 2012. The spliceosome as a target of novel antitumour drugs. *Nature Reviews Drug Discovery*, **11**(11), 847–859.

Borkowski, O M, Brown, N H, & Bate, M. 1995. Anterior-posterior subdivision and the diversification of the mesoderm in Drosophila. *Development (Cambridge, England)*, **121**(12), 4183–4193.

Borza, D B. 2000. The Goodpasture Autoantigen. IDENTIFICATION OF MULTIPLE CRYPTIC EPITOPES ON THE NC1 DOMAIN OF THE alpha 3(IV) COLLAGEN CHAIN. *Journal of Biological Chemistry*, **275**(8), 6030–6037.

Bowles, Kristian M, Vallier, Ludovic, Smith, Joseph R, Alexander, Morgan R J, & Pedersen, Roger A. 2006. HOXB4 overexpression promotes hematopoietic development by human embryonic stem cells. *Stem Cells*, **24**(5), 1359–1369.

Brabant, M C, & Brower, D L. 1993. PS2 integrin requirements in Drosophila embryo and wing morphogenesis. *Developmental Biology*, **157**(1), 49–59.

Brabant, M C, Fristrom, D, Bunch, T A, & Brower, D L. 1996. Distinct spatial and temporal functions for PS integrins during Drosophila wing morphogenesis. *Development (Cambridge, England)*, **122**(10), 3307–3317.

Brand, A H, & Perrimon, N. 1993. Targeted gene expression as a means of altering cell fates and generating dominant phenotypes. *Development (Cambridge, England)*, **118**(2), 401–415.

Brand, Andrea H, & Livesey, Frederick J. 2011. Neural Stem Cell Biology in Vertebrates and Invertebrates: More Alike than Different? *Neuron*, **70**(4), 719–729.

Brankatschk, Marko, & Eaton, Suzanne. 2010. Lipoprotein particles cross the blood-brain barrier in Drosophila. *Journal of Neuroscience*, **30**(31), 10441–10447.

Brian S Clark, Seth Blackshaw. 2014. Long non-coding RNA-dependent transcriptional regulation in neuronal development and disease. *Frontiers in Genetics*, **5**.

Briscoe, J, & Ericson, J. 2001. Specification of neuronal fates in the ventral neural tube. *Current Opinion in Neurobiology*, **11**(1), 43–49.

Britton, J S, & Edgar, B A. 1998. Environmental control of the cell cycle in Drosophila: nutrition activates mitotic and endoreplicative cells by distinct mechanisms. *Development (Cambridge, England)*, **125**(11), 2149–2158.

Brizzi, Maria Felice, Tarone, Guido, & Defilippi, Paola. 2012. Extracellular matrix, integrins, and growth factors as tailors of the stem cell niche. *Current Opinion in Cell Biology*, **24**(5), 645–651.

Broadie, Kendal, Baumgartner, Stefan, & Prokop, Andreas. 2011. Extracellular matrix and its receptors in Drosophila neural development. *Developmental Neurobiology*, **71**(11), 1102–1130.

Brody, Thomas, Stivers, Chad, Nagle, James, & Odenwald, Ward F. 2002. Identification of novel Drosophila neural precursor genes using a differential embryonic head cDNA screen. *Mechanisms of Development*, **113**(1), 41–59.

Brooker, G J, Kalloniatis, M, Russo, V C, Murphy, M, Werther, G A, & Bartlett, P F. 2000. Endogenous IGF-1 regulates the neuronal differentiation of adult stem cells. *Journal of Neuroscience Research*, **59**(3), 332–341.

Brower, D L, Bunch, T A, Mukai, L, Adamson, T E, Wehrli, M, Lam, S, Friedlander, E, Roote, C E, & Zusman, S. 1995. Nonequivalent requirements for PS1 and PS2 integrin at cell attachments in Drosophila: genetic analysis of the alpha PS1 integrin subunit. *Development (Cambridge, England)*, **121**(5), 1311–1320.

Brown, Judith C, Sasaki, Takako, Gohring, Walter, Yamada, Yoshihiko, & Timpl, Rupert. 1997. The C-Terminal Domain V of Perlecan Promotes beta1 Integrin-Mediated Cell Adhesion, Binds Heparin, Nidogen and Fibulin-2 and Can be Modified by Glycosaminoglycans. *European journal of biochemistry / FEBS*, **250**(1), 39–46.

Brown, N H. 1993. Integrins hold Drosophila together. *BioEssays*, **15**(6), 383–390.

Brown, N H. 1994. Null mutations in the alpha PS2 and beta PS integrin subunit genes have distinct phenotypes. *Development (Cambridge, England)*, **120**(5), 1221–1231.

Brown, N H, Gregory, S L, & Martin-Bermudo, M D. 2000. Integrins as mediators of morphogenesis in Drosophila. *Developmental Biology*, **223**(1), 1–16.

Brown, Nicholas H, Gregory, Stephen L, Rickoll, Wayne L, Fessler, Liselotte I, Prout, Mary, White, Robert A H, & Fristrom, James W. 2002. Talin is essential for integrin function in Drosophila. *Developmental Cell*, **3**(4), 569–579.

Bunch, T A, Graner, M W, Fessler, L I, Fessler, J H, Schneider, K D, Kerschen, A, Choy, L P, Burgess, B W, & Brower, D L. 1998. The PS2 integrin ligand tiggrin is required for proper muscle function in Drosophila. *Development (Cambridge, England)*, **125**(9), 1679–1689.

Bunt, Stephanie, Hooley, Clare, Hu, Nan, Scahill, Catherine, Weavers, Helen, & Skaer, Helen. 2010. Hemocyte-Secreted Type IV Collagen Enhances BMP Signaling to Guide Renal Tubule Morphogenesis in Drosophila. *Developmental Cell*, **19**(2), 296–306.

Bylund, Magdalena, Andersson, Elisabeth, Novitch, Bennett G, & Muhr, Jonas. 2003. Vertebrate neurogenesis is counteracted by Sox1–3 activity. *Nature Neuroscience*, **6**(11), 1162–1168.

Bystron, Irina, Blakemore, Colin, & Rakic, Pasko. 2008. Development of the human cerebral cortex: Boulder Committee revisited. *Nature Reviews Neuroscience*, **9**(2), 110–122.

Caldwell, M C, & Datta, S. 1998. Expression of cyclin E or DP/E2F rescues the G1 arrest of trol mutant neuroblasts in the Drosophila larval central nervous system. *Mechanisms of Development*, **79**(1-2), 121–130.

Cavener, Douglas R. 1987. Comparison of the consensus sequence flanking translational start sites in Drosophilaand vertebrates. *Nucleic acids research*, **15**(4), 1353–1361.

Chell, James M, & Brand, Andrea H. 2010. Nutrition-responsive glia control exit of neural stem cells from quiescence. *Cell*, **143**(7), 1161–1173.

Cheng, Louise Y, Bailey, Andrew P, Leevers, Sally J, Ragan, Timothy J, Driscoll, Paul C, & Gould, Alex P. 2011. Anaplastic Lymphoma Kinase Spares Organ Growth during Nutrient Restriction in Drosophila. *Cell*, **146**(3), 435–447.

Cheng, T, Rodrigues, N, Shen, H, Yang, Y, Dombkowski, D, Sykes, M, & Scadden, D T. 2000. Hematopoietic stem cell quiescence maintained by p21cip1/waf1. *Science*, **287**(5459), 1804–1808.

Choksi, Semil P, Southall, Tony D, Bossing, Torsten, Edoff, Karin, de Wit, Elzo, Fischer, Bettina E, van Steensel, Bas, Micklem, Gos, & Brand, Andrea H. 2006. Prospero Acts as a Binary Switch between Self-Renewal and Differentiation in Drosophila Neural Stem Cells. *Developmental Cell*, **11**(6), 775–789.

Cirelli, Chiara. 2003. Searching for sleep mutants ofDrosophila melanogaster. *BioEssays*, **25**(10), 940–949.

Cohen, Ehud, Paulsson, Johan F, Blinder, Pablo, Burstyn-Cohen, Tal, Du, Deguo, Estepa, Gabriela, Adame, Anthony, Pham, Hang M, Holzenberger, Martin, Kelly, Jeffery W, Masliah, Eliezer, & Dillin, Andrew. 2009. Reduced IGF-1 signaling delays age-associated proteotoxicity in mice. *Cell*, **139**(6), 1157–1169.

Cohn, Ronald D. 2005. Dystroglycan: important player in skeletal muscle and beyond. *Neuromuscular disorders : NMD*, **15**(3), 207–217.

Colombani, J, Andersen, D S, & Leopold, P. 2012. Secreted Peptide Dilp8 Coordinates Drosophila Tissue Growth with Developmental Timing. *Science*, **336**(6081), 582–585.

Colombani, Julien, Raisin, Sophie, Pantalacci, Sophie, Radimerski, Thomas, Montagne, Jacques, & Léopold, Pierre. 2003. A nutrient sensor mechanism controls Drosophila growth. *Cell*, **114**(6), 739–749.

Comisar, W A, Mooney, D J, & Linderman, J J. 2011. Integrin organization: linking adhesion ligand nanopatterns with altered cell responses. *Journal of theoretical biology*, **274**(1), 120–130.

Cordero-Llana, O, Scott, S A, Maslen, S L, Anderson, J M, Boyle, J, Chowhdury, R-R, Tyers, P, Barker, R A, Kelly, C M, Rosser, A E, Stephens, E, Chandran, S, & Caldwell, M A. 2011. Clusterin secreted by astrocytes enhances neuronal differentiation from human neural precursor cells. *Cell Death and Differentiation*, **18**(5), 907–913.

Costell, M, Gustafsson, E, Aszódi, A, Mörgelin, M, Bloch, W, Hunziker, E, Addicks, K, Timpl, R, & Fässler, R. 1999. Perlecan maintains the integrity of cartilage and some basement membranes. *Journal of Cell Biology*, **147**(5), 1109–1122.

Curtin, Kathryn D, Wyman, Robert J, & Meinertzhagen, Ian A. 2007. Basigin/EMMPRIN/CD147 mediates neuron-glia interactions in the optic lamina of Drosophila. *Glia*, **55**(15), 1542–1553.

Dalla, Christina, Bangasser, Debra A, Edgecomb, Carol, & Shors, Tracey J. 2007. Neurogenesis and learning: Acquisition and asymptotic performance predict how many new cells survive in the hippocampus. *Neurobiology of Learning and Memory*, **88**(1), 143–148.

Daneman, Richard, Zhou, Lu, Agalliu, Dritan, Cahoy, John D, Kaushal, Amit, & Barres, Ben A. 2010. The mouse blood-brain barrier transcriptome: a new resource for understanding the development and function of brain endothelial cells. *PloS One*, **5**(10), e13741.

Darios, Frédéric, Wasser, Catherine, Shakirzyanova, Anastasia, Giniatullin, Artur, Goodman, Kerry, Munoz-Bravo, Jose L, Raingo, Jesica, Jorgačevski, Jernej, Kreft, Marko, Zorec, Robert, Rosa, Juliana M, Gandia, Luis, Gutiérrez, Luis M, Binz, Thomas, Giniatullin, Rashid, Kavalali, Ege T, & Davletov, Bazbek. 2009. Sphingosine Facilitates SNARE Complex Assembly and Activates Synaptic Vesicle Exocytosis. *Neuron*, **62**(5), 683–694.

Dascher, C, Matteson, J, & Balch, W E. 1994. Syntaxin 5 regulates endoplasmic reticulum to Golgi transport. *The Journal of biological chemistry*, **269**(47), 29363–29366.

Datta, S. 1995. Control of proliferation activation in quiescent neuroblasts of the Drosophila central nervous system. *Development (Cambridge, England)*, **121**(4), 1173–1182.

DeCarlo, Arthur A, Belousova, Maria, Ellis, April L, Petersen, Donald, Grenett, Hernan, Hardigan, Patrick, O'Grady, Robert, Lord, Megan, & Whitelock, John M. 2012. Perlecan domain 1 recombinant proteoglycan augments BMP-2 activity and osteogenesis. *BMC Biotechnology*, **12**(1), 60.

DeSalvo, Michael K, Mayer, Nasima, Mayer, Fahima, & Bainton, Roland J. 2011. Physiologic and anatomic characterization of the brain surface glia barrier of Drosophila. *Glia*, **59**(9), 1322–1340.

Dietzl, Georg, Chen, Doris, Schnorrer, Frank, Su, Kuan-Chung, Barinova, Yulia, Fellner, Michaela, Gasser, Beate, Kinsey, Kaolin, Oppel, Silvia, Scheiblauer, Susanne, Couto, Africa, Marra, Vincent, Keleman, Krystyna, & Dickson, Barry J. 2007. A genome-wide transgenic RNAi library for conditional gene inactivation in Drosophila. *Nature*, **448**(7150), 151–156.

Donady, Seecof. 1972. Effect of the gene lethal 1 myospheroid on Drosophila embryonic cells in vitro. *In Vitro*, **8**(1), 7–12.

Dong, Jinghui, Revilla-Sanchez, Raquel, Moss, Stephen, & Haydon, Philip G. 2010. Multiphoton in vivo imaging of amyloid in animal models of Alzheimer's disease. *Neuropharmacology*, **59**(4-5), 268–275.

Dorner, S, Lum, L, Kim, M, Paro, R, Beachy, P A, & Green, R. 2006. A genomewide screen for components of the RNAi pathway in Drosophila cultured cells. *Proceedings of the National Academy of Sciences*, **103**(32), 11880–11885.

Drago, J, Murphy, M, Carroll, S M, Harvey, R P, & Bartlett, P F. 1991. Fibroblast growth factor-mediated proliferation of central nervous system precursors depends on endogenous production of insulin-like growth factor I. *Proceedings of the National Academy of Sciences of the United States of America*, **88**(6), 2199–2203.

Dudley, Andrew C, Thomas, David, Best, James, & Jenkins, Alicia. 2004. The STATs in cell stress-type responses. *Cell Communication and Signaling*, **2**(1), 8.

Durbeej, Madeleine. 2010. Laminins. *Cell and Tissue Research*, **339**(1), 259–268.

Ebens, A J, Garren, H, Cheyette, B N, & Zipursky, S L. 1993. The Drosophila anachronism locus: a glycoprotein secreted by glia inhibits neuroblast proliferation. *Cell*, **74**(1), 15–27.

Ehm, Oliver, Göritz, Christian, Covic, Marcela, Schäffner, Iris, Schwarz, Tobias J, Karaca, Esra, Kempkes, Bettina, Kremmer, Elisabeth, Pfrieger, Frank W, Espinosa, Lluis, Bigas, Anna, Giachino, Claudio, Taylor, Verdon, Frisén, Jonas, & Lie, D Chichung. 2010. RBPJkappa-dependent signaling is essential for long-term maintenance of neural stem cells in the adult hippocampus. *Journal of Neuroscience*, **30**(41), 13794–13807.

Elizabeth J Rideout, Lynne Marshall Savraj S Grewal. 2012. Drosophila RNA polymerase III repressor Maf1 controls body size and developmental timing by modulating tRNAiMet synthesis and systemic insulin signaling. *Proceedings of the National Academy of Sciences of the United States of America*, **109**(4), 1139.

Evdokimovskaya, Yulia, Skarga, Yuri, Vrublevskaya, Veronika, & Morenkov, Oleg. 2013. Secretion of the heat shock proteins HSP70 and HSC70 by baby hamster kidney (BHK-21) cells. *Cell Biology International*, **34**(10), 985–990.

Farhadian, Shelli F, Suárez-Fariñas, Mayte, Cho, Christine E, Pellegrino, Maurizio, & Vosshall, Leslie B. 2012. Post-fasting olfactory, transcriptional, and feeding responses in Drosophila. *Physiology & Behavior*, **105**(2), 544–553.

Farioli-Vecchioli, Stefano, Saraulli, Daniele, Costanzi, Marco, Leonardi, Luca, Cinà, Irene, Micheli, Laura, Nutini, Michele, Longone, Patrizia, Oh, S Paul, Cestari, Vincenzo, & Tirone, Felice. 2009. Impaired terminal differentiation of hippocampal granule neurons and defective contextual memory in PC3/Tis21 knockout mice. *PloS One*, **4**(12), e8339.

Farioli-Vecchioli, Stefano, Ceccarelli, Manuela, Saraulli, Daniele, Micheli, Laura, Cannas, Sara, D'Alessandro, Francesca, Scardigli, Raffaella, Leonardi, Luca, Cinà, Irene, Costanzi, Marco, Mattera, Andrea, Cestari, Vincenzo, & Tirone, Felice. 2014. Tis21 is required for adult neurogenesis in the subventricular zone and for olfactory behavior regulating cyclins, BMP4, Hes1/5 and Ids. *Frontiers in Cellular Neuroscience*, **8**.

Fietz, Simone A, Kelava, Iva, Vogt, Johannes, Wilsch-Bräuninger, Michaela, Stenzel, Denise, Fish, Jennifer L, Corbeil, Denis, Riehn, Axel, Distler, Wolfgang, Nitsch, Robert, & Huttner, Wieland B. 2010. OSVZ progenitors of human and ferret neocortex are epithelial-like and expand by integrin signaling. *Nature Neuroscience*, **13**(6), 690–699.

Fogerty, F J, Fessler, L I, Bunch, T A, Yaron, Y, Parker, C G, Nelson, R E, Brower, D L, Gullberg, D, & Fessler, J H. 1994. Tiggrin, a novel Drosophila extracellular matrix protein that functions as a ligand for Drosophila alpha PS2 beta PS integrins. *Development (Cambridge, England)*, **120**(7), 1747–1758.

Fraichard, Stéphane, Bougé, Anne-Laure, Kendall, Timmy, Chauvel, Isabelle, Bouhin, Hervé, & Bunch, Thomas A. 2010. Tenectin is a novel alphaPS2betaPS integrin ligand required for wing morphogenesis and male genital looping in Drosophila. *Developmental Biology*, **340**(2), 504–517.

Franceschini, Andrea, Szklarczyk, Damian, Frankild, Sune, Kuhn, Michael, Simonovic, Milan, Roth, Alexander, Lin, Jianyi, Minguez, Pablo, Bork, Peer, von Mering, Christian, & Jensen, Lars J. 2013. STRING v9.1: protein-protein interaction networks, with increased coverage and integration. *Nucleic acids research*, **41**(Database issue), D808–15.

Freeman, Marc R, & Doherty, Johnna. 2006a. Glial cell biology in Drosophila and vertebrates. *Trends in Neurosciences*, **29**(2), 82–90.

Freeman, Marc R, & Doherty, Johnna. 2006b. Glial cell biology in Drosophila and vertebrates. *Trends in Neurosciences*, **29**(2), 82–90.

Freeman, Marc R, Delrow, Jeffrey, Kim, Junhyong, Johnson, Eric, & Doe, Chris Q. 2003. Unwrapping glial biology: Gcm target genes regulating glial development, diversification, and function. *Neuron*, **38**(4), 567–580.

French, M M, Smith, S E, Akanbi, K, Sanford, T, Hecht, J, Farach-Carson, M C, & Carson, D D. 1999. Expression of the heparan sulfate proteoglycan, perlecan, during mouse embryogenesis and perlecan chondrogenic activity in vitro. *Journal of Cell Biology*, **145**(5), 1103–1115.

Friedrich, M V, Schneider, M, Timpl, R, & Baumgartner, S. 2000. Perlecan domain V of Drosophila melanogaster. Sequence, recombinant analysis and tissue expression. *European journal of biochemistry / FEBS*, **267**(11), 3149–3159.

Furuse, M. 1998. Claudin-1 and -2: Novel Integral Membrane Proteins Localizing at Tight Junctions with No Sequence Similarity to Occludin. *The Journal of Cell Biology*, **141**(7), 1539–1550.

Gao, Z, Ure, K, Ding, P, Nashaat, M, Yuan, L, Ma, J, Hammer, R E, & Hsieh, J. 2011. The Master Negative Regulator REST/NRSF Controls Adult Neurogenesis by Restraining the Neurogenic Program in Quiescent Stem Cells. *Journal of Neuroscience*, **31**(26), 9772–9786.

Garcia-Alonso, L, Fetter, R D, & Goodman, C S. 1996. Genetic analysis of Laminin A in Drosophila: extracellular matrix containing laminin A is required for ocellar axon pathfinding. *Development (Cambridge, England)*, **122**(9), 2611–2621.

Garelli, Andres, Gontijo, Alisson M, Miguela, Veronica, Caparros, Esther, & Dominguez, Maria. 2012. Imaginal discs secrete insulin-like peptide 8 to mediate plasticity of growth and maturation. *Science*, **336**(6081), 579–582.

Gavériaux-Ruff, Claire, & Kieffer, Brigitte L. 2007. Conditional gene targeting in the mouse nervous system: Insights into brain function and diseases. *Pharmacology & therapeutics*, **113**(3), 619–634.

Géminard, Charles, Rulifson, Eric J, & Léopold, Pierre. 2009. Remote Control of Insulin Secretion by Fat Cells in Drosophila. *Cell Metabolism*, **10**(3), 199–207.

Gibson, Daniel G. 2011. Enzymatic Assembly of Overlapping DNA Fragments. *Pages 349–361 of: sciencedirect.com*. Elsevier.

Gibson, Daniel G, Young, Lei, Chuang, Ray-Yuan, Venter, J Craig, Hutchison, Clyde A, & Smith, Hamilton O. 2009. Enzymatic assembly of DNA molecules up to several hundred kilobases. *Nature Methods*, **6**(5), 343–345.

Girós, Amparo, Morante, Javier, Gil-Sanz, Cristina, Fairén, Alfonso, & Costell, Mercedes. 2007. Perlecan controls neurogenesis in the developing telencephalon. *BMC Developmental Biology*, **7**, 29.

Goberdhan, Deborah C I, & Wilson, Clive. 2003. The functions of insulin signaling: size isn't everything, even in Drosophila. *Differentiation*, **71**(7), 375–397.

Gobeske, Kevin T, Das, Sunit, Bonaguidi, Michael A, Weiss, Craig, Radulovic, Jelena, Disterhoft, John F, & Kessler, John A. 2009. BMP signaling mediates effects of exercise on hippocampal neurogenesis and cognition in mice. *PloS One*, **4**(10), e7506.

Gotwals, P J, Paine-Saunders, S E, Stark, K A, & Hynes, R O. 1994. Drosophila integrins and their ligands. *Current Opinion in Cell Biology*, **6**(5), 734–739.

Götz, Magdalena, & Huttner, Wieland B. 2005. The cell biology of neurogenesis. *Nature Publishing Group*, **6**(10), 777–788.

Gould, Douglas B, Phalan, F Campbell, Breedveld, Guido J, van Mil, Saskia E, Smith, Richard S, Schimenti, John C, Aguglia, Umberto, van der Knaap, Marjo S, Heutink, Peter, & John, Simon W M. 2005. Mutations in Col4a1 cause perinatal cerebral hemorrhage and porencephaly. *Science*, **308**(5725), 1167–1171.

Graner, M W, Bunch, T A, Baumgartner, S, Kerschen, A, & Brower, D L. 1998. Splice variants of the Drosophila PS2 integrins differentially interact with RGD-containing fragments of the extracellular proteins tiggrin, ten-m, and D-laminin 2. *The Journal of biological chemistry*, **273**(29), 18235–18241.

Green, Edward W, Fedele, Giorgio, Giorgini, Flaviano, & Kyriacou, Charalambos P. 2014. A Drosophila RNAi collection is subject to dominant phenotypic effects. *Nature Methods*, **11**(3), 222–223.

Grigorian, Melina, Liu, Ting, Banerjee, Utpal, & Hartenstein, Volker. 2013. The proteoglycan Trol controls the architecture of the extracellular matrix and balances proliferation and differentiation of blood progenitors in the Drosophila lymph gland. *Developmental Biology*, Mar.

Grönke, Sebastian, Clarke, David-Francis, Broughton, Susan, Andrews, T Daniel, & Partridge, Linda. 2010. Molecular evolution and functional characterization of Drosophila insulin-like peptides. *PLoS Genetics*, **6**(2), e1000857.

Groos, Stephanie, Reale, Enrico, Hünefeld, Günter, & Luciano, Liliana. 2003. Changes in epithelial cell turnover and extracellular matrix in human small intestine after TPN. *The Journal of surgical research*, **109**(2), 74–85.

Groszer, M, Erickson, R, Scripture-Adams, D D, Lesche, R, Trumpp, A, Zack, J A, Kornblum, H I, Liu, X, & Wu, H. 2001. Negative regulation of neural stem/progenitor cell proliferation by the Pten tumor suppressor gene in vivo. *Science*, **294**(5549), 2186–2189.

Groszer, M, Erickson, R, Scripture-Adams, D D, Dougherty, J D, Le Belle, J, Zack, J A, Geschwind, D H, Liu, X, Kornblum, H I, & Wu, H. 2006. PTEN negatively regulates neural stem cell self-renewal by modulating G0-G1 cell cycle entry. *Proceedings of the National Academy of Sciences*, **103**(1), 111–116.

Groth, Amy C, Fish, Matthew, Nusse, Roel, & Calos, Michele P. 2004. Construction of transgenic Drosophila by using the site-specific integrase from phage phiC31. *Genetics*, **166**(4), 1775–1782.

Guerra, R R, Trotta, M R, Parra, O M, Avanzo, J L, Bateman, A, Aloia, T P A, Dagli, M L Z, & Hernandez-Blazquez, F J. 2009. Modulation of extracellular matrix by nutritional hepatotrophic factors in thioacetamide-induced liver cirrhosis in the rat. *Brazilian journal of medical and biological research = Revista brasileira de pesquisas médicas e biológicas / Sociedade Brasileira de Biofísica ... [et al.]*, **42**(11), 1027–1034.

H Asha, Istvan Nagy Gabor Kovacs Daniel Stetson Istvan Ando Charles R Dearolf. 2003. Analysis of Ras-induced overproliferation in Drosophila hemocytes. *Genetics*, **163**(1), 203.

Häcker, Udo, Nybakken, Kent, & Perrimon, Norbert. 2005. Heparan sulphate proteoglycans: the sweet side of development. *Nature reviews. Molecular cell biology*, **6**(7), 530–541.

Haigo, Saori L, & Bilder, David. 2011. Global tissue revolutions in a morphogenetic movement controlling elongation. *Science*, **331**(6020), 1071–1074.

Handke, Björn, Poernbacher, Ingrid, Goetze, Sandra, Ahrens, Christian H, Omasits, Ulrich, Marty, Florian, Simigdala, Nikiana, Meyer, Imke, Wollscheid, Bernd, Brunner, Erich, Hafen, Ernst, & Lehner, Christian F. 2013. The Hemolymph Proteome of Fed and Starved Drosophila Larvae. *PloS One*, **8**(6), e67208.

Harburger, David S, & Calderwood, David A. 2009. Integrin signalling at a glance. *Journal of cell science*, **122**(Pt 2), 159–163.

Harrison, D E, Astle, C M, & Delaittre, J A. 1978. Loss of proliferative capacity in immunohemopoietic stem cells caused by serial transplantation rather than aging. *The Journal of experimental medicine*, **147**(5), 1526–1531.

Helgason, C D, Sauvageau, G, Lawrence, H J, Largman, C, & Humphries, R K. 1996. Overexpression of HOXB4 enhances the hematopoietic potential of embryonic stem cells differentiated in vitro. *Blood*, **87**(7), 2740–2749.

Henchcliffe, C, Garcia-Alonso, L, Tang, J, & Goodman, C S. 1993. Genetic analysis of laminin A reveals diverse functions during morphogenesis in Drosophila. *Development (Cambridge, England)*, **118**(2), 325–337.

Herold, N, Will, C L, Wolf, E, Kastner, B, Urlaub, H, & Luhrmann, R. 2008. Conservation of the Protein Composition and Electron Microscopy Structure of Drosophila melanogaster and Human Spliceosomal Complexes. *Molecular and Cellular Biology*, **29**(1), 281–301.

Higami, Yoshikazu, Barger, Jamie L, Page, Grier P, Allison, David B, Smith, Steven R, Prolla, Tomas A, & Weindruch, Richard. 2006. Energy restriction lowers the expression of genes linked to inflammation, the cytoskeleton, the extracellular matrix, and angiogenesis in mouse adipose tissue. *The Journal of nutrition*, **136**(2), 343–352.

Ho, Matthew S P, Böse, Kerstin, Mokkapati, Sharada, Nischt, Roswitha, & Smyth, Neil. 2008. Nidogens-Extracellular matrix linker molecules. *Microscopy research and technique*, **71**(5), 387–395.

Hoang, B, & Chiba, A. 1998. Genetic analysis on the role of integrin during axon guidance in Drosophila. *The Journal of neuroscience : the official journal of the Society for Neuroscience*, **18**(19), 7847–7855.

Hodge, R D. 2004. Insulin-Like Growth Factor-I Accelerates the Cell Cycle by Decreasing G1 Phase Length and Increases Cell Cycle Reentry in the Embryonic Cerebral Cortex. *Journal of Neuroscience*, **24**(45), 10201–10210.

Hopf, M, Göhring, W, Kohfeldt, E, Yamada, Y, & Timpl, R. 1999. Recombinant domain IV of perlecan binds to nidogens, laminin-nidogen complex, fibronectin, fibulin-2 and heparin. *European journal of biochemistry / FEBS*, **259**(3), 917–925.

Hu, Yanhui, Flockhart, Ian, Vinayagam, Arunachalam, Bergwitz, Clemens, Berger, Bonnie, Perrimon, Norbert, & Mohr, Stephanie E. 2011. An integrative approach to ortholog prediction for disease-focused and other functional studies. *BMC Bioinformatics*, **12**, 357.

Huang, Da Wei, Sherman, Brad T, & Lempicki, Richard A. 2009. Bioinformatics enrichment tools: paths toward the comprehensive functional analysis of large gene lists. *Nucleic acids research*, **37**(1), 1–13.

Humphries, Jonathan D, Byron, Adam, & Humphries, Martin J. 2006a. Integrin ligands at a glance. *Journal of cell science*, **119**(Pt 19), 3901–3903.

Humphries, Jonathan D, Byron, Adam, & Humphries, Martin J. 2006b. Integrin ligands at a glance. *Journal of cell science*, **119**(Pt 19), 3901–3903.

Hynes, R O. 1992. Integrins: versatility, modulation, and signaling in cell adhesion. *Cell*, **69**(1), 11–25.

Ikeya, Tomoatsu, Galic, Milos, Belawat, Priyanka, Nairz, Knud, & Hafen, Ernst. 2002. Nutrient-Dependent Expression of Insulin-like Peptides from Neuroendocrine Cells in the CNS Contributes to Growth Regulation in Drosophila. *Current Biology*, **12**(15), 1293–1300.

Imayoshi, I, Sakamoto, M, Yamaguchi, M, Mori, K, & Kageyama, R. 2010. Essential Roles of Notch Signaling in Maintenance of Neural Stem Cells in Developing and Adult Brains. *Journal of Neuroscience*, **30**(9), 3489–3498.

Iozzo, R V, Cohen, I R, Grässel, S, & Murdoch, A D. 1994. The biology of perlecan: the multifaceted heparan sulphate proteoglycan of basement membranes and pericellular matrices. *The Biochemical Journal*, **302 (Pt 3)**(Sept.), 625–639.

Iresjö, Britt-Marie, Svensson, Johan, Ohlsson, Claes, & Lundholm, Kent. 2013. Liver-derived endocrine IGF-I is not critical for activation of skeletal muscle protein synthesis following oral feeding. *BMC physiology*, **13**, 7.

Ito, K, & Hotta, Y. 1992. Proliferation pattern of postembryonic neuroblasts in the brain of Drosophila melanogaster. *Developmental Biology*, **149**(1), 134–148.

Jahn, Reinhard, & Scheller, Richard H. 2006. SNAREs — engines for membrane fusion. *Nature Publishing Group*, **7**(9), 631–643.

Jan, Y N, & Jan, L Y. 1998. Asymmetric cell division. *Nature*, **392**(6678), 775–778.

Jessen, Kristjan R. 2004. Glial cells. *The International Journal of Biochemistry & Cell Biology*, **36**(10), 1861–1867.

Jiménez-García, L F, & Spector, D L. 1993. In vivo evidence that transcription and splicing are coordinated by a recruiting mechanism. *Cell*, **73**(1), 47–59.

Jin, Kunlin, Zhu, Yonghua, Sun, Yunjuan, Mao, Xiao Ou, Xie, Lin, & Greenberg, David A. 2002. Vascular endothelial growth factor (VEGF) stimulates neurogenesis in vitro and in vivo. *Proceedings of the National Academy of Sciences of the United States of America*, **99**(18), 11946–11950.

Joseph D'Ercole, A., & Ye, Ping. 2008. Expanding the Mind: Insulin-Like Growth Factor I and Brain Development. *Endocrinology*, **149**(12), 5958.

Kaido, T, Yebra, M, Cirulli, V, & Montgomery, A M. 2004. Regulation of Human -Cell Adhesion, Motility, and Insulin Secretion by Collagen IV and Its Receptor 1 1. *Journal of Biological Chemistry*, **279**(51), 53762–53769.

Kalluri, Raghu. 2003. Angiogenesis: Basement membranes: structure, assembly and role in tumour angiogenesis. *Nature Reviews Cancer*, **3**(6), 422–433.

Kamimura, Keisuke, Ueno, Kohei, Nakagawa, Jun, Hamada, Rie, Saitoe, Minoru, & Maeda, Nobuaki. 2013. Perlecan regulates bidirectional Wnt signaling at the Drosophila neuromuscular junction. *The Journal of Cell Biology*, Jan.

Kamminga, Leonie M, Bystrykh, Leonid V, de Boer, Aletta, Houwer, Sita, Douma, José, Weersing, Ellen, Dontje, Bert, & de Haan, Gerald. 2006. The Polycomb group gene Ezh2 prevents hematopoietic stem cell exhaustion. *Blood*, **107**(5), 2170–2179.

Karpac, Jason, Younger, Andrew, & Jasper, Heinrich. 2011. Dynamic Coordination of Innate Immune Signaling and Insulin Signaling Regulates Systemic Responses to Localized DNA Damage. *Developmental Cell*, **20**(6), 841–854.

Kazanis, Ilias. 2011. Can Adult Neural Stem Cells Create New Brains? Plasticity in the Adult Mammalian Neurogenic Niches: Realities and Expectations in the Era of Regenerative Biology. *The Neuroscientist : a review journal bringing neurobiology, neurology and psychiatry*, May.

Kazanis, Ilias, & ffrench Constant, Charles. 2011. Extracellular matrix and the neural stem cell niche. *Developmental Neurobiology*, **71**(11), 1006–1017.

Kazanis, Ilias, Lathia, Justin D, Vadakkan, Tegy J, Raborn, Eric, Wan, Ruiqian, Mughal, Mohamed R, Eckley, D Mark, Sasaki, Takako, Patton, Bruce, Mattson, Mark P, Hirschi, Karen K, Dickinson, Mary E, & ffrench Constant, Charles. 2010. Quiescence and activation of stem and precursor cell populations in the subependymal zone of the mammalian brain are associated with distinct cellular and extracellular matrix signals. *Journal of Neuroscience*, **30**(29), 9771–9781.

Kennea, Nigel L, & Mehmet, Huseyin. 2002. Neural stem cells. *The Journal of Pathology*, **197**(4), 536–550.

Khoshnoodi, Jamshid, Pedchenko, Vadim, & Hudson, Billy G. 2008. Mammalian collagen IV. *Microscopy research and technique*, **71**(5), 357–370.

Kibbe, W A. 2007. OligoCalc: an online oligonucleotide properties calculator. *Nucleic acids research*, **35**(Web Server), W43–W46.

Killip, L E, & Grewal, S S. 2012. DREF is required for cell and organismal growth in Drosophila and functions downstream of the nutrition/TOR pathway. *Developmental Biology*, **371**(2), 191–202.

Kim, Kimberly H, & Roberts, Charles W M. 2013. CHD7 in charge of neurogenesis. *Cell Stem Cell*, **13**(1), 1–2.

Kim, Nam Chul, & Marqués, Guillermo. 2010. Identification of downstream targets of the Bone Morphogenetic Protein pathway in the Drosophila nervous system. *Developmental Dynamics*, **239**(9), 2413–2425.

Kim, YongJoong, Kim, Hag Dong, Youn, Buhyun, Park, Yun Gyu, & Kim, Joon. 2013. Ribosomal protein S3 is secreted as a homodimer in cancer cells. *Biochemical and Biophysical Research Communications*, **441**(4), 805–808.

Kintner, Chris. 2002. Neurogenesis in embryos and in adult neural stem cells. *Journal of Neuroscience*, **22**(3), 639–643.

Kippin, Tod E, Martens, David J, & van der Kooy, Derek. 2005. p21 loss compromises the relative quiescence of forebrain stem cell proliferation leading to exhaustion of their proliferation capacity. *Genes and Development*, **19**(6), 756–767.

Kokovay, Erzsebet, Goderie, Susan, Wang, Yue, Lotz, Steve, Lin, Gang, Sun, Yu, Roysam, Badrinath, Shen, Qin, & Temple, Sally. 2010. Adult SVZ lineage cells home to and leave the vascular niche via differential responses to SDF1/CXCR4 signaling. *Cell Stem Cell*, **7**(2), 163–173.

Kraut, Rachel. 2011. Roles of sphingolipids in Drosophila development and disease. *Journal of neurochemistry*, **116**(5), 764–778.

Krishnamurthy, Mansa, Li, Jinming, Al-Masri, Maia, & Wang, Rennian. 2008. Expression and function of alphabeta1 integrins in pancretic beta (INS-1) cells. *Journal of cell communication and signaling*, **2**(3-4), 67–79.

Kucherenko, Mariya M, Pantoja, Mario, Yatsenko, Andriy S, Shcherbata, Halyna R, Fischer, Karin A, Maksymiv, Dariya V, Chernyk, Yaroslava I, & Ruohola-Baker, Hannele. 2008. Genetic modifier screens reveal new components that interact with the Drosophila dystroglycan-dystrophin complex. *PloS One*, **3**(6), e2418.

Kusche-Gullberg, M, Garrison, K, MacKrell, A J, Fessler, L I, & Fessler, J H. 1992. Laminin A chain: expression during Drosophila development and genomic sequence. *The EMBO Journal*, **11**(12), 4519–4527.

Le Parco, Y., Knibiehler, B, Cecchini, J P, & Mirre, C. 1986. Stage and tissue-specific expression of a collagen gene during Drosophila melanogaster development. *Experimental cell research*, **163**(2), 405–412.

LeBleu, Valerie S, MacDonald, Brian, & Kalluri, Raghu. 2007. Structure and function of basement membranes. *Experimental biology and medicine (Maywood, N.J.)*, **232**(9), 1121–1129.

Lee, J, Duan, W, Long, J M, Ingram, D K, & Mattson, M P. 2000. Dietary restriction increases the number of newly generated neural cells, and induces BDNF expression, in the dentate gyrus of rats. *Journal of molecular neuroscience : MN*, **15**(2), 99–108.

Lee, Jaewon, Duan, Wenzhen, & Mattson, Mark P. 2002. Evidence that brain-derived neurotrophic factor is required for basal neurogenesis and mediates, in part, the enhancement of neurogenesis by dietary restriction in the hippocampus of adult mice. *Journal of neurochemistry*, **82**(6), 1367–1375.

Lee, S K, & Pfaff, S L. 2001. Transcriptional networks regulating neuronal identity in the developing spinal cord. *Nature Neuroscience*, **4 Suppl**(Nov.), 1183–1191.

Lehtinen, Maria K, Zappaterra, Mauro W, Chen, Xi, Yang, Yawei J, Hill, Anthony D, Lun, Melody, Maynard, Thomas, Gonzalez, Dilenny, Kim, Seonhee, Ye, Ping, D'Ercole, A Joseph, Wong, Eric T, LaMantia, Anthony S, & Walsh, Christopher A. 2011. The cerebrospinal fluid provides a proliferative niche for neural progenitor cells. *Neuron*, **69**(5), 893–905.

Leitinger, Birgit, & Hohenester, Erhard. 2007. Mammalian collagen receptors. *Matrix Biology*, **26**(3), 146–155.

Leptin, M, Bogaert, T, Lehmann, R, & Wilcox, M. 1989. The function of PS integrins during Drosophila embryogenesis. *Cell*, **56**(3), 401–408.

Liang, Huixuan, Hippenmeyer, Simon, & Ghashghaei, H Troy. 2012. A Nestin-cre transgenic mouse is insufficient for recombination in early embryonic neural progenitors. *Biology open*, **1**(12), 1200–1203.

Lichtenwalner, R J, Forbes, M E, Bennett, S A, Lynch, C D, Sonntag, W E, & Riddle, D R. 2001. Intracerebroventricular infusion of insulin-like growth factor-I ameliorates the age-related decline in hippocampal neurogenesis. *Neuroscience*, **107**(4), 603–613.

Lie, Dieter-Chichung, Colamarino, Sophia A, Song, Hong-Jun, Désiré, Laurent, Mira, Helena, Consiglio, Antonella, Lein, Edward S, Jessberger, Sebastian, Lansford, Heather, Dearie, Alejandro R, & Gage, Fred H. 2005. Wnt signalling regulates adult hippocampal neurogenesis. *Nature*, **437**(7063), 1370–1375.

Lin, Guonan, Zhang, Xi, Ren, Juan, Pang, Zhimin, Wang, Chenhui, Xu, Na, & Xi, Rongwen. 2013. Integrin signaling is required for maintenance and proliferation of intestinal stem cells in Drosophila. *Developmental Biology*, **377**(1), 177–187.

Lin, H M, Lee, J H, Yadav, H, Kamaraju, A K, Liu, E, Zhigang, D, Vieira, A, Kim, S J, Collins, H, Matschinsky, F, Harlan, D M, Roberts, A B, & Rane, S G. 2009. Transforming Growth Factor- /Smad3 Signaling Regulates Insulin Gene Transcription and Pancreatic Islet -Cell Function. *Journal of Biological Chemistry*, **284**(18), 12246–12257.

Lin, Xinhua. 2004a. Functions of heparan sulfate proteoglycans in cell signaling during development. *Development (Cambridge, England)*, **131**(24), 6009–6021.

Lin, Xinhua. 2004b. Functions of heparan sulfate proteoglycans in cell signaling during development. *Development (Cambridge, England)*, **131**(24), 6009–6021.

Lindner, Jonathan R, Hillman, Paul R, Barrett, Andrea L, Jackson, Megan C, Perry, Trinity L, Park, Youngji, & Datta, Sumana. 2007. The Drosophila Perlecan gene trol regulates multiple signaling pathways in different developmental contexts. *BMC Developmental Biology*, **7**(1), 121.

Livingstone, Callum, & Borai, Anwar. 2014. Insulin-like growth factor-II: its role in metabolic and endocrine disease. *Clinical Endocrinology*, Mar., n/a–n/a.

Loulier, Karine, Lathia, Justin D, Marthiens, Veronique, Relucio, Jenne, Mughal, Mohamed R, Tang, Sung-Chun, Coksaygan, Turhan, Hall, Peter E, Chigurupati, Srinivasulu, Patton, Bruce, Colognato, Holly, Rao, Mahendra S, Mattson, Mark P, Haydar, Tarik F, & ffrench Constant, Charles. 2009. β1 Integrin Maintains Integrity of the Embryonic Neocortical Stem Cell Niche. *PLoS Biology*, **7**(8), e1000176.

Marshall, Lynne, Rideout, Elizabeth J, & Grewal, Savraj S. 2012. Nutrient/TOR-dependent regulation of RNA polymerase III controls tissue and organismal growth in Drosophila. *The EMBO Journal*, **31**(8), 1916–1930.

Martin, D. 1999. wing blister, A New Drosophila Laminin alpha Chain Required for Cell Adhesion and Migration during Embryonic and Imaginal Development. *The Journal of Cell Biology*, **145**(1), 191–201.

Martin-Bermudo, M D, & Brown, N H. 1999. Uncoupling integrin adhesion and signaling: the betaPS cytoplasmic domain is sufficient to regulate gene expression in the Drosophila embryo. *Genes and Development*, **13**(6), 729–739.

Martinek, Nathalie, Shahab, Jaffer, Saathoff, Manuela, & Ringuette, Maurice. 2008. Haemocyte-derived SPARC is required for collagen-IV-dependent stability of basal laminae in Drosophila embryos. *Journal of cell science*, **121**(Pt 10), 1671–1680.

Martinez, E, Palhan, V B, Tjernberg, A, Lymar, E S, Gamper, A M, Kundu, T K, Chait, B T, & Roeder, R G. 2001. Human STAGA Complex Is a Chromatin-Acetylating Transcription Coactivator That Interacts with Pre-mRNA Splicing and DNA Damage-Binding Factors In Vivo. *Molecular and Cellular Biology*, **21**(20), 6782–6795.

Martynoga, Ben, Mateo, Juan L, Zhou, Bo, Andersen, Jimena, Achimastou, Angeliki, Urbán, Noelia, van den Berg, Debbie, Georgopoulou, Dimitra, Hadjur, Suzana, Wittbrodt, Joachim, Ettwiller, Laurence, Piper, Michael, Gronostajski, Richard M, & Guillemot, Francois. 2013. Epigenomic enhancer annotation reveals a key role for NFIX in neural stem cell quiescence. *Genes and Development*, **27**(16), 1769–1786.

Mason, Jeffrey L, Xuan, Shouhong, Dragatsis, Ioannis, Efstratiadis, Argiris, & Goldman, James E. 2003. Insulin-like growth factor (IGF) signaling through type 1 IGF receptor plays an important role in remyelination. *Journal of Neuroscience*, **23**(20), 7710–7718.

Matsumoto, K, Toh-e, A, & Oshima, Y. 1978. Genetic control of galactokinase synthesis in Saccharomyces cerevisiae: evidence for constitutive expression of the positive regulatory gene gal4. *Journal of bacteriology*, **134**(2), 446–457.

McDonald, Thomas J, Nijland, Mark J, & Nathanielsz, Peter W. 2007. The insulin-like growth factor system and the fetal brain: effects of poor maternal nutrition. *Reviews in endocrine & metabolic disorders*, **8**(2), 71–84.

McGuire, Sean E, Le, Phuong T, Osborn, Alexander J, Matsumoto, Kunihiro, & Davis, Ronald L. 2003. Spatiotemporal rescue of memory dysfunction in Drosophila. *Science*, **302**(5651), 1765–1768.

Medioni, C, & Noselli, S. 2005. Dynamics of the basement membrane in invasive epithelial clusters in Drosophila. *Development*, **132**(13), 3069–3077.

Mehrabian, Shima, Raycheva, Margarita, Gateva, Antoaneta, Todorova, Gergana, Angelova, Petia, Traykova, Martina, Stankova, Tonya, Kamenov, Zdravko, & Traykov, Latchezar. 2012. Cognitive dysfunction profile and arterial stiffness in type 2 diabetes. *Journal of the neurological sciences*, **322**(1-2), 152–156.

Melrose, James, Hayes, Anthony J, Whitelock, John M, & Little, Christopher B. 2008. Perlecan, the "jack of all trades" proteoglycan of cartilaginous weight-bearing connective tissues. *BioEssays*, **30**(5), 457–469.

Michele, Daniel E, & Campbell, Kevin P. 2003. Dystrophin-glycoprotein complex: post-translational processing and dystroglycan function. *The Journal of biological chemistry*, **278**(18), 15457–15460.

Mira, Helena, Andreu, Zoraida, Suh, Hoonkyo, Lie, D Chichung, Jessberger, Sebastian, Consiglio, Antonella, Emeterio, Juana San, Hortigüela, Rafael, Marqués-Torrejón, María Angeles, Nakashima, Kinichi, Colak, Dilek, Götz, Magdalena, Fariñas, Isabel, & Gage, Fred H. 2010. Signaling through BMPR-IA Regulates Quiescence and Long-Term Activity of Neural Stem Cellsin the Adult Hippocampus. *Stem Cell*, **7**(1), 78–89.

Miura, Yutaka, Kato, Hisanori, & Noguchi, Tadashi. 2007. Effect of dietary proteins on insulin-like growth factor-1 (IGF-1) messenger ribonucleic acid content in rat liver. *British Journal of Nutrition*, **67**(02), 257.

Mizee, Mark R, Wooldrik, Desiree, Lakeman, Kim A M, van het Hof, Bert, Drexhage, Joost A R, Geerts, Dirk, Bugiani, Marianna, Aronica, Eleonora, Mebius, Reina E, Prat, Alexandre, de Vries, Helga E, & Reijerkerk, Arie. 2013. Retinoic acid induces blood-brain barrier development. *Journal of Neuroscience*, **33**(4), 1660–1671.

Mobley, Aaron K, & McCarty, Joseph H. 2011. β8 integrin is essential for neuroblast migration in the rostral migratory stream. *Glia*, **59**(11), 1579–1587.

Mobley, Aaron K, Tchaicha, Jeremy H, Shin, Jaekyung, Hossain, Mohammad G, & McCarty, Joseph H. 2009. Beta8 integrin regulates neurogenesis and neurovascular homeostasis in the adult brain. *Journal of cell science*, **122**(Pt 11), 1842–1851.

Mochizuki, Toshio, Lemmink, Henny H, Mariyama, Mariko, Antignac, Corinne, Gubler, Marie-Claire, Pirson, Yves, Verellen-Dumoulin, Christine, Chan, Belinda, Schröder, Cornelis H, Smeets, Hubert J, & Reeders, Stephen T. 1994. Identification of mutations in the α3(IV) and α4(IV) collagen genes in autosomal recessive Alport syndrome. *Nature genetics*, **8**(1), 77–82.

Moline, M M, Southern, C, & Bejsovec, A. 1999. Directionality of wingless protein transport influences epidermal patterning in the Drosophila embryo. *Development (Cambridge, England)*, **126**(19), 4375–4384.

Morgan, Mark R, Humphries, Martin J, & Bass, Mark D. 2007. Synergistic control of cell adhesion by integrins and syndecans. *Nature Publishing Group*, **8**(12), 957–969.

Morin, X, Daneman, R, Zavortink, M, & Chia, W. 2001. A protein trap strategy to detect GFP-tagged proteins expressed from their endogenous loci in Drosophila. *Proceedings of the National Academy of Sciences of the United States of America*, **98**(26), 15050–15055.

Mount, S M. 2000. Pre-messenger RNA Processing Factors in the Drosophila Genome. *The Journal of Cell Biology*, **150**(2), 37F–44.

Müller, Hannah, Schmidt, David, Steinbrink, Sandra, Mirgorodskaya, Ekaterina, Lehmann, Verena, Habermann, Karin, Dreher, Felix, Gustavsson, Niklas, Kessler, Thomas, Lehrach, Hans, Herwig, Ralf, Gobom, Johan, Ploubidou, Aspasia, Boutros, Michael, & Lange, Bodo M H. 2010. Proteomic and functional analysis of the mitotic Drosophila centrosome. *The EMBO Journal*, **29**(19), 3344–3357.

Nagele, Robert G, Wegiel, Jerzy, Venkataraman, Venkat, Imaki, Humi, Wang, Kuo-Chiang, & Wegiel, Jarek. 2004. Contribution of glial cells to the development of amyloid plaques in Alzheimer's disease. *Neurobiology of aging*, **25**(5), 663–674.

Nässel, Dick R, Kubrak, Olga A, Liu, Yiting, Luo, Jiangnan, & Lushchak, Oleh V. 2013. Factors that regulate insulin producing cells and their output in Drosophila. *Invertebrate Physiology*, **4**.

Neumüller, Ralph A, Richter, Constance, Fischer, Anja, Novatchkova, Maria, Neumüller, Klaus G, & Knoblich, Juergen A. 2011. Genome-Wide Analysis of Self-Renewal in Drosophila Neural Stem Cells by Transgenic RNAi. *Stem Cell*, **8**(5), 580–593.

Ni, Jian-Quan, Liu, Lu-Ping, Binari, Richard, Hardy, Robert, Shim, Hye-Seok, Cavallaro, Amanda, Booker, Matthew, Pfeiffer, Barret D, Markstein, Michele, Wang, Hui, Villalta, Christians, Laverty, Todd R, Perkins, Lizabeth A, & Perrimon, Norbert. 2009. A Drosophila resource of transgenic RNAi lines for neurogenetics. *Genetics*, **182**(4), 1089–1100.

Ni, Jian-Quan, Zhou, Rui, Czech, Benjamin, Liu, Lu-Ping, Holderbaum, Laura, Yang-Zhou, Donghui, Shim, Hye-Seok, Tao, Rong, Handler, Dominik, Karpowicz, Phillip, Binari, Richard, Booker, Matthew, Brennecke, Julius, Perkins, Lizabeth A, Hannon, Gregory J, & Perrimon, Norbert. 2011. A genome-scale shRNA resource for transgenic RNAi in Drosophila. *Nature Methods*, **8**(5), 405–407.

Nidhi Batra, Sirisha Burra Arlene J Siller-Jackson Sumin Gu Xuechun Xia Gregory F Weber Douglas DeSimone Lynda F Bonewald Eileen M Lafer Eugene Sprague Martin A Schwartz Jean X Jiang. 2012. Mechanical stress-activated integrin $\alpha 5\beta 1$ induces opening of connexin 43 hemichannels. *Proceedings of the National Academy of Sciences of the United States of America*, **109**(9), 3359.

Nievers, M G, Schaapveld, R Q, & Sonnenberg, A. 1999. Biology and function of hemidesmosomes. *Matrix biology : journal of the International Society for Matrix Biology*, **18**(1), 5–17.

Niu, W, Zou, Y, Shen, C, & Zhang, C L. 2011. Activation of Postnatal Neural Stem Cells Requires Nuclear Receptor TLX. *Journal of Neuroscience*, **31**(39), 13816–13828.

O'Brien, Lucy Erin, Soliman, Sarah S, Li, Xinghua, & Bilder, David. 2011. Altered Modes of Stem Cell Division Drive Adaptive Intestinal Growth. *Cell*, **147**(3), 603–614.

Okamoto, Naoki, Yamanaka, Naoki, Yagi, Yoshimasa, Nishida, Yasuyoshi, Kataoka, Hiroshi, O'Connor, Michael B, & Mizoguchi, Akira. 2009. A fat body-derived IGF-like peptide regulates postfeeding growth in Drosophila. *Developmental Cell*, **17**(6), 885–891.

Orford, Keith W, & Scadden, David T. 2008. Deconstructing stem cell self-renewal: genetic insights into cell-cycle regulation. *Nature Reviews Genetics*, **9**(2), 115–128.

Ortega, Nathalie, & Werb, Zena. 2002. New functional roles for non-collagenous domains of basement membrane collagens. *Journal of cell science*, **115**(Pt 22), 4201–4214.

Paik, Ji-hye, Ding, Zhihu, Narurkar, Rujuta, Ramkissoon, Shakti, Muller, Florian, Kamoun, Walid S, Chae, Sung-Suk, Zheng, Hongwu, Ying, Haoqiang, Mahoney, Jed, Hiller, David, Jiang, Shan, Protopopov, Alexei, Wong, Wing H, Chin, Lynda, Ligon, Keith L, & DePinho, Ronald A. 2009. FoxOs Cooperatively Regulate Diverse Pathways Governing Neural Stem Cell Homeostasis. *Stem Cell*, **5**(5), 540–553.

Papaemmanuil, E, Cazzola, M, Boultwood, J, Malcovati, L, Vyas, P, Bowen, D, Pellagatti, A, Wainscoat, J S, Hellstrom-Lindberg, E, Gambacorti-Passerini, C, Godfrey, A L, Rapado, I, Cvejic, A, Rance, R, McGee, C, Ellis, P, Mudie, L J, Stephens, P J, McLaren, S, Massie, C E, Tarpey, P S, Varela, I, Nik-Zainal, S, Davies, H R, Shlien, A, Jones, D, Raine, K, Hinton, J, Butler, A P, Teague, J W, Baxter, E J, Score, J, Galli, A, Della Porta, M G, Travaglino, E, Groves, M, Tauro, S, Munshi, N C, Anderson, K C, El-Naggar, A,

Fischer, A, Mustonen, V, Warren, A J, Cross, N C P, Green, A R, Futreal, P A, Stratton, M R, & Campbell, P J. 2011. Somatic SF3B1Mutation in Myelodysplasia with Ring Sideroblasts. *New England Journal of Medicine*, **365**(15), 1384–1395.

Paralkar, V M, Vukicevic, S, & Reddi, A H. 1991. Transforming growth factor beta type 1 binds to collagen IV of basement membrane matrix: implications for development. *Developmental Biology*, **143**(2), 303–308.

Parham, Christi, Auckland, Lisa, Rachwal, Jessica, Clarke, Douglas, & Bix, Gregory. 2013. Perlecan Domain V Inhibits Amyloid-β Induced Brain Endothelial Cell Toxicity and Restores Angiogenic Function. *Journal of Alzheimer's disease : JAD*, Aug.

Park, Hee Ra, Park, Mikyung, Choi, Jehun, Park, Kun-Young, Chung, Hae Young, & Lee, Jaewon. 2010. A high-fat diet impairs neurogenesis: involvement of lipid peroxidation and brain-derived neurotrophic factor. *Neuroscience Letters*, **482**(3), 235–239.

Park, Youngji, Rangel, Carolina, Reynolds, M Megan, Caldwell, M Craig, Johns, Misty, Nayak, Mamatha, Welsh, C Jane R, McDermott, Sean, & Datta, Sumana. 2003. Drosophila perlecan modulates FGF and hedgehog signals to activate neural stem cell division. *Developmental Biology*, **253**(2), 247–257.

Pastor-Pareja, José Carlos, & Xu, Tian. 2011. Shaping cells and organs in Drosophila by opposing roles of fat body-secreted Collagen IV and perlecan. *Developmental Cell*, **21**(2), 245–256.

Peltier, Joseph, O'Neill, Analeah, & Schaffer, David V. 2007. PI3K/Akt and CREB regulate adult neural hippocampal progenitor proliferation and differentiation. *Developmental Neurobiology*, **67**(10), 1348–1361.

Phelan, Pauline. 2005. Innexins: members of an evolutionarily conserved family of gap-junction proteins. *Biochimica et biophysica acta*, **1711**(2), 225–245.

Popken, Gregory J, Hodge, Rebecca D, Ye, Ping, Zhang, Jihui, Ng, Winnie, O'Kusky, John R, & D'Ercole, A Joseph. 2004. In vivo effects of insulin-like growth factor-I (IGF-I) on prenatal and early postnatal development of the central nervous system. *The European journal of neuroscience*, **19**(8), 2056–2068.

Porlan, Eva, Morante-Redolat, José Manuel, Marqués-Torrejón, María Angeles, Andreu-Agulló, Celia, Carneiro, Carmen, Gómez-Ibarlucea, Esther, Soto, Atenea, Vidal, Anxo, Ferrón, Sacri R, & Fariñas, Isabel. 2013. Transcriptional repression of Bmp2 by p21(Waf1/Cip1) links quiescence to neural stem cell maintenance. *Nature Neuroscience*, **16**(11), 1567–1575.

Porlan, Eva, Martí-Prado, Beatriz, Morante-Redolat, José Manuel, Consiglio, Antonella, Delgado, Ana C, Kypta, Robert, López-Otín, Carlos, Kirstein, Martina, & Fariñas, Isabel. 2014. MT5-MMP regulates adult neural stem cell functional quiescence through the cleavage of N-cadherin. *Nature Cell Biology*, **16**(7), 629–638.

Pöschl, Ernst, Schlötzer-Schrehardt, Ursula, Brachvogel, Bent, Saito, Kenji, Ninomiya, Yoshifumi, & Mayer, Ulrike. 2004. Collagen IV is essential for basement membrane stability but dispensable for initiation of its assembly during early development. *Development (Cambridge, England)*, **131**(7), 1619–1628.

Prokop, A, Martin-Bermudo, M D, Bate, M, & Brown, N H. 1998. Absence of PS integrins or laminin A affects extracellular adhesion, but not intracellular assembly, of hemiadherens and neuromuscular junctions in Drosophila embryos. *Developmental Biology*, **196**(1), 58–76.

Qin, Song, Niu, Wenze, Iqbal, Nida, Smith, Derek K, & Zhang, Chun-Li. 2014. Orphan nuclear receptor TLX regulates astrogenesis by modulating BMP signaling. *Frontiers in neuroscience*, **8**, 74.

Qu, Qiuhao, Sun, Guoqiang, Li, Wenwu, Yang, Su, Ye, Peng, Zhao, Chunnian, Yu, Ruth T, Gage, Fred H, Evans, Ronald M, & Shi, Yanhong. 2010. Orphan nuclear receptor TLX activates Wnt/beta-catenin signalling to stimulate neural stem cell proliferation and self-renewal. *Nature Cell Biology*, **12**(1), 31–40– sup pp 1–9.

Radakovits, Randor, Barros, Claudia S, Belvindrah, Richard, Patton, Bruce, & Müller, Ulrich. 2009. Regulation of radial glial survival by signals from the meninges. *Journal of Neuroscience*, **29**(24), 7694–7705.

Rafalski, Victoria A, & Brunet, Anne. 2011. Energy metabolism in adult neural stem cell fate. *Progress in Neurobiology*, **93**(2), 182–203.

Rajan, Akhila, & Perrimon, Norbert. 2012. Drosophila cytokine unpaired 2 regulates physiological homeostasis by remotely controlling insulin secretion. *Cell*, **151**(1), 123–137.

Ramírez-Weber, F A, & Kornberg, T B. 1999. Cytonemes: cellular processes that project to the principal signaling center in Drosophila imaginal discs. *Cell*, **97**(5), 599–607.

Reinhardt, R R, & Bondy, C A. 1994. Insulin-like growth factors cross the blood-brain barrier. *Endocrinology*, **135**(5), 1753–1761.

Renault, ValErie M, Rafalski, Victoria A, Morgan, Alex A, Salih, Dervis A M, Brett, Jamie O, Webb, Ashley E, Villeda, Saul A, Thekkat, Pramod U, Guillerey, Camille, Denko, Nicholas C, Palmer, Theo D, Butte, Atul J, & Brunet, Anne. 2009. FoxO3 Regulates Neural Stem Cell Homeostasis. *Stem Cell*, **5**(5), 527–539.

Reuter, R, Grunewald, B, & Leptin, M. 1993. A role for the mesoderm in endodermal migration and morphogenesis in Drosophila. *Development (Cambridge, England)*, **119**(4), 1135–1145.

Reynolds, B, Laynes, R, Ögmundsdóttir, M H, Boyd, C A R, & Goberdhan, D C I. 2007. Amino acid transporters and nutrient-sensing mechanisms: new targets for treating insulin-linked disorders? *Biochemical Society Transactions*, **35**(5), 1215.

Riopel, M, Krishnamurthy, M, Li, J, Liu, S, Leask, A, & Wang, R. 2011. Conditional β1-integrin-deficient mice display impaired pancreatic β cell function. *The Journal of Pathology*, **224**(1), 45–55.

Roberts, Jacqueline M, Ennajdaoui, Hanane, Edmondson, Carina, Wirth, Brunhilde, Sanford, Jeremy R, & Chen, Bin. 2014. Splicing factor TRA2B is required for neural progenitor survival. *The Journal of Comparative Neurology*, **522**(2), 372–392.

Roberts, Jill, Kahle, Michael P, & Bix, Gregory J. 2012. Perlecan and the Blood-Brain Barrier: Beneficial Proteolysis? *Frontiers in Pharmacology*, **3**.

Rodriguez, A, Zhou, Z, Tang, M L, Meller, S, Chen, J, Bellen, H, & Kimbrell, D A. 1996. Identification of immune system and response genes, and novel mutations causing melanotic tumor formation in Drosophila melanogaster. *Genetics*, **143**(2), 929–940.

Rohrbough, J, Grotewiel, M S, Davis, R L, & Broadie, K. 2000. Integrin-mediated regulation of synaptic morphology, transmission, and plasticity. *The Journal of neuroscience : the official journal of the Society for Neuroscience*, **20**(18), 6868–6878.

Rondas, D, Tomas, A, Soto-Ribeiro, M, Wehrle-Haller, B, & Halban, P A. 2012. Novel Mechanistic Link between Focal Adhesion Remodeling and Glucose-stimulated Insulin Secretion. *Journal of Biological Chemistry*, **287**(4), 2423–2436.

Roote, C E, & Zusman, S. 1996. Alternatively spliced forms of the Drosophila alphaPS2 subunit of integrin are sufficient for viability and can replace the function of the alphaPS1 subunit of integrin in the retina. *Development (Cambridge, England)*, **122**(6), 1985–1994.

Rulifson, Eric J, Kim, Seung K, & Nusse, Roel. 2002. Ablation of insulin-producing neurons in flies: growth and diabetic phenotypes. *Science*, **296**(5570), 1118–1120.

Sawala, Annick, Sutcliffe, Catherine, & Ashe, Hilary L. 2012. Multistep molecular mechanism for bone morphogenetic protein extracellular transport in the Drosophila embryo. *Proceedings of the National Academy of Sciences*, **109**(28), 11222–11227.

Scharfman, Helen, Goodman, Jeffrey, Macleod, Adam, Phani, Sudar, Antonelli, Cara, & Croll, Susan. 2005. Increased neurogenesis and the ectopic granule cells after intrahippocampal BDNF infusion in adult rats. *Experimental neurology*, **192**(2), 348–356.

Schlaepfer, David D, Sieg, David J, Hauck, Christof R, Ilic, Dusko, Klingbeil, Candice K, Schaefer, Erik, & Damsky, Caroline H. 2000. FAK integrates growth-factor and integrin signals to promote cell migration : Abstract : Nature Cell Biology. *Nature Cell Biology*, **2**(5), 249–256.

Schneller, M, Vuori, K, & Ruoslahti, E. 1997. Alphavbeta3 integrin associates with activated insulin and PDGFbeta receptors and potentiates the biological activity of PDGF. *The EMBO Journal*, **16**(18), 5600–5607.

Schoenherr, C J, & Anderson, D J. 1995. Silencing is golden: negative regulation in the control of neuronal gene transcription. *Current Opinion in Neurobiology*, **5**(5), 566–571.

Scott, Charlotte E, Wynn, Sarah L, Sesay, Abdul, Cruz, Catarina, Cheung, Martin, Gaviro, Maria-Victoria Gomez, Booth, Sarah, Gao, Bo, Cheah, Kathryn S E, Lovell-Badge, Robin, & Briscoe, James. 2010. SOX9 induces and maintains neural stem cells. *Nature Neuroscience*, **13**(10), 1181–1189.

Scott, Ryan C, Schuldiner, Oren, & Neufeld, Thomas P. 2004. Role and regulation of starvation-induced autophagy in the Drosophila fat body. *Developmental Cell*, **7**(2), 167–178.

Segev, Amit, Nili, Nafiseh, & Strauss, Bradley H. 2004. The role of perlecan in arterial injury and angiogenesis. *Cardiovascular research*, **63**(4), 603–610.

Segretain, Dominique, & Falk, Matthias M. 2004. Regulation of connexin biosynthesis, assembly, gap junction formation, and removal. *Biochimica et biophysica acta*, **1662**(1-2), 3–21.

Sengle, G, Ono, R N, Sasaki, T, & Sakai, L Y. 2011. Prodomains of Transforming Growth Factor (TGF) Superfamily Members Specify Different Functions: EXTRACELLULAR MATRIX INTERACTIONS AND GROWTH FACTOR BIOAVAILABILITY. *Journal of Biological Chemistry*, **286**(7), 5087–5099.

Sepp, K. 2001. Peripheral Glia Direct Axon Guidance across the CNS/PNS Transition Zone. *Developmental Biology*, **238**(1), 47–63.

Shen, Qin, Wang, Yue, Kokovay, Erzsebet, Lin, Gang, Chuang, Shu-Mien, Goderie, Susan K, Roysam, Badrinath, & Temple, Sally. 2008. Adult SVZ stem cells lie in a vascular niche: a quantitative analysis of niche cell-cell interactions. *Cell Stem Cell*, **3**(3), 289–300.

Shetty, Ashok K, Hattiangady, Bharathi, & Shetty, Geetha A. 2005. Stem/progenitor cell proliferation factors FGF-2, IGF-1, and VEGF exhibit early decline during the course of aging in the hippocampus: role of astrocytes. *Glia*, **51**(3), 173–186.

Shie, Feng-Shiun, Nivison, Mary, Hsu, Pei-Chien, & Montine, Thomas. 2009. Modulation of Microglial Innate Immunity in Alzheimers Disease by Activation of Peroxisome Proliferator-activated Receptor Gamma. *Current Medicinal Chemistry*, **16**(6), 643–651.

Simone A Fietz, Robert Lachmann Holger Brandl Martin Kircher Nikolay Samusik Roland Schröder Naharajan Lakshmanaperumal Ian Henry Johannes Vogt Axel Riehn Wolfgang Distler Robert Nitsch Wolfgang Enard Svante Pääbo Wieland B Huttner. 2012. Transcriptomes of germinal zones of human and mouse fetal neocortex suggest a role of extracellular matrix in progenitor self-renewal. *Proceedings of the National Academy of Sciences of the United States of America*, **109**(29), 11836.

Slaidina, Maija, Delanoue, Rénald, Grönke, Sebastian, Partridge, Linda, & Léopold, Pierre. 2009. A Drosophila insulin-like peptide promotes growth during nonfeeding states. *Developmental Cell*, **17**(6), 874–884.

Söderberg, Jeannette A E, Birse, Ryan T, & Nässel, Dick R. 2011. Insulin Production and Signaling in Renal Tubules of Drosophila Is under Control of Tachykinin-Related Peptide and Regulates Stress Resistance. *PloS One*, **6**(5), e19866.

Song, Hongjun, Stevens, Charles F, & Gage, Fred H. 2002. Astroglia induce neurogenesis from adult neural stem cells. *Nature*, **417**(6884), 39–44.

Song, Juan, Zhong, Chun, Bonaguidi, Michael A, Sun, Gerald J, Hsu, Derek, Gu, Yan, Meletis, Konstantinos, Huang, Z Josh, Ge, Shaoyu, Enikolopov, Grigori, Deisseroth, Karl, Luscher, Bernhard, Christian, Kimberly M, Ming, Guo-Li, & Song, Hongjun. 2012. Neuronal circuitry mechanism regulating adult quiescent neural stem-cell fate decision. *Nature*, **489**(7414), 150–154.

Sousa-Nunes, Rita, Yee, Lih Ling, & Gould, Alex P. 2011. Fat cells reactivate quiescent neuroblasts via TOR and glial insulin relays in Drosophila. *Nature*, **471**(7339), 508–512.

Southall, Tony D, Gold, Katrina S, Egger, Boris, Davidson, Catherine M, Caygill, Elizabeth E, Marshall, Owen J, & Brand, Andrea H. 2013. Cell-Type-Specific Profiling of Gene Expression and Chromatin Binding without Cell Isolation: Assaying RNA Pol II Occupancy in Neural Stem Cells. *Developmental Cell*, June.

Spéder, Pauline, Liu, Jun, & Brand, Andrea H. 2011. Nutrient control of neural stem cells. *Current Opinion in Cell Biology*, **23**(6), 724–729.

Staquicini, Fernanda I, Dias-Neto, Emmanuel, Li, Jianxue, Snyder, Evan Y, Sidman, Richard L, Pasqualini, Renata, & Arap, Wadih. 2009. Discovery of a functional protein complex of netrin-4, laminin gamma1 chain, and integrin alpha6beta1 in mouse neural stem cells. *Proceedings of the National Academy of Sciences*, **106**(8), 2903–2908.

Stevens, Adrienne, & Jacobs, J Roger. 2002. Integrins regulate responsiveness to slit repellent signals. *Journal of Neuroscience*, **22**(11), 4448–4455.

Stopa, E G, Berzin, T M, Kim, S, Song, P, Kuo-LeBlanc, V, Rodriguez-Wolf, M, Baird, A, & Johanson, C E. 2001. Human choroid plexus growth factors: What are the implications for CSF dynamics in Alzheimer's disease? *Experimental neurology*, **167**(1), 40–47.

Stork, Tobias, Engelen, Daniel, Krudewig, Alice, Silies, Marion, Bainton, Roland J, & Klämbt, Christian. 2008. Organization and function of the blood-brain barrier in Drosophila. *Journal of Neuroscience*, **28**(3), 587–597.

Stork, Tobias, Bernardos, Rebecca, & Freeman, Marc R. 2012. Analysis of glial cell development and function in Drosophila. *Cold Spring Harbor protocols*, **2012**(1), 1–17.

Stranahan, Alexis M, Arumugam, Thiruma V, Cutler, Roy G, Lee, Kim, Egan, Josephine M, & Mattson, Mark P. 2008a. Diabetes impairs hippocampal function through glucocorticoid-mediated effects on new and mature neurons. *Nature Neuroscience*, **11**(3), 309–317.

Stranahan, Alexis M, Norman, Eric D, Lee, Kim, Cutler, Roy G, Telljohann, Richard S, Egan, Josephine M, & Mattson, Mark P. 2008b. Diet-induced insulin resistance impairs hippocampal synaptic plasticity and cognition in middle-aged rats. *Hippocampus*, **18**(11), 1085–1088.

Subramanian, A, Wayburn, B, Bunch, T, & Volk, T. 2007. Thrombospondin-mediated adhesion is essential for the formation of the myotendinous junction in Drosophila. *Development*, **134**(7), 1269–1278.

Takagi, Y, Nomizu, M, Gullberg, D, MacKrell, A J, Keene, D R, Yamada, Y, & Fessler, J H. 1996. Conserved neuron promoting activity in Drosophila and vertebrate laminin alpha1. *The Journal of biological chemistry*, **271**(30), 18074–18081.

Takagi, Y, Ui-Tei, K, Miyake, T, & Hirohashi, S. 1998. Laminin-dependent integrin clustering with tyrosine-phosphorylated molecules in a Drosophila neuronal cell line. *Neuroscience Letters*, **244**(3), 149–152.

Tanimoto, H, Itoh, S, ten Dijke, P, & Tabata, T. 2000. Hedgehog creates a gradient of DPP activity in Drosophila wing imaginal discs. *Molecular cell*, **5**(1), 59–71.

Tapon, N, Ito, N, Dickson, B J, Treisman, J E, & Hariharan, I K. 2001. The Drosophila tuberous sclerosis complex gene homologs restrict cell growth and cell proliferation. *Cell*, **105**(3), 345–355.

Tian, A, & Jiang, J. 2014. Intestinal epithelium-derived BMP controls stem cell self-renewal in Drosophila adult midgut. *eLife*, **3**(0), e01857–e01857.

Timpl, R, Dziadek, M, Fujiwara, S, Nowack, H, & Wick, G. 1983. Nidogen: a new, self-aggregating basement membrane protein. *European journal of biochemistry / FEBS*, **137**(3), 455–465.

Truman, J W, & Bate, M. 1988. Spatial and temporal patterns of neurogenesis in the central nervous system of Drosophila melanogaster. *Developmental Biology*, **125**(1), 145–157.

Tsai, Pei-I, Kao, Hsiu-Hua, Grabbe, Caroline, Lee, Yu-Tao, Ghose, Aurnab, Lai, Tzu-Ting, Peng, Kuan-Po, Van Vactor, David, Palmer, Ruth H, Chen, Ruey-Hwa, Yeh, Shih-Rung, & Chien, Cheng-Ting. 2008. Fak56 functions downstream of integrin alphaPS3betanu and suppresses MAPK activation in neuromuscular junction growth. *Neural Development*, **3**, 26.

Tuckwell, Danny, & Humphries, Martin. 1996. Integrin–collagen binding. *Seminars in Cell & Developmental Biology*, **7**(5), 649–657.

van der Knaap, Marjo S, Smit, Leo M E, Barkhof, Frederik, Pijnenburg, Yolande A L, Zweegman, Sonja, Niessen, Hans W M, Imhof, Saskia, & Heutink, Peter. 2006. Neonatal porencephaly and adult stroke related to mutations in collagen IV A1. *Annals of Neurology*, **59**(3), 504–511.

van Praag, H, Kempermann, G, & Gage, F H. 1999. Running increases cell proliferation and neurogenesis in the adult mouse dentate gyrus. *Nature Neuroscience*, **2**(3), 266–270.

van Steensel, B, Delrow, J, & Henikoff, S. 2001. Chromatin profiling using targeted DNA adenine methyltransferase. *Nature genetics*, **27**(3), 304–308.

Van Vactor, David, Wall, Dennis P, & Johnson, Karl G. 2006. Heparan sulfate proteoglycans and the emergence of neuronal connectivity. *Current Opinion in Neurobiology*, **16**(1), 40–51.

Vanderploeg, Jessica, Vazquez Paz, L Lourdes, MacMullin, Allison, & Jacobs, J Roger. 2012. Integrins are required for cardioblast polarisation in Drosophila. *BMC Developmental Biology*, **12**, 8.

Vaynman, Shoshanna, Ying, Zhe, & Gomez-Pinilla, Fernando. 2004. Hippocampal BDNF mediates the efficacy of exercise on synaptic plasticity and cognition. *The European journal of neuroscience*, **20**(10), 2580–2590.

Veenstra, Jan A, Agricola, Hans-Jürgen, & Sellami, Azza. 2008. Regulatory peptides in fruit fly midgut. *Cell and Tissue Research*, **334**(3), 499–516.

Vega, Virginia L, Rodríguez-Silva, Monica, Frey, Tiffany, Gehrmann, Mathias, Diaz, Juan Carlos, Steinem, Claudia, Multhoff, Gabriele, Arispe, Nelson, & De Maio, Antonio. 2008. Hsp70 translocates into the plasma membrane after stress and is released into the extracellular environment in a membrane-associated form that activates macrophages. *Journal of immunology (Baltimore, Md. : 1950)*, **180**(6), 4299–4307.

Venere, Monica, Han, Young-Goo, Bell, Robert, Song, Jun S, Alvarez-Buylla, Arturo, & Blelloch, Robert. 2012. Sox1 marks an activated neural stem/progenitor cell in the hippocampus. *Development*, **139**(21), 3938–3949.

Voigt, Aaron, Pflanz, Ralf, Sch fer, Ulrich, & J ckle, Herbert. 2002. Perlecan participates in proliferation activation of quiescentDrosophila neuroblasts. *Developmental Dynamics*, **224**(4), 403–412.

Volk, T. 1999. Singling out Drosophila tendon cells: a dialogue between two distinct cell types. *Trends in genetics : TIG*, **15**(11), 448–453.

von Mering, Christian, Jensen, Lars J, Snel, Berend, Hooper, Sean D, Krupp, Markus, Foglierini, Mathilde, Jouffre, Nelly, Huynen, Martijn A, & Bork, Peer. 2005. STRING: known and predicted protein-protein associations, integrated and transferred across organisms. *Nucleic acids research*, **33**(Database issue), D433–7.

Wang, Huafang, & Su, Yunchao. 2011. Collagen IV contributes to nitric oxide-induced angiogenesis of lung endothelial cells. *AJP: Cell Physiology*, **300**(5), C979–88.

Wang, S, Tulina, N, Carlin, D L, & Rulifson, E J. 2007. The origin of islet-like cells in Drosophila identifies parallels to the vertebrate endocrine axis. *Proceedings of the National Academy of Sciences*, **104**(50), 19873–19878.

Wang, Xiaomeng, Harris, Robin E, Bayston, Laura J, & Ashe, Hilary L. 2008. Type IV collagens regulate BMP signalling in Drosophila. *Nature*, **455**(7209), 72–77.

Webb, Thomas R, Joyner, Amanda S, & Potter, Philip M. 2013. The development and application of small molecule modulators of SF3b as therapeutic agents for cancer. *Drug discovery today*, **18**(1-2), 43–49.

Weber, Laney M, Hayda, Kirsten N, & Anseth, Kristi S. 2008. Cell–Matrix Interactions Improve β-Cell Survival and Insulin Secretion in Three-Dimensional Culture. *Tissue Engineering Part A*, **14**(12), 1959–1968.

Weng, Ruifen, & Cohen, Stephen M. 2012. Drosophila miR-124 regulates neuroblast proliferation through its target anachronism. *Development*, Feb.

Whitelock, John M, Melrose, James, & Iozzo, Renato V. 2008. Diverse Cell Signaling Events Modulated by Perlecan †. *Biochemistry*, **47**(43), 11174–11183.

Will, C L. 2002. Characterization of novel SF3b and 17S U2 snRNP proteins, including a human Prp5p homologue and an SF3b DEAD-box protein. *The EMBO Journal*, **21**(18), 4978–4988.

Williams, Gwyn T, & Farzaneh, Farzin. 2012. Are snoRNAs and snoRNA host genes new players in cancer? *Nature Reviews Cancer*, **12**(2), 84–88.

Wilson, S I, & Edlund, T. 2001. Neural induction: toward a unifying mechanism. *Nature Neuroscience*, **4 Suppl**(Nov.), 1161–1168.

Wojcik-Stanaszek, Luiza, Gregor, Anna, & Zalewska, Teresa. 2011. Regulation of neurogenesis by extracellular matrix and integrins. *Acta neurobiologiae experimentalis*, **71**(1), 103–112.

Wolfstetter, Georg, & Holz, Anne. 2012. The role of LamininB2 (LanB2) during mesoderm differentiation in Drosophila. *Cellular and molecular life sciences : CMLS*, **69**(2), 267–282.

Woolford, J L, & Baserga, S J. 2013. Ribosome Biogenesis in the Yeast Saccharomyces cerevisiae. *Genetics*, **195**(3), 643–681.

Wright, S, Parham, C, Lee, B, Clarke, D, Auckland, L, Johnston, J, Lawrence, A L, Dickeson, S K, Santoro, S A, Griswold-Prenner, I, & Bix, G. 2012. Perlecan domain V inhibits. *Neurobiology of aging*, **33**(7), 1379–1388.

Wyatt, G R, & KALE, G F. 1957. The chemistry of insect hemolymph. II. Trehalose and other carbohydrates. *The Journal of general physiology*, **40**(6), 833–847.

Xavier, Miguel J, & Williams, Michael J. 2011. The Rho-family GTPase Rac1 regulates integrin localization in Drosophila immunosurveillance cells. *PloS One*, **6**(5), e19504.

Yager, J, Richards, S, Hekmat-Scafe, D S, Hurd, D D, Sundaresan, V, Caprette, D R, Saxton, W M, Carlson, J R, & Stern, M. 2001. Control of Drosophila perineurial glial growth by interacting neurotransmitter-mediated signaling pathways. *Proceedings of the National Academy of Sciences of the United States of America*, **98**(18), 10445–10450.

Yan, D, & Lin, X. 2009. Shaping Morphogen Gradients by Proteoglycans. *Cold Spring Harbor Perspectives in Biology*, **1**(3), a002493–a002493.

Yan, Yi-Ping, Sailor, Kurt A, Vemuganti, Raghu, & Dempsey, Robert J. 2006. Insulin-like growth factor-1 is an endogenous mediator of focal ischemia-induced neural progenitor proliferation. *The European journal of neuroscience*, **24**(1), 45–54.

Yasothornsrikul, S, Davis, W J, Cramer, G, Kimbrell, D A, & Dearolf, C R. 1997. viking: identification and characterization of a second type IV collagen in Drosophila. *Gene*, **198**(1-2), 17–25.

Ye, Ping, Popken, Greg J, Kemper, April, McCarthy, Ken, Popko, Brian, & D'Ercole, A Joseph. 2004. Astrocyte-specific overexpression of insulin-like growth factor-I promotes brain overgrowth and glial fibrillary acidic protein expression. *Journal of Neuroscience Research*, **78**(4), 472–484.

Yi, Peng, Park, Ji-Sun, & Melton, Douglas A. 2013. Betatrophin: A Hormone that Controls Pancreatic β Cell Proliferation. *Cell*, Apr.

You, Jia, Zhang, Yan, Li, Zhouhua, Lou, Zhefeng, Jin, Longjin, & Lin, Xinhua. 2014. Drosophila Perlecan Regulates Intestinal Stem Cell Activity via Cell-Matrix Attachment. *Stem Cell Reports*, **2**(6), 761–769.

Yu, Hui, Yuan, Youzhong, Shen, Hongmei, & Cheng, Tao. 2006. Hematopoietic stem cell exhaustion impacted by p18 INK4C and p21 Cip1/Waf1 in opposite manners. *Blood*, **107**(3), 1200–1206.

Yuan, Youzhong, Shen, Hongmei, Franklin, David S, Scadden, David T, & Cheng, Tao. 2004. In vivo self-renewing divisions of haematopoietic stem cells are increased in the absence of the early G1-phase inhibitor, p18INK4C. *Nature Cell Biology*, **6**(5), 436–442.

Yurchenco, P D, & Ruben, G C. 1987. Basement membrane structure in situ: evidence for lateral associations in the type IV collagen network. *Journal of Cell Biology*, **105**(6 Pt 1), 2559–2568.

Yurchenco, Peter D, & Patton, Bruce L. 2009. Developmental and pathogenic mechanisms of basement membrane assembly. *Current pharmaceutical design*, **15**(12), 1277–1294.

Zhang, Guohong, Taneja, Krishan L, Singer, Robert H, & Green, Michael R. 1994. Localization of pre-mRNA splicing in mammalian nuclei. *Nature*, **372**(6508), 809–812.

Zhu, Changqi C, Boone, Jason Q, Jensen, Philip A, Hanna, Scott, Podemski, Lynn, Locke, John, Doe, Chris Q, & O'Connor, Michael B. 2008. Drosophila Activin- and the Activin-like product Dawdle function redundantly to regulate proliferation in the larval brain. *Development (Cambridge, England)*, **135**(3), 513–521.

Zhu, Sijun, Lin, Suewei, Kao, Chih-Fei, Awasaki, Takeshi, Chiang, Ann-Shyn, & Lee, Tzumin. 2006. Gradients of the Drosophila Chinmo BTB-zinc finger protein govern neuronal temporal identity. *Cell*, **127**(2), 409–422.

Ziegler, A N, Chidambaram, S, Forbes, B E, Wood, T L, & Levison, S W. 2014. Insulin-like Growth Factor-II (IGF-II) and IGF-II Analogs with Enhanced Insulin Receptor-a Binding Affinity Promote Neural Stem Cell Expansion. *Journal of Biological Chemistry*, **289**(8), 4626–4633.

Ziegler, Amber N, Schneider, Joel S, Qin, Mei, Tyler, William A, Pintar, John E, Fraidenraich, Diego, Wood, Teresa L, & Levison, Steven W. 2012. IGF-II Promotes Stemness of Neural Restricted Precursors. *Stem Cells*, **30**(6), 1265–1276.

Zigova, T, Pencea, V, Wiegand, S J, & Luskin, M B. 1998. Intraventricular administration of BDNF increases the number of newly generated neurons in the adult olfactory bulb. *Molecular and cellular neurosciences*, **11**(4), 234–245.

Zinke, Ingo, Schütz, Christina S, Katzenberger, Jörg D, Bauer, Matthias, & Pankratz, Michael J. 2002. Nutrient control of gene expression in Drosophila: microarray analysis of starvation and sugar-dependent response. *The EMBO Journal*, **21**(22), 6162–6173.

Appendix A

RNAi Lines Used For Screening

Table A.0.1 List of genes unregulated in the fat body encoding for predicted secreted proteins by Secretome P and/or Signal P

Gene symbol	Signal P	Secretome P	GO Cellular component	GO Biological processes
CG14629	y	y	-	-
CG15369	y	y	-	-
Hsc70-3	y	y	lipid particle	sleep
CG11529	y	y	-	proteolysis; neurogenesis
Lsp1beta	y	y	lipid particle	lateral inhibition
CG5945	y	y	-	-
CG11425	y	n	membrane	dephosphorylation
CG32829	y	n	cellular_component	-
Crc	y	n	lipid particle	central nervous system development;olfactory behavior; brain morphogenesis
CG9269	y	n	-	-
CG6415	n	y	lipid particle	glycine catabolic process
CG15482	n	y	-	-
Pepck	n	y	mitochondrion	gluconeogenesis
Nop60B	n	y	nucleolus	pseudouridine synthesis;rRNA processing
sta	n	y	lipid particle	translation;mitotic spindle elongation
Uhg1	n	y	-	-

w	n	y	ATP-binding cassette transporter complex	eye pigment precursor transport
RpL23	n	y	cytosolic large ribosomal subunit	translation
RpL12	n	y	cytosolic large ribosomal subunit	translation
RpL39	n	y	ribosome	translation
CG13900	n	y	small nuclear ribonucleoprotein complex	mRNA splicing,via spliceosome
RpS5a	n	y	ribosome	translation
RpS12	n	y	ribosome	translation
RpL3	n	y	cytosolic large ribosomal subunit	translation
RpS27A	n	y	ribosome	translation
LanA	y	n	basement membrane	central nervous system development;heart development
CG11037	y	n	-	proteolysis
CG12491	y	n	-	-
CG13333	y	n	vesicle	neurogenesis
CG13641	y	n	-	-
CG14331	n	y	-	-
CG15021	y	n	-	-
CG15093	y	n	mitochondrion	cellular amino acid metabolic process;valine metabolic process
CG15554	y	n	-	-
RpS20	n	y	ribosome	translation
lectin-33A	y	n	-	-
Lip2	y	n	-	lipid metabolic process
Obp99a	y	n	extracellular region	olfactory behavior;response to pheromone
RpS7	n	y	lipid particle	translation
Lsp1alpha	y	n	lipid particle	-
RpL40	y	n	lipid particle	translation
CG31659	y	n	-	multicellular organism reproduction

CG32667	y	n	extracellular space	multicellular organism reproduction
l(1)G0320	y	n	lipid particle	-
CheA46a	y	n	cellular_component	sensory perception of chemical stimulus
sug	y	y	nuclear speck	negative regulation of transcription,DNA-templated;response to starvation
Cg25C	y	n	collagen type IV	dorsal closure;oviduct morphogenesis
CG5493	n	y	-	oxidation-reduction process
Gp93	y	n	lipid particle	protein folding;midgut development;response to stress
CG5989	n	y	-	-
Ef1beta	n	y	lipid particle	translational elongation
Pdi	y	n	lipid particle	protein folding;cell redox homeostasis
Eip71CD	n	y	-	sulfur amino acid metabolic process; autophagic cell death
CG7280	n	y	mitochondrial intermembrane space	protein catabolic process
RpL10Ab	n	y	cytosolic large ribosomal subunit	translation
CG8147	y	n	-	response to nicotine;metabolic process
CG8157	y	n	-	-
boss	y	n	microvillus	R7 cell fate commitment;sevenless signaling pathway
RpS15	n	y	lipid particle	translation
kek4	y	n	-	negative regulation of epidermal;growth factor receptor signaling pathway
PH4alphaNE2	y	n	procollagen-proline 4-dioxygenase complex	peptidyl-proline hydroxylation to 4-hydroxy-L-proline

Vkg	y	y		skeletal muscle tissue development;Malpighian tubule morphogenesis

Table A.0.2 VDRC Lines for Fat Body Signal Screen

CG number	VDRC transformant ID
CG10236	18873
CG10798	106066
CG11037	108803
CG11198	30517
CG11271	109381
CG11317	106863
CG11425	103037
CG11527	106812
CG11529	103207
CG11654	100177
CG12101	100697
CG1242	108568
CG12491	109101
CG12885	100107
CG13333	19555
CG13360	100997
CG13641	101688
CG13900	108248
CG14331	13355
CG14629	107496
CG14792	101495
CG15021	106362
CG15093	5655
CG1518	110709
CG15369	106111
CG15482	32614

CG1554	110340
CG15554	19522
CG15693	105298
CG16834	108412
CG16858	108631
CG16876	100036
CG17116	102033
CG17725	20529
CG1780	102269
CG18111	100475
CG1883	110558
CG2238	107268
CG2559	101101
CG2759	30033
CG2960	108730
CG30274	33693
CG31017	21284
CG31659	103022
CG3195	109447
CG32602	104968
CG32667	110126
CG32701	110344
CG32829	101223
CG3333	109616
CG33800	48522
CG34355	101438
CG3504	26211
CG3523	108339
CG3661	108402
CG3850	109584
CG3997	108821
CG4027	104500
CG4145	104536

CG4147	14883
CG4178	52386
CG4264	101734
CG4328	108648
CG4863	109820
CG4886	108734
CG5271	105501
CG5493	50637
CG5945	106894
CG5989	5149
CG6341	106636
CG6415	109458
CG6425	102310
CG6910	103766
CG6988	23359
CG7266	104465
CG7280	105942
CG7283	109345
CG7434	104506
CG7459	5804
CG7490	28619
CG7974	106966
CG8147	100052
CG8157	18585
CG8280	104502
CG8285	4366
CG8332	104439
CG8422	110708
CG8922	101472
CG9057	5584
CG9269	104109
CG9429	51272
CG9431	105647

CG9720	100523
CR34603	101915

Table A.0.3 TRiP Glial ECM Receptor Screen

ECM Receptor Gene Symbol	Bloomington TRiP NO.
mew	27543
if	38958/27544
scb	38959/27545
alphaPS4	28535
alphaPS5	Not available
mys	33642/27735
betaInt_v	Not available
Dg	34895
dally	33952
dlp	34091/34089
sdc	Not available

Table A.0.4 TRiP Glial Signalling Pathway Screen

Receptors for Major Signalling Pathways	Bloomington TRiP NO.
htl	35024
tl	35628
pvr	37520
Fz2	27568
tkv	35653
put	35195
babo	25933
fz	34321
wit	25946
egfr	36770

tor	35316
sev	36778
Ras85D	34619
sax	36131
os	33680
dome	34618
ptc	28793

Appendix B

Gene Lists of Interest From Glial TaDa Transcriptional Profiling

Table B.0.3 Glial subtype specific genes involved in neurogenesis based on subtype TaDa transcriptional profiling

Gene Symbol	Glial subtype	Molecular function (GO)
RpI135	SPG	DNA-directed RNA polymerase activity
aop	SPG	protein binding
Pdsw	SPG	NADH dehydrogenase (ubiquinone) activity
CG8086	SPG	-
alien	SPG	signal transducer activity
numb	SPG	Notch binding
CG4364	SPG	-
Srp54	SPG	mRNA binding
CG4901	SPG	ATP-dependent RNA helicase activity
cdc2	SPG	cyclin-dependent protein serine/threonine kinase activity
da	SPG	sequence-specific DNA binding transcription factor activity
CG6734	SPG	-
CG5525	SPG	ATPase activity, coupled ;
Tap42	SPG	-

Continued...

Gene Symbol	Glial subtype	Molecular function (GO)
l(2)35Df	SPG	ATP-dependent RNA helicase activity
fzy	SPG	mitotic anaphase-promoting complex activity
Nedd8	SPG	-
Ars2	SPG	-
CG12042	SPG	-
nito	SPG	mRNA binding
Ggamma1	SPG	GTPase activity
Not1	SPG	protein binding
CG1671	SPG	-
CG12343	SPG	-
Cct5	SPG	ATPase activity, coupled
UbcD10	SPG	ubiquitin-protein ligase activity
Hsf	SPG	DNA binding
GstE11	SPG	glutathione transferase activity
CG15100	SPG	methionine-tRNA ligase activity
dom	SPG	helicase activity
zip	SPG	ATPase activity, coupled
CG7028	SPG	protein kinase activity
CG32344	SPG	helicase activity
CG42554	SPG	-
pUf68	SPG	poly(U) RNA binding
Cdc37	SPG	chaperone binding
CG9004	SPG	RNA binding
Scsalpha	SPG	succinate-CoA ligase (GDP-forming) activity
ida	SPG	mitotic anaphase-promoting complex activity
Rpd3	SPG	histone deacetylase activity
CG33523	SPG	structural molecule activity
SrpRbeta	SPG	signal recognition particle binding
Use1	SPG	-
klu	SPG	nucleic acid binding
CG32075	SPG	-
CG6273	SPG	protein heterodimerization activity

Continued...

Gene Symbol	Glial subtype	Molecular function (GO)
Prp31	SPG	-
CG7375	SPG	-
CG12301	SPG	-
brm	SPG	DNA-dependent ATPase activity
Rpn12	SPG	endopeptidase activity
Dab	SPG	SH2 domain binding
Su(z)12	SPG	histone methyltransferase activity (H3-K27 specific) ;
polo	SPG	protein serine/threonine kinase activity
Hr78	SPG	ligand-activated sequence-specific DNA binding RNA polymerase II transcription factor activity
Cdk12	SPG	cyclin-dependent protein serine/threonine kinase activity
ctrip	SPG	ligand-dependent nuclear receptor binding
mRpL44	SPG	structural constituent of ribosome
CG2656	SPG	purine nucleotide binding
gfzf	SPG	glutathione transferase activity
CG10903	SPG	S-adenosylmethionine-dependent methyltransferase activity
Scm	SPG	sequence-specific DNA binding transcription factor activity
Hrb87F	SPG	mRNA binding
CG6455	SPG	-
CG5857	SPG	structural constituent of nuclear pore
CG5808	SPG	mRNA binding
CG11859	SPG	protein kinase activity
ball	SPG	protein kinase activity
CG7346	SPG	-
nej	SPG	transcription coactivator activity
Rx	CG	sequence-specific DNA binding transcription factor activity
CG7084	CG	secondary active organic cation transmembrane transporter activity

Continued...

Gene Symbol	Glial subtype	Molecular function (GO)
AdoR	PG	G-protein coupled adenosine receptor activity

Table B.0.1 Top upregulated glial genes under fed conditions 12-36hph

Gene Symbol	GO biological processes	Log ratio_fed vs st	FDR_fed vs st
RpL24	translation	3.62	1.55E-07
CG14756	-	3.33	2.4E-05
RpL13	translation	3.19	1.29E-07
CG17440	-	3.14	7.62E-12
CG11635	-	2.92	1.45E-06
CG17107	-	2.81	3.6E-06
CG42240	-	2.72	1.88E-08
Cfp1	histone H3-K4 methylation	2.64	1.74E-09
lmgA	mitotic anaphase	2.61	4.81E-09
lmgB	-	2.61	4.81E-09
CG10014	-	2.54	4.90E-09
CG9451	-	2.33	5.33E-08
CG9184	-	2.32	1.4E-04
CG17036	transport	2.24	1.48E-06
CG44044	-	2.17	2.8E-04
Chi	axon guidance	2.15	2.80E-06
a6	embryonic development	2.15	2.4E-04
CG42809	-	2.11	6.9E-03
CG17929	transmembrane transport	2.08	8.24E-08
RpS27A	translation	2.07	7.43E-08
GstD9	glutathione metabolic process	2.07	1.25E-06
RpL34b	translation	2.05	6.50E-05
CG7974	-	2.029	5.24E-05
CG13900	mRNA splicing	1.98	1.55E-07
SmB	mRNA splicing	1.98	1.4E-04
CG12848	-	1.98	1.1E-04
CG12985	-	1.94	4.59E-06
CG15459	-	1.93	6.69E-07
CG5036	regulation of G-protein coupled receptor protein signaling pathway	1.92	4.64E-09
CG42764	-	1.92	1.6E-04
fs(1)K10	dorsal/ventral pattern formation	1.91	1.18E-11
CG18810	protein palmitoylation	1.91	1.8E-04
CG32119	-	1.91	3.52E-05
cola	-	1.90	1.98E-05
CG1124	-	1.90	1.82E-09
RpLP0	translation	1.90	2.03E-05
RpS29	translation	1.89	1.3E-04
RpL5	translation	1.89	1.03E-05
eve	regulation of axonogenesis	1.88	1.4E-04
NT5E-2	nucleotide catabolic process	1.88	2.22E-12

Table B.0.2 Top upregulated glial genes under starved conditions 12-36hph

Gene Symbol	GO biological processes	Log ratio_st vs fed	FDR_st vs fed
CG13309	chitin metabolic process	2.07	1.4E-04
CG44037	-	1.82	1.17E-12
CG13541	-	1.58	4.07E-06
Cyp4p3	oxidation-reduction process	1.56	3.44E-09
eater	phagocytosis, recognition	1.54	3.20E-10
CG6733	cellular amino acid metabolic process	1.54	1.66E-05
CG42536	-	1.49	2.5E-05
CG3955	-	1.44	3.3E-04
CG7059	glycolysis	1.42	1.23E-05
CG6738	cellular amino acid metabolic process	1.38	2.7E-04
Brd	Notch signaling pathway	1.38	1.4E-04
rib	regulation of transcription, DNA-templated	1.25	2.57E-12
unk	chaeta morphogenesis	1.14	2.69E-09
CG13117	-	1.07	3.1E-03
danr	central nervous system formation	1.03	3.4E-02
Ubc84D	-	1.00	0.01
CG34194	-	0.96	1.5E-05
CG13857	-	0.93	2.5E-04
CG43230	-	0.91	1.4E-04
mab-21	embryonic organ development	0.89	1.30E-06
CG6398	establishment of glial blood-brain barrier	0.88	7.68E-09
TM4SF	-	0.87	9.25E-05
2mit	short-term memory	0.84	8.28E-22
CG43921	regulation of establishment of planar Polarity	0.83	1.77E-14
beat-IIIa	heterophilic cell-cell adhesion	0.81	1.91E-37
CG33639	G-protein coupled receptor signaling pathway	0.80	2.14E-12
Snmp1	response to pheromone	0.79	6.5E-04
alpha-Est7	determination of adult lifespan	0.78	3.4E-04
CG2269	-	0.78	3.90E-12
CG14989	-	0.75	7.4E-04
CG16787	-	0.70	2.4E-04
slou	muscle cell fate determination	0.67	6.62E-08
CG11317	neurogenesis	0.65	2.9E-04
jeb	axon guidance	0.62	2.87E-28
VAChT	neurotransmitter transport	0.60	5.22E-09
comm	axon guidance	0.58	5.15E-06